

## PDF hosted at the Radboud Repository of the Radboud University Nijmegen

The following full text is a publisher's version.

For additional information about this publication click this link.

<http://hdl.handle.net/2066/51043>

Please be advised that this information was generated on 2017-12-06 and may be subject to change.

# **The podocyte and parietal epithelial cell in proteinuria and glomerulosclerosis**

Henry Dijkman

The podocyte and parietal epithelial cell in proteinuria and glomerulosclerosis  
Dijkman, Henry B.P.M.

ISBN 90-8559-200-3

This thesis was prepared at the Departments of Pathology and Nephrology, Radboud University Nijmegen Medical Center, Nijmegen, The Netherlands

The printing of this thesis was supported by grants from the Dutch Kidney Foundation

Cover illustration: Three-dimensional reconstruction of parietal epithelial cells 'invading' the glomerular tuft, illustrated by Henry Dijkman

Printed by Optima grafische communicatie, Rotterdam

# **The podocyte and parietal epithelial cell in proteinuria and glomerulosclerosis**

Een wetenschappelijke proeve op het gebied van de Medische Wetenschappen

Proefschrift

ter verkrijging van de graad van doctor  
aan de Radboud Universiteit Nijmegen  
op gezag van de Rector Magnificus prof. dr. C.W.P.M. Blom,  
volgens besluit van het College van Decanen  
in het openbaar te verdedigen op dinsdag 28 november 2006  
des namiddags om 1.30 uur precies

door

Hendrikus Bernardus Paulus Martinus Dijkman

geboren op 11 oktober 1962  
te 's-Heerenberg

Promotor: Prof. dr. J.F.M. Wetzels

Co-promotores: Dr. K.J.M. Assmann  
Dr. E.J. Steenbergen

Manuscriptcommissie: Prof. dr. J.H.M. Berden  
Prof. dr. J.J. Weening (UvA)  
Dr. R. Goldschmeding (UU)

## CONTENTS

Chapter 1	Introduction	7
Chapter 2	Expression and Effect of Inhibition of Aminopeptidase-A during Nephrogenesis <i>Journal of Histochemistry &amp; Cytochemistry 2006;54:253-262</i>	19
Chapter 3	Podocyte Changes after Induction of Acute Albuminuria in Mice by Anti-Aminopeptidase-A mAbs <i>Nephron Exp Nephrol 2003;94:85-93</i>	35
Chapter 4	Automated magnification calibration in transmission electron microscopy using Fourier analysis of replica images <i>Ultramicroscopy 2006;106:255-260</i>	51
Chapter 5	The parietal epithelial cell is crucially involved in human idiopathic focal segmental glomerulosclerosis <i>Kidney International 2005;68:1562-1572</i>	65
Chapter 6	Proliferating cells in HIV and pamidronate-associated collapsing focal segmental glomerulosclerosis are parietal epithelial cells <i>Kidney International 2006;70:338-344</i>	87
Chapter 7	Glomerular involution: An unrecognized form of glomerulosclerosis? <i>Kidney International 2006; Accepted for publication in combination with chapter 8</i>	103
Chapter 8	Characteristics of glomerular involution in children with frequently relapsing minimal change nephrotic syndrome <i>Kidney International 2006; Accepted for publication in combination with chapter 7</i>	119
Chapter 9	A mouse model of glomerular involution <i>Submitted</i>	127
Chapter 10	General discussion: Parietal epithelial cell injury: tipping the balance between glomerulosclerosis and glomerular involution	143
Chapter 11	Summary: The role of the glomerular epithelial cells in focal segmental glomerulosclerosis	153
Chapter 12	Samenvatting	159
	Dankwoord	167
	Curriculum vitae	171
	List of publications	175



# 1

## INTRODUCTION





## INTRODUCTION

Kidneys are paired structures that lie in the retroperitoneum. Each kidney contains approximately 1,000,000 glomeruli, which are small balls of capillaries (diameter 0.1 mm) through which the blood is filtered. Glomeruli are present only in the cortex (Figure 1).

The functions of the kidneys are: 1) excretion of toxins and waste products (urea, creatinine, and many others); 2) maintaining homeostasis (balance) in the body's volume and chemistry; 3) production of hormones (erythropoietin, vitamin D, angiotensin). Blood flows into the glomerulus via the afferent arteriole and out via the efferent arteriole. Approximately 20-25% of the plasma that enters the glomerulus is filtered through the capillary wall into the urinary space. The capillary wall functions as a filtration barrier allowing the passage of water and small molecules (toxins, salts) into the urinary space while keeping cells and proteins in the capillary loop. The glomerular capillary wall is composed of three components: the fenestrated endothelium which lines the capillaries; the glomerular basement membrane, a thin sheet composed of negatively charged extracellular matrix proteins; the visceral epithelial cells, which are also called podocytes because of their characteristic interdigitating foot processes that cover the GBM. The filtered plasma is first collected in Bowman's space, covered by Bowman's capsule which is lined by the parietal epithelial cells (PECs), and subsequently transported via the tubular system to the ureter. The filtration barrier is believed to be a size-selective and charge-selective filter. Recent studies have made important contributions to our understanding of the role of the various constituents of this barrier. The fenestrated endothelium, which lines the capillary wall, is critically dependent on vascular endothelial growth factor (VEGF), produced by the adjacent podocytes [1;2]. The glomerular basement membrane is an acellular matrix with a thickness of 300 to 350 nm that provides structural support for the capillary wall. Its main components are type IV collagen, proteoglycans, laminin, and nidogen. Anionic sites in the glomerular basement membrane are believed to be located on the heparan sulfate and chondroitin sulfate side chains of perlecan and agrin. The anionic charges have been thought to be important for the restricted passage of negatively charged proteins. However, genetically engineered mice whose glomerular basement membrane contains heparan sulfate-deficient perlecan or lacks agrin do not have proteinuria but are sensitive with respect to albumin overload [3]. S-laminin/laminin beta 2 is a major component of adult renal glomerular basement membrane (GBM), and mutant mice that lack beta 2, develop massive proteinuria [4]. More recently, the podocyte is being recognized as the most important determinant of capillary wall permeability. The podocyte is a terminally differentiated cell with a complex structure and is composed of primary processes which form interdigitating extensions that form the characteristic foot processes which rest on the GBM. The foot processes are connected by a tiny membrane, the so-called slit diaphragm. The slit diaphragm complex is composed of several proteins that contribute to the structure of the slit diaphragm, connect the diaphragm to the intracellular actin cytoskeleton, and participate

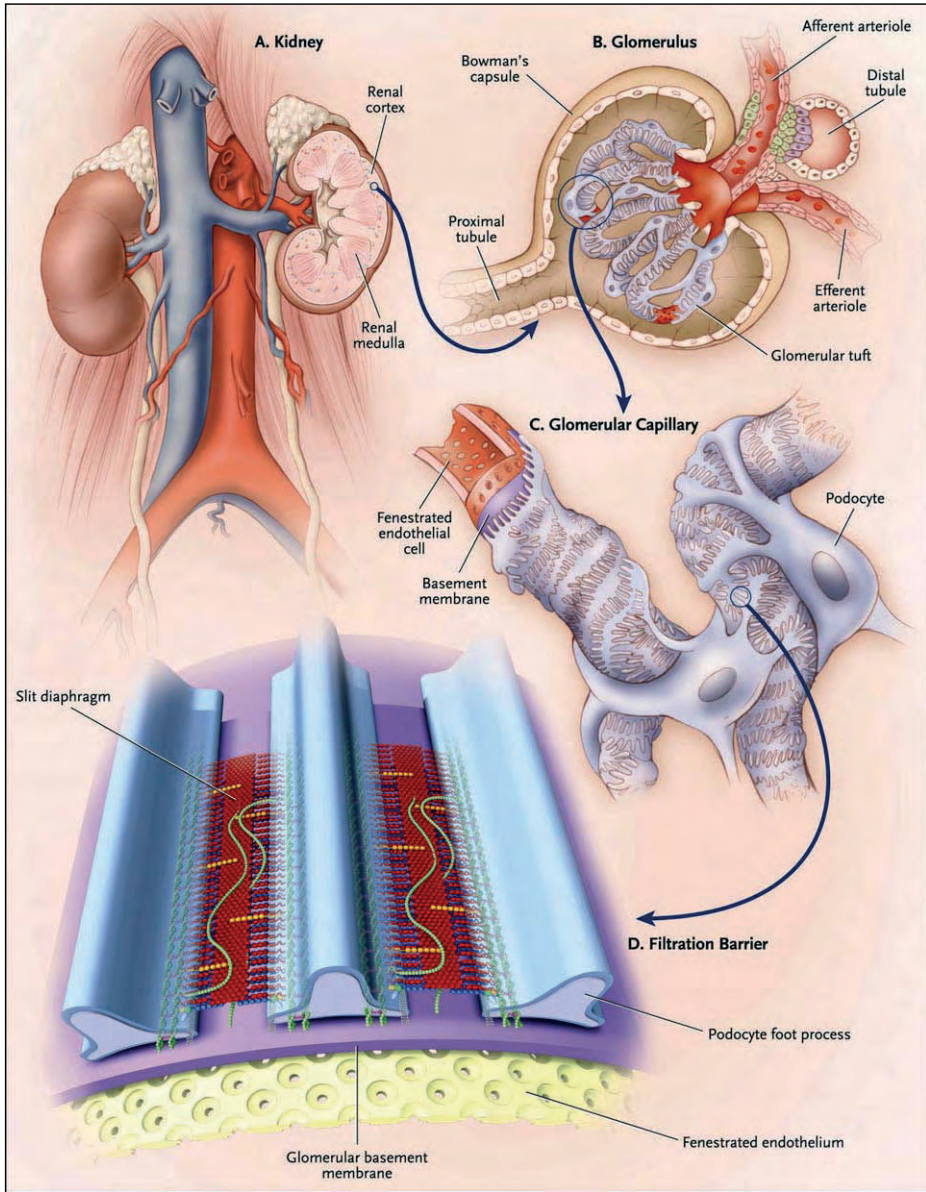


**Figure 1. Filtration System of the kidney.** The kidneys contain glomeruli in the renal cortex (Panel A). Arterioles enter Bowman's capsule and form the glomerular tuft; the capillary wall functions as a filter. The filtered plasma is collected in Bowman's space and then further transported to the proximal tubules (B). The capillary wall is composed of fenestrated endothelium, the glomerular basement membrane and a layer of podocytes (C). Panel D shows a cross section through the capillary wall with the fenestrated endothelium at the bottom, the glomerular basement membrane with overlying podocyte foot processes. In between these processes the slit diaphragm complex is located (D). Reprinted with permission [5].

in podocytic signalling processes (Figure 2). Well-known examples of slit diaphragm complex proteins are nephrin, podocin,  $\alpha$ -actinin-4 and CD2AP. Most of these proteins are essential for a functional slit diaphragm and maintenance of glomerular permselectivity, since mutation or inactivation of the corresponding genes causes proteinuria [5]. Thus, proteinuria is considered to be predominantly caused by alterations of the slit diaphragm complex. Proteinuria is mostly accompanied by disturbances of the architecture of the foot processes, so called effacement.

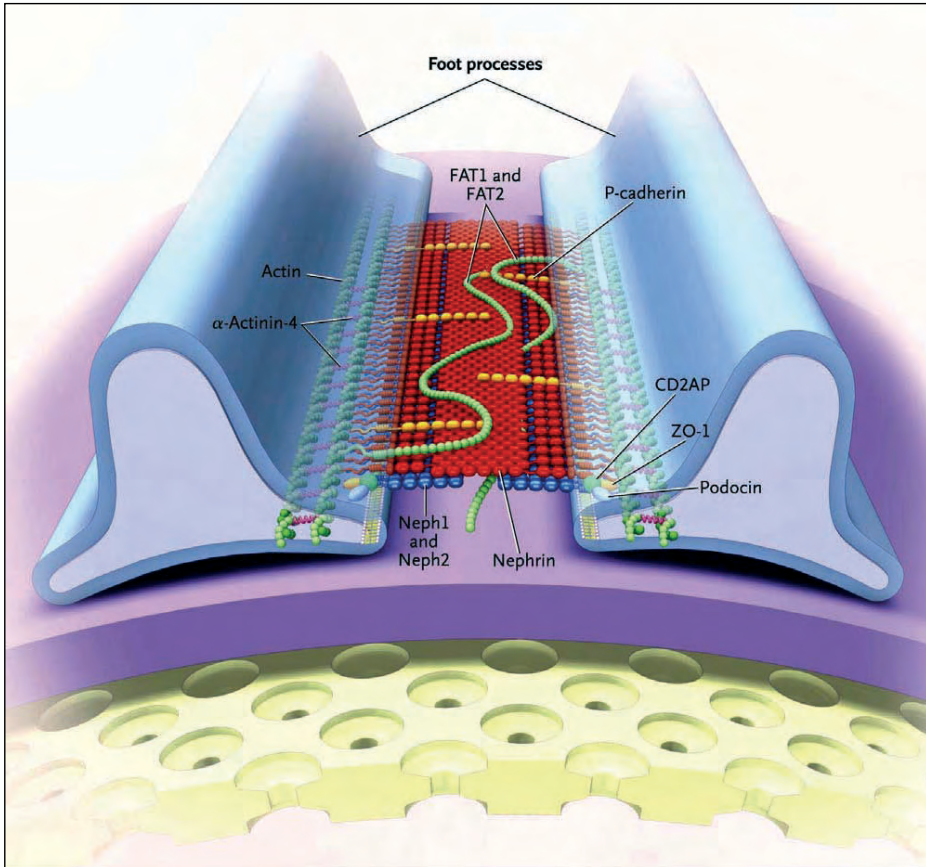


**Figure 2. The Slit-Diaphragm Complex.** Components which form the Filter; From the opposite foot processes nephrin molecules form a central density with pores, a zipper-like structure which probably maintains the width of the slit. Nephrin also interact with other proteins in the slit, such as FAT1 and FAT2. Nephrin interact with the intracellular podocin and CD2-associated protein (CD2AP). These molecules presumably connect the slit-diaphragm protein complex with ZO-1 and actin strands. Reprinted with permission [5].

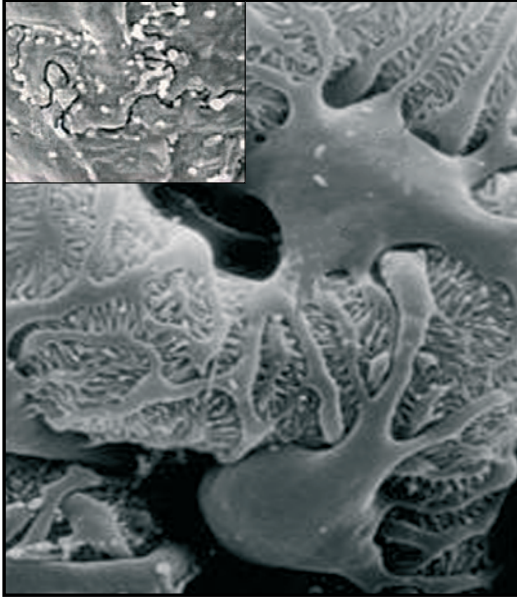


**Figure 3.** Scanning electron microscopy pictures of podocytes on glomerular capillaries. The interdigitating foot processes are nicely illustrated. The inset shows podocyte effacement.

This can be illustrated by scanning electron microscopy (Figure 3) and by transmission electron microscopy (Figure 4). Proteinuria is a hallmark of glomerular diseases and an independent predictor of renal function deterioration. Histologically, renal insufficiency is characterised by glomerulosclerosis and tubulo-interstitial fibrosis. Focal segmental glomerulosclerosis (FSGS) has become one of the most common glomerular diseases. In its classical form FSGS is characterized by mesangial sclerosis, obliteration of glomerular capillaries, formation

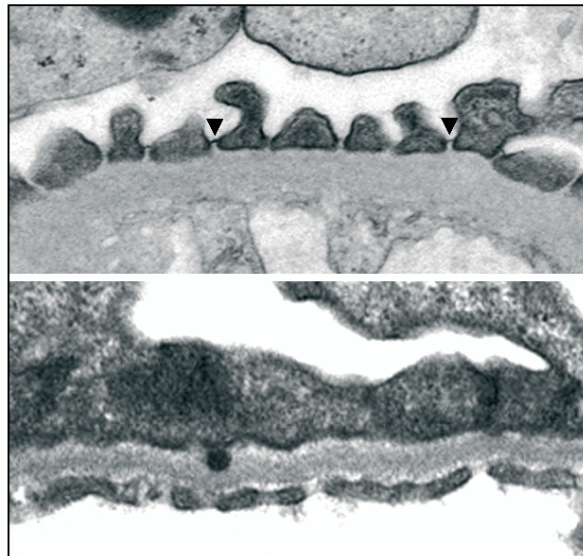


**Figure 4.** Transmission electron microscopy pictures of podocyte foot processes resting on the GBM. The arrowheads point to the slit diaphragm. The lower picture illustrates podocyte effacement.

of adhesions between the glomerular tuft and Bowman's capsule, podocyte hypertrophy, hyalinosis of the vessel wall and intracapillary foam cells. Notably, FSGS is merely a descriptive diagnosis, and not a disease entity. FSGS may be secondary to glomerular hyperfiltration and thus the result of longstanding and ongoing glomerular injury ending with chronic renal disease. Recently, various morphological variants have been defined and a classification has been proposed to better address the diversity of FSGS [6].

Five light microscopic variants of FSGS were defined: the perihilar variant (lesions predominantly located at the vascular pole), the tip variant (the presence of lesions located at the urinary pole), the cellular variant (characterized by endocapillary hypercellularity), the collapsing variant (collapse of the glomerular tuft associated with epithelial cell hypertrophy and hyperplasia), and finally FSGS not otherwise specified (NOS), if lesions do not fit into one of the above mentioned categories (Figure 5).

All morphological variants are accompanied by some degree of epithelial cell proliferation, being minimal or absent in the perihilar variant and often very prominent in the cellular and collapsing variant (Figure 6). In recent studies the podocytes have received a central role in the pathogenesis of FSGS [7]. Normal podocytes are unable to proliferate and to compensate for damaged neighbouring podocytes. Studies by Kriz and co-workers in various rat models of FSGS indicated loss of podocytes and adherence of the parietal epithelial cell (PEC) to the naked GBM as the critical event in the formation of FSGS lesions [8;9]. The adhesions allow filtration of proteins to the periglomerular space and this process is held responsible for the periglomerular fibrosis and tubulointerstitial fibrosis that typically accompanies FSGS. These studies can not explain the pathogenesis of the more cellular FSGS lesions. The collapsing variant of FSGS is the prototypical example. Studies in collapsing FSGS have suggested that the proliferating cells are podocytes that have lost their podocyte markers, and have

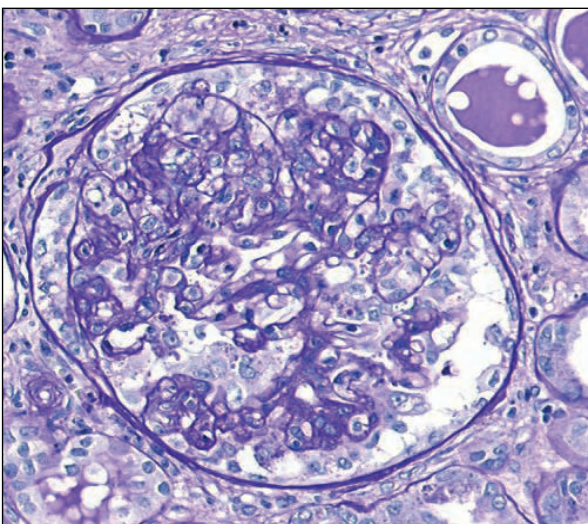


**Figure 5.** FSGS not otherwise specified (NOS).

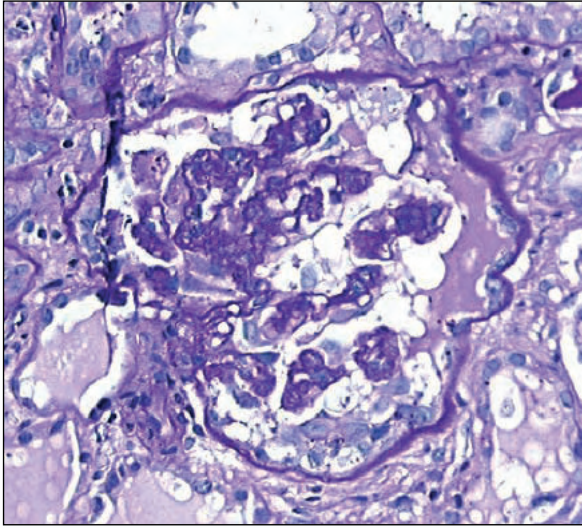


Figure 6. Collapsing FSGS.

regained the ability to proliferate [10-14]. This is the concept of the dedifferentiated dys-regulated podocyte. Based on these findings epithelial hyperplasia, which is also commonly observed in 'active' FSGS lesions other than collapsing lesions, is generally considered to be the result of proliferation of dedifferentiated podocytes.

## AIMS OF THE STUDY

The studies presented in this thesis were aimed at:

- 1) Unraveling mechanisms of proteinuria
- 2) Evaluating the role of glomerular epithelial cells in FSGS

### *Mechanisms of proteinuria*

We have used the anti-aminopeptidase-A mouse model to study mechanisms of proteinuria [15-17]. This model is characterized by a massive and acute albuminuria, induced by a single intravenous injection of a combination of two mAbs directed against specific epitopes of mouse aminopeptidase-A (APA). APA (EC 3.4.11.7) is a membrane bound zinc metalloprotease which, in mouse kidney, is expressed on podocytes, epithelial cells of the proximal convoluted tubules and, to a lesser extent, on the endothelial cells of the peritubular capillaries and the smooth muscle cells of the media of arteries. APA is involved in the degradation of peptides. It's best-known substrate is angiotensin II (Ang II), the most active component of the renin-angiotensin system. APA inactivates Ang II by hydrolyzing the N-terminal aspartyl residue, thus forming angiotensin III (Ang III) [18].

The induction of albuminuria in this model is not related to any of the known systemic mediators of glomerular injury, such as complement, coagulation factors, monocytes, neutrophils, or platelets [15]. In subsequent studies we have shown that injection of the anti-APA mAbs increased glomerular Ang II levels [19]. However, in adult mice induction of albuminuria was independent from Ang II, as proven by our studies in angiotensinogen knock-out mice [17]. We questioned if the effects of anti-APA administration may be dependent in the developmental stage of the glomeruli. It is well known that Ang II is important during nephrogenesis. Most components of the RAS are expressed in the developing kidney. The role of APA is unknown. We have studied the expression of APA during nephrogenesis and the effect of APA inhibition in newborn mice (chapter 2).

In the experiments described in chapter 3, we have examined the expression of several important podocytic proteins in relation to the time course of the albuminuria in our anti-APA mouse model. We have included cytoskeleton (-associated) proteins, adhesion molecules, slit-diaphragm proteins and heparan sulfate proteoglycans, all known to affect podocyte integrity, associated with podocytic injury or proteinuria. In addition, we measured ultra-structurally the number of foot processes per  $\mu\text{m}$  GBM and the width of the slit pore between the podocytes by morphometric methods. In subsequent studies we have improved the methodology of calibrating the morphometric measurements on electron microscopical images (chapter 4).

#### *Pathogenesis of focal segmental glomerulosclerosis*

In recent years we have used the Thy-1.1 transgenic mouse model for the study of focal segmental glomerulosclerosis [20;21]. Thy-1.1 transgenic mice carry a mouse-human transgene that causes ectopic expression of the mouse Thy-1.1 antigen on podocytes. Injection of mAbs directed against the Thy-1.1 antigen induces an acute albuminuria within 10 min and a dose dependent development of FSGS within 3 weeks. The early stages of FSGS in this model are characterised by prominent cell proliferation and the lesions clearly resemble human collapsing FSGS. We noted that the proliferating cells were parietal epithelial cells (PECs), rather than podocytes. Moreover we showed that the extracellular matrix that formed the adhesion was produced by the PECs [22].

To evaluate the role of the PECs in human FSGS we have used a nephrectomy specimen of a patient with recurrent FSGS after transplantation (chapter 5). This enabled us to evaluate over 400 serial sections. We could demonstrate that parietal epithelial cells also play an important role in the formation of the cellular lesions and the scar in human idiopathic FSGS. We subsequently have investigated the origin of the proliferating cells in collapsing FSGS associated with HIV and pamidronate (chapter 6).



### *Global glomerulosclerosis*

Progressive glomerular injury is eventually characterized by global glomerulosclerosis. Two types of global glomerulosclerosis can be distinguished: the vascular type (also referred to as obsolescent type) and the glomerulopathic type (also referred to as solidified type). The latter type is often observed in patients with FSGS. In biopsies of children with a nephrotic syndrome we observed small glomeruli, which somewhat resembled global glomerulosclerosis. We have coined the term involuted glomeruli to describe them. The involuted glomeruli can be distinguished from the above mentioned forms of global glomerulosclerosis (chapter 7). We have evaluated biopsies of a cohort of children with frequently relapsing minimal change nephrotic syndrome for the presence of involuted glomeruli and have tried to relate their presence with clinical parameters (chapter 8). Finally, in chapter 9 we describe the long term follow-up of mice injected twice with the proteinuric anti-APA mAbs. We did not observe development of FSGS. Intriguing was the observation that these mice developed small dense glomeruli, clearly resembling the involuted glomeruli in humans.

We discuss and summarize our findings in chapters 10 and 11

## REFERENCES

1. Eremina V, Sood M, Haigh J *et al.*: Glomerular-specific alterations of VEGF-A expression lead to distinct congenital and acquired renal diseases. *J Clin Invest* 111:707-716, 2003.
2. Eremina V, Quaggin SE: The role of VEGF-A in glomerular development and function. *Curr Opin Nephrol Hypertens* 13:9-15, 2004.
3. Morita H, Yoshimura A, Inui K *et al.*: Heparan sulfate of perlecan is involved in glomerular filtration. *J Am Soc Nephrol* 16:1703-1710, 2005.
4. Noakes PG, Miner JH, Gautam M *et al.*: The renal glomerulus of mice lacking s-laminin/laminin beta 2: nephrosis despite molecular compensation by laminin beta 1. *Nat Genet* 10:400-406, 1995.
5. Tryggvason K, Patrakka J, Wartiovaara J: Hereditary proteinuria syndromes and mechanisms of proteinuria. *N Engl J Med* 354:1387-1401, 2006.
6. D'Agati V: Pathologic classification of focal segmental glomerulosclerosis. *Semin Nephrol* 23:117-134, 2003.
7. Mundel P, Shankland SJ: Podocyte biology and response to injury. *J Am Soc Nephrol* 13:3005-3015, 2002.
8. Kriz W: Progressive renal failure--inability of podocytes to replicate and the consequences for development of glomerulosclerosis. *Nephrol Dial Transplant* 11:1738-1742, 1996.
9. Kriz W, Gretz N, Lemley KV: Progression of glomerular diseases: is the podocyte the culprit? *Kidney Int* 54:687-697, 1998.
10. Barisoni L, Kriz W, Mundel P, D'Agati V: The dysregulated podocyte phenotype: a novel concept in the pathogenesis of collapsing idiopathic focal segmental glomerulosclerosis and HIV-associated nephropathy. *J Am Soc Nephrol* 10:51-61, 1999.
11. Bariety J, Bruneval P, Hill G *et al.*: Posttransplantation relapse of FSGS is characterized by glomerular epithelial cell transdifferentiation. *J Am Soc Nephrol* 12:261-274, 2001.
12. Yang Y, Gubler MC, Beauflis H: Dysregulation of podocyte phenotype in idiopathic collapsing glomerulopathy and HIV-associated nephropathy. *Nephron* 91:416-423, 2002.
13. Ohtaka A, Ootaka T, Sato H, Ito S: Phenotypic change of glomerular podocytes in primary focal segmental glomerulosclerosis: developmental paradigm? *Nephrol Dial Transplant* 17 Suppl 9:11-5:11-15, 2002.
14. Ohtaka A, Ootaka T, Sato H *et al.*: Significance of early phenotypic change of glomerular podocytes detected by Pax2 in primary focal segmental glomerulosclerosis. *Am J Kidney Dis* 39:475-485, 2002.
15. Assmann KJ, van Son JP, Dijkman HB, Koene RA: A nephritogenic rat monoclonal antibody to mouse aminopeptidase-A. Induction of massive albuminuria after a single intravenous injection. *J Exp Med* 175:623-635, 1992.
16. Mentzel S, van Son JP, Dijkman HB *et al.*: Induction of albuminuria in mice: synergistic effect of two monoclonal antibodies directed to different domains of aminopeptidase-A. *Kidney Int* 55:1335-1347, 1999.
17. Gerlofs-Nijland ME, Assmann KJ, Dijkman HB *et al.*: Albuminuria in mice after injection of antibodies against aminopeptidase-A: role of angiotensin II. *J Am Soc Nephrol* 12:2711-2720, 2001.
18. Wolf G, Mentzel S, Assmann KJ: aminopeptidase-A: a key enzyme in the intrarenal degradation of angiotensin II. *Exp Nephrol* 5:364-369, 1997.
19. Mentzel S, Assmann KJ, Dijkman HB *et al.*: Inhibition of aminopeptidase-A activity causes an acute albuminuria in mice: an angiotensin II-mediated effect? *Nephrol Dial Transplant* 11:2163-2169, 1996.
20. Assmann KJ, van Son JP, Dijkman HB *et al.*: Antibody-induced albuminuria and accelerated focal glomerulosclerosis in the Thy-1.1 transgenic mouse. *Kidney Int* 62:116-126, 2002.
21. Smeets B, Dijkman HB, Te Loeke NA *et al.*: Podocyte changes upon induction of albuminuria in Thy-1.1 transgenic mice. *Nephrol Dial Transplant* 18:2524-2533, 2003.
22. Smeets B, Te Loeke NA, Dijkman HB *et al.*: The parietal epithelial cell: a key player in the pathogenesis of focal segmental glomerulosclerosis in Thy-1.1 transgenic mice. *J Am Soc Nephrol* 15:928-939, 2004.



# 2

## **EXPRESSION AND EFFECT OF INHIBITION OF AMINOPEPTIDASE-A DURING NEPHROGENESIS**

Henry B.P.M. Dijkman, Karel J.M. Assmann, Eric  
J. Steenbergen and Jack F.M. Wetzels,<sup>2</sup>

*Department of Pathology and Department of  
Internal Medicine<sup>2</sup>, Division of Nephrology, Radboud  
University Nijmegen Medical Centre, the Netherlands*

## ABSTRACT

Aminopeptidase-A (APA) is a metalloprotease that cleaves N-terminal aspartyl and glutamyl residues from peptides. Its best known substrate is angiotensin II (Ang II), the most active compound of the renin angiotensin system (RAS). The RAS is involved in renal development. Most components of the RAS system are expressed in the developing kidney. Thus far, APA has not been studied in detail.

In the present study we have evaluated the expression of APA at the protein-, mRNA-, and enzyme activity level in the kidney during nephrogenesis. Furthermore, we have studied the effect of inhibiting APA enzyme activity by injection of anti-APA antibodies into 1-day-old newborn mice. APA expression was observed from the comma stage onwards, predominantly in the developing podocytes and brush borders of proximal tubular cells. Notably, APA was absent in the medulla or the renal arterioles. Inhibition of APA enzyme activity caused temporary podocyte foot process effacement, suggesting a minimum role for APA during nephrogenesis.

Keywords: podocyte, nephrogenesis, aminopeptidase-A, albuminuria, monoclonal antibodies, inhibition, enzyme activity, mouse

## INTRODUCTION

Angiotensin II (Ang II) is the most active component of the renin angiotensin system (RAS). The RAS is involved in the regulation of vascular tone and maintenance of blood pressure. Ang II is also involved in the regulation of cell growth. In adult life Ang II contributes to renal injury by increasing the blood pressure, initiating glomerular injury and inducing fibrosis [1]. These effects of Ang II are predominantly mediated by activation of the angiotensin type 1a receptor (AT1a). Indeed, overexpression of the AT1a receptor in rat podocytes resulted in focal glomerulosclerosis [2]. Inhibitors of the RAS system thus have become important tools in the treatment of patients with renal diseases [3]. In contrast, in the fetal kidney an intact RAS system is essential for a normal development [4,5]. Treatment of newborn mice or rats with angiotensin converting enzyme (ACE) inhibition resulted in abnormal development of the kidney characterised by papillary atrophy and severe wall thickening of the cortical arteries and arterioles. Similar abnormalities were observed in mice with a targeted disruption of genes involved in the RAS system such as angiotensinogen, ACE and the AT1 receptor (reviewed in Guron and Friberg, 2000). Most components of the RAS system are expressed in the developing kidney in a time and site specific manner. Detailed studies have demonstrated expression of angiotensin, renin, ACE and the AT1 and AT2 receptor (reviewed in Guron and Friberg, 2000). Thus far little attention has been given to aminopeptidase-A (APA).

APA (EC 3.4.11.7) is a membrane-bound metalloprotease that cleaves N-terminal aspartyl and glutamyl residues from peptides. Its best known substrate is angiotensin II [6]. APA has a wide-spread organ distribution suggesting that this enzyme has a role in many diverse biological processes [7].

Investigators have suggested that APA may be involved in blood pressure regulation and the pathogenesis of preeclampsia [8]. In the adult mouse kidney APA is expressed on podocytes and brush borders of proximal tubular epithelial cells, and to a lesser degree on juxtaglomerular (JC) cells, endothelial cells of peritubular capillaries (PTC) and in pars media of arteries. In our studies on membranous nephropathy we have developed a panel of antibodies directed against APA [9]. Injection of a combination of antibodies that inhibit APA enzyme activity, increased renal All levels and induced an acute and profound albuminuria [10]. The mAbs are highly specific for APA since we observed no binding upon injection into APA-deficient mice [10]. These monoclonal antibodies have provided us with tools to study the tissue distribution of APA [7]. In the present study we have evaluated the expression of APA at the mRNA -, protein -, and enzyme activity level during nephrogenesis in mice. In addition we examined the effect of APA inhibition during nephrogenesis.

## MATERIALS AND METHODS

### *Animals*

Female BALB/c mice in late pregnancy, aged 2 to 3 months, were purchased from Charles River, Sulzfeld, Germany. E18 old BALB/c mouse embryos or newborns, day 1 (E18-19 days post coitum (d.p.c.)), were used to study the nephrogenesis of the mouse kidney. In mice nephrogenesis starts at E11-12 (forming metanephros) and continues for 7-10 days (P1-2) after birth. In mice, 80% of the glomeruli form after birth. Microscopic examination of kidneys from E18 old embryos allows studying glomeruli at various developmental stages, ranging from the earliest developmental stage (vesicle formation) in the outer cortex to mature glomeruli in the inner cortex. 1-day-old mice were used to study the effect of inhibiting APA enzyme activity during nephrogenesis. All procedures involving mice were approved by the Animal Care Committee of the University of Nijmegen and conformed to the Dutch Council for Animal Care and National Institutes of Health guidelines.

### *Animal experiments*

For the distribution study kidneys from E18 old embryos were removed from BALB/c mice, snap frozen in liquid nitrogen for immunofluorescence, enzyme histochemistry and mRNA in situ hybridization, or immersion fixed for light microscopy (LM) and immunoelectron microscopy (IEM).

To study the effect of APA inhibition during nephrogenesis we injected combinations of anti-APA antibodies in 1-day-old mice. The characteristics of the three rat mAbs used in this study (ASD-3, ASD-37 and ASD-41) have been described previously [9]. The anti-APA mAbs have been propagated in vitro by hollow fiber culture (Nematology Department, Agriculture University Wageningen, The Netherlands). Injection of the combination ASD-37/41 inhibited the APA enzyme activity completely and induced a massive acute albuminuria at day 1. In contrast, the combination ASD-3/41, which did partly inhibit APA activity on the podocyte and completely inhibited the enzyme activity of the brush border (BB), did not induce proteinuria. We have used a single intravenous injection of a total dose of 0.8 mg of the nephritogenic combination ASD-37/41 or the non-nephritogenic combination ASD-3/41 (both with 1:1 weight ratio). Groups of mice (n=5) were studied 9, 21 days and 3 months after injection. Urine samples were collected via spontaneously voiding at day 1 and via bladder puncture at days 9, 21 and 3 months, after which mice were killed and the kidneys processed for light microscopy, immunofluorescence, enzyme histochemistry and electron microscopy.

### *Morphologic studies*

To study the expression of APA by immunofluorescence (IF), we have used the mAbs ASD-3, an anti-APA mAbs of subclass IgG1. All the three rat mAbs used in this study (ASD-3, ASD-37 and ASD-41) give the same staining pattern of APA. Kidneys from E18 old embryos were snap

frozen in liquid nitrogen. Two  $\mu\text{m}$ -thick, acetone fixed sections were incubated for 60 minutes at room temperature. Binding of the mAbs was visualized with FITC-labeled rabbit anti-rat IgG containing 4% normal mouse serum (Dako, Glostrup, Denmark) as described before [9,11].

The enzyme activity of APA was visualized by enzyme histochemistry according to Lojda and Gossrau, as described before [12], with the APA-specific substrate L-glutamic acid-4-methoxy- $\beta$ -naphthylamide (Bachem, Bubendorf, Switzerland). The intensity of the developed colour was recorded semi quantitatively on a scale from 0 to 4+ [13].

APA mRNA was detected by RNA in situ hybridization using both a sense and an antisense 344 bp digoxigenin-labeled cRNA probe, as described before [9].

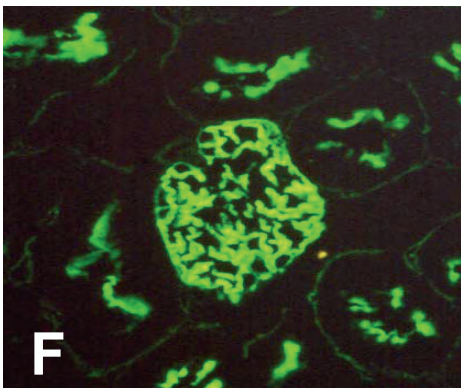
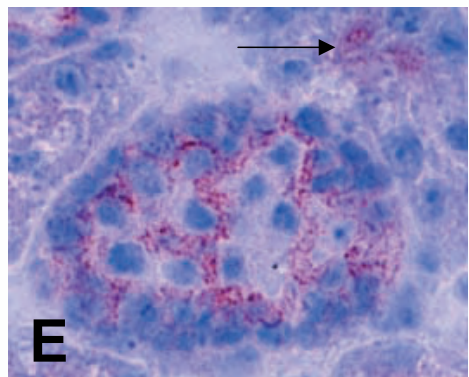
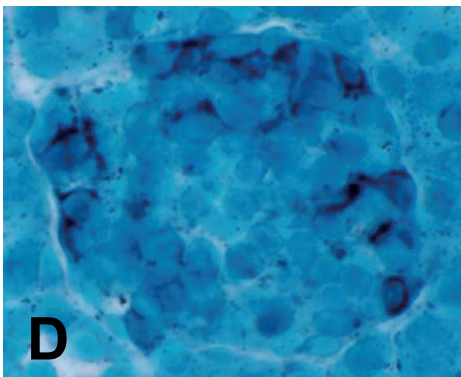
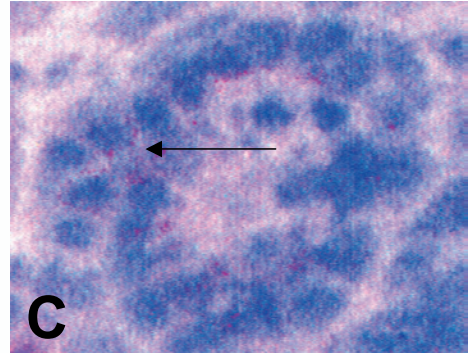
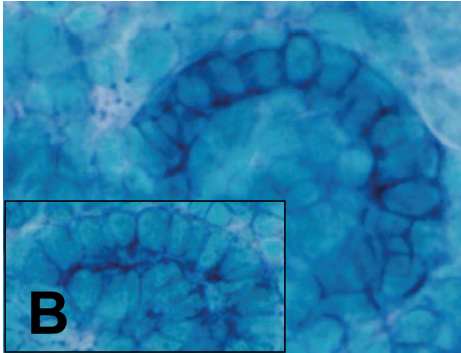
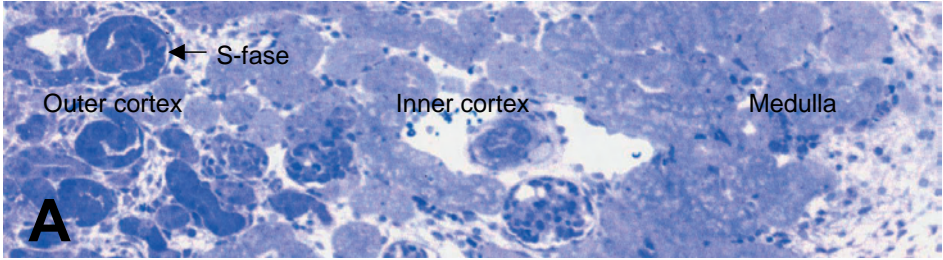
For light- and electronmicroscopy (LM / EM) the kidneys were immersion-fixed in 2.5% glutaraldehyde dissolved in 0.1 M sodium cacodylate buffer, pH 7.4, overnight at 4°C and washed in the same buffer. The tissue fragments were post fixed in palade buffered 2% OsO<sub>4</sub> for 1 hr, dehydrated, and embedded in Epon 812, Luft's procedure (Merck, Darmstadt, Germany). Semithin (1 $\mu\text{m}$ ) and ultrathin sections were cut on an ultratome, Reichert Ultracut S (Leica Microsystems). The semithin slices were stained with toluidine blue and examined using light microscopy. Ultrathin sections were stained with 4% uranyl acetate for 45 min and subsequently with lead citrate for 4 min at room temperature. Sections were examined in a JEOL 1200 EX2 electron microscope (JEOL, Tokyo, Japan).

For IEM the kidneys were immersion-fixed in a mixture of 10 mM periodate, 75 mM lysine and 2% paraformaldehyde, pH 6.2 (PLP) for 3 hr. After rinsing several times in PBS, the embryonic kidneys were cryoprotected by immersion in 2.3 M sucrose, pH 7.2, for 1 hr, and then frozen in liquid nitrogen. Twenty  $\mu\text{m}$ -thick sections were incubated with ASD-3, for 18 hr at 4°C. Binding of the mAbs was visualized with peroxidase-labeled rabbit anti-rat IgG containing 4% normal mouse serum (Seralab/Sanbio, Uden, The Netherlands), as described before. For IEM ultrathin sections were cut on an ultratome (Leica, Reichert Ultracuts, Wien, Austria). The sections were examined in a Jeol 1200 EX2 electron microscope (JEOL, Tokyo, Japan).

## RESULTS

In mice nephrogenesis starts at E11-12 (metanephros formation) and continues for 7-10 days after birth. Formation of the kidney epithelium involves reciprocal inductive interactions between two mesoderm-derived structures, the uretic bud, an outgrowth of the Wolffian duct, and the adjacent metanephric mesenchyme. The bud branches into collecting ducts, and the mesenchyme differentiates into nephrons [14,15]. In mice, 80% of the glomeruli form after





← **Figure 1. Developmental stages:** kidneys from E18 old embryos show glomeruli at various developmental stages ranging from the earliest developmental stage (vesicle formation) in the outer cortex to glomerular maturation in the inner cortex (A, overview toluidine blue staining). The APA mRNA expression during nephrogenesis could be demonstrated during all stages, especially in the S-stage (B) the developing podocytes could be nicely recognized, in massive amounts in some proximal tubules (B, insert) and in developing podocytes in the capillary stage (D). In addition, APA enzyme activity could already be demonstrated in these early stages (C), (arrow developing podocytes) and was continuously demonstrable and increased in the more advanced capillary stage (E). In the proximal tubules APA enzyme activity could also be demonstrated in the brush border membranes, arrow (E). In mature kidney the immunohistological presence of glomerular APA in the podocytes and brush borders of the proximal tubules stain for APA, faint APA expression can also be observed in the granular juxtaglomerular cells and on the endothelial cells of the peritubular capillaries (F). IEM (G) illustrates the membranous podocytic pattern (A x150, B-C x600, D x1000, E x600, F x300, G x5000).

birth. Microscopic examination of kidneys from E18 old embryos reveals glomeruli at various developmental stages ranging from the earliest developmental stage (vesicle formation) in the outer cortex to mature glomeruli in the inner cortex, a low magnification overview shows several stages (Figure 1a). The various stages of glomerular development can be nicely distinguished by transmission electron microscopy. Figure 2 illustrates a typical example of a developing glomerulus in the comma stage (Figure 2a), the S-stage (Figure 2b) and the early capillary stage (Figure 2c).

#### *Histology and immunofluorescence*

In the earliest histologically definable glomerular stage, the comma stage, (Figure 3a) there was only trace staining for APA by immunofluorescence (Figure 3b). Controls for background were completely negative. Its morphological shape and the presence of the earliest ingrowth of capillaries, recognized by using our antibody ASD-13, which is specific for glomerular endothelium, identified the comma stage.

In the next stage, the S-stage (Figure 3c), there was staining for APA of the cells lining the vascular cleft destined to become podocytes and with lower intensity also of the epithelial cells destined to become parietal epithelial cells. In addition cells that will develop into the proximal tubule stained faintly positive for APA without a clear polarity (Figure 3d, arrow). In the more advanced early capillary stage (Figure 3e), the staining of cells destined to become podocytes is more intense (Figure 3f). Staining is membranous and strongest nearest to the capillary tuft. At this stage there is luminal staining of the proximal tubules, restricted to the brush border (Figure 3f, arrow). In addition there is still weak staining of the developing parietal epithelial cells. Finally, in the mature glomerulus (Figure 3g), APA staining shows a homogeneous podocytic pattern. In addition the brush borders of the proximal tubules stain for APA (Figure 3h). In the mature kidney, faint APA expression can also be observed in the granular juxtaglomerular cells and on the endothelial cells of the peritubular capillaries (PTC) (Figure 1f), whereas no expression is observed in the efferent and afferent arterioles, the distal tubules, the loops of Henle or the collecting ducts.

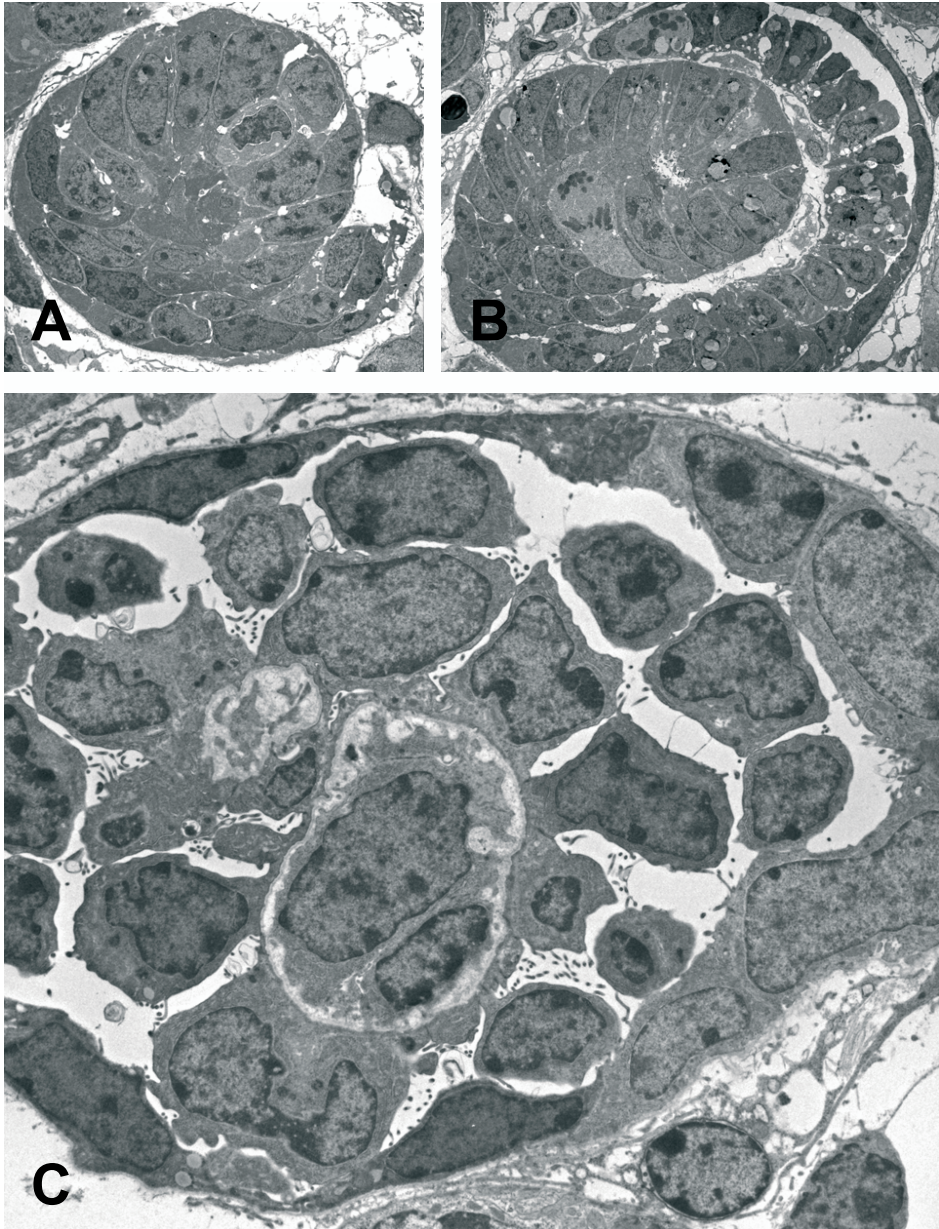


**Figure 2.** At the electronmicroscopical level the different stages and the developing podocytes could be nicely distinguished, the comma-stage (A), the S-stage (B) and the more advanced early capillary stage (C) (A-B x900, C x2500).

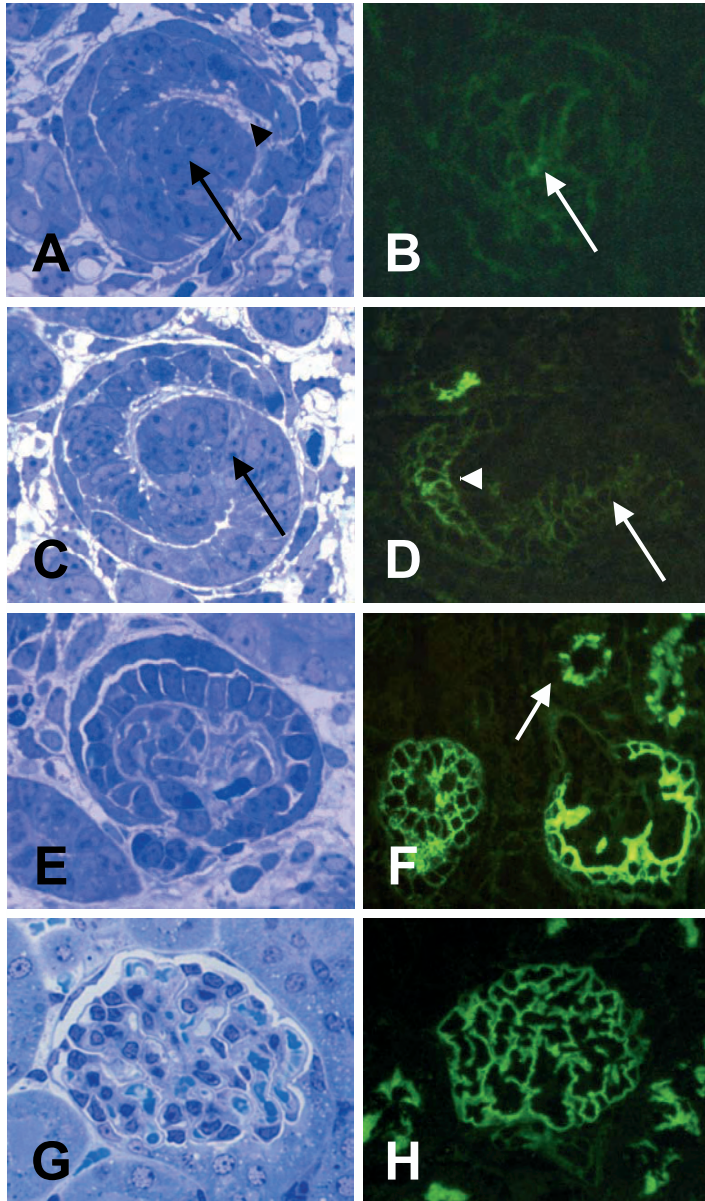
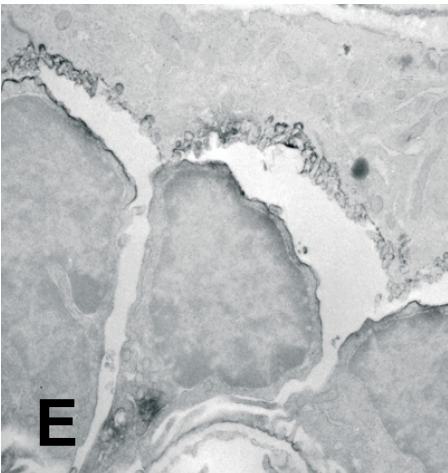
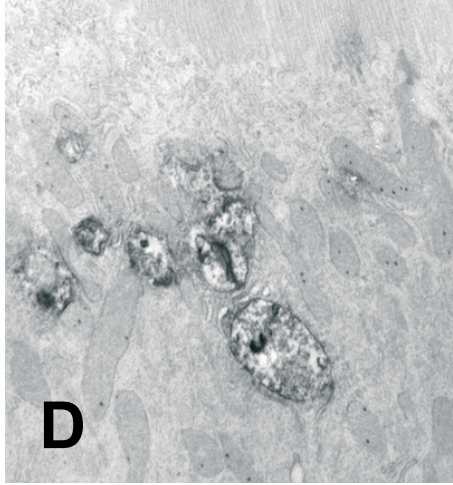
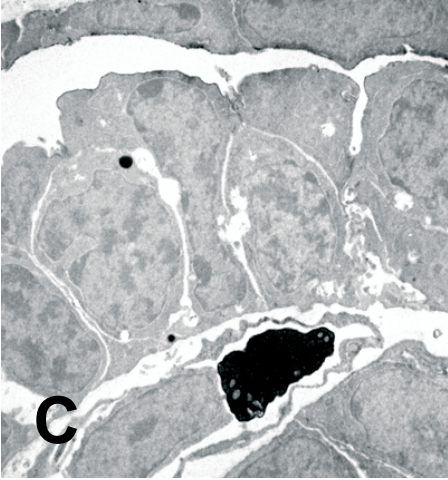
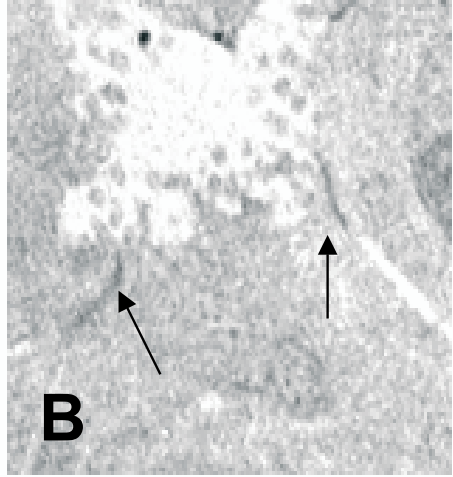
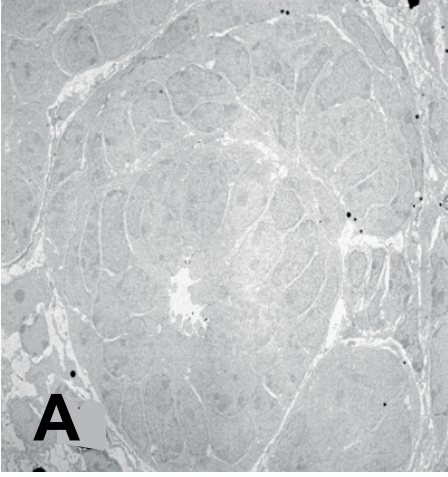


**Figure 3. Expression of APA in the developing glomeruli studied by immunofluorescence:** APA (demonstrated with the mAbs ASD-3) could already be detected in the earliest histological definable glomerular stage, the comma stage and proximal tubular stages in the cortex but not in the medulla. In the comma stage the vascular cleft, arrowhead (A), could be nicely distinguished (also the capillaries could be recognized via ASD-13, a specific antibody for glomerular endothelium, data not shown). APA staining could be seen in the developing podocytes and in a somewhat stronger degree in the center of the earliest developing proximal tubules, arrow (A,B). In the S-stage there was staining for APA of the cells lining the vascular cleft that are destined to become podocytes (arrowhead) (D). In addition cells that will develop into the proximal tubule stained faintly positive for APA without a clear polarity (arrow) (C,D). In the more advanced early capillary stage, several capillary loops start to develop within the glomerulus. These capillary loops are positively stained for APA (E,F). In the proximal tubules expression is now polarised, with predominant localization at the apical site in the brush border (arrow) (F). In the capillary stage APA was present in the glomerular capillary loops and in the brush borders of the proximal tubules (G,H) (A–H x600).



← **Figure 4. Immunoelectron microscopy on day E18 old embryos:** In the comma stage APA was faintly observed on the membranes of the early epithelial cells. APA was only seen on those epithelial cells that first came in contact with the ingrowing endothelial cells of the vascular cleft (A). In the more advanced S-stage the APA staining on the membranes of the epithelial cells was much more pronounced. Furthermore, APA on these epithelial cells was only stained on the membranes lining the earliest developing Bowman's space (C). APA was present on the early apical membranes of the parietal epithelial cells lining Bowman's capsule and on the top membranes and early foot processes of the developing podocytes. The occluding junctions were located between the visceral epithelial cells (C,E). In the developing proximal tubules APA was first observed on the apical/lateral membranes (B) and predominantly in the cytoplasm in distinct vesicles of these early proximal tubular epithelial cells (D). Later in development the formation of the proximal tubular brush borders becomes more pronounced and APA was found in massive amounts on the brush border membranes, then the strong cytoplasmic staining of APA was absent (F) (A x900, B x25000, C x3500, D x12000, E x5000, F x2500).

To obtain more insight in the exact sub cellular localization of APA during nephrogenesis IEM on E18 old embryos was carried out (Figure 4). In the comma stage there was only a faint APA expression (Figure 4a). In the S-stage there was strong membrane staining of both developing podocytes and parietal epithelial cells. Staining was predominantly seen on surfaces lining Bowman's space (Figure 4c). In the S-stage proximal tubular epithelial cells showed some expression of the apical/lateral membranes, arrows (Figure 4b) and strong staining of cytoplasmic vesicles close to the luminal surface of the epithelial cells (Figure 4d). In the early capillary stage membranes lining Bowman's capsule were still strongly positive, probably apical BB staining. In addition the early podocytes showed staining of apical, lateral and basal membranes and sometimes carried cytoplasmic vesicles (Figure 4e). At this later stage the epithelial cells of the proximal tubules showed merely brush border staining and no longer staining of cytoplasmic vesicles (Figure 4f). In the mature kidney IEM confirmed the membranous staining pattern of the podocytes (Figure 1g).

Enzyme histochemistry with a specific APA substrate on frozen sections of E18 old embryonic kidneys showed that APA enzyme activity could already be demonstrated in early stages (Figure 1c) and further increased in glomeruli in a more advanced developmental stage, early capillary stage (Figure 1e). In the proximal tubules APA enzyme activity could be demonstrated in the brush border (Figure 1e, arrows).

We also determined APA mRNA expression during nephrogenesis by non-radioactive RNA in situ hybridization. Glomerular APA mRNA could be demonstrated in all developmental stages. Nicely the expression is seen in cells destined to become podocytes (Figure 1b, S-stage). In addition we could demonstrate APA mRNA in developing proximal tubules (Figure 1b, inset). In the early capillary stage expression is restricted to the podocytes (Figure 1d). In the mature kidney APA mRNA expression was restricted to the perinuclear zone of podocytes, expression in other compartments could not be detected or was very low [9].

Table 1 summarizes our findings.

**Table 1:** Expression of APA during kidney development.

Developmental phase	APA IF	APA IEM	APA mRNA	APA E.A.
<i>Comma phase (E18-P1)<sup>1</sup></i>				
Tubular	±	±	±	±
Epithelial	±	±	±	±
Endothelial	-	-	-	-
<i>S-phase: (E18-P1)</i>				
Tubular (proximal); Cytoplasm	+	+	++	+
Apical (BB)	±	±		
Bas. Lateral	-	-		
Epithelial (podocyte)	++	++	+++	+++
Endothelial	-	-	-	-
<i>Pre- / Capillary phase: (E18-P1)</i>				
Tubular (proximal); Cytoplasm		-	++	
Apical (BB)	+	+		++
Bas. Lateral	-	-		
Epithelial (podocyte)	+++	+++	++	+++
Endothelial	-	-	-	-
<i>Adult phase: P3<sup>2</sup></i>				
Tubular (proximal); Cytoplasm		-	±	
Apical (BB)	++	++		+++
Bas. Lateral	-	±		
Epithelial (podocyte)	++	++	+	++++
Endothelial <sup>3</sup>	-	-	-	-

1) Embryonic day 18-postnatal week 1.

2) Postnatal week 3.

3) APA expression was observed on endothelial cells of peritubular capillaries and in the pars media of arteries.

IF, immunofluorescence; IEM, immunoelectronmicroscopy; EA, enzyme activity; BB, brush border.

Injection of the nephritogenic APA antibody combination ASD-37/41 in 1 day-old mice completely blocked enzyme activity (Figure 5a) and cause albuminuria at day 1 ( $60,000 \pm 4,000$   $\mu\text{g/ml}$ ) whereas the combination ASD-3/41 albuminuria only partly blocked enzyme activity (Figure 5b) and did not induce albuminuria ( $140 \pm 21$   $\mu\text{g/ml}$ ). APA enzyme activity was still absent at day 9 after injection of ASD-37/41 and was normalized at day 21 (Figure 5c). Partial foot process effacement was present at day 1 and persisted at day 9 and 21 (Figure 5e). These abnormalities were not accompanied by albuminuria (day 9 ASD-37/41 ( $240 \pm 47$   $\mu\text{g/ml}$ ); ASD-3/41 ( $120 \pm 20$   $\mu\text{g/ml}$ ); day 21 ASD-37/41 ( $180 \pm 25$   $\mu\text{g/ml}$ ); ASD-3/41 ( $120 \pm 20$   $\mu\text{g/ml}$ ); mice were followed for 3 months after injection of antibodies. At 3 months there were no abnormalities either by light microscopy (Figure 5d), electronmicroscopy (Figure 5f) or enzyme histochemistry.

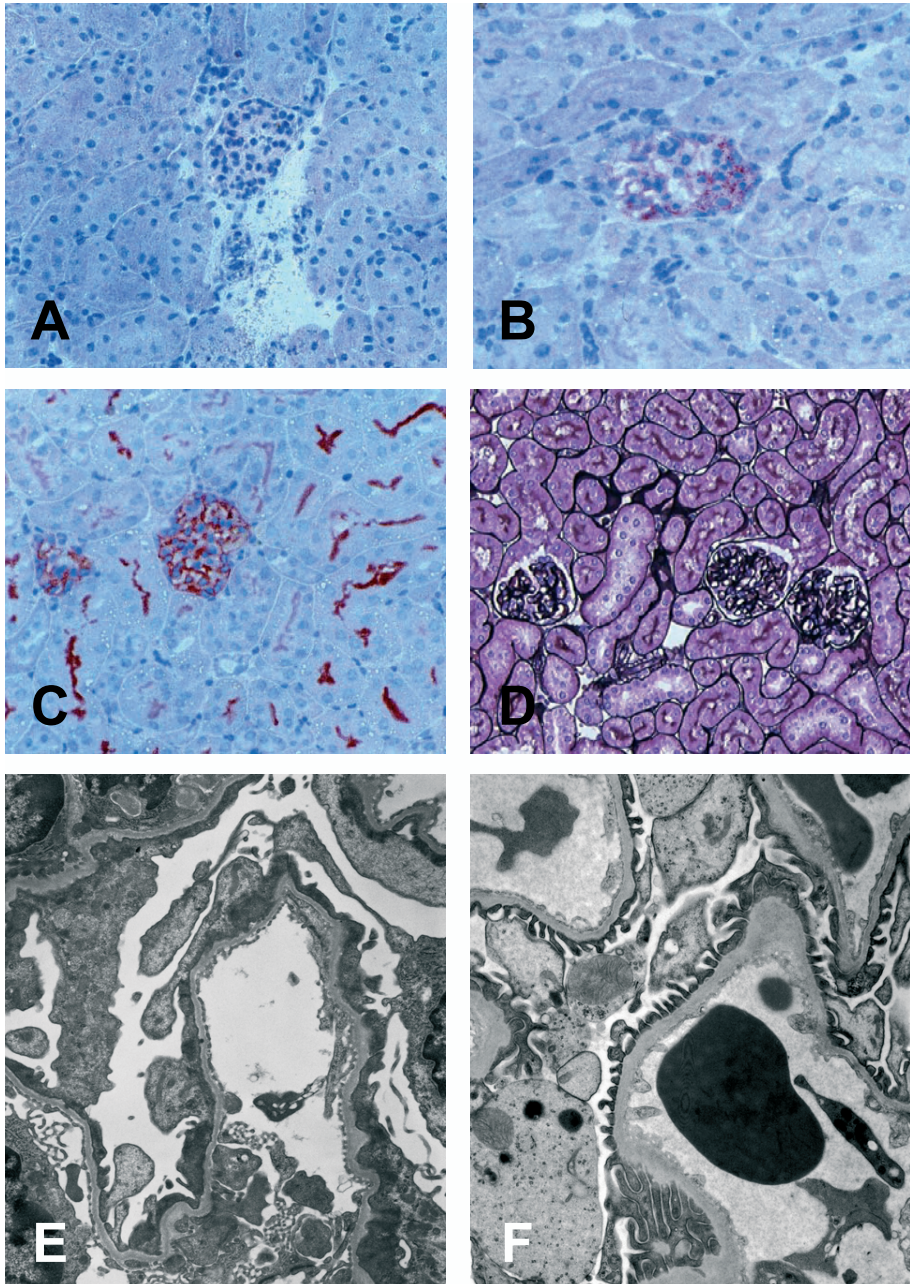


**Figure 5. Blocking APA enzyme activity:** Injection of the nephritogenic APA antibody combination ASD-37/41 in 1 day-old mice, blocked enzyme activity completely for 9 days (A). In mice treated with the combination ASD-3/41 enzyme activity was partly blocked in the glomeruli and completely in the proximal tubular brush borders (B). Total blocking of the renal APA activity did not lead to abnormal development of the kidney. In kidneys removed at days 9 and 21 after injection of the combination ASD-37/41, we observed partial podocyte foot-process effacement (E). At day 21 enzyme activity was completely returned at normal levels (C). After 3 months foot-process effacement disappeared (F) and no morphological abnormalities were observed at either the light microscopical (D) or electron microscopical level (F) (A-D x300, E-F x5000).



## DISCUSSION

From our study it is evident that APA is expressed in the kidney during nephrogenesis. APA was detectable from the earliest stage of glomerular development, the comma stage, onwards. In later stages APA expression was confined to the podocytes and the brush border membranes of the proximal tubular epithelial cells. The subcellular localisation of APA was confirmed by IEM [7]. We have confirmed the activity of APA by enzymehistochemistry. Of note, APA was not expressed in the medulla nor in the endothelium of the renal arteries or arterioles. Only in the mature glomerulus faint expression was observed in the juxtaglomerular cells (JC), the peritubular capillaries (PTC) and pars media of arteries.

We were interested in APA since this enzyme is involved in the degradation of Ang II, the most active compound of the RAS system. Ang II is a cytokine that participates in renal damage and has vasoactive and profibrotic properties and contributes to kidney injury by causing hypertension and glomerulosclerosis. Impairment of Ang II degradation may influence Ang II action and indeed animal studies have suggested a role for APA in blood pressure regulation [8,16]. Ang II components of the renin-angiotensin system (RAS) are highly expressed in the developing kidney. A role for angiotensin II in renal development has been suggested. The cellular distribution of angiotensin II type 1 (AT1) and type 2 (AT2) receptor mRNA in mouse kidneys at several embryonic stages and up to three weeks after birth by *in situ* hybridization is widespread. The expression is extra high at E18-P1 and is localised in tubular-, epithelial-, endothelial cells and in the papilla. In support of this notion, pharmacological interruption of angiotensin II type-1 (AT1) receptor signalling in animals with ongoing nephrogenesis produces specific renal abnormalities characterized by papillary atrophy, abnormal wall thickening of intrarenal arterioles, tubular atrophy associated with expansion of the interstitium, and a marked impairment in urinary concentrating ability, suggesting a role for angiotensin II in renal development. Similar changes in renal morphology and function develop also in mice with targeted inactivation of genes encoding renin, angiotensinogen, angiotensin-converting enzyme, or both AT(1) receptor isoforms simultaneously. Taken together, these results clearly indicate that an intact signalling through AT(1) receptors is a prerequisite for normal renal development [5]. So an intact RAS system is important for a normal development of the kidney. However, in our experiments blockade of APA enzyme activity for 9 days only led to temporary effacement of foot processes, with no morphological abnormalities present after 3 months. Our findings are in line with studies demonstrating normal renal development in APA-knockout mice [17] or in rats with an increased expression of the AT1a receptor on podocytes [2]. In view of the dependence of normal kidney development on Ang II, adverse effects of impaired Ang II degradation by blockade of APA might not be expected. Of note, we observed no APA expression in the areas of the kidney which are most dependent on intact Ang II for development i.e. the papilla, the collecting ducts and the intra renal arterioles. We observed APA expression in the podocytes and the brush borders of the proximal tubules.

The expression partly overlaps with the expression of the AT1 receptor. In the fetal kidney high circulating levels of AngII are present. It has been demonstrated that the expression of APA increases upon stimulation by AngII [8]. Upregulation of APA is directed by the AT1a receptor [18].

Therefore, it is possible that the expression of APA in the developing kidney follows and is dependent on the local Ang II levels. We cannot exclude that APA is becoming more important after birth when Ang II exerts negative effects. These negative effects are shown via short-term infusion of Ang II in rats which causes renal injury leading to the development of salt dependent hypertension in these rats in later life [19]. Furthermore, Ang II is involved in the development of hypertension in the spontaneously hypertensive rat, since ACE-inhibitors administered at young age prevented hypertension. The development of hypertension has been attributed to an increased expression of the AT1a receptor in the proximal tubules [20]. Thus, future studies should evaluate the effects of APA inhibition in young mice on long-term blood pressure regulation.

## **CONCLUSION**

APA is highly expressed in the developing kidney. Complete inhibition of APA enzyme activity during nephrogenesis for 9 days after birth, only led to podocyte effacement at day 9 and day 21 which disappeared after 3 months, suggesting a minimum role for APA in embryonal development.

## REFERENCES

1. Ma L, Fogo AB. Role of angiotensin II in glomerular injury. *Semin Nephrol* 21: 544-553, 2001.
2. Hoffmann S, Podlich D, Hahnel B, Kriz W, Gretz N. Angiotensin II type 1 receptor overexpression in podocytes induces glomerulosclerosis in transgenic rats. *J Am Soc Nephrol* 15: 1475-1487, 2004.
3. Wolf G, Ritz E. Combination therapy with ACE inhibitors and angiotensin II receptor blockers to halt progression of chronic renal disease: pathophysiology and indications. *Kidney Int* 67: 799-812, 2005.
4. Guron G, Friberg P. An intact renin-angiotensin system is a prerequisite for normal renal development. *J Hypertens* 18: 123-137, 2000.
5. Chen Y, Lasaitiene D, Friberg P. The renin-angiotensin system in kidney development. *Acta Physiol Scand* 181: 529-535, 2004.
6. Wolf G, Mentzel S, Assmann KJ. aminopeptidase-A: a key enzyme in the intrarenal degradation of angiotensin II. *Exp Nephrol* 5: 364-369, 1997.
7. Mentzel S, Dijkman HB, van Son JP, Koene RA, Assmann KJ. Organ distribution of aminopeptidase-A and dipeptidyl peptidase IV in normal mice. *J Histochem Cytochem* 44: 445-461, 1996.
8. Mitsui T, Nomura S, Itakura A, Mizutani S. Role of aminopeptidases in the blood pressure regulation. *Biol Pharm Bull* 27: 768-771, 2004.
9. Mentzel S, Assmann KJ, Dijkman HB, De Jong AS, van Son JP, Wetzels JF, Koene RA. Inhibition of aminopeptidase-A activity causes an acute albuminuria in mice: an angiotensin II-mediated effect? *Nephrol Dial Transplant* 11: 2163-2169, 1996.
10. Gerlofs-Nijland ME, Assmann KJ, Dijkman HB, Dieker JW, van Son JP, Mentzel S, van Kats JP, Danser AH, Smithies O, Groenen PJ, Wetzels JF. Albuminuria in mice after injection of antibodies against aminopeptidase-A: role of angiotensin II. *J Am Soc Nephrol* 12: 2711-2720, 2001.
11. Assmann KJ, van Son JP, Dijkman HB, Koene RA. A nephritogenic rat monoclonal antibody to mouse aminopeptidase-A. Induction of massive albuminuria after a single intravenous injection. *J Exp Med* 175: 623-635, 1992.
12. Lojda Z, Gossrau R. Study on aminopeptidase-A. *Histochemistry* 67: 267-290, 1980.
13. Assmann KJ, Tangelder MM, Lange WP, Tadema TM, Koene RA. Membranous glomerulonephritis in the mouse. *Kidney Int* 24: 303-312, 1983.
14. Woolf AS, Loughna S. Origin of glomerular capillaries: is the verdict in? *Exp Nephrol* 6: 17-21, 1998.
15. Piscione TD, Rosenblum ND. The malformed kidney: disruption of glomerular and tubular development. *Clin Genet* 56: 341-356, 1999.
16. Mitsui T, Nomura S, Okada M, Ohno Y, Kobayashi H, Nakashima Y, Murata Y, Takeuchi M, Kuno N, Nagasaka T, Wang J, Cooper MD, Mizutani S. Hypertension and angiotensin II hypersensitivity in aminopeptidase-A-deficient mice. *Mol Med* 9: 57-62, 2003.
17. Lin Q, Taniuchi I, Kitamura D, Wang J, Kearney JF, Watanabe T, Cooper MD. T and B cell development in BP-1/6C3/aminopeptidase-A-deficient mice. *J Immunol* 160: 4681-4687, 1998.
18. Ino K, Uehara C, Kikkawa F, Kajiyama H, Shibata K, Suzuki T, Khin EE, Ito M, Takeuchi M, Itakura A, Mizutani S. Enhancement of aminopeptidase-A expression during angiotensin II-induced choriocarcinoma cell proliferation through AT1 receptor involving protein kinase C- and mitogen-activated protein kinase-dependent signaling pathway. *J Clin Endocrinol Metab* 88: 3973-3982, 2003.
19. Lombardi D, Gordon KL, Polinsky P, Suga S, Schwartz SM, Johnson RJ. Salt-sensitive hypertension develops after short-term exposure to angiotensin II. *Hypertension* 33: 1013-1019, 1999.
20. Cheng HF, Wang JL, Vinson GP, Harris RC. Young SHR express increased type 1 angiotensin II receptors in renal proximal tubule. *Am J Physiol* 274: F10-F17, 1998.

# 3

## **PODOCYTE CHANGES AFTER INDUCTION OF ACUTE ALBUMINURIA IN MICE BY ANTI-AMINOPEPTIDASE-A MABS**

Henry B.P.M. Dijkman<sup>1</sup>, Miriam E. Gerlofs-  
Nijland<sup>1</sup>, Jeroen A.W.M van der Laak<sup>1</sup>, Jack F.M.  
Wetzels<sup>2</sup>, Patricia J.T.A. Groenen<sup>1</sup> and Karel J.M.  
Assmann<sup>1</sup>,

*Department of Pathology<sup>1</sup> and Department of  
Internal Medicine<sup>2</sup>, Division of Nephrology, University  
Medical Center Nijmegen, The Netherlands*

## ABSTRACT

Administration of a specific combination of anti-aminopeptidase-A (APA) mAbs (ASD-37/41) in mice induces an acute albuminuria, which is independent of angiotensin II, a well known substrate of APA. In the present experiments, we examined whether binding of the mAbs initiated changes in the podocytic expression of cytoskeleton (- associated), adhesion and slit diaphragm proteins in relation to the time-course of albuminuria. In addition, we measured ultrastructurally the extent of foot process retraction (the number of foot processes per  $\mu\text{m}$  GBM) and the width of the slit pore between the podocytes by morphometric methods. An injection of the mAbs combination ASD-37/41 induced a massive but transient albuminuria that started at 6 hr, and peaked at 8 hr after which it declined. However, even at day 7 after injection of the mAbs some albuminuria was present. Injection of the combination ASD-3/41 or saline did not induce an albuminuria. Notably, we observed changes in the staining of CD2AP and podocin, two slit-pore associated proteins, that coincided with the start of the albuminuria. Nephlin staining was reduced and podocytic actin staining became more granular only at a time albuminuria was declining (24 hr). The number of foot processes per  $\mu\text{m}$  GBM was already decreased at 4 hr with a further reduction thereafter. The width of the slit pore was unchanged at the time of peak albuminuria and gradually decreased thereafter. At day 7 podocytic foot process effacement was even more prominent although albuminuria was only slightly abnormal. Expression of CD2AP was still granular. We observed however a change toward normal in the expression of podocin. Injection of saline or ASD-3/41 had no effect on the expression of podocytic proteins, the number of foot processes or width of the slit pore. Our data show that the onset of albuminuria in the anti-APA model is related to alterations in CD2AP and podocin, proteins that are important for maintaining slit diaphragm structure and podocytic function. Extended studies at day 7 demonstrated uncoupling of albuminuria, podocytic foot process effacement and CD2AP staining. Changes in podocin more closely paralleled changes in albuminuria.

Keywords: podocyte, slit-diaphragm, aminopeptidase-A, albuminuria, mouse

## INTRODUCTION

In recent years we have described a mouse model of podocytic activation or injury characterized by a massive but transient acute albuminuria, and induced by a single intravenous injection of a combination of two mAbs directed against specific epitopes of mouse aminopeptidase-A (APA) [1]. Induction of the albuminuria is not dependent on systemic mediators, such as inflammatory cells, complement, or the coagulation system [1,2,7]. Recently we have demonstrated that the induction of albuminuria is not dependent on the presence of angiotensin II [2]. Thus it is unlikely that systemic factors or hemodynamic changes are involved in our anti-APA model and evidence for a local mechanism must be sought. APA has a widespread organ distribution, but in the mouse kidney it has a high expression on the cell membranes of podocytes and brush borders of proximal tubular epithelial cells [3,7]. It is therefore hypothesized that the enhanced glomerular permeability in this model is initiated by the binding of anti-APA mAbs to at least two pathogenic domains on glomerular APA resulting in an altered morphology and physiology of the podocyte and maybe the release of mediators that are involved in the albuminuria.

In the present experiments, we have examined the expression of several important podocytic proteins, in relation to the time course of the albuminuria. We have included cytoskeleton (-associated) proteins, adhesion molecules, slit-diaphragm proteins and heparan sulfate proteoglycans, all known to affect podocyte integrity, associated with podocytic injury or proteinuria in several experimental and human forms of glomerulonephritis [4]. In addition we have quantitated the degree of foot process retraction and the width of the slit pore.

## MATERIALS AND METHODS

### *Animals*

BALB/c mice, aged 6 to 10 weeks and weighing 20-25 gr, were purchased from Charles River, Sulzfeld, Germany. All procedures involving mice were approved by the Animal Care Committee of the University of Nijmegen and conformed to the Dutch Council for Animal Care and National Institutes of Health guidelines.

### *Animal experiments*

The characteristics of the three rat mAbs against different epitopes of mouse APA used in this study (ASD-3, ASD-37 and ASD-41) have been described previously [5]. The anti-APA mAbs have been propagated in vitro by hollow fiber culture (Nematology Department, Agriculture University Wageningen, The Netherlands). Injection of the combination ASD-37/41 into BALB/c mice induced a massive acute albuminuria at day 1, whereas the combination ASD-3/41 had no effect. The administration of ASD-37/41 almost completely inhibited the APA

enzyme activity *in vivo*, whereas ASD-3/41 did not alter the enzyme activity [5]. Mice received a single intravenous injection of a total dose of 4 mg of the nephritogenic combination ASD-37/41 or the non-nephritogenic combination ASD-3/41 (both with 1:1 weight ratio). Groups of mice ( $n=3$ ) were studied at defined time-points after injection of mAbs (see results). Urine was collected via bladder puncture, after which mice were killed and the kidneys processed for light microscopy, immunofluorescence and electron microscopy. The amount of albumin in the urine samples was determined by radial immunodiffusion [6].

## MORPHOLOGIC STUDIES

### *Immunofluorescence*

For immunofluorescence, kidney fragments were snap frozen in liquid nitrogen and two- $\mu\text{m}$  acetone fixed cryostat sections were stained with Alexa 488-labeled goat anti-rat Ig (Molecular Probes, Eugene, OR) for 60 min at room temperature to investigate the presence of the injected anti-APA mAb. Glomerular APA expression was analyzed using the anti-APA mAbs ASD-38 followed by incubation with FITC-labeled sheep anti-rat IgG2b (Serotec, Oxford, UK) as described before [2]. The expression of important podocytic proteins and GBM was examined at 0, 1, 2, 4, 6, 8, 16, 24, 48 hr and 7 days using unlabeled primary mAbs and FITC-labeled secondary antibodies as listed in Table 1. The sections were analysed by a confocal system, the Leica TCS NT (Leica Lasertechnik GmbH, Heidelberg, Germany).

### *Light microscopy and electron microscopy*

For light microscopy pieces of kidneys were fixed in Bouin's solution overnight at room temperature, dehydrated and embedded in paraplast (Amstelstad Amsterdam The Netherlands). Two  $\mu\text{m}$ -thick sections were stained with periodic acid Schiff and methenamine silver [7]. For electron microscopy small pieces of kidneys were fixed in 2.5% glutaraldehyde dissolved in 0.1M sodium cacodylate buffer, pH 7.4 overnight at 4° C and washed in the same buffer. The tissue fragments were postfixed in cacodylate-buffered 1%  $\text{OsO}_4$  for 2 hr, dehydrated, and embedded in Epon 812 (Merck, Darmstadt, Germany). Ultrathin sections were cut on an ultratome (Leica, Reichert Ultracuts, Wien, Austria), and contrasted with 4% uranyl acetate for 45 min and subsequently with lead citrate for 4 min at room temperature. Sections were examined in a Jeol 1200 EX2 electron microscope (JEOL, Tokyo, Japan).

### *Measurements of foot processes, slit pores and GBM*

Negatives of electron micrographs (magnification  $\times 6000$ ) were scanned at 600 dpi resolution using a flatbed scanner (Epson Perfection 1200 Photo, Epson Europe, Amsterdam), resulting in a specimen-level pixel size of approximately  $7 \times 7 \text{ nm}^2$ . Measurement of resulting images was performed using Leica QWin Pro V2.4 (Leica Imaging Systems Ltd, Cambridge, UK) under

Microsoft Windows NT 4.0. The system was calibrated using the marker bar on the electron micrographs. For five open random capillary loops in each of five randomly selected glomeruli per specimen, the GBM was indicated interactively using a graphic tablet. The image analysis software was used to measure the length of the GBM for each loop. Also, for each loop the number of podocytic foot processes was manually counted and expressed as the number of foot processes per  $\mu\text{m}$  GBM length; resulting in 25 measurement points for each specimen. Using QWin, the width of 100 individual slitpores was measured interactively for each specimen in the same set of digitized electron micrographs.

### *Statistical analysis*

Group comparisons were performed using Anova with Tukey post-hoc testing. For the number of podocytes per  $\mu\text{m}$  GBM, glomeruli were taken as a random factor to study the effect of heterogeneity within individual mice. P-values less than 0.05 were considered significant. All statistics were performed using SPSS statistical software (SPSS 9.0 for Windows, SPSS Inc., Chicago, IL)

## **RESULTS**

### *Albuminuria*

In mice injected with 4 mg of the nephritogenic combination ASD-37/41 albuminuria was first noted at 6 hr, and peaked at 8 hr at values of  $58,667 \pm 3,771 \mu\text{g/ml}$ . As shown in Figure 1, the albumin excretion decreased thereafter reaching a value of  $8,056 \pm 6,764 \mu\text{g/ml}$  at day 1,  $1,739 \pm 1,061 \mu\text{g/ml}$  at day 2, and  $2,249 \pm 1,447 \mu\text{g/ml}$  at day 7. Mice injected with the non-nephritogenic combination ASD-3/41 did not develop significant albuminuria ( $102 \pm 24 \mu\text{g/ml}$  at 8 hr).

### *Expression of podocytic and GBM components*

By immunofluorescence we investigated at 0,1,2,4,6,8,16,24,48 hr and 7 days the binding of the injected mAbs in the glomeruli and the presence of APA. In addition we examined at these timepoints the expression of several podocytic and GBM proteins that may be involved in the induction of albuminuria in this model. The proteins investigated are listed in Table 1.

After injection of ASD-37/41 we observed initial binding of the mAbs to capillary loops in a homogeneous pattern that changed into a fine granular pattern at 6 hr, and a more granular pattern at 24 hours. We also noted a similar change in the glomerular APA expression from a homogeneous staining pattern into a fine granular one (Figure 2). As described before, we observed binding of antibodies to the brush borders of the proximal epithelial cells as early as 2 hr after injection [8].

Interestingly we also observed changes in the expression pattern of the slit diaphragm



**Table 1.** Antibodies used for the detection of injected antibodies and glomerular antigens<sup>1</sup>

<b>Antigen<sup>2</sup></b>	<b>Primary antibody<sup>2</sup></b>	<b>Dil.</b>	<b>Suppl<sup>3</sup></b>	<b>Ref.</b>	<b>Secondary antibody</b>	<b>Dil.</b>	<b>Suppl<sup>3</sup></b>
<b>Antibodies injected</b>							
Rat anti-mouse							
APA mAbs							
(ASD3, 37, and 41)	Rabbit anti-rat Ig-FITC	100	Dako				
<b>Podocyte components</b>							
<i>Cell membrane</i>							
APA	Rat anti-mouse APA mAbs (ASD-38)	1		[ 7 ]	Sheep anti-rat IgG2b -FITC	100	Serotec
<i>Nuclear</i>							
WT1	Rabbit anti-nuclear protein	50	Santa Cruz		Swine anti-rabbit Ig-FITC	40	Dako
<i>Cytoskeleton</i>							
Synaptopodin	Mouse anti-synaptopodin	1	Progen		Sheep anti-mouse Ig-FITC	100	Cappel
Ezrin	Rabbit anti-ezrin	200		[ 34 ]	Swine anti-rabbit Ig-FITC	40	Dako
Talin	Mouse anti-talin	50	Sigma		Sheep anti-mouse Ig-FITC	100	Cappel
Vinculin	Mouse anti-vinculin	200	Sigma		Sheep anti-mouse Ig-FITC	100	Cappel
Paxillin	Mouse anti-paxillin	50	Transduction		Sheep anti-mouse Ig-FITC	100	Cappel
Actin	Phalloidin-FITC	20	Sigma				
Tubulin	Mouse anti-tubulin	200	Sigma		Sheep anti-mouse Ig-FITC	100	Cappel
<i>Slitpore</i>							
Nephrin	Rabbit anti-nephrin	50		[ 18 ]	Swine anti-rabbit Ig-FITC	40	Dako
ZO-1	Rabbit anti-ZO-1	200	Chemicon		Rabbit anti-rat Ig-FITC	100	Dako
P-Cadherin	Rat anti P-cadherin	10	Zymed		Rabbit anti-rat Ig-FITC	100	Dako
Podocin	Rabbit anti-podocin	40		[ 24 ]	Swine anti-rabbit Ig-FITC	40	Dako
CD2AP	Rabbit anti-CD2AP	200	Santa Cruz		Swine anti-rabbit Ig-FITC	40	Dako
<b>Adhesion molecules</b>							
$\alpha 3$ Integrin	Mouse anti- $\alpha 3$ integrin	1		[ 32 ]	Sheep anti-mouse Ig-FITC	100	Cappel
$\alpha$ Dystroglycan	Mouse anti- $\alpha$ dystroglycan	1	(Upstate)		Sheep anti-mouse Ig-FITC	100	Cappel
<b>GBM</b>							
Agrin	Hamster anti-agrin (MI-91)	800		[ 33 ]	Rabbit anti hamster Ig-FITC	200	Cappel
Heparan sulfate	Mouse anti-heparan sulfate(JM403)	200		[ 15 ]	Goat anti-mouse IgM-FITC	50	Nordic

1) Abbreviations: APA = aminopeptidase-A, mAbs = monoclonal antibodies, WT-1 = Wilf's tumor suppressor gene WT-1 product, CD2AP = CD2-associated protein, Dil. = dilution

2) Code between brackets

3) Serotec, Oxford, UK; Instruchemie, Hilversum, The Netherlands; Dako, Glostrup, Denmark; Progen, Heidelberg, Germany; Cappel, Organon Teknica, The Netherlands; Santa Cruz Biotechnology, Santa Cruz, California, Nordic, Tilburg, The Netherlands; Chemicon, Temecula, Canada; Transduction laboratories, Lexington, UK; Upstate Biotechnology Corp, Lake placid, USA; Zymed, San Francisco, USA.

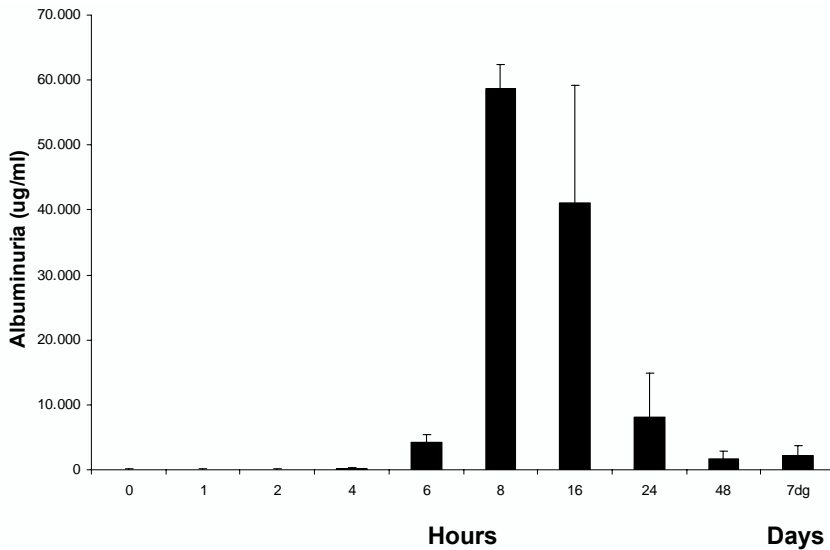


**Figure 1.** Albuminuria at different time points after injection of 4 mg of a combination of two mAbs against aminopeptidase-A (ASD-37/41; weight ratio 1:1) into BALB/c mice (mean  $\pm$  SD).

components podocin, CD2AP, and nephrin as well as the cytoskeleton protein actin. The normal homogeneous staining along the capillary loops of podocin became more granular at 6 hr with evidence of a recovery at day 7 (Figure 3). At the same time CD2AP expression changed from a normal fine granular into a granular pattern at 6 hr that persisted unchanged until day 7 (Figure 3). At the early time point no changes in the expression of nephrin were noted. The staining for nephrin at 24 hr was slightly less than in previous hours (Figure 2). Glomerular actin aggregated into a more granular pattern at 24 hr when albumin excretion was already declining (Figure 2). The expression of the other components listed in Table 1 did not change during the first 24 hr after injection of the mAb.

ASD-3/41 mAbs bound homogeneously to the periphery of the glomerular loops and this binding pattern remained the same during the first 24 hr. Also the expression of APA and all the components listed in Table 1 did not change upon injection of ASD-3/41 mAb.

### *Light and electron microscopy*

By light microscopy we did not see any changes in glomerular or tubular morphology in the BALB/c mice injected either with ASD-37/41 or ASD-3/41 during the time of the experiment. By electron microscopy we observed segmental fusion of podocytic foot processes during the experiment which was quantitated (see below).

### *Morphometric Measurements*

In mice that received the non-nephritogenic combination ASD-3/41 or saline, morphometry

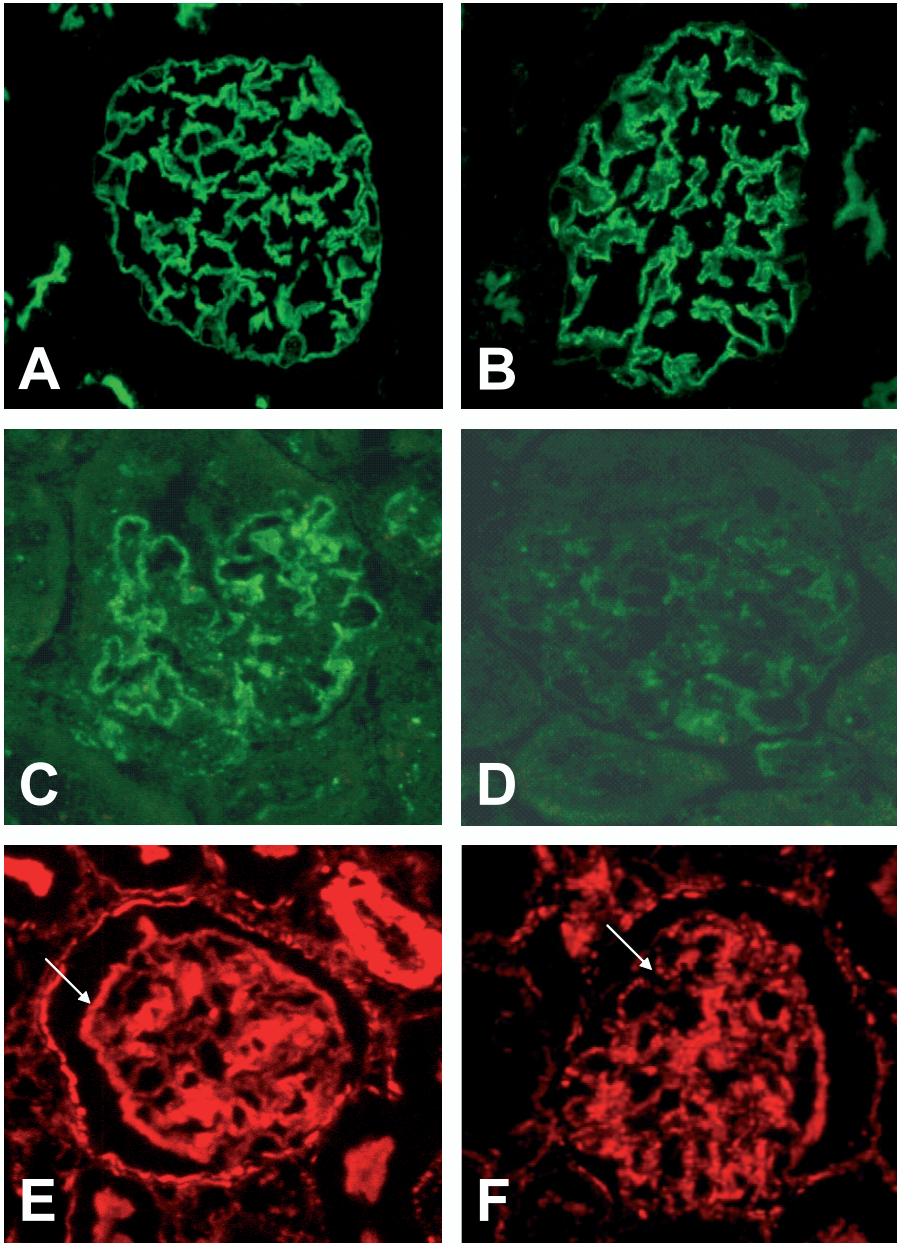


**Figure 2. The immunohistologic presence of glomerular APA after injection of the mAbs into BALB/c mice.** Panel A shows the normal homogeneous presence of APA at the periphery of the capillary tuft (corresponding to a podocytic pattern). After injection of the antibodies the expression pattern of APA changed from 6 hr onward into a fine granular one that persisted until day 7 (B; x700). The immunologic localization of the slit diaphragm associated protein nephrin and glomerular actin at 2 and 24 hr after injection of anti-APA mAb. The mild nephrin staining (C) at the periphery of the glomerular tuft was less intense at 24 hr (D). Glomerular actin as shown by TRITC-labeled phalloidin is present in mesangial cells and podocytes. The homogeneous staining for actin at 2 hr in podocytes (E, arrow) became more granular 16-24 hr after administration of the anti-APA mAbs (F, arrow) and persisted until day 7 (A-F x500).

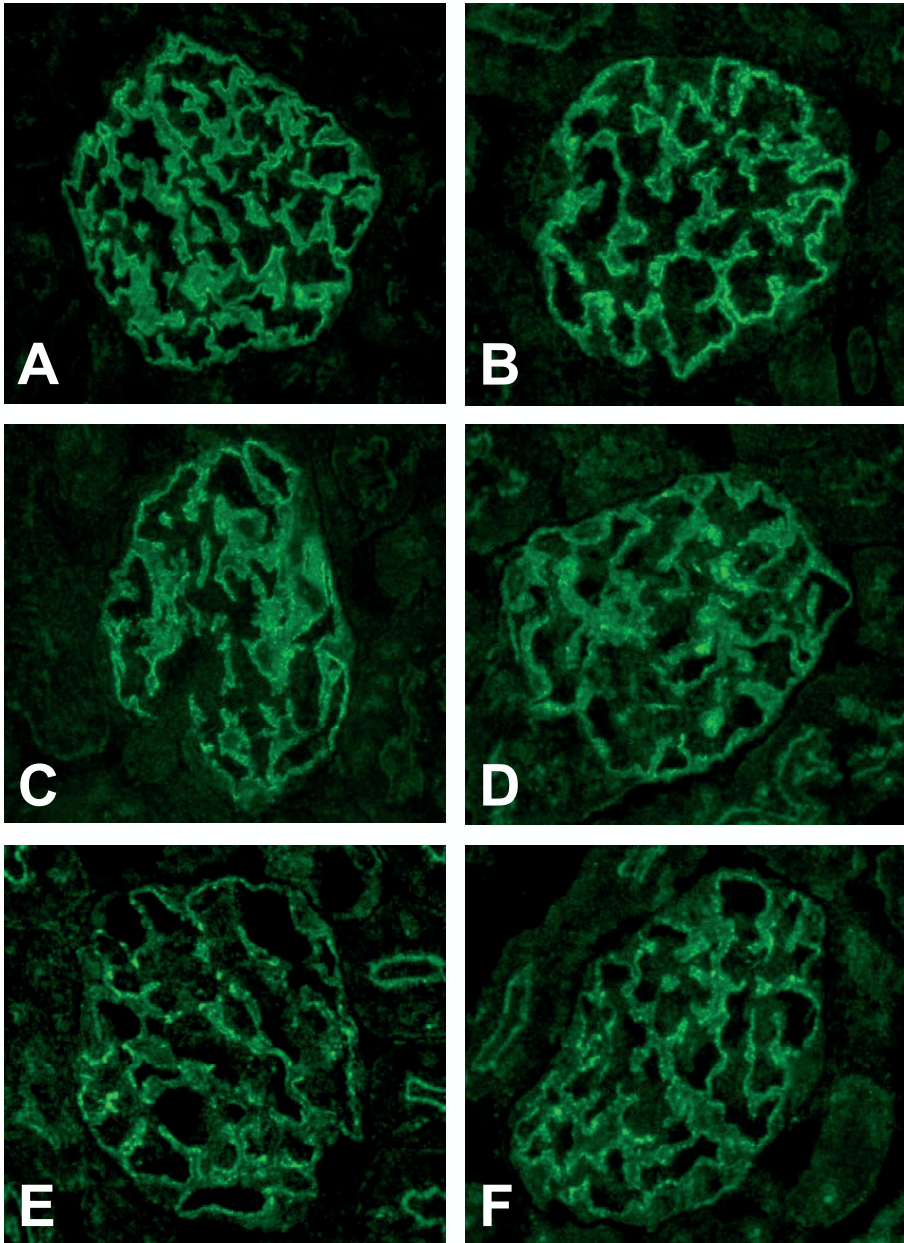


**Figure 3.** The immunologic localization of the slit diaphragm associated proteins podocin and CD2AP at 2 hr, 6 hr and 7 days after injection of anti-APA mAb. The prominent homogeneous staining for podocin along the capillary wall at 2 hr (A) became more granular and less intense from 6 hr onward (B). At day 7 the expression of podocin changed toward normal (C; x500). The immunologic localization of the slit diaphragm associated protein CD2AP changed from normal faint fine granular staining along the capillary wall at 2 hr (D) into a more granular and more intense staining at 6 hr (E), that persisted until day 7 (A-F x500).

was done on tissue samples obtained at 24 hr, and in mice that received the nephritogenic combination ASD-37/41 studies were done at 4, 8, 24 hr and 7 days. The slit pore width was unchanged at 4 hr and 8 hr after administration of ASD-37/41 (Table 2). We observed a decrease of the slit pore width only at 24 hr. In contrast, a reduction in the number of foot-processes occurred early and was already apparent at 4 hr after administration of ASD-37/41, at a time point that albuminuria was not detectable (Table 2). Foot process effacement progressed from 4 hr onward. As evident from the data in Table 2 foot process effacement was even more prominent at day 7.

**Table 2:** Slit pore width and number of foot processes as measured on electron microscopical sections.

	saline	ASD-3/41	ASD-37/41
<b>Slit pore width (nm)</b>			
4 hr			41 ± 11
8 hr			37 ± 10
24 hr	39 ± 7	40 ± 8	28 ± 5 <sup>a</sup>
<b>Foot process (n / μm GBM)</b>			
4 hr			1.4 ± 0.5 <sup>a</sup>
8 hr			1.2 ± 0.4 <sup>a</sup>
24 hr	1.7 ± 0.3	1.9 ± 0.4	0.9 ± 0.3 <sup>a1</sup>
Day 7			0.5 ± 0.3 <sup>a2</sup>

BALB/c-mice were injected with saline, the non-nephritogenic combination of two anti-APA mAbs (ASD-3/41), or the nephritogenic combination ASD-37/41 (see Methods section). At the indicated time points small pieces of renal cortex were processed for electron microscopy. Mean ± SD

<sup>a)</sup> p<0.001 vs saline and ASD3/41

<sup>1)</sup> p<0.001 vs ASD-37/41 at 4 hr

<sup>2)</sup> p<0.05 vs ASD-37/41 at 24 hr and p<0.001 vs others

## DISCUSSION

Injection of the combination of the anti-APA mAbs ASD-37 and ASD-41, which act synergistically on two nephritogenic epitopes of APA, induced an early massive albuminuria which started at 6 hr, reached its maximum at 8 hr and declined thereafter. In previous studies we have excluded complement, coagulation factors, inflammatory cells, and angiotensin II as mediators of proteinuria [1,2]. Therefore, in the present study we have evaluated the potential role of podocytic alterations in the development of albuminuria. Our anti-APA model in mice has some resemblance to an antibody mediated model in rats, in which a single injection of antibodies against podoplanin, a 43-kD protein on the podocytic cell membrane, leads to a transient proteinuria and effacement of foot processes that is independent of complement and inflammatory cells [9].

The GBM was for long considered the main size and charge selective filter. Recent studies have provided evidence that the podocyte and especially the slit diaphragms are important in maintaining the glomerular filtration barrier [4,10,11]. The slit diaphragm may function

as the size-selective barrier, while the negative charges of the GBM are responsible for the charge-selective barrier [12,13,14].

Theoretically proteinuria may be the result of loss of GBM negative charge, detachment of the podocyte from the GBM, cytoskeleton rearrangements of the podocyte that influence podocyte and slit diaphragm geometry, or functional abnormalities of the slit diaphragm complex or the GBM secondary to podocytic injury. Our study provided no arguments for one of the first three possibilities. The expression of JM403, an antibody against heparan sulfate used to characterize GBM negative charge [15,16], remained normal, thus suggesting that the acute albuminuria is not related to a defect or reduction of GBM negative charge. We also did not observe reduced expression of  $\alpha 3$ -integrin or dystroglycan, arguing against changes in podocyte-GBM adhesion. Of note, detachment was never observed by electron microscopy. An important role for primary cytoskeletal rearrangements is also unlikely. We only noted aggregation of podocytic actin at 24 hr, at a time point albuminuria was declining. Therefore, these changes are probably a consequence of podocytic foot process effacement or related to preceding changes in podocin and CD2AP.

Our data point to the slit diaphragm complex as the culprit of the increased permeability in our model. We observed changes in the expression pattern of CD2AP and podocin as early as 6 hr after administration of the antibodies, the earliest time point that albuminuria was noted. At this time point foot process density had decreased.

CD2AP and podocin are proteins that are involved in maintenance of the slit diaphragm. The important role of the slit diaphragm constituents in the functioning of the glomerular filtration barrier has been demonstrated by the proven relation between abnormalities of the slit diaphragm and podocytic specific proteins and the development of proteinuric renal diseases [4]. Nephrin was the first protein to be discovered as an essential component of the slit diaphragm. Nephrin, a protein product of the gene *NPHS1*, is a 1241 amino acid long plasma membrane protein that is exclusively expressed in the podocytes [17,18]. Mutations in nephrin are the cause of congenital nephrotic syndrome of the Finnish type [19]. Nephrin knock-out mice do not develop foot processes and are proteinuric [20]. Intravenous injection of the mAbs 5-1-6, which was recently discovered specific for rat nephrin, induces an acute, transient proteinuria in rats with effacement of foot processes and displacement of nephrin and slit diaphragm along the capillary loops [21,22]. Nephrin may function as a structural component of the slit diaphragm, although recent studies also have disclosed signalling properties [23]. Podocin, a product of the *NPHS2* gene, is a member of the stomatin family of proteins and forms hairloop structures with both the C and N terminal of the protein situated in the cytoplasm of the podocytes [24]. Mutations in podocin are associated with familial autosomal recessive forms of focal glomerulosclerosis in humans [25]. CD2AP (CD2-associated protein) was originally discovered in lymphocytes as an SH3 domain containing adaptor protein of the CD2 receptor. CD2AP is also present in podocytes, and CD2AP knock-out mice showed identical clinical and morphological features as nephrin knock-out mice [26]. Recent

studies have provided evidence that nephrin, CD2AP and podocin are closely linked; podocin interacts with nephrin and CD2AP [27,28], a cytoplasmic binding partner of nephrin. Nephrin and CD2AP are being linked to the actin cytoskeleton [29] and podocin augmenting the signalling properties of nephrin [23]. Normal functioning of each component is necessary for maintaining normal glomerular permeability.

Our data suggest that binding of the anti-APA mAbs cause alterations in the CD2AP-podocin-nephrin complex with resulting changes in the permeability. We did not observe early changes in the expression of nephrin. This might be explained by the relatively low specificity of our anti-nephrin antibody. Alternatively, we must conclude that the changes in podocin and CD2AP are most important. In this respect the recent studies in the Lmx1b knockout mouse seem relevant [30,31]. Lmx1b knock-out mice show phenotypic abnormalities in the glomeruli, with immature podocytes, a reduced number of foot processes and absent slit-diaphragms. In these mice mRNA and protein levels of podocin are greatly reduced. Also, changes in CD2AP expression were noted in one study [30]. Of note, expression of nephrin was normal in these knock-out mice [30,31].

We have extended our studies in order to find more convincing evidence for the relationship between albuminuria and alterations of the slit-pore complex. At day 7 albuminuria had decreased more than 20 fold, although values were still abnormal. The expression of CD2AP was unaltered, whereas the expression of podocin had slightly changed toward normal. These observations indicate an uncoupling between albuminuria and the expression of CD2AP and podocin, and question the role of alterations in these slit-pore proteins in the pathogenesis of albuminuria. The initial changes in expression of CD2AP and podocin may be an epiphenomenon, possibly related to alterations in foot process morphology i.e. foot process effacement. However, our morphometric analyses point to clear discrepancies between podocin and CD2AP staining and foot process morphology. Despite the enormous reduction in albuminuria foot process effacement was more prominent at day 7. If the observed alterations in podocin and CD2AP were merely epiphenomena, one would have expected an even more granular expression pattern. In contrast, the expression of CD2AP remained unchanged and the expression of podocin changed toward normal. How can we reconcile the above mentioned findings? We suggest the following sequence of events: binding of anti APA mAbs to podocytic APA results in injury or activation of the podocyte, with ensuing changes in slit-pore structure. As a consequence albuminuria occurs. Antibody binding is present for 7 days and more. The slit-pore structure remains altered, which explains ongoing albuminuria. However, progressive effacement of the podocytic foot process leads to a reduction in the number of slit-pores and thus attenuates albuminuria.

## CONCLUSION

We have found that albuminuria in the anti-APA model started 6 hr after injection of the nephritogenic combination of mAb, ASD-37/41. Albuminuria reached its peak at 8 hr, and decreased rapidly thereafter. Foot process effacement occurred before the onset of albuminuria and increased until day 7. We also noted early changes in the staining pattern of two slit diaphragm associated components, i.e. podocin and CD2AP. The data suggest that injection of anti-APA mAbs results in albuminuria by causing podocytic alterations at the level of the slit-pore.

## ACKNOWLEDGEMENT

We thank dr. Paul Mangeate and the Department of Cell Biology, dr. C. Antignac from the Hospital Necker-Enfants-Malades INSERM U423, Paris, France, dr. H. Holthöfer from the Haartman Institute, Department of Bacteriology and Immunology, University of Helsinki, and University of Helsinki Central Hospital, Helsinki, Finland, prof. dr. J.H. Berden from the Department of Internal Medicine, Division of Nephrology, and dr. L.P. v.d. Heuvel, Department of Pediatrics, University Medical Center Nijmegen, Nijmegen, and dr. A. Sonnenberg from the Netherlands Cancer Institute, Amsterdam for providing the anti-ezrin antibody, the anti-podocin antibody, the anti-nephrin antibody, JM403 mAb, anti-agrin mAb, and anti- $\alpha$ 3 integrin mAbs respectively.



## REFERENCES

1. Mentzel S, van Son JP, Dijkman HB, Wetzels JF, Assmann KJ: Induction of albuminuria in mice: synergistic effect of two monoclonal antibodies directed to different domains of aminopeptidase-A. *Kidney Int* 55:1335-1347, 1999.
2. Gerlofs-Nijland ME, Assmann KJ, Dijkman HB, Dieker JW, van Son JP, Mentzel S, van Kats JP, Danser AH, Smithies O, Groenen PJ, Wetzels JF: Albuminuria in mice after injection of antibodies against aminopeptidase-A: role of angiotensin II. *J Am Soc Nephrol* 12:2711-2720, 2001.
3. Mentzel S, Dijkman HB, van Son JP, Koene RA, Assmann KJ: Organ distribution of aminopeptidase-A and dipeptidyl peptidase IV in normal mice. *J Histochem Cytochem* 44:445-461, 1996.
4. Kerjaschki D: Caught flat-footed: podocyte damage and the molecular bases of focal glomerulosclerosis. *J Clin Invest* 108:1583-1587, 2001.
5. Mentzel S, Assmann KJ, Dijkman HB, De Jong AS, van Son JP, Wetzels JF, Koene RA: Inhibition of aminopeptidase-A activity causes an acute albuminuria in mice: an angiotensin II-mediated effect? *Nephrol Dial Transplant* 11:2163-2169, 1996.
6. Mancini G, Carbonara AO, Heremans JF: Immunochemical quantitation of antigens by single radial immunodiffusion. *Immunochemistry* 2:235-254, 1965.
7. Assmann KJ, van Son JP, Dijkman HB, Koene RA: A nephritogenic rat monoclonal antibody to mouse aminopeptidase-A. Induction of massive albuminuria after a single intravenous injection. *J Exp Med* 175:623-635, 1992.
8. Mentzel S, Dijkman HB, van Son JP, Wetzels JF, Assmann KJ: In vivo antibody-mediated modulation of aminopeptidase-A in mouse proximal tubular epithelial cells. *J Histochem Cytochem* 47:871-880, 1999.
9. Matsui K, Breiteneder-Geleff S, Kerjaschki D: Epitope-specific antibodies to the 43-kD glomerular membrane protein podoplanin cause proteinuria and rapid flattening of podocytes. *J Am Soc Nephrol* 9:2013-2026, 1998.
10. Somlo S, Mundel P: Getting a foothold in nephrotic syndrome. *Nat Genet* 24:333-335, 2000.
11. Endlich K, Kriz W, Witzgall R: Update in podocyte biology. *Curr Opin Nephrol Hypertens* 10:331-340, 2001.
12. Farquhar MG: Editorial: The primary glomerular filtration barrier--basement membrane or epithelial slits? *Kidney Int* 8:197-211, 1975.
13. van den Born J, van Kraats AA, Bakker MA, Assmann KJ, Dijkman HB, van der Laak JA, Berden JH: Reduction of heparan sulphate-associated anionic sites in the glomerular basement membrane of rats with streptozotocin-induced diabetic nephropathy. *Diabetologia* 38:1169-1175, 1995.
14. Tryggvason K, Wartiovaara J: Molecular basis of glomerular permselectivity. *Curr Opin Nephrol Hypertens* 10:543-549, 2001.
15. van den Born J, van den Heuvel LP, Bakker MA, Veerkamp JH, Assmann KJ, Berden JH: A monoclonal antibody against GBM heparan sulfate induces an acute selective proteinuria in rats. *Kidney Int* 41:115-123, 1992.
16. Raats CJ, van den BJ, Berden JH: Glomerular heparan sulfate alterations: mechanisms and relevance for proteinuria. *Kidney Int* 57:385-400, 2000.
17. Ruotsalainen V, Ljungberg P, Wartiovaara J, Lenkkeri U, Kestila M, Jalanko H, Holmberg C, Tryggvason K: Nephrin is specifically located at the slit diaphragm of glomerular podocytes. *Proc Natl Acad Sci U.S.A* 96:7962-7967, 1999.
18. Holthofer H, Ahola H, Solin ML, Wang S, Palmén T, Luimula P, Miettinen A, Kerjaschki D: Nephryn localizes at the podocyte filtration slit area and is characteristically spliced in the human kidney. *Am J Pathol* 155:1681-1687, 1999.
19. Lenkkeri U, Mannikko M, McCready P, Lamerdin J, Gribouval O, Niaudet PM, Antignac CK, Kashtan CE, Homberg C, Olsen A, Kestila M, Tryggvason K: Structure of the gene for congenital nephrotic syndrome of the Finnish type (NPHS1) and characterization of mutations. *Am J Hum Genet* 64:51-61, 1999.
20. Rantanen M, Palmén T, Patari A, Ahola H, Lehtonen S, Astrom E, Floss T, Vauti F, Wurst W, Ruiz P, Kerjaschki D, Holthofer H: Nephryn TRAP Mice Lack Slit Diaphragms and Show Fibrotic Glomeruli and Cystic Tubular Lesions. *J Am Soc Nephrol* 13:1586-1594, 2002.
21. Orikasa M, Matsui K, Oite T, Shimizu F: Massive proteinuria induced in rats by a single intravenous injection of a monoclonal antibody. *J Immunol* 141:807-814, 1988.
22. Topham PS, Kawachi H, Haydar SA, Chugh S, Addona TA, Charron KB, Holzman LB, Shia M, Shimizu F, Salant DJ: Nephritogenic mAbs 5-1-

- 6 is directed at the extracellular domain of rat nephrin. *J Clin Invest* 104:1559-1566, 1999.
23. Huber TB, Kottgen M, Schilling B, Walz G, Benzing T: Interaction with podocin facilitates nephrin signaling. *J Biol Chem* 276:41543-41546, 2001.
  24. Roselli S, Gribouval O, Boute N, Sich M, Benessy F, Attie T, Gubler MC, Antignac C: Podocin localizes in the kidney to the slit diaphragm area. *Am J Pathol* 160:131-139, 2002.
  25. Boute N, Gribouval O, Roselli S, Benessy F, Lee H, Fuchshuber A, Dahan K, Gubler MC, Niaudet P, Antignac C: NPHS2, encoding the glomerular protein podocin, is mutated in autosomal recessive steroid-resistant nephrotic syndrome. *Nat Genet* 24:349-354, 2000.
  26. Shih NY, Li J, Karpitskii V, Nguyen A, Dustin ML, Kanagawa O, Miner JH, Shaw AS: Congenital nephrotic syndrome in mice lacking CD2-associated protein. *Science* 286:312-315, 1999.
  27. Schwarz K, Simons M, Reiser J, Saleem MA, Faul C, Kriz W, Shaw AS, Holzman LB, Mundel P: Podocin, a raft-associated component of the glomerular slit diaphragm, interacts with CD2AP and nephrin. *J Clin Invest* 108:1621-1629, 2001.
  28. Shih NY, Li J, Cotran R, Mundel P, Miner JH, Shaw AS: CD2AP localizes to the slit diaphragm and binds to nephrin via a novel C-terminal domain. *Am J Pathol* 159:2303-2308, 2001.
  29. Yuan H, Takeuchi E, Salant DJ: Podocyte slit-diaphragm protein nephrin is linked to the actin cytoskeleton. *Am J Physiol Renal Physiol* 282:F585-F591, 2002.
  30. Miner JH, Morello R, Andrews KL, Li C, Antignac C, Shaw AS, Lee B: Transcriptional induction of slit diaphragm genes by Lmx1b is required in podocyte differentiation. *J Clin Invest* 109:1065-1072, 2002.
  31. Rohr C, Prestel J, Heidet L, Hosser H, Kriz W, Johnson RL, Antignac C, Witzgall R: The LIM-homeodomain transcription factor Lmx1b plays a crucial role in podocytes. *J Clin Invest* 109:1073-1082, 2002.
  32. de Melker AA, Sterk LM, Delwel GO, Fles DL, Daams H, Weening JJ, Sonnenberg A: The A and B variants of the alpha 3 integrin subunit: tissue distribution and functional characterization. *Lab Invest* 76:547-563, 1997.
  33. Groffen AJ, Ruegg MA, Dijkman H, van de Velden TJ, Buskens CA, van den BJ, Assmann KJ, Monnens LA, Veerkamp JH, van den Heuvel LP: Agrin is a major heparan sulfate proteoglycan in the human glomerular basement membrane. *J Histochem Cytochem* 46:19-27, 1998.
  34. Mangeat P, Gusdinari T, Sahuquet A, Hanzel DK, Forte JG, Magous R.: Acid secretion and membrane reorganization in single gastric parietal cell in primary culture. *Biol Cell* 69(3):223-31, 1990.



# 4

## **AUTOMATED MAGNIFICATION CALIBRATION IN TRANSMISSION ELECTRON MICROSCOPY USING FOURIER ANALYSIS OF REPLICA IMAGES**

Jeroen A.W.M. van der Laak, Henry B.P.M.  
Dijkman, Martin M.M. Pahlplatz

*Department of Pathology, Radboud University  
Nijmegen Medical Centre, Nijmegen, The Netherlands.*

## ABSTRACT

The magnification factor in transmission electron microscopy is not very precise, hampering for instance quantitative analysis of specimens. Calibration of the magnification is usually performed interactively using replica specimens, containing line or grating patterns with known spacing. In the present study, a procedure is described for automated magnification calibration using digital images of a line replica. This procedure is based on analysis of the power spectrum of Fourier transformed replica images, and is compared to interactive measurement in the same images. Images were used with magnification ranging from 1,000x to 200,000x. The automated procedure deviated on average 0.10% from interactive measurements. Especially for catalase replicas, the coefficient of variation of automated measurement was considerably smaller (average 0.28%) compared to that of interactive measurement (average 3.5%). In conclusion, calibration of the magnification in digital images from transmission electron microscopy may be performed automatically, using the procedure presented here, with high precision and accuracy.

Keywords: Transmission electron microscopy, calibration, digital image analysis, pattern recognition, geometry.

## INTRODUCTION

Transmission electron microscopy (TEM) is widely used for the ultrastructural study of cells and tissues. At present, traditional photography of EM images is increasingly replaced by digital techniques, capturing a digital image directly from the microscope. Digital image acquisition also facilitates stereological techniques, which enable reliable measurement of microscopic features such as length, area and diameter of particles. To perform stereology in an accurate and reproducible way, geometrical calibration of the imaging device is critical. Unfortunately, TEM magnification is not very precise. Even when adjustments have been made using standardized procedures [1], magnification aberration may be as high as 5% with modern TEMs, increasing with equipment age [2,3]. The calibration options found on modern TEMs are aimed at calibration of the viewing console, of which the magnification may deviate from digitally acquired images. Internal (inside the specimen of interest) or external (using a separate calibration specimen) reference standards are required to calibrate the magnification of digitally acquired images with each recording session. For this purpose, replica specimens may be used, which show a line or grating pattern with a known number of lines per unit area. For moderate magnifications up to 25,000x (25K), an external shadow-cast carbon replica may be used, typically containing 2160 lines/mm (line spacing 463 nm). Higher magnifications may be calibrated with an internal line replica, e.g. a replica based on catalase crystals (line spacing 8.75 nm) [1,2]. Alternatively, the MAG\*<sup>1</sup>\*CAL™ calibration specimen may be used [4]. This specimen consists of an ion milled cross section of a silicon single crystal consisting of a series of atomically flat layers of Si and SiGe, resulting in different layer spacings which may be used to calibrate the entire TEM magnification range (1,000x to 1,000,000x). Next to these replica specimens, colloidal particles [5] and for higher magnifications spherical virus diameters may be used as internal calibration standards [3].

Using the line or grating pattern of a replica for magnification calibration in digitally acquired images is usually performed manually, by interactively indicating the distance between a manually counted number of lines. If the average distance between replica lines in pixels is known, the specimen level pixel size (in nm) can easily be calculated using the replica specifications. Interactive calibration is laborious and may lack precision. The aim of the present study was development of an automated procedure for calibration of digital TEM images, using a line replica image. The automated method was evaluated against interactive calibration using the same replica images.

## MATERIALS AND METHODS

### *Electron microscopy*

All images were produced using a JEM-1200EX II (Jeol Europe B.V., The Netherlands). The TEM was aligned and adjusted (column alignment, depolarization of magnification forming lenses, tilt axis alignment [6]) according to manufacturer's instructions. Image acquisition was performed using digital imaging plate technology for TEM via the Dibus Micron Vario (Ditabis, Pforzheim, Germany). This system uses reusable image plates which are exposed in the TEM identical to classical photo negatives. Plates were read out digitally in a separate system (read out pixel size  $17.5 \times 17.5 \mu\text{m}^2$ ). Resulting images (size  $4910 \times 4340$  pixels) were stored as uncompressed tiff files. In this study, a carbon replica of 2160 lines/mm (line replica; EMS, Hatfield, UK) and a catalase replica (inter line distance 8.75 nm; EMS, Hatfield, UK) were used.

### *Digital image analysis*

Image analysis was performed using custom written macros for KS400 software (Carl Zeiss GMBH, Germany). Calculation of the average distance between replica lines was based on the fact that the repetition of replica lines is represented by local maxima in the power spectrum of the Fourier transformed replica image (Fourier image). Figure 1A shows an example of a digitally acquired replica image at magnification 1200x. A subimage of this image (white frame in Figure 1A) was Fourier transformed (power spectrum of the result is shown in Figure 1B). The local maxima in the Fourier image correspond to the base frequency of the replica lines and multiples of this frequency (higher order moments; Figure 1B). Because the input image is real valued (as opposed to complex valued), the Fourier transformed image is fully symmetric. To simplify the analysis, the left half of the Fourier image is cleared.

Segmentation of local maxima in the power spectrum of the Fourier transformed image was performed using a dynamic segmentation: the Fourier image was filtered using a low pass filter (mean filter, size  $45 \times 45$  pixels) and the result was subtracted from the Fourier image. Pixels with difference  $>25$  were considered to be part of a local maximum and were labeled "object" pixels. If the distance  $d$  between replica lines (in pixels) is small (e.g. when a low magnification is used, relative to the replica line spacing), the local maxima in the Fourier image are relatively far apart. In these cases, segmentation of a single local maximum in the Fourier image sometimes resulted in multiple small objects, located very close together. In these cases, a binary closing was performed on the resulting binary image (structuring element 8-connected neighborhood). The number of iterations for the binary closing (1 or 2) depended on the combination of magnification and replica line spacing. Object pixels resulting after the binary closing were grouped together to form (8 connected) binary objects. The binary object at the Fourier image origin (centre of the image) was removed. In cases with local maxima very close to each other, this resulted in removal of the first one or two maxima as well.

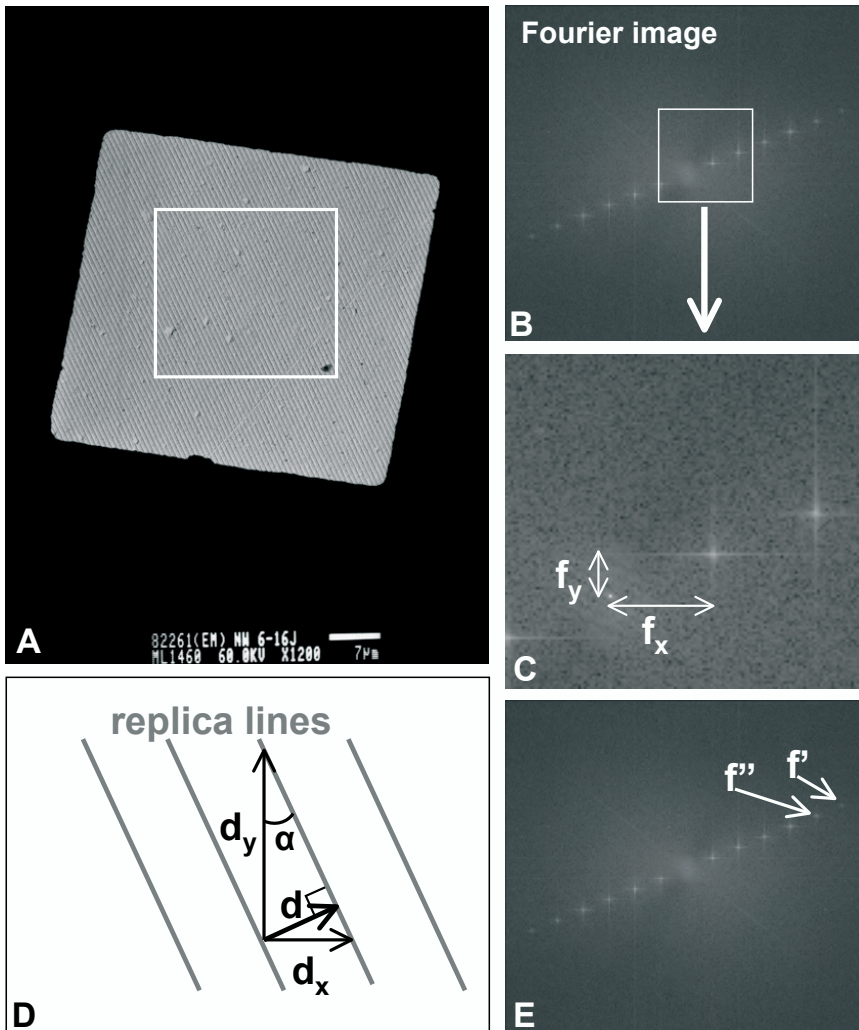


**Figure 1.** Example of a TEM image of a carbon line replica (A) at 1200x magnification. The sub image indicated by a white frame was Fourier transformed, of which the power spectrum was calculated (B). The location of the local maxima in the Fourier power spectrum (C) may be used to calculate the distance between replica lines in the original replica image (D). To increase precision, the two most distant maxima were used in the present study (E).

The local maximum in the Fourier image closest to the origin corresponds to the base frequency of replica lines in the original image (Figure 1C). The distance between Fourier origin and first local maximum ( $f_x$ ,  $f_y$ ) is the reciprocal of the distance between replica lines ( $d_x$ ,  $d_y$ ) in the original image (Figures 1C, D). From the measured ( $f_x$ ,  $f_y$ ) the distance  $d$  between replica lines can be calculated [7] (Appendix A). To decrease the error caused by the imprecision of locating the local Fourier maxima, and because in some cases the first local maximum has erroneously been erased together with the centre of origin, the two detected local maxima



most distant from the origin were used instead of the first local maximum (Appendix B). The centre of mass was determined for each detected binary object. Polar coordinates were calculated describing the distance of the object centre of mass to the Fourier image origin and the angle with the positive x-axis. In some cases, local maxima were present in the Fourier image which were not a representation of the replica pattern. To distinguish between these maxima and the maxima representing the replica line pattern, a histogram was calculated of the angles of all objects to the positive x-axis (bin size 0.025 radians). All higher order moments of the maxima representing the replica pattern are located on a line through the Fourier image origin. Therefore, the histogram bin with the highest number of maxima (histogram mode) was considered to contain the maxima representing the replica line pattern. Of all local maxima within this histogram bin, the two maxima with the largest distance to the image origin were selected (Figure 1E). The distance between replica lines was calculated using the equations in Appendix A and B. The KS400 macro developed in this study is available on request, please contact the corresponding author.

### *Interactive calibration*

Interactive calibration was performed using standard KS400 functions. The digitally acquired replica image was shown on a computer screen and the user interactively indicated one replica line near the edge of the image by drawing a straight line segment along the (left or right) side of the replica line in the image overlay. Next, a second replica line, as far distant from the first as possible, was interactively defined by clicking on the side (identical side as for the first replica line) of this line with the computer cursor. The system automatically calculated the shortest distance between the indicated line and point (Appendix C). The user manually counted the number of lines in between the two indicated lines. From these, the average distance between replica lines in pixels was calculated.

### *Experiments*

Digital TEM images of the carbon line replica (inter line spacing 463 nm) were acquired at 1K, 2K, 3K, 4K, 6K, 7.5K, 10K, 12K, 15K, 20K and 25K magnification. Digital TEM images of the catalase replica (inter line spacing 8.75 nm) were acquired at 50K, 100K, 150K and 200K magnification. Digital images were produced with 4910x4340 pixels resolution. Inter line spacing was manually measured in all carbon line replica images by two observers (JAWMvdL / HBPMd), using the procedure described above. Measurements were made in the centre of the images, with a software zoom factor (on the computer screen) which was determined by the observer for each individual case. To study intraobserver variability, one observer also performed the interactive measurement in 5 manually selected sub-images of different parts of all (carbon and catalase) replica images.

The automated procedure was used to measure the inter line spacing in all replica images. To ensure that the entire analyzed images were filled with the replica line pattern, and to

speed up the Fourier transform, subimages were taken from the originally acquired images. Subimage size was chosen such that enough replica lines were present in the image for accurate analysis: 1024x1024 pixels for the image acquired at 1K magnification, 2048x2048 pixels for magnifications 2K to 15K and 50K, and 4096x4096 pixels for magnifications 25K and 100K to 200K. The number of iterations for the binary closing was related to the distance between local maxima in the Fourier image. Two iterations were used for magnifications 10K and 50K to 200K, 1 iteration for magnification 15K and no binary closing at all for magnifications 20K and 25K. To study the variability of the automated procedure, the same analysis was performed 5 times for sub-images taken from different parts of each replica image.

### Statistics

For statistics and production of graphs, SPSS for Windows was used (version 11.0.1; SPSS Inc, Chicago, IL). The interobserver effect for manual measurements was studied using a one-sample t-test for the relative difference between observers. The difference between manual and automated measurements was evaluated using Wilcoxon signed ranks test. Strength of the relationship between variables was tested using Spearman rank correlations. P-values below 0.05 were considered to be statistically significant.

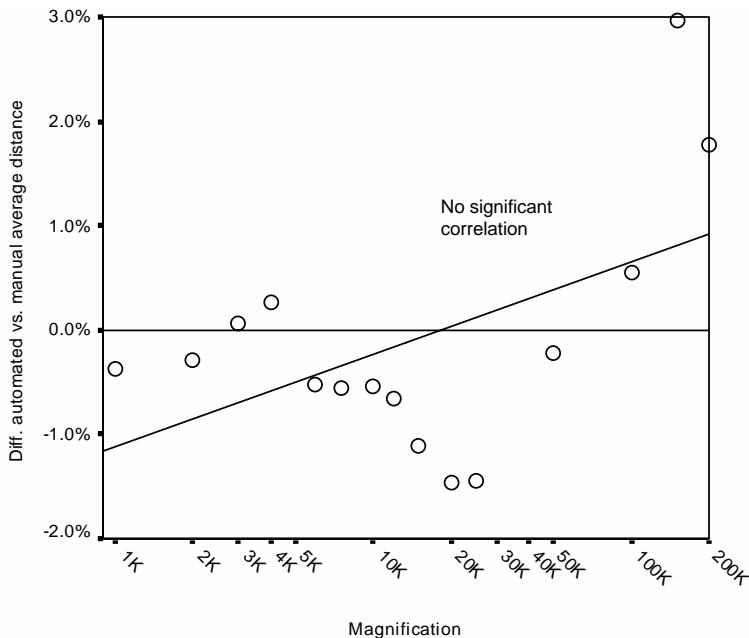


**Figure 2.** The relative difference between automated and manual measurement of the inter line distance in replica images of different magnifications. Magnifications are shown on a logarithmic axis.

## RESULTS

The interobserver effect for manual measurement of the replica inter line distance was found to be small (mean 0.20%, range 0.028% – 0.47%) but significant ( $p < 0.005$ ). Results from the automated procedure were on average 0.10% (range -1.46 to 2.97%) below manual measurements (Figure 2). This difference was not statistically significant. The largest differences between manual and automated measurement were seen for the two highest magnifications. No significant correlation was found between magnification and difference between automated and manual measurement.

For each magnification the expected inter line distance in pixels can be calculated from the imaging and replica parameters. Figure 3 shows measured distances as compared to this calculated distance. Intraobserver variability and the variability in the automated procedure were small for the carbon replica (Figure 3A), with average coefficient of variation (CV) 0.45% (maximum 0.7%) for manual and 0.56% (maximum 1.0%) for automated measurements. The largest deviation from the calculated inter line distance was seen for 1K magnification, which TEM setting is known to be less precise. For the catalase replica (Figure 3B) the intraobserver CV was on average 3.5% (maximum 5.3%), for the automated measurements the average CV was 0.28% (maximum 0.43%). For this replica, manual assessment of the inter line spacing is hampered by low image contrast and the presence of noise (Figure 4). No significant correlation was found between CV and magnification.

## DISCUSSION

Digital image acquisition has become the standard in transmission electron microscopy. It is well known that the magnification factor given by the microscope is in general not very precise. If precision of the magnification in digitally acquired TEM images is of importance, e.g. when performing measurements, image calibration is required. Traditionally, interactive manual calibration is performed to determine the specimen level pixel size, using replica images with known inter line spacing. In the present study, a fully automated procedure is described for use with replica images to perform magnification calibration in digital TEM images. This procedure, which is based on analysis of the power spectrum of the Fourier transform, was found to give results comparable to those obtained by manual calibration. When using a catalase replica, the automated procedure was superior to manual calibration in terms of measurement precision. The catalase replica images show considerably less contrast and more noise than the carbon replica images, making manual calibration less reliable.

In general, accuracy is considered to be of higher importance than precision in stereology [8]. Measurement lacking precision may be improved by increasing the number of samples, whereas poor accuracy leads to biased data. However, imprecise calibration of an entire set

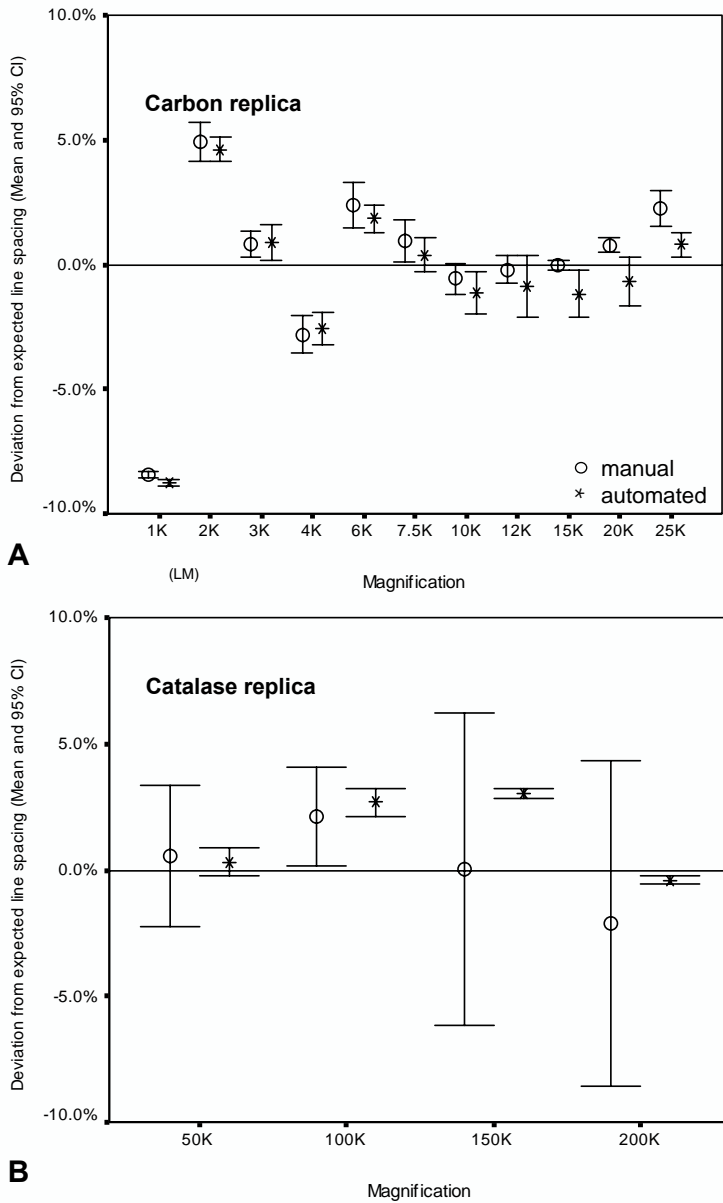


**Figure 3.** The relative deviation (average and 95% confidence interval) from the expected replica inter line distance in pixels, for manual and automated measurement. (A) shows results for the carbon replica, (B) for the catalase replica.

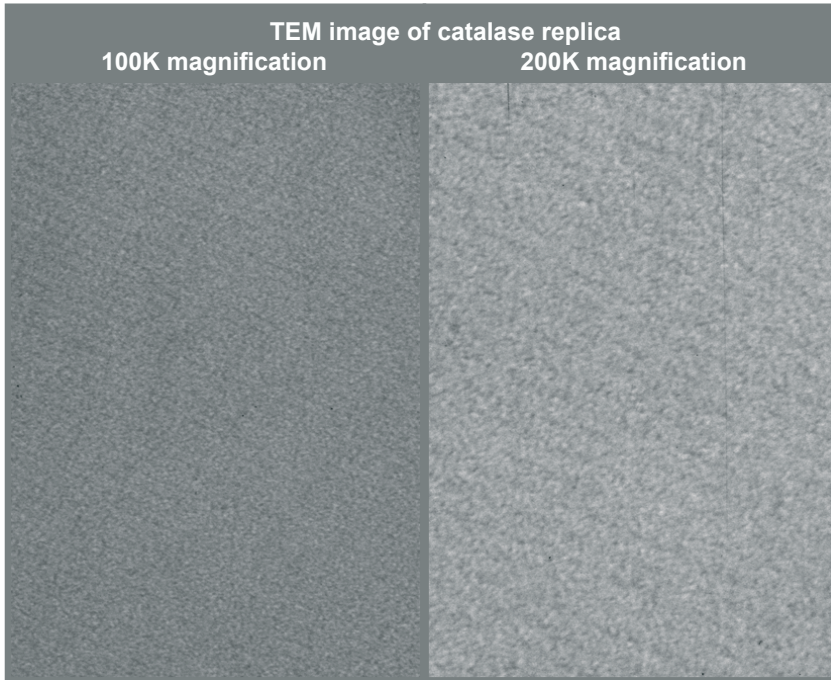


**Figure 4.** TEM image of the catalase replica at 100K and 200K magnification. Clearly, the line patterns in these images suffer from low contrast and noise, resulting in imprecise manual magnification calibration. The automated calibration procedure was capable of measuring the inter line spacing with high precision.

of images (e.g. comprising a patient data set) may lead to biased measurement results on patient level. Therefore, precision and accuracy are equally important for magnification calibration.

The automated procedure is widely applicable, as it is insensitive to local image artifacts, and to image contrast and brightness to a large extent. Also, the procedure is insensitive to mechanical rotation of the replica image, as rotation of an image causes rotation of the corresponding Fourier transform over the same angle, resulting in the same distances between local maxima. In this study a commonly used carbon line replica with 2160 lines/mm was used, as well as a catalase replica with inter line spacing of 8.75 nm. The procedure, however, will work with any replica containing a fixed number of repeating lines with constant spacing. For example, the general purpose MAG\**I*\*CAL™ specimen [4] can be used with the automated procedure, enabling magnification calibration over a large range of magnifications. Also, this procedure may be applied to a grating replica, for which minor adaptations will be required to handle the different pattern of local maxima in the Fourier image. Use of jpeg compression should be avoided, as this compression causes multiple false maxima in the power spectrum of the Fourier transform.

The size of the subwindow and the number of iterations for the binary closing step have to be selected to match the images used. Subimages should be selected which are filled as much as possible with the replica line pattern. Optimal parameters for taking subimages and binary closings have to be determined for each setup, as these depend on the used replica, magnification and also on the parameters of the digital imaging procedure.

## CONCLUSION

This paper describes a procedure for accurate automated calibration of TEM magnification in digital replica images. Next to be less labor intensive, the procedure is also more reproducible than manual calibration using a replica specimen.

### Appendix A

The distance  $d$  between replica lines (Figure 1D) can be expressed as:

$$d = \sin \alpha \cdot d_y$$

with:

$$\sin \alpha = \frac{d_x}{\sqrt{d_x^2 + d_y^2}}$$

with  $d_x, d_y$  the distance between replica lines in  $x$  respectively  $y$  direction (Figure 1D). Therefore:

$$d = \frac{d_x \cdot d_y}{\sqrt{d_x^2 + d_y^2}}$$

The location  $(f_x, f_y)$  of the first local maximum in the Fourier image (Figure 1C, see also Materials and Methods) equals:  $f_x = \frac{x_s}{d_x}$  and  $f_y = \frac{y_s}{d_y}$  with  $(x_s, y_s)$  the size of the Fourier image in pixels. Therefore:

$$d = \frac{x_s \cdot y_s / f_x \cdot f_y}{\sqrt{x_s^2 / f_x^2 + y_s^2 / f_y^2}} = \frac{x_s \cdot y_s}{\sqrt{x_s^2 \cdot f_y^2 + y_s^2 \cdot f_x^2}}$$

In case of a rectangular Fourier image ( $y_s = x_s$ ) [7]:

$$d = \frac{x_s}{\sqrt{f_x^2 + f_y^2}}$$

## Appendix B

Instead of using the first local maximum in the Fourier image, higher order moments may be used, decreasing the imprecision caused by determination of the location of local maxima. Higher order moments are found at multiples of  $(f_x, f_y)$ . In the present study, all local maxima with similar orientation (in relation to the Fourier image origin) were detected (see Materials and Methods). The two local maxima most distant from the origin were used for calculation of  $(f_x, f_y)$ . The most distant local maximum detected by the automated segmentation will be called  $(f'_x, f'_y)$  and the second most distant local maximum  $(f''_x, f''_y)$  (Figure 1E). The most precise estimation of  $(f_x, f_y)$  is:

$$f_x, f_y = \frac{f'_x}{n}, \frac{f'_y}{n}$$

with  $n$  the number of maxima detected.

Because the segmentation procedure is not always capable of discriminating between the Fourier origin and the first few local maxima,  $n$  can not reliably be determined directly. Instead, the number of maxima detected can be calculated by:

$$n = \frac{\sqrt{f'^2_x + f'^2_y}}{\sqrt{(f'_x - f''_x)^2 + (f'_y - f''_y)^2}}$$

The value of  $n$  has to be rounded to the nearest integer.

## Appendix C

The smallest distance  $d$  between a line through points  $(x_0, y_0)$  and  $(x_1, y_1)$  and a point  $(x_p, y_p)$  can be expressed as:

$$d = \sqrt{(x_p - X)^2 + (y_p - Y)^2}$$

with:

$$X = \frac{x_p \cdot A^2 + x_1 \cdot B^2 + (y_p - y_1) \cdot A \cdot B}{A^2 + B^2}$$

$$Y = \begin{cases} \frac{B}{A} \cdot (X - x_1) + y_1 & \text{if } A \neq 0 \\ y_p & \text{if } A = 0 \end{cases}$$

$$A = (x_1 - x_0); B = (y_1 - y_0)$$

## REFERENCES

1. R. Luftig, An accurate measurement of the catalase crystal period and its use as an internal marker for electron microscopy, *J. Ultrastruct. Res.* 20:91, 1967.
2. N.G. Wrigley, The lattice spacing of crystalline catalase as an internal standard of length in electron microscopy, *J. Ultrastruct. Res.* 24:454, 1968.
3. J.P. McCaffrey, J.M. Baribeau, A transmission electron microscope, TEM calibration standard sample for all magnification, camera constant, and image/diffraction pattern rotation calibrations, *Microsc. Res. Tech.* 32:449, 1995.
4. N.H. Olson, T.S. Baker, Magnification calibration and the determination of spherical virus diameters using cryo-microscopy, *Ultramicroscopy* 30:281, 1989.
5. J.A. Derosé, J. Revel, A comparative study of colloidal particles as imaging standards for microscopy, *J. Microsc.* 195:64, 1999.
6. I.M. Watt, The analytical electron microscope, *J. Phys. E.: Sci. Instrum.* 19:668, 1986.
7. R.O. Duda, P.E. Hart, Pattern classification and scene analysis, John Wiley & Sons, New York, Chapter 8, 1973.
8. C.V. Howard, M.G. Reed, Unbiased stereology, Springer-Verlag, New York, Chapter 1, 1998.





# 5

## THE PARIETAL EPITHELIAL CELL IS CRUCIALLY INVOLVED IN HUMAN IDIOPATHIC FOCAL SEGMENTAL GLOMERULOSCLEROSIS<sup>1</sup>

Henry B.P.M. Dijkman\*, Bart Smeets\*, Jeroen  
A.W.M. van der Laak, Eric J. Steenbergen and  
Jack F.M. Wetzels<sup>2</sup>

*Dept. of Pathology, Nephrology<sup>2</sup>, Radboud University  
Nijmegen medical centre, Nijmegen, the Netherlands*

*\* Both authors contributed equally to this work.*

<sup>1</sup> *See editorial by Schwartz, Kidney International  
2005;68: p. 1894*

## ABSTRACT

Focal segmental glomerulosclerosis (FSGS) is one of the most common patterns of glomerular injury encountered in human renal biopsies. Epithelial hyperplasia, which can be prominent in FSGS has been attributed to dedifferentiation and proliferation of podocytes. Based on observations in a mouse model of FSGS, we pointed to the role of parietal epithelial cells (PECs). In the present study we investigated the relative role of PECs and podocytes in human idiopathic FSGS.

We performed a detailed study of lesions from a patient with recurrent idiopathic FSGS by serial sectioning, marker analysis and 3D reconstruction of glomeruli. We have studied the expression of markers for podocytes, PECs, mesangial cells, endothelium and myofibroblasts. We also looked at proliferation and composition of the deposited extracellular matrix.

We found that proliferating epithelial cells in FSGS lesions are negative for podocyte and macrophage markers, but stain for PEC markers. The composition of the matrix deposited by these cells is identical to Bowman's capsule.

Conclusion; Our study demonstrates that PECs are crucially involved in the pathogenesis of FSGS lesions.

Keywords: parietal epithelial cell, podocyte, epithelial cell proliferation and glomerulosclerosis.

## INTRODUCTION

Focal segmental glomerulosclerosis (FSGS) has become one of the most common glomerular diseases [1]. FSGS is characterized by focal and segmental occurrence of lesions with mesangial sclerosis, obliteration of glomerular capillaries with hyalinosis and intracapillary foam cells, formation of adhesions between the glomerular tuft and Bowman's capsule, and podocyte hypertrophy [2]. FSGS is not a disease entity, but rather a pattern of injury with quite diverse clinical behaviour, morphology, and possibly also pathogenesis [3]. Recently, various morphological variants have been defined and a classification has been proposed to better address the diversity of FSGS [4]. Five light microscopic variants of FSGS were defined: the perihilar variant (lesions predominantly located at the vascular pole), the tip variant (the presence of lesions located at the urinary pole), the cellular variant (characterized by endocapillary hypercellularity), the collapsing variant (collapse of the glomerular tuft associated with epithelial cell hypertrophy and hyperplasia), and finally FSGS not otherwise specified (NOS) if lesions do not fit into one of the above mentioned categories. All morphological variants are accompanied by some degree of epithelial proliferation, being minimal or absent in the perihilar variant and sometimes very prominent in the cellular and collapsing variant.

The pathogenesis of FSGS has been the subject of recent studies. Many investigators have focussed on the visceral epithelial cell, the so-called podocyte. Normal podocytes are considered terminally differentiated, post-mitotic cells, which are unable to proliferate and to compensate for damaged neighbouring podocytes. Studies by Kriz et al [5;6] in various rat models of FSGS indicated loss of podocytes and adherence of the parietal epithelial cell (PEC) to the naked GBM as the critical event in the formation of FSGS lesions. Studies on the pathogenesis of the more cellular FSGS lesions have focused on the collapsing variant of FSGS [7]. From these studies the concept of the dedifferentiated and dysregulated podocyte emerged [8-12]. Dysregulated podocytes are characterized by loss of podocyte markers, and are no longer growth restricted and have regained the ability to proliferate. Based on these findings epithelial hyperplasia, which is also commonly observed in 'active' FSGS lesions other than collapsing lesions, is generally considered to be the result of proliferation of dedifferentiated podocytes. Recently, we have reported on FSGS in Thy-1.1 transgenic mice (a model of collapsing FSGS) and have provided evidence that proliferating epithelial cells in lesions are of PEC origin and that these cells deposit the extracellular matrix that eventually forms the scars [13].

We now investigated the role of PECs in human idiopathic FSGS by detailed analysis of FSGS lesions in a nephrectomy specimen of a patient with recurrence of idiopathic FSGS in his renal allograft.

## METHODS

### *Patient and methods*

Our patient developed a steroid-resistant nephrotic syndrome in 1994, at the age of 8 years. In 1995 bilateral nephrectomy was performed because of untreatable nephrotic syndrome and deteriorating renal function. He was treated by peritoneal dialysis. In October 1996 patient received a renal transplant. The postoperative course was characterized by an early recurrence of proteinuria, which persisted despite plasma filtration. Approximately 6 months after transplantation the allograft was removed and peritoneal dialysis was resumed. In August 2002 a second transplant was performed, with a 3-mismatched kidney from a cadaveric donor. In view of the previous experience pre-emptive plasma filtration was performed. The initial immunosuppressive regimen consisted of the anti-CD25 antibody daclizumab, mycophenolate mofetil, prednisone and cyclosporine. The kidney functioned immediately, and serum creatinine decreased to values of 1.4 mg/dl. The patient was treated with plasma filtration three times weekly, and only mild proteinuria was noted (0,2 – 1,0 g/day). In October 2002, while reducing the number of plasmapheresis sessions and lowering the immunosuppressive dose, proteinuria gradually increased reaching values between 3-4 g/day in November 2002. Switching from cyclosporine to tacrolimus was ineffective. A renal biopsy was performed in December. Light microscopically we found 13 glomeruli. One glomerulus showed advanced sclerosis, the others had a normal aspect. Ultrastructural analysis showed particular podocyte effacement and microvillous transformation, compatible with a recurrence FSGS.

In view of the reported efficacy in a French study, the patient was treated with added cyclophosphamide for 8 weeks and more intensive plasmapheresis [14]. There was no major effect, although after ending this treatment a definite increase of proteinuria was observed. Over the next months, proteinuria remained severe, patient was frankly nephrotic and finally developed moderate renal insufficiency, which did not respond to replacement of tacrolimus by rapamycin. After lengthy discussions, and in view of the clinical and psychological condition of the patient, it was decided to perform a nephrectomy, and resume renal replacement therapy with haemodialysis. Nephrectomy was performed October 2003, one year after transplantation.

### *Preparation of the kidney specimen for Light microscopy, Immunohistochemistry and Electron Microscopy*

The nephrectomized kidney measured 13 x 7 x 6 cm and weighed 290 grams. The outer aspect of the kidney was normal, the vessels contained no thrombi nor were there any macroscopical abnormalities when dissecting the kidney. Some pyramid-shaped segments were dissected and separately fixed in bouin, buffered formalin and snap frozen in liquid nitrogen. For electron microscopy we divided the cortex in five equal parts.

### *Light microscopy*

For light microscopy, kidney fragments were fixed in Bouin's solution and formaldehyde, dehydrated, and embedded in paraplast (Amstelstad, Amsterdam The Netherlands). 2 µm sections were stained with periodic acid-Schiff, and with silver methenamine [15].

### *Immunohistochemistry*

Immunohistochemical staining was performed on kidney sections fixed in 4% buffered formaldehyde for 24 hr and embedded in paraffin. 4 µm sections were incubated with monoclonal antibodies (mAb) and polyclonal antibodies (pAb) directed at various markers for podocytes, PECs, macrophages and myofibroblasts as detailed in table 1. As secondary antibody we used powervision Poly-HRP-anti Mouse/Rabbit/Rat IgG (Immunologic, Klinipath, Duiven, The Netherlands). Detection was carried out with the use of peroxidase as label and diaminobenzidine as substrate. For the doublestaining, first the polyclonal antibody (pAb) was detected and completed. As detecting antibody we used Envision AF-anti Rabbit IgG (Immunologic, Klinipath, Duiven, The Netherlands), detection was carried out with the use of alkaline phosphatase as label and FastBlue as substrate. Thereafter samples were incubated with the second antibody, as detecting antibody we used powervision Poly-HRP-anti Mouse/Rabbit/Rat IgG (Immunologic, Klinipath, Duiven, The Netherlands). Detection was carried out with the use of peroxidase as label and AEC/red as substrate.

### *Immunofluorescence microscopy*

Kidney fragments were snap-frozen in liquid nitrogen, and 2 µm acetone fixed cryostat sections were used. Kidney sections were incubated with antibodies directed against synaptopodin, collagen IV chains, and heparan sulfate species (Table 1). Detection of the anti-collagen antibodies was done using goat anti-mouse Alexa™ 488 antibodies (Molecular probes Inc, Leiden, The Netherlands). We have performed double staining for synaptopodin (a marker of differentiated podocytes) and heparan sulfate species with exclusive presence in either Bowman's capsule or the GBM. Synaptopodin was detected using an anti-synaptopodin mAbs (Progen Biotechnik, Heidelberg, Germany), followed by a FITC labelled sheep anti-mouse IgG1 (Nordic Immunologicals, Tilburg, The Netherlands). The single chain antibodies used for staining of heparan sulfate species [16;17] were detected via a rabbit antibody directed against the VSV-g epitope tag (ICL, Oregon, USA) and finally detected with a goat anti-rabbit Alexa™ 568 antibodies (Molecular probes Inc, Leiden, The Netherlands). The sections were examined with a confocal laser scanning microscope (CLSM) (Leica lasertechnik GmbH, Heidelberg, Germany).

**Table 1:** Antibodies used for the detection of glomerular antigens

Antigen	Primary antibody	Dil.	Supplier / Reference
<b>Podocyte components</b>			
Synaptopodin	Mouse anti-synaptopodin	1	Progen, Heidelberg, Germany
CD 10	Mouse anti human CD10	50	Monosan, Caltag lab., Burlingame
Vimentin	Mouse anti human Vimentin	800	Biogenex, Ramon, CA
VEGF	ISH m-RNA Probe (*ng/ml)	100*	[18]
<b>PEC components</b>			
PAX-2	Rabbit anti human PAX-2	50	Zymed laboratories Inc. San Francisco, USA
Cytokeratin	Mouse anti human CAM 5.2 (CK8)	50	BD Biosciences, San Diego, CA
Pan cadherine	Mouse anti human Pan cadherin	500	Sigma, St. Louis, USA
<b>Proliferation</b>			
KI 67	Mouse anti human MIB-1	200	Dako, Glostrup, Denmark
<b>Miscellaneous</b>			
Macrophage	Mouse anti human CD68	2000	Dako, Glostrup, Denmark
$\alpha$ smooth muscle actin	Mouse anti human SMA	15000	Sigma, St. Louis, USA
<b>Bouwman's Capsule</b>			
Collagen IV $\alpha$ 1	Mouse anti- $\alpha$ 1 collagen	10	Wieslab, Lund, Sweden
Heparan sulfate Single chain	Single chain antibody HS4E4	1	[16]
<b>GBM</b>			
Collagen IV $\alpha$ 3	Mouse anti- $\alpha$ 3 collagen	10	Wieslab, Lund, Sweden
Heparan sulfate Single chain	Single chain antibody HS4C3	1	[17]

### *In situ hybridisation*

Kidney sections were fixed in 4% buffered formaldehyde for 24 hr and embedded in paraffin. 4  $\mu$ m sections were incubated and subjected to VEGF in situ hybridization (ISH) using a digoxigenin-labeled VEGF-A antisense RNA probe [18]. The corresponding sense probe was used as a control. This ISH was followed by Immunohistochemical staining with the monoclonal antibody (mAb) CK8. As secondary antibody we used powervision Poly-HRP-anti Mouse/Rabbit/Rat IgG (Immunologic, Klinipath, Duiven, The Netherlands). Detection was carried out with the use of AF as label and AEC as substrate.

### *Three-dimensional reconstruction of infiltrating PECs*

The nephrectomy specimen gave us the opportunity to cut serial sections of a relatively large area segment (containing more than 250 glomeruli). At least 400 serial sections were cut and incubated for CK8 as described under Immunohistochemistry of the Patient and Methods section. In a selected set of sections covering 300 microns we digitized 40-50 serial images of each glomerulus. These section images visualized by DAB staining were directly digitized from a light microscope into the KS400 Universal Image Processing and Analysis software via a CCD color camera; binary images of the structures were created and the binary images were exported into 3D reconstruction software '3D doctor' (Able software cooperation, Lexington, USA) to reconstruct and to view still and rotating 3D images on a computer monitor, enabling us to produce a 3D model of the glomerulus. 3D reconstruction was performed to reconstruct 3D models of 14 glomeruli showing early to more advanced lesions.

### *Transmission Electron Microscopy*

For electron microscopy, we used immersion fixation, small fragments of cortex were fixed in 2.5% glutaraldehyde dissolved in 0.1 M sodium cacodylate buffer, pH 7.4, overnight at 4°C and washed in the same buffer. The tissue fragments were postfixed in palade-buffered 2% OsO<sub>4</sub> for 1 hr, dehydrated, and embedded in Epon 812, Luft's procedure (Merck, Darmstadt, Germany). Ultrathin sections were contrasted with 4% uranyl acetate for 45 min and subsequently with lead citrate for 5 min at room temperature. Sections were examined in a Jeol 1200 EX2 electron microscope (JEOL, Tokyo, Japan).

### *Analysis of glomeruli in consecutive tissue sections*

A pyramid-shaped segment in paraffin was cut and provided over 400 serial sections. Examination glomerular profile: Assessment of glomeruli for FSGS lesions was performed using a stack of 145 micron. Seven PAS-stained tissue sections equal divided over this stack were completely scanned. Of each glomerulus 3 - 5 PAS-stained cross sections were evaluated. In total 137 whole glomeruli were evaluated. Images were acquired using an AxioCam MRc (Carl Zeiss, Germany) connected to an AxioPlan 2 Imaging microscope (Carl Zeiss, Germany). The microscope was equipped with a computer controlled scanning stage (8 specimen stage, Märzhäuser GmbH, Wetzlar, Germany controlled by a Ludl MAC5000 controller, Ludl Electronic Products Ltd., Hawthorne, NY). Images were acquired using a 20x objective (Plan Aplanachromat, NA=0.6), resulting in a specimen level pixel size of 53x53µm<sup>2</sup>. Image acquisition was performed using custom written macros in KS400 image analysis software (version 3.0, Carl Zeiss, Germany). For each tissue section, a user-defined region of interest was automatically scanned and consecutive individual microscopic fields were stitched together into large 24 bit RGB TIFF images. Each individual microscopic field was autofocussed, and grabbed images were shading corrected.

Pairs of images of consecutive tissue sections were opened in Aperio ImageScope (v.4.14; Aperio Technologies, Vista, CA) and 'synchronized', i.e. both tissue sections could be viewed simultaneously and a change of the view position (location or magnification) in one 'virtual' section automatically caused an identical movement in the view of the second section. All glomeruli were numerically labeled in the image overlay, so that a single glomerulus could be followed in each section in which it was present. Each glomerular profile was examined. For the scoring of FSGS lesions each glomerular cross-section was subdivided into four quadrants. The position of the vascular pole was defined in this way; data were obtained with respect to the location and extent of lesions in each of 137 whole glomeruli contained in the kidney segment. For each glomerulus 3 to 5 PAS-stained sections could be studied. Lesions were categorized in four different groups. The first group contained only normal or ischemic quadrants sometimes associated with wrinkling or even collapse of the capillaries of the glomerular tuft, without cellular hypertrophy or hyperplasia. Second group showed early lesions defined by collapse of the capillaries, accompanied by hypertrophy and epithelial prolifera-



tion (hyperplasia) of glomerular epithelial cells and early adhesions between the glomerular tuft and Bowman's capsule. The third contained more advanced lesions, characterized by collapse of the capillaries of the glomerular tuft, with foam cells, ECM accumulation, sclerotic segments and various degrees of hypercellularity. The last group consisted of quadrants of glomeruli with advanced sclerosis.

To analyze the distribution of the various marker proteins and to determine the cellular origin, consecutive sections were used for incubations with the various antibodies as described in Table 1. Using our system, two consecutive profiles of the same glomerulus could be viewed simultaneously. In addition, we have performed doublestaining using different sets of marker proteins to strengthen our findings.

## RESULTS

### *Histopathology*

We have evaluated 137 whole glomeruli. Of each glomerulus 3 - 5 PAS-stained cross sections were scored. A total of 2232 glomerular quadrants were each assigned to one of the 4 categories normal, collapsing lesion, 'typical' FSGS and advanced sclerosis (Figure 1). In 1541 quadrants we saw a normal glomerular tuft (69%), 30 quadrants showed pure collapse with epithelial cell proliferation (hyperplasia) (1.5%), 588 quadrants showed 'typical' FSGS lesions with segmental collapse, adhesions, foam cells, ECM accumulation and variable epithelial cell swelling and hyperplasia (26%), and 73 quadrants were affected by advanced sclerosis (3.5%). Lesions of all categories could be located anywhere in the glomerulus (perihilar, at the tubular pole, or elsewhere). Within a single glomerulus affected quadrants were sometimes assigned to different categories. In these cases it often turned out that in such a glomerulus there was one confluent lesion with different morphology depending on the plain of sectioning. Glomeruli in the juxtamedullary half of the cortex were more frequently affected (38.4% of quadrants demonstrating FSGS lesions) than the more peripherally located glomeruli (23.9% involved). Overall, lesions showed a wide morphological spectrum with at the one end collapse and prominent epithelial cell proliferation and at the other end sclerosis without prominent hypercellularity. Morphological appearance of lesions was presumably related to the age/developmental stage of the lesions. We focussed on the lesions with prominent epithelial cell proliferation to study the relative role of podocytes and PECs.

We studied the phenotype of epithelial cells in Bowman's space using consecutive sections and double stainings. We investigated the expression of markers specific for podocytes; (synaptopodin, CD10, vimentin and VEGF), PECs; (CK8, Pan-cadherin and PAX-2) macrophages; (CD68) and myofibroblasts; ( $\alpha$  smooth muscle actin). In both normal and affected glomeruli we observed a uniform staining of the PECs lining Bowman's capsule for PAX-2 and Pan-cad-

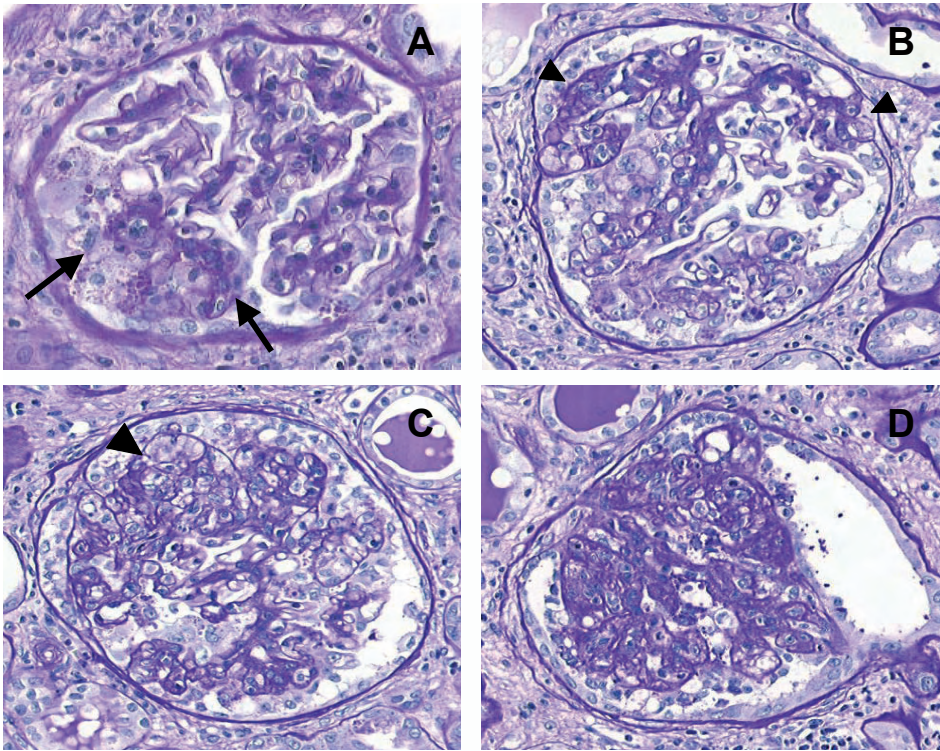


**Figure 1. Glomerular histology:** The morphology of the FSGS lesions was highly variable, ranging from segmental collapse of a few capillaries to advanced global sclerosis. Panel A shows an early lesion with segmental capillary collapse and epithelial hyperplasia (arrows). Some of the epithelial cells have prominent resorption droplets. The upper part of the glomerulus appears unremarkable. Glomeruli in panels B and C show more extensive abnormalities with on top of collapsed capillaries with epithelial hyperplasia more advanced ('typical') FSGS lesions (arrowheads) with sclerosis, adhesions, epithelial hyperplasia and mild endocapillary hypercellularity with endocapillary foam cells. Panel D shows a hypocellular globally sclerotic glomerulus covered with a single layer of epithelial cells, which do not appear, activated (x450).

herin. In glomeruli of normal control kidney tissue and in non-affected glomeruli of our patient CK8 staining was generally faint or absent (not shown). In our patient, in all glomeruli with FSGS lesions cells lining Bowman's capsule were segmentally CK8 positive. Notably, in our patient also in some glomeruli without FSGS lesions (serial sections were examined) we observed strong CK8 positivity of PEC's with a segmental and patchy distribution. Thus, CK8 staining appears to be a marker of early PEC activation. In collapsing lesions synaptopodin expressing podocytes were seen covering the collapsed tuft (Figure 2A, synaptopodin). These synaptopodin expressing podocytes were covered by synaptopodin negative but CK8 and PAX-2 positive epithelial cells (Figure 2A, CK8). This finding was confirmed via double staining for synaptopodin and PAX-2 (Figure 2B, C). We did an additional double staining for VEGF mRNA and CK8. VEGF mRNA is specifically expressed by podocytes [19]. Again we observed VEGF positive cells and CK8 positive cells but never double positive cells (Figure 2D, E, VEGF/CK8). In FSGS lesions with significant ECM accumulation (the 'typical' FSGS category),

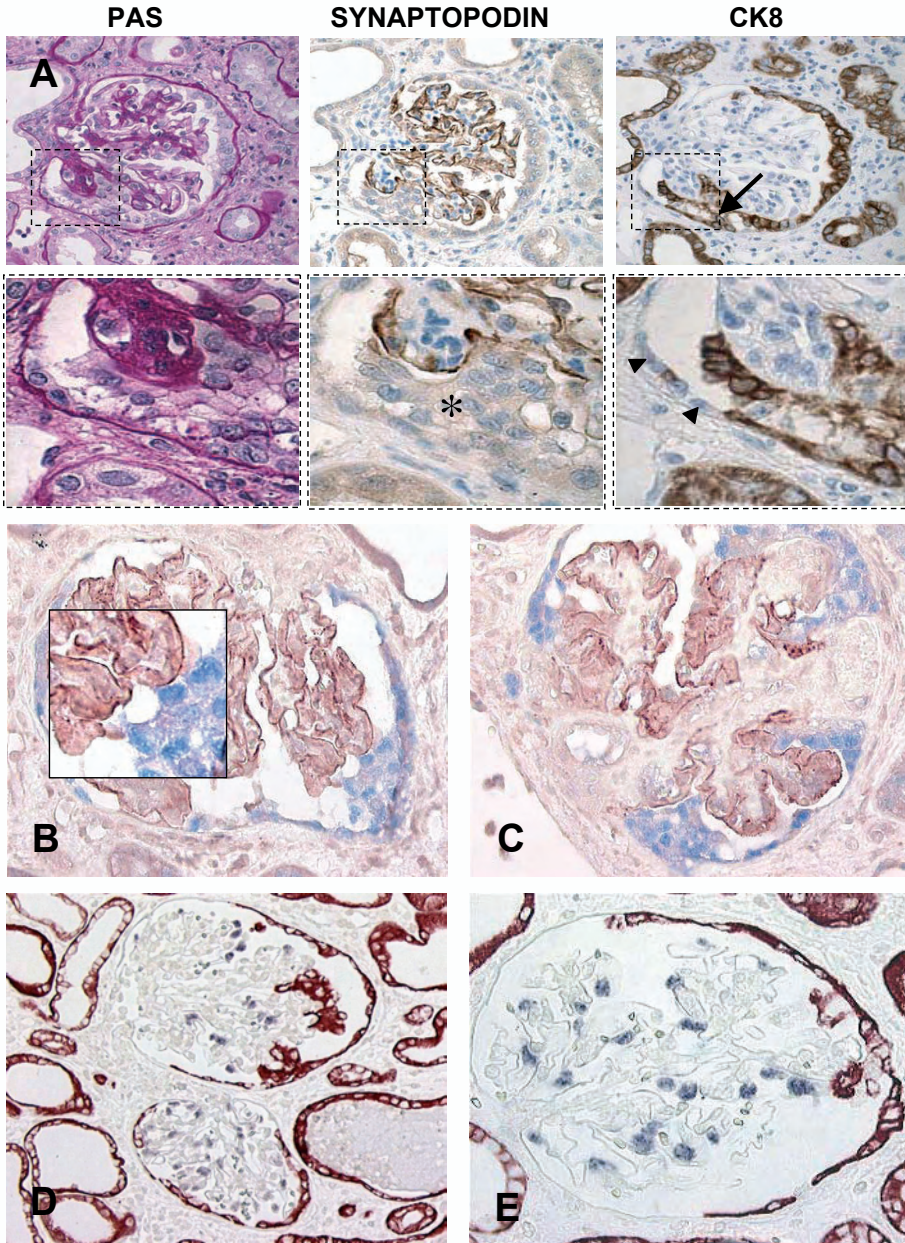


**Figure 2. Phenotype of proliferating epithelial cells:** Panel A shows serial sections of a glomerulus with a collapsing lesion. The epithelial cells (asterisk) that cover the collapsed segment are strongly CK8 positive. Also most of the PECs lining Bowman's capsule are CK8 positive. Some PECs are CK8 negative (arrowheads). Podocytes covering the collapsed segment stain positive for synaptopodin. Panel B,C show a double staining for synaptopodin (red) and PAX-2 (blue). Sometimes PAX-2 positive cells were located on top of synaptopodin expressing podocytes (panel B), whereas in lesions with more sclerosis synaptopodin expression in affected segments was lost. Double positive cells were not present. Panel D,E shows a double staining for VEGF mRNA and CK8. Podocytes are VEGF positive and PECs and epithelial cells that are part of an FSGS lesion are CK8 positive. Double positive cells were not present (A x200, detail x800, B,C x600, D x400, E x600).

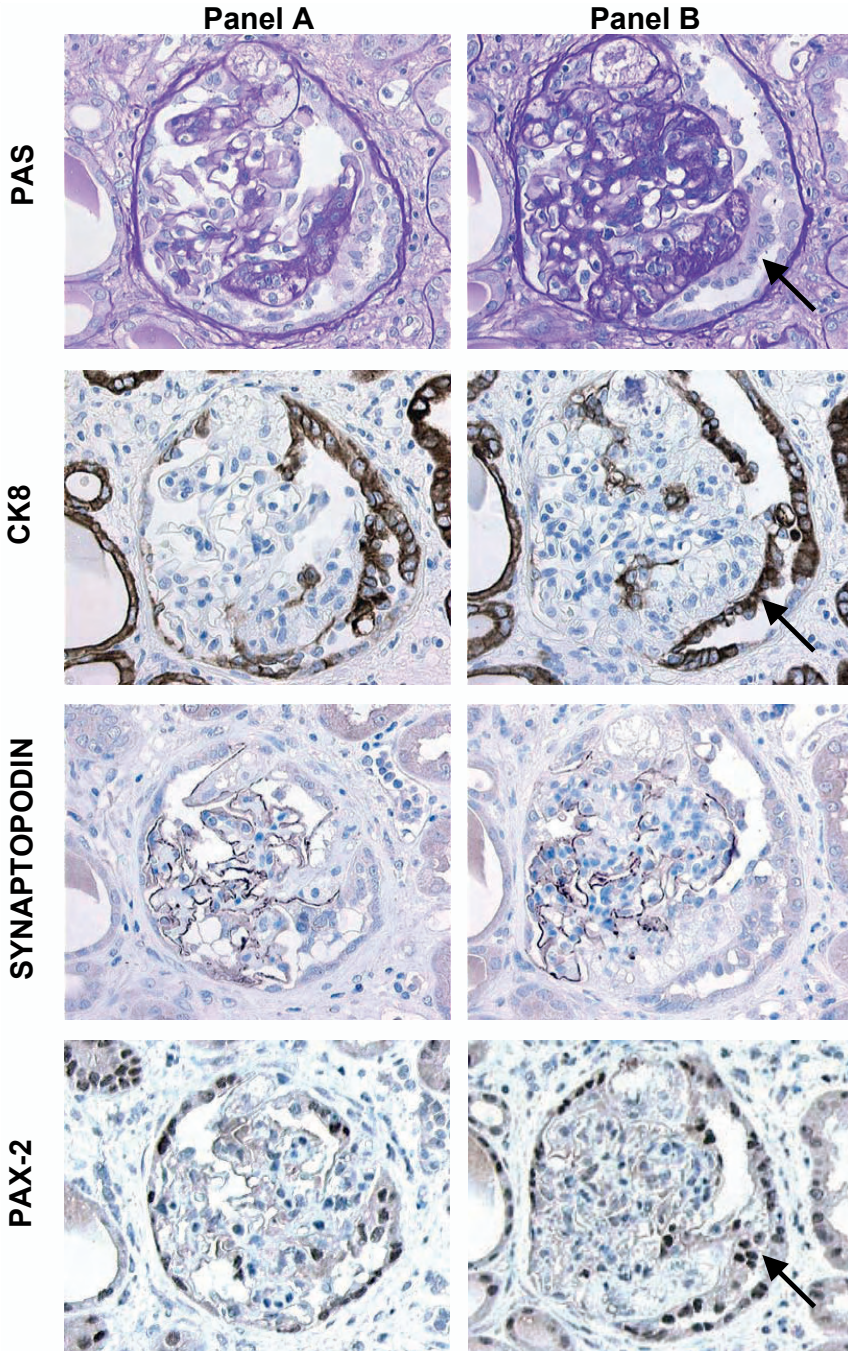


**Figure 3. Phenotype of epithelial cells in Bowman's space in lesions with sclerosis ('typical' FSGS lesions):** Two sections through the same glomerulus are shown in panel A and B. For each plain of sectioning consecutive sections were stained for CK8, synaptopodin and PAX-2. Epithelial cells in Bowman's space are positive for CK8 and PAX-2, but negative for synaptopodin. In affected segments synaptopodin positivity is lost (x375).

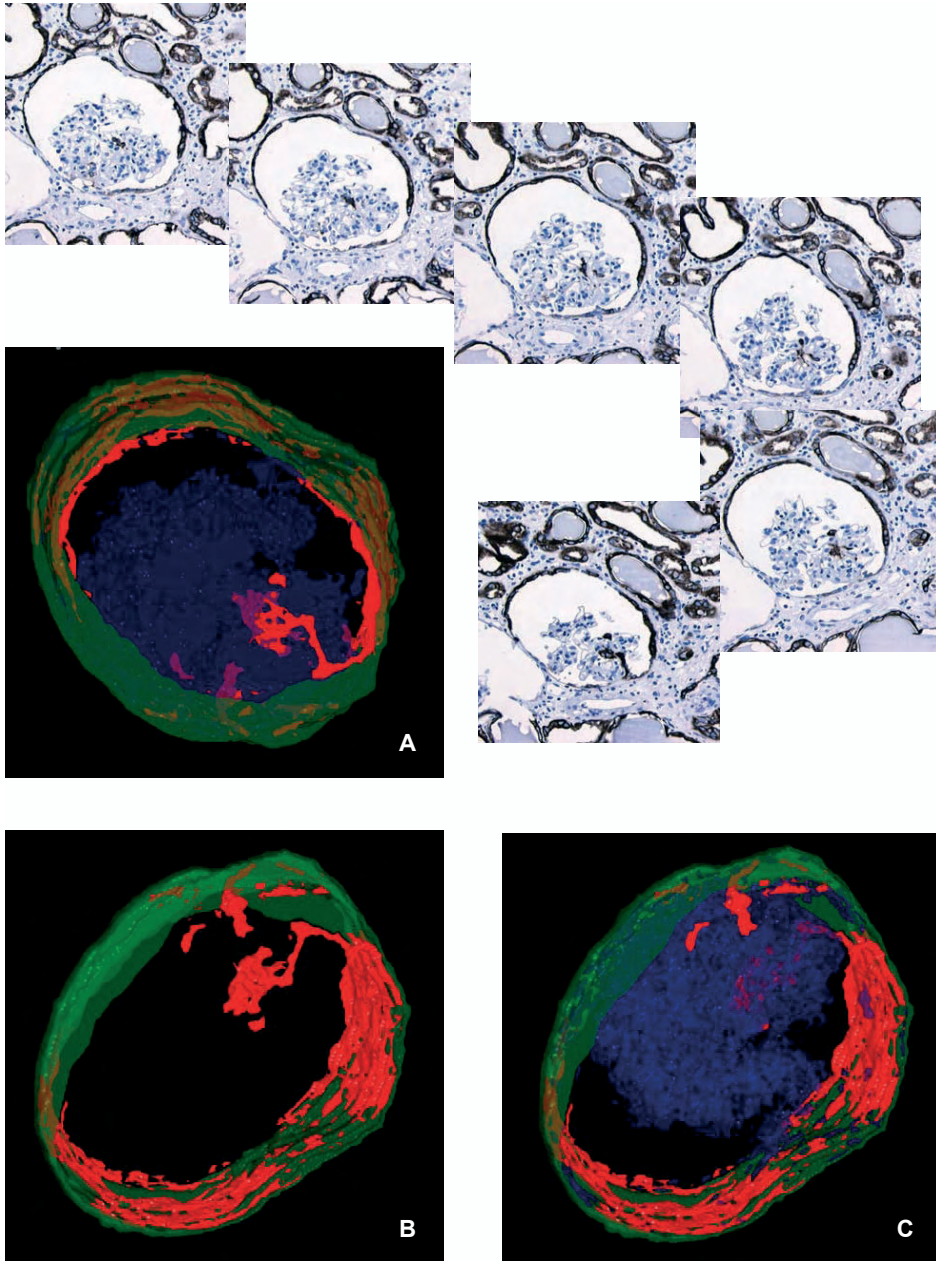


**Figure 4. Parietal epithelial cells ‘invade’ the glomerular tuft:** 3D reconstruction of glomeruli demonstrated that CK8 positive cells (red) are always in continuity with CK8 positive cells lining Bowman’s capsule (green). The glomerular tuft is shown in blue and was deleted from panel B to better visualize the deep penetration of CK8 positive cells. Panel B and C show the same glomerulus as panel A but from a different angle. For clarity 6 of the sections used for the 3D reconstruction are also shown. CK positive cells, whether positioned at the outer aspect of the collapsed segment or even within the central areas, are always connected to the CK8 positive layer of PECs lining Bowman’s capsule. The 3D images can best be appreciated in the Supplementary Material (Compact Disc).

we observed a decreased expression or even a total loss of expression of podocyte markers, while the non-affected-segments still did express podocyte markers (Figure 3, synaptopodin). Epithelial cells in Bowman's space were negative for synaptopodin (Figure 3, synaptopodin) and all other tested podocyte markers (not shown) but stained positive for PAN-cadherin, CK8 (Figure 3, CK8) and PAX-2 (Figure 3, PAX-2). We also observed PAN-cadherin, CK8 and PAX-2 positive cells in the central areas of the glomerular tuft (Figure 3 and 4). The 3D images demonstrated that these CK8 positive cells were always in continuity with the CK8 positive layer of PECs lining Bowman's capsule (Figure 4). MIB-1 staining showed positive cells along Bowman's capsule near affected segments of the glomerulus (Figure 5), whereas MIB-1 staining was only sporadically observed in normal kidney tissue. Notably, we did not observe cells that stained positive for either vimentin or CD68 in Bowman's space or the lumens of the proximal or distal tubules.

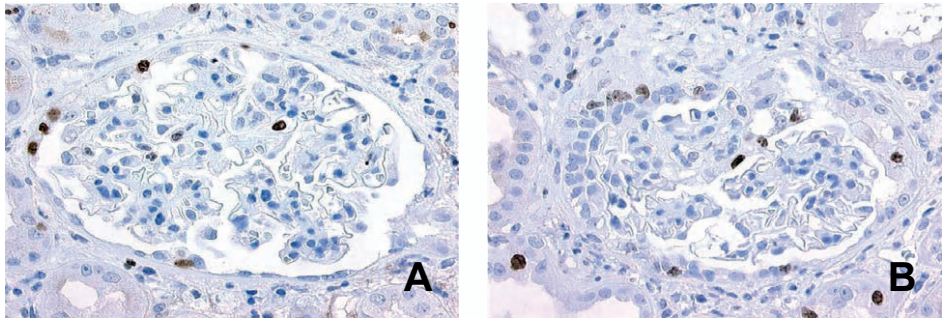


**Figure 5. KI-67 staining:** Most proliferating cells are seen along Bowman's capsule in segmental lesions or elsewhere in the glomerulus. A minority of positive cells is located more centrally in the glomerulus (x375).

We analysed the composition of the extracellular matrix deposited in lesions by staining serial sections with antibodies directed against the  $\alpha 1$  (Figure 6A), and  $\alpha 3$  (Figure 6B) chains of collagen IV. In addition, we have used an anti-HS single chain antibody (HS4E4) that in normal kidney tissue predominantly stains Bowman's capsule and not the GBM, and HS4C3, which stains the GBM and mesangial matrix. The ECM in adhesions stained for collagen  $\alpha 1$  (IV) (Figure 6C) and HS4E4 (Figure 6D), and was negative for collagen  $\alpha 3$  (IV) and HS4C3. Thus, the staining properties of the newly formed ECM were identical to those of Bowman's capsule, indicating that the deposited matrix was produced by PECs rather than podocytes.

This conclusion was strengthened by double immunostaining of kidney sections using anti-synaptopodin antibodies and the single chain antibody HS4E4 (Figure 7A, control). In glomeruli with collapsing lesions we observed expression of synaptopodin underneath a layer of newly formed, HS4E4 positive ECM (Figure 7B, arrow white). In lesions with more sclerosis there was loss of the synaptopodin expression (Figure 7C, white asterisks).

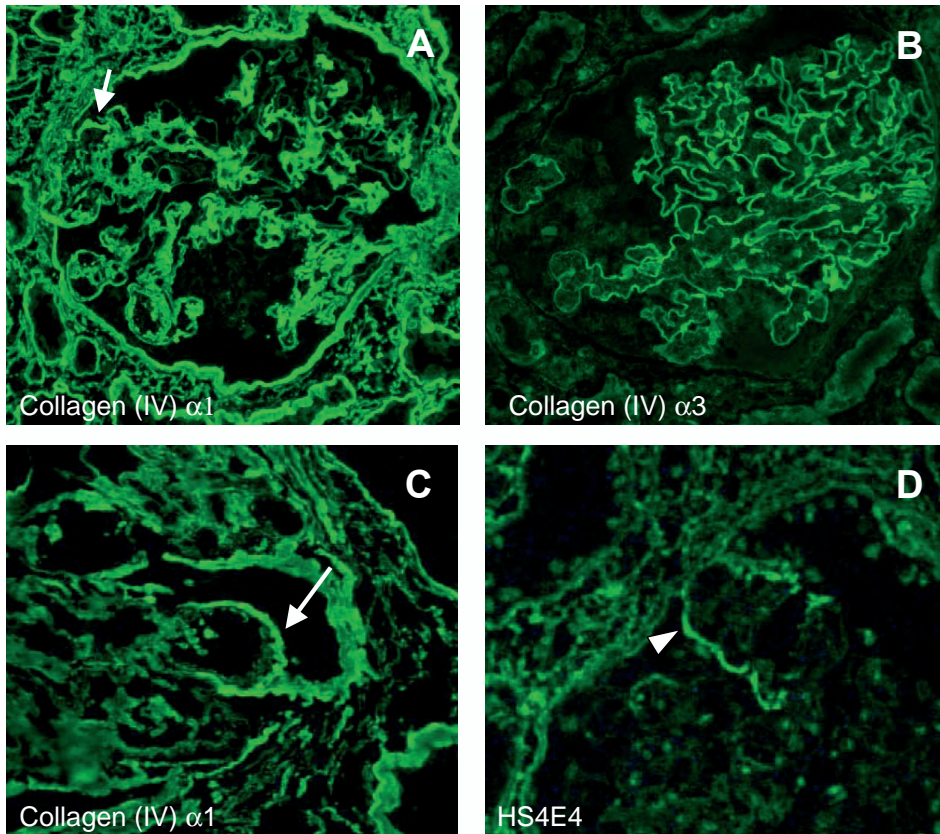


**Figure 6. The ECM deposited by proliferating epithelial cells has the same staining characteristics as Bowman's capsule:** Serial sections were stained with collagen IV  $\alpha$  1 (panel A, C) and collagen IV  $\alpha$  3 (panel B). Collagen IV  $\alpha$  1 strongly stains Bowman's capsule, the newly deposited matrix forming the adhesions (arrows panel A, C) and the mesangial matrix. There is weak GBM staining for Collagen IV  $\alpha$  1 (panel A), Collagen IV  $\alpha$  3 (panel B) stains the GBM and not Bowman's capsule. Panel D shows positive staining of an adhesion for the single chain antibody HS4E4 (arrowhead). In control kidney, this antibody directed against a heparan sulphate species only stains Bowman's capsule and not the GBM (A,B x450, C,D x900).

Ultrastructural analysis by transmission electron microscopy showed that in hypercellular lesions without prominent ECM deposition podocytes appeared activated with foot process effacement and microvillous transformation. In these non-sclerotic lesions we never observed podocyte detachment nor areas of denuded GBM. In contrast, denuded segments of Bowman's capsule were frequently observed and podocytes were sometimes positioned against these naked segments of Bowman's capsule (Figure 8A) or against activated appearing cells lining Bowman's capsule, presumably PECs (Figure 8C). These latter cells resembled parietal epithelial cells as defined by Gaffney et al [20] i.e. enlarged cells with a somewhat cubical appearance with round and enlarged nuclei. In most cells the cytoplasm was vacuolated and more appreciable than in normal PECs. Some of these cells had swollen mitochondria and disrupted cell membranes consistent with injury. Sometimes the number of nuclei along

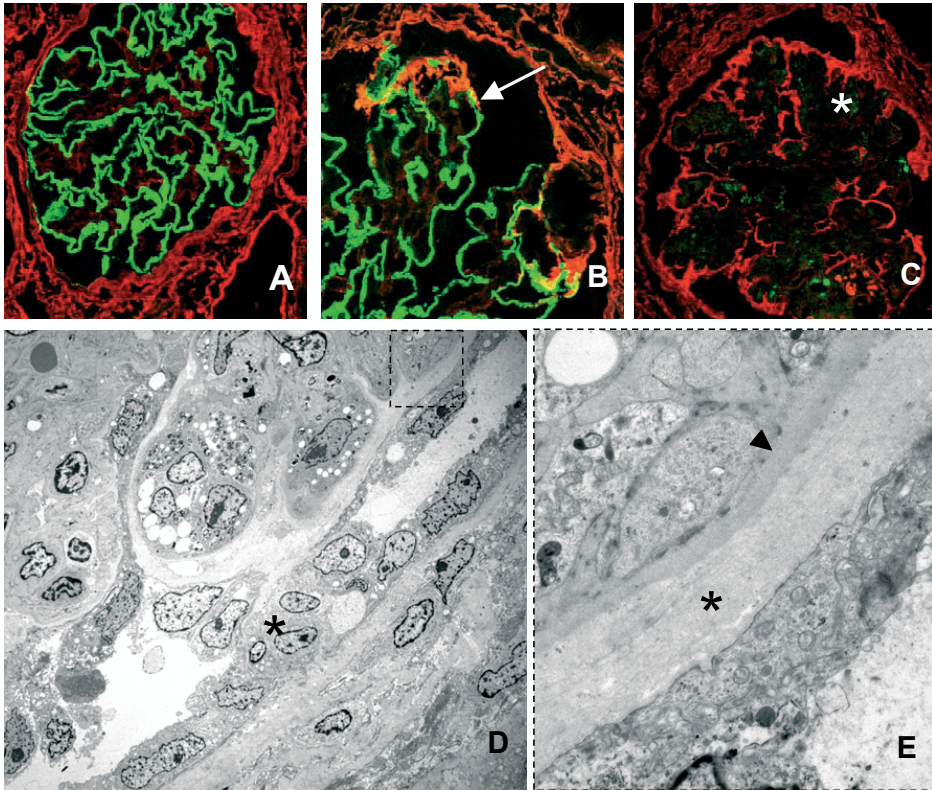


**Figure 7. Newly formed extracellular matrix is deposited on top of the GBM and sometimes on top of synaptopodin expressing podocytes:** Double staining for HS4E4 (red) and synaptopodin (green) is shown for a normal glomerulus (panel A), a segmental lesion (panel B) and a glomerulus with advanced global sclerosis (panel C). In control glomeruli HS4E4 stains Bowman's capsule and not the GBM. Adhesions stain for HS4E4 and sometimes HS4E4 positive ECM is deposited on top of synaptopodin positive podocytes (arrow panel B). In glomeruli with advanced sclerosis synaptopodin expression is lost (asterisk panel C). In panels D and E transmission electron micrographs show that in a segment with prominent sclerosis podocytes are absent and newly formed ECM (asterisk panel E) is deposited on top of the GBM (arrowhead panel E). Hyperplastic cells lining Bowman's capsule cover this matrix (asterisk panel D) (A,C x300, B x700, D x1200, E x7000).

Bowman's capsule was increased and occasionally mitotic figures were observed, indicating proliferative activity. Deposition of ECM-like material between the tuft and epithelial cells in Bowman's space was sometimes observed (figure 8B-asterisk). In lesions with more advanced sclerosis we did see areas of denuded GBM, indicating loss of podocytes at this stage. In such denuded areas we sometimes saw deposition of newly formed ECM directly on top of the GBM (Figure 7D-E, black asterisks). We have looked for evidence of podocyte apoptosis. However, we did not see apoptotic bodies in affected glomerular segments (there was also no caspase-3 positivity, data not shown).



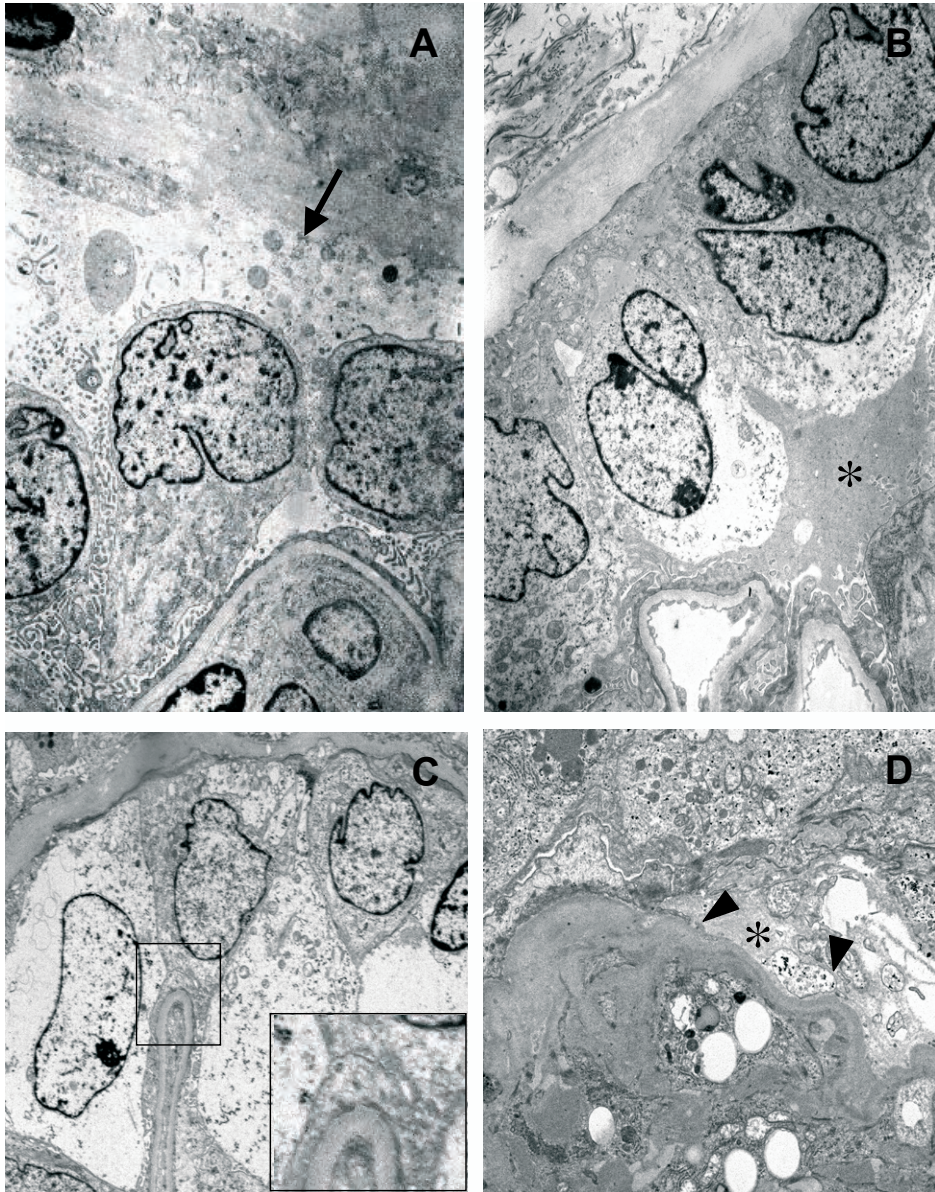


**Figure 8. Transmission electron microscopy:** Panels A to C show glomerular segments with an increase of epithelial cells in Bowman's space without prominent sclerosis (early lesions). Podocytes appear activated with extensive foot process effacement, microvillous transformation and enlarged nuclei (panel A). Locally, the parietal epithelium appeared damaged and denuded segments Bowman's capsule were present (arrow panel A). Segmentally, there appeared to be an increased number of nuclei along Bowman's capsule (panel B). We sometimes observed bridging epithelial cells between activated podocytes and Bowman's capsule (panel C). The insert shows the cell contact between the podocyte and the bridging cell with apparent fusion of cell membranes. Amorphous extracellular matrix was sometimes present surrounding the epithelial cells in Bowman's space (asterisk panel B). In lesions with more advanced sclerosis (panel D) we did see denuded GBM segments and sometimes remnants of podocytes (arrowhead) appeared to be present. Amorphous extracellular matrix was sometimes deposited on top of the naked GBM (asterisk) (A,B x7000, C,D x5000).

## DISCUSSION

Our patient suffered from recurrent FSGS after transplantation, and the etiology of the glomerular lesion in this condition is considered identical with that of primary FSGS. The FSGS lesions in our patient were morphologically diverse, ranging from recent collapse with prominent epithelial hyperplasia to advanced sclerosis. Based on the classification of FSGS variants proposed by D'Agati and co-workers [4], FSGS in our patient would have to be classified as collapsing type FSGS, although only a small proportion of glomerular segments showed pure collapse. Within a single glomerulus, we often observed large confluent lesions which in one plane of sectioning could appear hypercellular and in another plane of sectioning could appear mostly sclerotic. We therefore postulate that the different morphology of the lesions reflects differences in the developmental stage of the FSGS lesions. In the present manuscript we focussed on the origin of the proliferating epithelial cells in early hypercellular lesions.

Our study indicates that parietal epithelial cells are critically involved in the development of FSGS lesions in humans. We have demonstrated that the epithelial cells that for a large part constitute the early hypercellular lesions stained positively for PAX-2, CK8 and PAN-cadherin, were connected to cells lining Bowman's capsule and did not express podocyte markers synaptopodin or VEGF. Obviously, the validity of markers to determine a cell type can be questioned in view of the prospect of (de-)differentiation. For instance It has been shown that in developing kidney immature podocytes are PAX-2 positive, making it hardly possible to differentiate between mature PECs and dedifferentiated podocytes. Therefore we have used many other markers (CK8, PAN-cadherin, synaptopodin, VEGF) and performed double staining experiments (PAX-2/synaptopodin, VEGF/CK8) and results were always in perfect agreement: proliferating cells were positive for all PEC markers and negative for the podocyte markers. It is worth mentioning that a recent study showed that PAN-cadherin is not expressed on activated podocytes after injection of puromycin [22]. In our study CK8 proved a marker of activated PECs. In normal kidney PECs are negative or stained only faintly positive for CK8. In some of the normal appearing glomeruli in our patient there was strong CK8 staining of cells lining Bowman's capsule in a segmental distribution. By serial sectioning we could show that in these glomeruli adhesions between the glomerular tuft and Bowman's capsule were absent, thus providing a strong argument that PECs acquire the CK8 positive phenotype upon activation. Additional evidence supporting the PEC origin of the proliferating epithelial cells comes from the finding that the staining characteristics of the extracellular matrix that is produced by these cells are identical to those of Bowman's capsule. Finally, 3D analysis confirmed that all CK8 positive cells within a glomerulus are in continuity with cells lining Bowman's capsule. Taken together, these data argue that proliferating epithelial cells in early FSGS lesions are PECs and question the contribution of the so called dedifferentiated podocyte.

The findings in our patient are very similar to our previous observations in the Thy-1.1 transgenic mouse. In this mouse model of collapsing FSGS we observed that the proliferating epithelial cells strongly expressed CD10 (a specific PEC marker in mouse). In addition we noted that the composition of the newly formed ECM resembled Bowman's capsule and thus was produced by PECs [13]. Double staining for the podocytic transgene Thy-1.1 and the proliferation marker Ki-67 proved that there was no proliferation of the podocytes during the development of early FSGS lesions.

How do our findings relate to those of other authors? The early hypercellular lesions we studied are classified by many authors as collapsing FSGS lesions although in the earliest description by Valeri, it was suggested that the term collapsing FSGS should be restricted to biopsies in which any glomerulus contained global collapse or at least 20% of the glomeruli showed segmental collapse [22]. Nonetheless, the histology observed in our patient is very similar to the glomerular profiles shown in papers by Schwartz [23], Bariety [9], and Othaka [11;12], and were defined as cellular or collapsing lesions. The latter authors have used immunostaining to identify the cell types and concluded that the proliferating epithelial cells were dedifferentiated podocytes, since these cells showed no expression of mature podocyte markers. In contrast, these cells stained for PEC markers such as PAX-2, hence the idea of dedifferentiation. It is evident that immunostaining of unknown cells has limitations in judging their cellular origin, since in fact during nephrogenesis in the S-shaped body stage, podocytes have features comparable to mature PECs [24]. Therefore, the authors have used the localization of the cells to define their origin and since the hyperplastic epithelial cells covered the glomerular tuft and often lacked an apparent connection to Bowman's capsule, these cells were identified as podocytes. However in a recent review it was clearly pointed out that the absence of a connection between the epithelial cells and Bowman's capsule is not a very good criterion without proper three dimensional (3D) analysis [25].

In seminal studies of Nagata et al [26;27] and Kihara et al [28] it has already been suggested that PECs do contribute to the cellular lesions. These authors however proposed that PECs proliferate and cover the capillary tuft as a consequence of denudation of the GBM due to detachment and loss of podocytes. In our patient we never observed podocyte detachment in early lesions, nor did we note podocytes in the urinary space. Rather, we observed proliferating PECs directly on top of podocytes. We can only speculate about the stimulus for PEC proliferation. Possibly, the interaction between activated/injured podocytes and activated/injured PECs or between activated/injured podocytes and denuded areas of Bowman's capsule plays a role.

It is important to emphasize that our data do not dispute the fact that in the chain of events that leads to full blown FSGS lesions it is the podocyte that is initially injured, causing pro-

teinuria. However, we do challenge the concept that ensuing epithelial cell proliferation, which is important for progression of the FSGS lesions, is due to proliferation of dedifferentiated podocytes. An exception may be HIV-induced collapsing FSGS which is characterized by global collapse in many glomeruli and by the absence of adhesions. It is therefore likely that podocyte proliferation does occur in this condition, probably related to incorporation of viral genome in podocytic DNA [29;30]. In some forms of FSGS there is little or no proliferation of epithelial cells and the mechanism of FSGS development may be different in these conditions. For example studies by Kriz et al have pointed to the role of podocyte loss in the development of FSGS in various rat models. These models are all characterized by glomerular hypertension and capillary ballooning and may therefore be more relevant for secondary FSGS than for idiopathic FSGS. Most patients with secondary FSGS have rather inactive, hypocellular lesions, with lesions predominantly involving the perihilar region of the glomerulus.

## **CONCLUSION**

Parietal epithelial cells are crucially involved in the pathogenesis of idiopathic FSGS.

## **ACKNOWLEDGEMENTS**

This work was supported by a grant from the Dutch Kidney Foundation (C04.2079). We gratefully acknowledge dr. Toin van Kuppevelt (Department of Biochemistry, University Medical Center Nijmegen) for providing the single chain antibodies HS4E4 and HS4C3. Further, we thank dr. William Leenders for providing the VEGF-probe, Kiek Verrijp, Vincent Cuijpers and the members of the EM-, Immuno/ISH laboratory (all of the Department of Pathology, University Medical Center Nijmegen, Nijmegen), for their expert technical assistance.

## **SUPPLEMENTARY MATERIAL**

The following supplementary material is available for this article on CD: Video Clip. Three-dimensional reconstruction of parietal epithelial cells 'invading' the glomerular tuft.

## REFERENCES

1. Haas M, Meehan SM, Karrison TG, Spargo BH: Changing etiologies of unexplained adult nephrotic syndrome: a comparison of renal biopsy findings from 1976-1979 and 1995-1997. *Am.J.Kidney Dis.* 30:621-631, 1997.
2. Jennette JC, Olson JL, Schwartz MM, et al (editors): *Heptinstall's Pathology of the Kidney*, 5th ed., Philadelphia, New York, LippincottWilliams & Wilkins, 1998, pp 212-223.
3. Cameron JS: The enigma of focal segmental glomerulosclerosis. *Kidney Int.Suppl* 57:S119-31.:S119-S131, 1996.
4. D'Agati VD, Fogo AB, Bruijn JA, Jennette JC: Pathologic classification of focal segmental glomerulosclerosis: a working proposal. *Am.J.Kidney Dis.* 43:368-382, 2004.
5. Kriz W, Gretz N, Lemley KV: Progression of glomerular diseases: is the podocyte the culprit? *Kidney Int* 54:687-697, 1998.
6. Kriz W: Progressive renal failure--inability of podocytes to replicate and the consequences for development of glomerulosclerosis. *Nephrol.Dial.Transplant.* 11:1738-1742, 1996.
7. Kriz W, Lemley KV: The role of the podocyte in glomerulosclerosis. *Curr.Opin.Nephrol Hypertens.* 8:489-497, 1999.
8. Barisoni L, Kriz W, Mundel P, D'Agati V: The dysregulated podocyte phenotype: a novel concept in the pathogenesis of collapsing idiopathic focal segmental glomerulosclerosis and HIV-associated nephropathy. *J.Am.Soc. Nephrol.* 10:51-61, 1999.
9. Bariety J, Bruneval P, Hill G, et al: Posttransplantation relapse of FSGS is characterized by glomerular epithelial cell transdifferentiation. *J.Am.Soc.Nephrol.* 12:261-274, 2001.
10. Yang Y, Gubler MC, Beauflis H: Dysregulation of Podocyte Phenotype in Idiopathic Collapsing Glomerulopathy and HIV-Associated Nephropathy. *Nephron* 91:416-423, 2002.
11. Ohtaka A, Ootaka T, Sato H, Ito S: Phenotypic change of glomerular podocytes in primary focal segmental glomerulosclerosis: developmental paradigm? *Nephrol.Dial.Transplant.* 17 *Suppl* 9:11-5.:11-15, 2002.
12. Ohtaka A, Ootaka T, Sato H, et al: Significance of early phenotypic change of glomerular podocytes detected by Pax2 in primary focal segmental glomerulosclerosis. *Am.J.Kidney Dis.* 39:475-485, 2002.
13. Smeets B, Te Loeke NA, Dijkman HB, et al: The parietal epithelial cell: a key player in the pathogenesis of focal segmental glomerulosclerosis in Thy-1.1 transgenic mice. *J.Am.Soc. Nephrol.* 15:928-939, 2004.
14. Cochat P, Kassir A, Colon S, et al: Recurrent nephrotic syndrome after transplantation: early treatment with plasmapheresis and cyclophosphamide. *Pediatr.Nephrol.* 7:50-54, 1993.
15. Assmann KJ, Tangelder MM, Lange WP, et al: Membranous glomerulonephritis in the mouse. *Kidney Int* 24:303-312, 1983.
16. Dennissen MA, Jenniskens GJ, Pieffers M, et al: Large, tissue-regulated domain diversity of heparan sulfates demonstrated by phage display antibodies. *J.Biol.Chem.* 277:10982-10986, 2002.
17. van Kuppevelt TH, Dennissen MA, van Venrooij WJ, et al: Generation and application of type-specific anti-heparan sulfate antibodies using phage display technology. Further evidence for heparan sulfate heterogeneity in the kidney. *J Biol.Chem* 273:12960-12966, 1998.
18. Leenders WP, Kusters B, Verrijp K, et al: Antiangiogenic therapy of cerebral melanoma metastases results in sustained tumor progression via vessel co-option. *Clin.Cancer Res.* 10:6222-6230, 2004.
19. Kretzler M, Schroppel B, Merkle M, et al: Detection of multiple vascular endothelial growth factor splice isoforms in single glomerular podocytes. *Kidney Int.Suppl* 67:S159-61.:S159-S161, 1998.
20. Gaffney EF: Prominent parietal epithelium: a common sign of renal glomerular injury. *Hum. Pathol.* 13:651-660, 1982.
21. Yaoita E, Sato N, Yoshida Y, et al: Cadherin and catenin staining in podocytes in development and puromycin aminonucleoside nephrosis. *Nephrol.Dial.Transplant.* 17 *Suppl* 9:16-9.:16-19, 2002.
22. Valeri A, Barisoni L, Appel GB, et al: Idiopathic collapsing focal segmental glomerulosclerosis: a clinicopathologic study. *Kidney Int.* 50:1734-1746, 1996.
23. Schwartz MM, Lewis EJ: Focal segmental glomerular sclerosis: the cellular lesion. *Kidney Int.* 28:968-974, 1985.
24. Moll R, Hage C, Thoenes W: Expression of intermediate filament proteins in fetal and adult human kidney: modulations of intermediate filament patterns during development and in damaged tissue. *Lab Invest* 65:74-86, 1991.
25. Nagata M, Tomari S, Kanemoto K, et al: Podocytes, parietal cells, and glomerular pathology:

- the role of cell cycle proteins. *Pediatr.Nephrol.* 18:3-8, 2003.
26. Nagata M, Horita S, Shu Y, et al: Phenotypic characteristics and cyclin-dependent kinase inhibitors repression in hyperplastic epithelial pathology in idiopathic focal segmental glomerulosclerosis. *Lab.Invest.* 80:869-880, 2000.
  27. Nagata M, Hattori M, Hamano Y, et al: Origin and phenotypic features of hyperplastic epithelial cells in collapsing glomerulopathy. *Am.J.Kidney Dis.* 32:962-969, 1998.
  28. Kihara I, Yaoita E, Kawasaki K, et al: Origin of hyperplastic epithelial cells in idiopathic collapsing glomerulopathy. *Histopathology* 34:537-547, 1999.
  29. Husain M, Gusella GL, Klotman ME, et al: HIV-1 Nef Induces Proliferation and Anchorage-Independent Growth in Podocytes. *J Am Soc Nephrol* 13:1806-1815, 2002.
  30. Marras D, Bruggeman LA, Gao F, et al: Replication and compartmentalization of HIV-1 in kidney epithelium of patients with HIV-associated nephropathy. *Nat.Med.* 8:522-526, 2002.



# 6

## **PROLIFERATING CELLS IN HIV AND PAMIDRONATE ASSOCIATED COLLAPSING FOCAL SEGMENTAL GLOMERULOSCLEROSIS ARE PARIETAL EPITHELIAL CELLS\***

Henry B.P.M. Dijkman<sup>1</sup>, Jan J. Weening<sup>2</sup>,  
Bart Smeets<sup>1</sup>, Kiek C.N. Verrijp<sup>1</sup>, Toin H. van  
Kuppevelt<sup>3</sup>, Karel J.M. Assmann<sup>1</sup>, Eric J.  
Steenbergen<sup>1</sup> and Jack F.M. Wetzels<sup>4</sup>

*Departments of Pathology<sup>1</sup>, Biochemistry<sup>3</sup>, and  
Nephrology<sup>4</sup>, Radboud University Nijmegen Medical  
Center and Department of Pathology, Academic  
Medical Center Amsterdam<sup>2</sup>, The Netherlands.*

*\*Contribution to the cover, Kidney International  
volume 70, issue 2.*



## ABSTRACT

Collapsing focal segmental glomerulosclerosis (cFSGS) is characterized by hyperplasia of glomerular epithelial cells. In a mouse model of FSGS and in a patient with recurrent idiopathic FSGS we identified the proliferating cells as parietal epithelial cells (PECs). In the present study we have evaluated the origin of the proliferating cells in cFSGS associated with HIV and pamidronate. We performed a detailed study of glomerular lesions in biopsies of two patients with HIV associated cFSGS and a nephrectomy specimen of a patient with pamidronate associated cFSGS. Glomeruli were studied by serial sectioning using light and electron microscopy and immunohistochemistry to determine the epithelial cell phenotype. We used synaptopodin, VEGF and CD10 as podocyte markers, CK8 and PAX2 as PEC markers and Ki-67 as marker of cell proliferation. The newly deposited extracellular matrix was characterized using anti-heparan sulphate single chain antibodies.

The proliferating cells were negative for the podocyte markers, but stained positive for the PEC markers and the cell proliferation marker Ki-67. The proliferating PAX-2 and CK8 positive cells that covered the capillary tuft were always in continuity with PAX-2/CK8 positive cells lining Bowman's capsule. The matrix deposited by these proliferating cells stained identically to Bowman's capsule.

Our study demonstrates that PECs proliferate in HIV and pamidronate associated cFSGS. Our data do not support the concept of the proliferating, dedifferentiated podocyte.

Keywords: HIV, pamidronate, parietal epithelial cell, podocyte, epithelial cell proliferation, collapsing lesions and glomerulosclerosis.

## INTRODUCTION

Focal segmental glomerulosclerosis (FSGS) is one of the most common patterns of glomerular injury [1]. Recently, various morphological variants have been described and a new classification was proposed [2]. The traditional forms of FSGS now classified as perihilar and FSGS-not otherwise specified, lack epithelial cell proliferation and are characterized by mesangial sclerosis, obliteration of glomerular capillaries, formation of adhesions between the glomerular tuft and Bowman's capsule, podocyte hypertrophy, hyalinosis and intracapillary foam cells. In contrast, epithelial cell proliferation is prominent in the other variants, in particular in collapsing FSGS, defined by segmental or global collapse of the glomerular tuft associated with epithelial cell hypertrophy and hyperplasia.

In recent studies on the pathogenesis of FSGS a central role was assigned to the visceral epithelial cell, the so-called podocyte. The podocyte is considered to be a highly specialized and differentiated cell, unable to replicate. Kriz and co-workers have studied the development of FSGS in various rat models [3-5]. Based on these studies Kriz and Mundel (reviewed in [6]), proposed that podocyte loss (podocytopenia) was the critical starting event in FSGS. Neighbouring podocytes cannot compensate for this loss, resulting in denudation of the GBM and formation of an adhesion between the capillary tuft and the parietal epithelial cells.

The concept of the terminally differentiated, not-replicating podocyte seemed incompatible with the development of the proliferative lesions observed in collapsing FSGS. Since the proliferating cells cover the glomerular tuft they are considered by several investigators to be of podocytic origin [7;8], although they do not express podocyte markers such as synaptopodin, VEGF and WT1. These and similar observations have fostered the concept that proliferating, dedifferentiated podocytes are the main cell type involved in the formation of cellular lesions in collapsing FSGS [9-11]. Few studies have questioned this concept, apparently because of the localisation of the cells, despite the observation that the proliferating cells express cytokeratins, a marker expressed by parietal epithelial cells and not by podocytes [12-14].

We previously studied the origin of the proliferating epithelial cells in FSGS in more detail in the Thy-1.1 transgenic mouse (a model of collapsing FSGS), providing evidence that in this model the proliferating epithelial cells are of PEC origin [15]. Recently our conclusions were confirmed and strengthened by Asano et al, who found PEC proliferation in their transgenic mouse with LacZ expressing podocytes [16]. Subsequently, we performed detailed studies of glomerular lesions in a patient with recurrent idiopathic FSGS [17]. Using 3D analysis we were able to firmly establish that the proliferating cells were of PEC origin.

Thus our previous studies questioned a major contribution of proliferating podocytes to the formation of cellular lesions in FSGS in general and we discussed the possibility that in this respect HIV associated cFSGS may be an exception [17]. In the present study we have investigated the characteristics of the proliferating epithelial cells in glomerular lesions of

patients with HIV and pamidronate associated cFSGS. Our study indicates that also in these conditions, most proliferating cells are PECs.

## MATERIALS AND METHODS

### *Patients*

We studied biopsies from 2 HIV patients with collapsing FSGS and a nephrectomy specimen from a patient with pamidronate associated collapsing FSGS. The latter patient was treated with aminohydroxypropylidene bisphosphonate (APD: 'pamidronate') because of persistent hypercalcaemia after renal transplantation, she received oral APD in daily dosage of 300 mg for 20 months, 450 mg for 6 months and 600 mg for 2 months. Subsequently I.V. APD was administered in a dose of 60 mg at two-weekly intervals. Severe proteinuria was noted after the third infusion. The HIV biopsies contained 11 and 17 different glomeruli respectively, and the paraffin block from the nephrectomy specimen contained over 77 glomeruli. The material was serially sectioned and from each specimen more than 100 sections were examined. One of every 5 sections was PAS stained for LM evaluation and intervening sections were retained for immunostainings.

### *Light microscopy*

For light microscopy, kidney fragments were fixed in formaldehyde, dehydrated, and embedded in paraplast (Amstelstad, Amsterdam The Netherlands). 2  $\mu\text{m}$  sections were stained with periodic acid Schiff, and with silver methenamine [18].

### *Immunohistochemistry*

Immunohistochemical staining was performed on kidney sections fixed in 4% buffered formaldehyde for 24 hr and embedded in paraffin. 4  $\mu\text{m}$  sections were incubated with monoclonal antibodies (mAb) and polyclonal antibodies (pAb) directed at various markers for podocytes, PECs, as detailed in table 1. As secondary antibody we used power vision Poly-HRP –anti mouse/rabbit/rat IgG (Immunologic, Klinipath, Duiven, The Netherlands). Detection was carried out with the use of peroxidase as label and diaminobenzidine as substrate.

For the doublestaining CD10/CK8, first the polyclonal antibody (pAb) CD10 was detected and completed. As detecting antibody we used Envision AF-anti Rabbit IgG (Immunologic, Klinipath, Duiven, The Netherlands), detection was carried out with the use of alkaline phosphatase as label and FastBlue as substrate. Thereafter samples were incubated with the monoclonal antibody (mAb) CK8, as detecting antibody we used powervision Poly-HRP-anti Mouse/Rabbit/Rat IgG (Immunologic, Klinipath, Duiven, The Netherlands). Detection was carried out with the use of peroxidase as label and AEC/red as substrate.

For the doublestaining synaptopodin/CK8, first the monoclonal antibody (mAb) synaptopodin was incubated and as detecting antibody we used powerision Poly-HRP-anti Mouse/Rabbit/Rat IgG (Immunologic, Klinipath, Duiven, The Netherlands). Detection was carried out with the use of peroxidase as label and DAB as substrate. Thereafter samples were incubated with the monoclonal antibody (mAb) CK8, as detecting antibody we used powerision Poly-AP-anti-Mouse IgG (Immunologic, Klinipath, Duiven, The Netherlands). Detection was carried out with the use of alkaline phosphatase as label and AEC/red as substrate.

### *Immunofluorescence microscopy*

Kidney fragments were snap-frozen in liquid nitrogen, and 2  $\mu\text{m}$  acetone fixed cryostat sections were used. Kidney sections were incubated with antibodies directed against heparan sulfate species (Table 1). The single chain antibodies used for staining of heparan sulfate species [19;20] were detected via a rabbit antibody directed against the VSV-g epitope tag (ICL, Oregon, USA) and finally detected with a goat anti-rabbit Alexa™ 488 antibody (Molecular probes Inc, Leiden, The Netherlands). The sections were examined with a fluorescence microscope (Leica microsystems GmbH, Heidelberg, Germany).

**Table 1:** Antibodies used for the detection of glomerular antigens

Antigen	Primary antibody	Dil.	Supplier / Reference
<b>Podocyte components</b>			
Synaptopodin	Mouse anti-synaptopodin	1	Progen, Heidelberg, Germany
CD 10	Rabbit anti-human CD10	50	Monosan, Caltag lab., Burlingame
VEGF	ISH m-RNA Probe (*ng/ml)	100*	[21]
<b>PEC components</b>			
PAX-2	Rabbit anti-human PAX-2	50	Zymed laboratories Inc. San Francisco, USA
Cytokeratin 8	Mouse anti-human CAM 5.2 (CK8)	50	BD Biosciences, San Diego, CA
<b>Proliferation</b>			
KI 67	Mouse anti-human MIB-1	200	Dako, Glostrup, Denmark
<b>Bouwman's capsule</b>			
Heparan sulfate single chain	Single chain antibody HS4E4	1	[20]
<b>GBM</b>			
Heparan sulfate single chain	Single chain antibody HS4C3	1	[19]

### *In situ hybridization*

Kidney sections were fixed in 4% buffered formaldehyde for 24 hr and embedded in paraffin. 4  $\mu\text{m}$  sections were incubated and subjected to VEGF in situ hybridization (ISH) using a digoxigenin-labeled VEGF-A antisense RNA probe [21], as secondary antibody we used sheep anti-digoxigenin alkaline phosphatase. Detection was carried out with NBT/BCIP, the corresponding sense probe was used as a control. This ISH was followed by immunohistochemical staining with the monoclonal antibody (mAb) CK8. As secondary antibody we used biotin-labeled rabbit anti-mouse (Immunologic, Klinipath, Duiven, The Netherlands). Detection was carried out with the use of ABC Vectastain, peroxidase as label and AEC/red as substrate.

### *Transmission Electron Microscopy*

For electron microscopy, we used immersion fixation, small fragments of cortex were fixed in 2.5% glutaraldehyde dissolved in 0.1 M sodium cacodylate buffer, pH 7.4, overnight at 4°C and washed in the same buffer. The tissue fragments were postfixed in palade-buffered 2% OsO<sub>4</sub> for 1 hr, dehydrated, and embedded in Epon 812, Luft's procedure (Merck, Darmstadt, Germany). Ultrathin sections were contrasted with 4% uranyl acetate for 45 min and subsequently with lead citrate for 5 min at room temperature. Sections were examined in a Jeol 1200 EX2 electron microscope (JEOL, Tokyo, Japan).

## **RESULTS**

We studied biopsies from 2 HIV patients with collapsing FSGS and a nephrectomy specimen from a patient with pamidronate associated collapsing FSGS. The latter patient was treated with aminohydroxypropylidene bisphosphonate (APD: 'pamidronate') because of persistent hypercalcaemia after renal transplantation; she received oral APD in daily dosage of 300 mg for 20 months, 450 mg for 6 months and 600 mg for 2 months. Subsequently I.V. APD was administered in a dose of 60 mg at two-weekly intervals. Severe proteinuria was noted after the third infusion.

The HIV biopsies contained 11 and 17 different glomeruli respectively, and the paraffin block from the nephrectomy specimen contained over 77 glomeruli. The material was serially sectioned and from each specimen more than 100 sections were examined. One of every 5 sections was PAS stained for LM evaluation and intervening sections were retained for immunostainings.

In the biopsies with HIV associated nephropathy (HIVAN) we observed a wide spectrum of glomerular lesions by light microscopy. At the one end of the spectrum there were normal appearing glomeruli and at the other end glomeruli with advanced sclerosis. For our analyses we focussed on glomeruli with 'early' collapsing lesions, as defined by collapse of the glomerular tuft without, or with only minimal, sclerosis (deposition of new matrix). In these glomeruli the collapsed tuft was either still covered with a single layer of epithelial cells with only limited segmental proliferation (2 out of 28) or collapse was accompanied by a prominent increase of epithelial cells, filling Bowman's space (18 out of 28). These epithelial cells appeared activated, with enlarged nuclei with prominent nucleoli and vacuolation of the cytoplasm with the presence of reabsorption droplets (Figure 1A). Some glomeruli showed advanced sclerosis (7 out of 28) and one glomerulus appeared normal. True adhesions of the tuft to Bowman's capsule were not found when analysing serial sections. Ultrastructural analysis by transmission electron microscopy showed the presence of tubuloreticular inclusions (TRIs) in the glomerular endothelial cells of both HIV biopsies. Podocytes appeared activated

and showed foot process effacement and microvillous transformation. The podocytes in pamidronate nephropathy were enlarged and highly vacuolated. The morphological appearance of collapsing lesions in pamidronate associated cFSGS differed from those in HIVAN, as in this condition we usually observed only a single layer of epithelial cells in Bowman's space, covering the glomerular tuft (34 out of 77). In 5 of 77 glomeruli we observed segmental multilayering of epithelial cells in Bowman's space. It was noted that these cells on top of the tuft appeared severely injured with extreme vacuolation and ballooning, more so than in HIVAN (Figure 1B). Also in pamidronate associated cFSGS adhesions were not found.

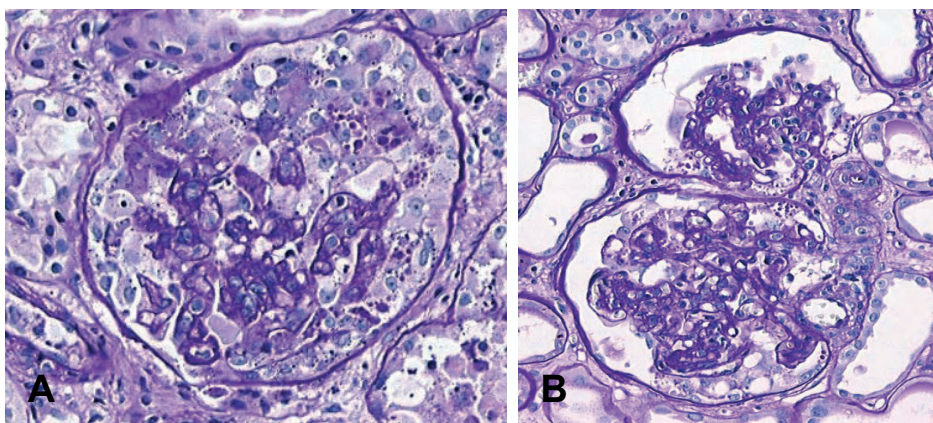


**Figure 1. Glomerular histology (PAS staining) in HIV associated cFSGS (panel A) and pamidronate associated cFSGS (panel B):** Panel A HIV associated cFSGS (HIVAN) shows a glomerulus with collapse of the capillary tuft and prominent epithelial cell proliferation in Bowman's space. Most of the glomeruli in our HIV biopsies had this appearance (18 out of 28). The epithelial cells appeared activated, with enlarged nuclei with prominent nucleoli and vacuolation of the cytoplasm with the presence of reabsorption droplets. Podocyte injury with enlargement, vacuolation and ballooning was more evident in pamidronate associated cFSGS (panel B) and multilayering of epithelial cells in Bowman's space was only sporadically and segmentally observed (A, B x450).

For phenotypic analysis of the epithelial cells in Bowman's space serial sections were stained with podocyte markers (synaptopodin, CD10, and VEGF), PEC markers (CK8 and PAX-2) and proliferation marker Ki-67. To characterise the ECM we stained with an anti-HS single chain antibody that in normal glomeruli predominantly stains Bowman's capsule and not the GBM (HS4E4) and one that stains only the GBM and the mesangial matrix (HS4C3) (markers are described in Table 1). To strengthen our findings, we additionally performed VEGF/CK8, synaptopodin/CK8 and CD10/CK8 double stainings.

In normal control kidney tissue the cells lining Bowman's capsule (PECs) uniformly stained for PAX-2 and were negative (occasional weak positivity was observed) for CK8 (not shown). Podocytes uniformly stain for synaptopodin and CD10. CD10/CALLA is not a podocyte specific marker but in humans strongly stains podocytes in addition to brush border and vascular smooth muscle cells [22]. In HIVAN normal looking glomeruli also demonstrated uniform

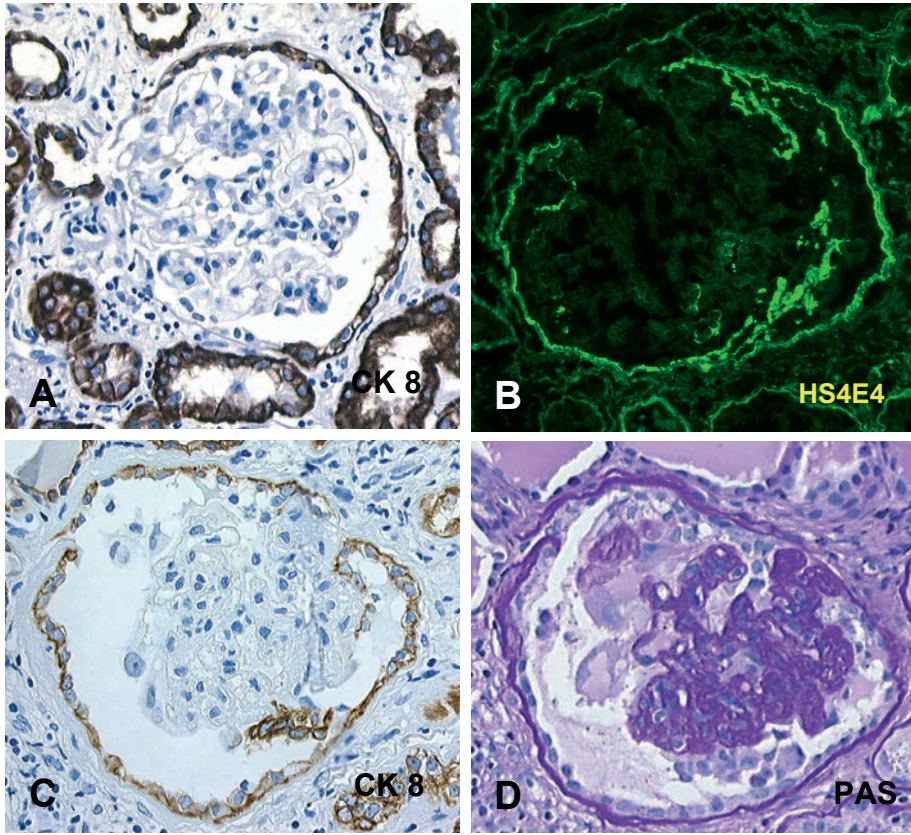


**Figure 2. Phenotype of proliferating epithelial cells in HIV associated nephropathy in segmental lesions:** Panel A shows a section of a normal looking glomerulus (no lesions) with segmental CK8 positive cells lining Bowman's capsule. The anti HS single chain antibody HS4E4 showed that newly deposited matrix in areas of epithelial proliferation stained as Bowman's capsule, shown for a glomerulus with more advanced sclerosis (Figure 2B). In glomeruli with collapse, podocyte hypertrophy and limited cell proliferation, CK8 positive cells segmentally covered the capillary tuft. These cells were always in contact with CK8 positive cells lining Bowman's capsule, as demonstrated in serial sections (Figure 2C,D) (A-D x450).

PAX-2 staining and additionally showed strong CK8 staining in a segmental pattern, compatible with activation of PECs (Figure 2A). In glomeruli with collapse and limited cell proliferation, CK8 positive cells segmentally covered the capillary tuft (Figure 2C,D). These cells were always in contact with CK8 positive cells lining Bowman's capsule. The remainder of the tuft was covered with a single layer of cells that were negative for all PEC and podocyte markers except for CD10, which was strongly and uniformly positive. In glomeruli with prominent hypercellularity epithelial proliferation was confirmed by positive staining for Ki-67 (Figure 3B). Most cells in Bowman's space were CK8 and PAX 2 positive (Figure 3A). In these glomeruli there was often no or only faint expression of synaptopodin (Figure 3C). Notably, most cells in the periphery of the glomerular tuft were positive for CD10 (Figure 3D), thus confirming that podocytes were still present. To strengthen these findings, we additionally performed

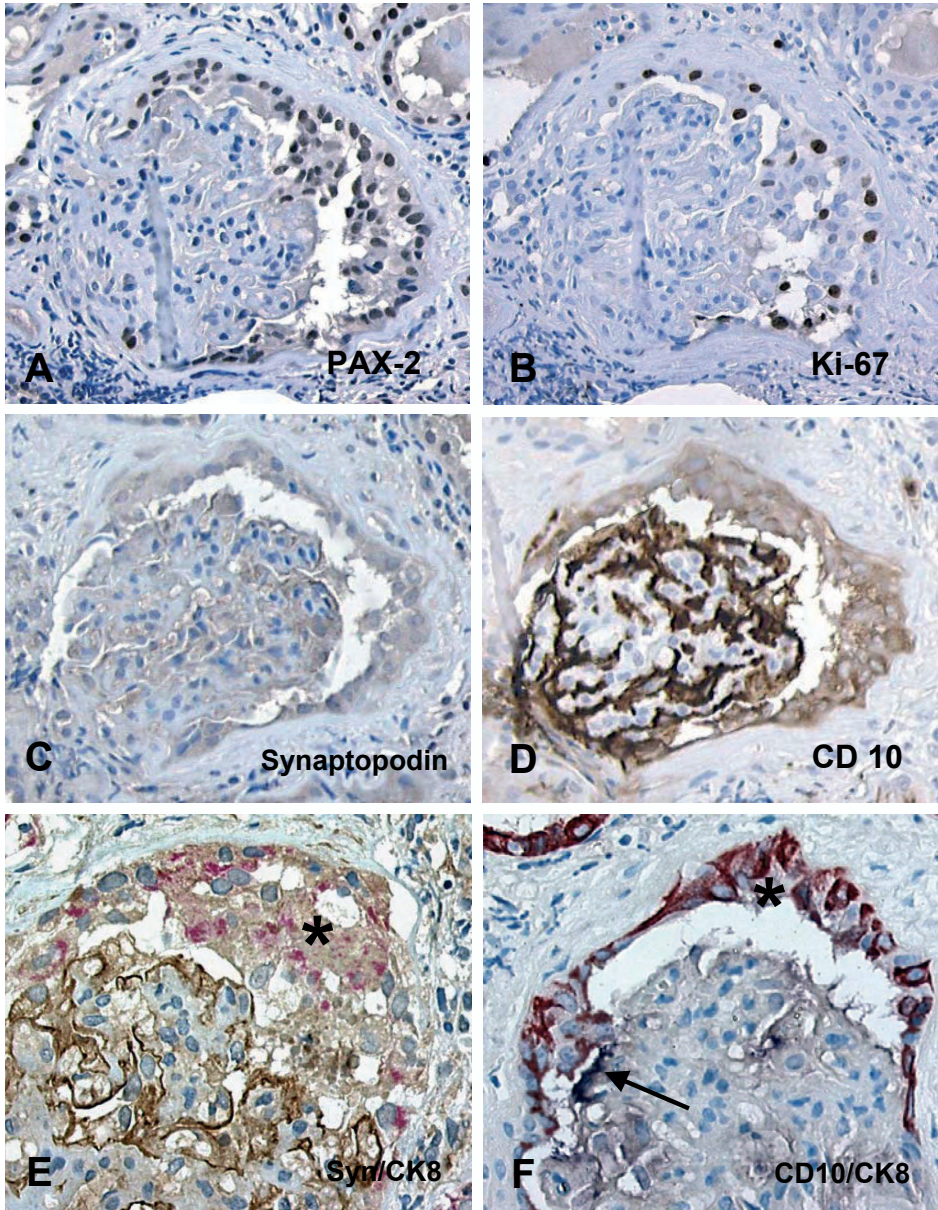


**Figure 3. Phenotype of proliferating epithelial cells in HIV associated nephropathy in glomeruli with extensive proliferation:**

In A-D serial sections are shown. The proliferating cells were mostly CK8 positive (E, F-red staining) and almost all were PAX 2 positive (panel A). Proliferation was confirmed by Ki-67 (panel B). Dedifferentiated podocytes lost expression of synaptopodin (panel C), but were still positive for CD10 (panel D). Doublestainings synaptopodin/CK8 (panel E) and CD10/CK8 (panel F) confirmed that the proliferating cells (asterisk) were positive for CK8 and are found adjacent / on top of synaptopodin or CD 10 positive residual podocytes. No cells were found doubly positive for synaptopodin/CD10 and CK8. In more advanced lesions podocytes lost all these markers. In panel F (arrow) a single podocyte has kept its expression for CD10 (A-D x450, E,F x700).



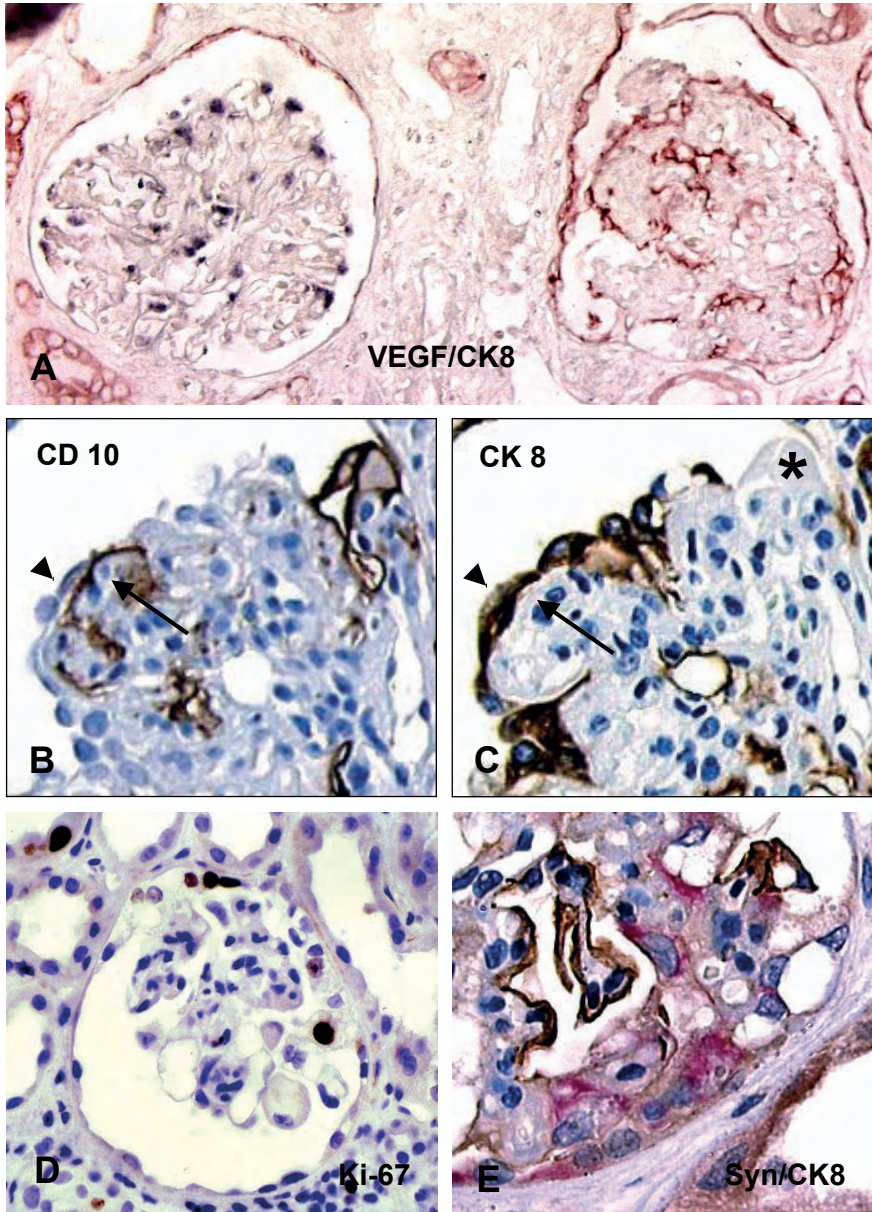


**Figure 4. Phenotype of epithelial cells in pamidronate nephropathy:** We observed a focal and segmental CK8 expression by PECs lining Bowman's capsule, in normal appearing glomeruli (Figure 4A-left, red staining). In more advanced glomerular lesions CK8 positive cells were also found overlying the capillary tuft (panel A-right). VEGF expression is present in podocytes of a normal appearing glomerulus (panel A-left, blue staining) and is absent in an affected glomerulus (panel A-right). In serial sections segmental CD10 positivity was observed (panel B, arrow), underneath CK8 positive cells (panel D, arrowhead), indicating the presence of some residual podocytes. Sometimes CK8 positive cells covering the tuft were interspersed with CK8 negative but CD10 positive cells. These CD10 positive cells showed already vacuolisation and ballooning (panel B, C, asterisk). This latter finding was also confirmed by a synaptopodin/CK8 double staining (panel E). We never observed VEGF/CK8 co-expression or synaptopodin/CK8 co-expression. Epithelial cells lining Bowman's capsule and the glomerular tuft were mitotically active (panel D) although proliferation in HIVAN was more extensive (A,D x450, B,C,E x900).

synaptopodin/CK8 (Figure 3E) and CD10/CK8 (Figure 3F) double stainings. No cells were found doubly positive for synaptopodin/CD10 or CK8. In more advanced lesions eventually the podocytes lost all these markers.

Also in pamidronate nephropathy we observed focal and segmental CK8 expression in normal appearing glomeruli (Figure 4A-left). In glomeruli with collapse CK8 positive cells were found overlying the capillary tuft (Figure 4A-right) and occasionally continuity of CK8 positive cells covering the tuft and CK8 positive cells covering Bowman's capsule was seen away from the vascular pole. VEGF expression is present in a normal appearing glomerulus (Figure 4A-left) and is absent in an affected glomerulus (Figure 4A-right). The expression pattern observed in the normal appearing glomerulus is identical to the expression observed in normal glomeruli in humans or mice (see Figure S1, as supplemental material). Ki-67 positivity was noted in PEC's covering Bowman's capsule (Figure 4D). Segmentally CD10 positivity was observed underneath CK8 positive cells (Figure 4B,C). Of note, CK8 positive cells covering the tuft were interspersed with CK8 negative CD10 positive cells, indicating the presence of residual podocytes (Figure 4C, asterisk). This latter finding was also confirmed by a synaptopodin/CK8 (Figure 4E) double staining. We never observed co-expression of CK8/PAX2 with podocytemarkers!

In both HIV and Pamidronate associated cFSGS staining with the anti HS single chain antibody HS4E4 showed that new matrix that stained as Bowman's capsule was sometimes deposited in areas of epithelial proliferation. More extensive deposition of HS4E4 positive ECM was seen in glomeruli with more advanced sclerosis (Figure 2B).

## DISCUSSION

Our study demonstrates that most of the proliferating cells in HIV and pamidronate associated collapsing FSGS are parietal epithelial cells. This conclusion is based on the finding that the proliferating cells are often positive for CK8, always positive for the PEC marker PAX2 and negative for the podocyte markers synaptopodin, CD10 and VEGF. In addition, the staining characteristics of the extracellular matrix that is produced by the proliferating cells are identical to those of Bowman's capsule. Admittedly, the use of cellular markers to define the origin of proliferating cells can be questioned, since it can be argued that cellular activation may induce phenotypic changes and could cause a switch from an activated podocyte phenotype to a parietal cell phenotype. However, the CK8 and PAX-2 positivity strongly supports the PEC origin of these cells as shown in our previous study [17]. In normal kidney PECs are negative or stain only faintly positive for CK8. In some of the normal appearing glomeruli in our patients there was strong CK8 staining of cells lining Bowman's capsule in a segmental distribution. By serial sectioning we could show that in these glomeruli adhesions between

the glomerular tuft and Bowman's capsule were absent, thus providing a strong argument that these PECs acquire the CK8 positive phenotype upon activation, prior to proliferation. Perhaps the most striking argument for our conclusion is the demonstration of CK8 positive cells on top of residual CD10 and even synaptopodin positive podocytes by double staining.

Our present findings in HIV and pamidronate associated cFSGS confirm and extend the conclusions of our previous studies. In the Thy-1.1 transgenic mouse, a model of collapsing FSGS, we observed that the proliferating epithelial cells strongly express PEC markers. In addition we noted that the staining characteristics of the newly formed ECM are identical to Bowman's capsule arguing that this matrix is produced by PECs [15]. Double staining for the podocytic transgene Thy-1.1 and the proliferation marker Ki-67 proved that there is no proliferation of podocytes during the development of FSGS lesions. Asano et al confirmed these findings in a recent study [16]. These authors have generated a transgenic mouse with podocytes that express LacZ. Injection of LMB2, an immunotoxin against the podocytic CD25 antigen, into these Nphs1-Cre/ ROSA26-loxP/NEP25 mice, causes podocyte injury characterized by vacuolar degeneration eventually leading to glomerular sclerosis. In this model proliferating epithelial cells accumulated in Bowman's space, as seen in cFSGS. These authors found no evidence for proliferation or transdifferentiation of podocyte-derived cells but did find proliferating PECs migrating onto the visceral site.

A detailed study of FSGS lesions in the kidney of a patient with recurrent idiopathic FSGS [17] revealed that also in humans the proliferating cells in collapsing lesions are parietal epithelial cells (PECs).

Although these studies firmly established a role for PECs in the cellular lesion of cFSGS in mice as well as in a patient with idiopathic FSGS, we questioned if similar events would occur in HIV associated cFSGS. HIV associated cFSGS is the prototypical example of cFSGS, characterized by a very high proliferation rate. Proliferating cells are by some authors considered to be dysregulated podocytes, but data from the literature are conflicting. Evidence from in vitro studies showed that incorporation of HIV-1 Nef induces proliferation of podocytes [23]. However, in mice podocyte specific expression of HIV-1 Nef does cause podocytes to enter the cell cycle, but does not lead to completion of mitosis [24]. A recent study in a mouse model of HIV-nephropathy (the HIV13FBV mouse) has provided additional support for our conclusions [25]. These mice express HIV-1 genes in podocytes and avid cell proliferation is observed within Bowman's space. The extracapillary proliferating cells adjacent to the parietal epithelial cells lining Bowman's capsule were often positive for Ki-67 and cytokeratin, whereas the cells adjacent to the GBM were rarely positive for Ki-67. No cells were found doubly positive for synaptopodin and Ki-67. From their observations the authors conclude that most proliferating cells in Bowman's space are derived from parietal epithelial cells [25].

Barisoni and Bariety et al proposed that the loss of specific podocyte markers defines a novel dysregulated and proliferating podocyte phenotype and suggests a common pathogenetic mechanism in collapsing FSGS [7;9]. In our studies we found that in collapsing idiopathic FSGS and HIV-associated nephropathy, there was disappearance of podocyte markers, consistent with dedifferentiation. Synaptopodin disappeared very early but remarkably CD10/CALLA [26] remained positive longer, to disappear in advanced lesions. Other investigators also observed a variable degree of expression reduction for different podocyte markers, especially in unaffected portions of the tuft in segmentally injured glomeruli, or in glomeruli without any visible collapse or other histologic abnormalities [7]. Our findings are therefore consistent with dysregulation of podocytes but do not support proliferation of podocytes.

To summarize our data, in HIV and pamidronate associated cFSGS we do find dedifferentiation of podocytes but most of the epithelial cells in Bowman's space are derived from the parietal epithelium. These findings are similar to what we previously observed in a patient with recurrent idiopathic FSGS in both the segmental collapsing lesions and non-collapsing FSGS lesions with prominent epithelial hyperplasia. Therefore, it can be argued that in all forms of FSGS with prominent epithelial hyperplasia there is proliferation of PECs and that in this respect collapsing FSGS can be included in the spectrum of FSGS and need not be regarded as a distinct entity caused by a dysregulated podocyte phenotype. It can be hypothesized that a common pathogenetic mechanism applies to all variants of FSGS and that the type of lesion that is seen depends on the extent of podocyte activation. In FSGS secondary to hyperfiltration (often peri-hilar variant), podocyte activation may be focal and mere loss of podocytes with subsequent adherence of PECs to the glomerular tuft results in sclerosis [5]. If podocyte activation is more widespread and acute, as we believe is the case in primary (idiopathic) FSGS, PEC proliferation is more prominent. Presumably, PEC proliferation is the direct result of interactions between activated podocytes and PECs and growth factors produced by podocytes may play an important role. In HIV associated collapsing FSGS prominent epithelial proliferation follows massive podocyte activation upon integration of the viral genome. In pamidronate collapsing FSGS rapid widespread toxic loss of podocytes may lead to the collapsing phenotype with less PEC proliferation as compared to HIV associated collapsing FSGS.

## CONCLUSION

Most of the proliferating cells in collapsing glomerulopathy are derived from the parietal epithelium. This conclusion holds for all forms of cFSGS i.e. idiopathic, Pamidronate and HIV associated FSGS.

## ACKNOWLEDGEMENTS

We gratefully acknowledge dr. William Leenders for providing the VEGF-probe, the members of the EM-, Immuno/ISH laboratory (all of the Department of Pathology, University Medical Center Nijmegen, Nijmegen), for their expert technical assistance.

Ing. B. Smeets is supported by a grant from the Dutch Kidney Foundation (NSN nr. C04.2079)

## SUPPLEMENTARY MATERIAL

Figure S1. In situ hybridisation of mRNA VEGF in (A,B) normal human and (C) mice glomeruli.

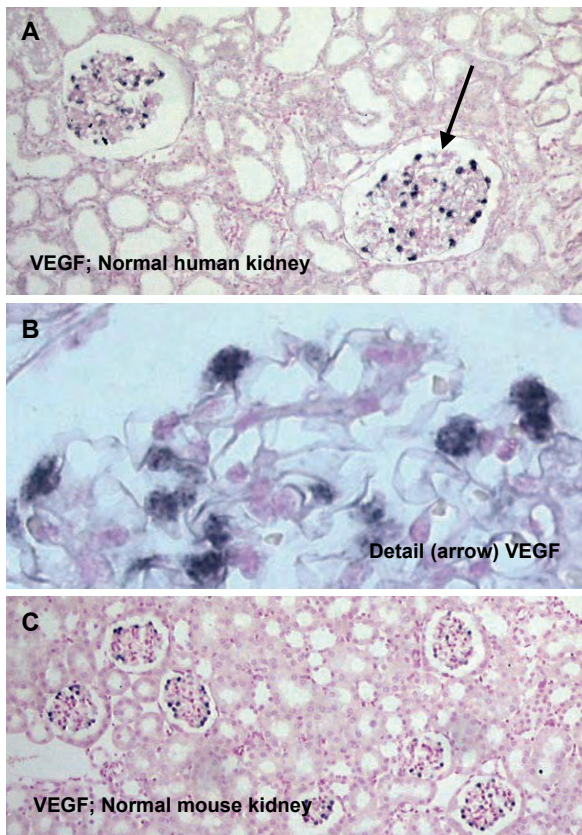


**Figure S1.** In situ hybridisation of mRNA VEGF in (A,B) normal human and (C) mice glomeruli.

## REFERENCES

1. Haas M, Meehan SM, Karrison TG *et al.*: Changing etiologies of unexplained adult nephrotic syndrome: a comparison of renal biopsy findings from 1976-1979 and 1995-1997. *Am J Kidney Dis* 30:621-631, 1997.
2. D'Agati V: Pathologic classification of focal segmental glomerulosclerosis. *Semin Nephrol* 23:117-134, 2003.
3. Kriz W, Elger M, Nagata M *et al.*: The role of podocytes in the development of glomerular sclerosis. *Kidney Int Suppl* 45:S64-72.:S64-S72, 1994.
4. Kriz W, Kretzler M, Nagata M *et al.*: A frequent pathway to glomerulosclerosis: deterioration of tuft architecture-podocyte damage-segmental sclerosis. *Kidney Blood Press Res* 19:245-253, 1996.
5. Kriz W, Gretz N, Lemley KV: Progression of glomerular diseases: is the podocyte the culprit? *Kidney Int* 54:687-697, 1998.
6. Mundel P, Shankland SJ: Podocyte biology and response to injury. *J Am Soc Nephrol* 13:3005-3015, 2002.
7. Barisoni L, Kriz W, Mundel P *et al.*: The dysregulated podocyte phenotype: a novel concept in the pathogenesis of collapsing idiopathic focal segmental glomerulosclerosis and HIV-associated nephropathy. *J Am Soc Nephrol* 10:51-61, 1999.
8. Barisoni L, Mokrzycki M, Sablay L *et al.*: Podocyte cell cycle regulation and proliferation in collapsing glomerulopathies. *Kidney Int* 58:137-143, 2000.
9. Bariety J, Nochy D, Mandet C *et al.*: Podocytes undergo phenotypic changes and express macrophagic-associated markers in idiopathic collapsing glomerulopathy. *Kidney Int* 53:918-925, 1998.
10. Bariety J, Bruneval P, Hill G *et al.*: Posttransplantation relapse of FSGS is characterized by glomerular epithelial cell transdifferentiation. *J Am Soc Nephrol* 12:261-274, 2001.
11. Barisoni L, Kopp JB: Modulation of podocyte phenotype in collapsing glomerulopathies. *Microsc Res Tech* 57:254-262, 2002.
12. Nagata M, Horita S, Shu Y *et al.*: Phenotypic characteristics and cyclin-dependent kinase inhibitors repression in hyperplastic epithelial pathology in idiopathic focal segmental glomerulosclerosis. *Lab Invest* 80:869-880, 2000.
13. Nagata M, Tomari S, Kanemoto K *et al.*: Podocytes, parietal cells, and glomerular pathology: the role of cell cycle proteins. *Pediatr Nephrol* 18:3-8, 2003.
14. Kihara I, Yaoita E, Kawasaki K *et al.*: Origin of hyperplastic epithelial cells in idiopathic collapsing glomerulopathy. *Histopathology* 34:537-547, 1999.
15. Smeets B, Te Loeke NA, Dijkman HB *et al.*: The parietal epithelial cell: a key player in the pathogenesis of focal segmental glomerulosclerosis in Thy-1.1 transgenic mice. *J Am Soc Nephrol* 15:928-939, 2004.
16. Asano T, Niimura F, Pastan I *et al.*: Permanent genetic tagging of podocytes: fate of injured podocytes in a mouse model of glomerular sclerosis. *J Am Soc Nephrol* 16:2257-2262, 2005.
17. Dijkman H, Smeets B, van der Laak J *et al.*: The parietal epithelial cell is crucially involved in human idiopathic focal segmental glomerulosclerosis. *Kidney Int* 68:1562-1572, 2005.
18. Assmann KJ, Tangelder MM, Lange WP *et al.*: Membranous glomerulonephritis in the mouse. *Kidney Int* 24:303-312, 1983.
19. van Kuppevelt TH, Dennissen MA, van Venrooij WJ *et al.*: Generation and application of type-specific anti-heparan sulfate antibodies using phage display technology. Further evidence for heparan sulfate heterogeneity in the kidney. *J Biol Chem* 273:12960-12966, 1998.
20. Dennissen MA, Jenniskens GJ, Pieffers M *et al.*: Large, tissue-regulated domain diversity of heparan sulfates demonstrated by phage display antibodies. *J Biol Chem* 277:10982-10986, 2002.
21. Leenders WP, Kusters B, Verrijp K *et al.*: Antiangiogenic therapy of cerebral melanoma metastases results in sustained tumor progression via vessel co-option. *Clin Cancer Res* 10:6222-6230, 2004.
22. Ronco P, Ardaillou N, Verroust P *et al.*: Pathophysiology of the podocyte: A target and a major player in glomerulonephritis. *Adv Nephrol Necker Hosp* 23: 91-131, 1994.
23. He JC, Husain M, Sunamoto M *et al.*: Nef stimulates proliferation of glomerular podocytes through activation of Src-dependent Stat3 and MAPK1,2 pathways. *J Clin Invest* 114:643-651, 2004.
24. Husain M, D'Agati VD, He JC *et al.*: HIV-1 Nef induces dedifferentiation of podocytes in vivo: a characteristic feature of HIVAN. *AIDS* 19:1975-1980, 2005.

25. Zhong J, Zuo Y, Ma J *et al.*: Expression of HIV-1 genes in podocytes alone can lead to the full spectrum of HIV-1-associated nephropathy. *Kidney Int* 68:1048-1060, 2005.
26. Platt JL, LeBien TW, Michael AF: Stages of renal ontogenesis identified by monoclonal antibodies reactive with lymphohemopoietic differentiation antigens. *J Exp Med* 157:155-172, 1983.

# 7

## **GLOMERULAR INVOLUTION: AN UNRECOGNIZED FORM OF GLOMERULOSCLEROSIS?**

Henry B.P.M. Dijkman, Jack F.M. Wetzels<sup>1</sup>,  
Johanna H. Gemmink, Elena N. Levtchenko<sup>2</sup>  
and Eric J. Steenbergen

*Department of Pathology, Nephrology<sup>1</sup>, Pediatric  
Nephrology<sup>2</sup>, Radboud University Nijmegen Medical  
Centre, Nijmegen, the Netherlands*

**Kidney International 2006; Accepted for  
publication in combination with chapter 8**



## ABSTRACT

Global glomerulosclerosis can be divided in the vascular (obsolescent) type and the glomerulopathic (solidified) type. In biopsies from children with recurrent nephrotic syndrome we noticed small, globally sclerosed glomeruli that appeared to be distinct from global glomerulosclerosis. These small sclerosed glomeruli, best described as involuted glomeruli, are characterised by a marked reduction in size and a lack of accompanying tubular atrophy and interstitial fibrosis.

We have characterised these involuted glomeruli in detail by light microscopy and electron microscopy. Via immunostainings we have studied the expression of markers for podocytes (synaptopodin, CD10), parietal epithelial cells (PAX-2), miscellaneous matrix components (Col I, III & IV), endothelium (CD 34), myofibroblasts (SMA) and made a comparison with the classical vascular type and glomerulopathic type.

The involuted glomeruli contain discontinuous matrix components which form an interconnecting network with matrix continuity (adhesions) between the glomerular tuft and Bowman's capsule. They can be differentiated from the other types of global glomerulosclerosis. Most notable is the presence of vital podocytes and parietal epithelial cells, which have retained their staining characteristics, in between the matrix, and the absence of periglomerular and peritubular inflammation.

Our study demonstrates that glomerular involution is a special form of global glomerulosclerosis. The absence of periglomerular and tubulo-interstitial fibrosis suggests a different pathogenesis.

**Keywords:** global glomerulosclerosis, parietal epithelial cell, podocyte, periglomerular fibrosis, glomerulopathic glomerulosclerosis, vascular glomerulosclerosis, involution.

## INTRODUCTION

With advancing age the number of globally sclerosed glomeruli in the human kidney increases. This is a more or less physiological phenomenon that is related to arteriosclerosis. More than 10% globally sclerosed glomeruli is considered as pathological for persons over the age of 40 years [1;2]. Two types of global glomerulosclerosis can be distinguished: the vascular type (also referred to as obsolescent type) and the glomerulopathic type (also referred to as solidified type) [3]. Vascular glomerulosclerosis is characterised by a retracted glomerular tuft without tuft adhesions, surrounded by a hypocellular homogeneous collagenous matrix in the former Bowman's space (only recognizable in a silver or PAS stain). Glomerulopathic sclerosis is characterized by a solidified non-retracted glomerular tuft with often recognizable tuft adhesions and without the homogeneous collagenous matrix in Bowman's space. The former is mostly associated with decreased perfusion resulting from arterial intimal fibrosis in aging or hypertension, whereas the latter form is the result of ongoing damage in glomerular diseases. It has been suggested that global sclerosis may also occur without renal disease as part of a normal damage and repair process. In fact, globally sclerosed glomeruli have been found in children below the age of 2 years [4]. Notably, global glomerulosclerosis is always accompanied by tubulo-interstitial fibrosis. In recent years Kriz and co-workers have proposed the concept of misdirected filtration as a mechanism by which glomerulosclerosis leads to periglomerular and tubulointerstitial fibrosis [5].

We recently noticed globally sclerosed glomeruli that appeared to be distinct from either vascular or glomerulopathic glomerulosclerosis in biopsies from children with recurrent nephrotic syndrome. These sclerosed glomeruli are characterised by a marked reduction in size and apparent lack of accompanying tubular atrophy and interstitial fibrosis. Small globally sclerosed glomeruli in the setting of congenital or childhood nephrotic syndrome in children < 1 year have been previously noticed by others and were referred to as 'microglomeruli' in the old literature [6]. However, it has not been investigated whether these glomeruli truly represent a distinct type of sclerosis. It was reported that their presence does not predict prognosis in the setting of congenital nephrotic syndrome, but other than that their potential meaning has not been addressed. In the present study we have characterised these glomeruli in detail by light microscopy, immunostainings and electron microscopy, and made a comparison with the classical vascular type of glomerulosclerosis and the glomerulopathic type of glomerulosclerosis in the setting of focal and segmental glomerulosclerosis. Our findings indicate that the small globally sclerosed glomeruli in the setting of childhood nephrotic syndrome represent a unique type of glomerular injury, best described by the term glomerular involution. We hypothesize that this is a special form of glomerulosclerosis with a different pathogenesis.

## METHODS

### *Patients*

Small glomeruli are often recognized in renal biopsies of children with minimal change disease. We have counted the number of small globally sclerosed glomeruli in the biopsies of 8 children (age 3-9 years) with minimal change nephropathy. All patients had presented with a nephrotic syndrome and were biopsied because of a frequent relapsing or steroid dependent course. For comparison we studied 5 biopsies from children without proteinuria. Their primary diagnosis was hyperoxaluria and thin basement membrane nephropathy. To investigate the involuted glomeruli in more detail we used biopsies of three patients with minimal change disease. For comparison we used nephrectomy specimens with evidence of the other types of global glomerulosclerosis. Vascular sclerosis was investigated in the normal cortex of a male, 74 years old patient, nephrectomized because of a renal clear cell carcinoma. We studied the solidified type of global sclerosis in a nephrectomized kidney from a patient with end stage FSGS.

### Light microscopy, Immunohistochemistry and Electron Microscopy

#### *Light microscopy*

For light microscopy, kidney fragments were fixed in Bouin's solution or formaldehyde, dehydrated, and embedded in paraplast (Amstelslad, Amsterdam The Netherlands). 2  $\mu$ m sections were stained with periodic acid-Schiff, and with silver methenamine.

#### *Immunohistochemistry*

Immunohistochemical staining was performed on kidney sections fixed in 4% buffered formaldehyde for 24 hr fixation and embedded in paraffin. 4  $\mu$ m sections were incubated with monoclonal antibodies (mAb) and polyclonal antibodies (pAb) directed at various markers for podocytes, parietal epithelial cells (PECs), macrophages, endothelium, myofibroblasts and matrix components such as collagen as detailed in table 1. As secondary antibody we used powervision Poly-HRP-anti Mouse/Rabbit/Rat IgG (Immunologic, Klinipath, Duiven, The Netherlands). Detection was carried out with the use of peroxidase as label and diaminobenzidine as substrate.

#### *Transmission Electron Microscopy*

For electron microscopy, we used immersion fixation. Small fragments of cortex were fixed in 2.5% glutaraldehyde dissolved in 0.1 M sodium cacodylate buffer, pH 7.4, overnight at 4°C and washed in the same buffer. The tissue fragments were postfixated in palade-buffered 2% OsO<sub>4</sub> for 1 hr, dehydrated, and embedded in Epon 812, Luft's procedure (Merck, Darmstadt, Germany). Ultrathin sections were contrasted with 4% uranyl acetate for 45 min and subse-

quently with lead citrate for 5 min at room temperature. Sections were examined in a Jeol 1200 EX2 electron microscope (JEOL, Tokyo, Japan).

**Table 1:** Antibodies used for the detection of glomerular antigens

Antigen	Primary antibody	Dil.	Supplier / Reference
<b>Podocyte components</b>			
Synaptopodin	Mouse anti-synaptopodin	1	Progen, Heidelberg, Germany
CD 10	Mouse anti human CD10	50	Monosan, Caltag lab.,Burlinggame
<b>PEC components</b>			
PAX-2	Rabbit anti human PAX-2	50	Zymed laboratories Inc. San Francisco, USA
Cytokeratin	Mouse anti human CAM 5.2 (CK8)	50	BD Biosciences, San Diego, CA
<b>Miscellaneous</b>			
$\alpha$ smooth muscle actin	Mouse anti human SMA	15000	Sigma, St. Louis, USA
Endothelium	Mouse anti human CD34	40	Monosan, Caltag lab.,Burlinggame
Vimentin	Mouse anti human Vimentin	800	Biogenex, Ramon, CA
Collagen IV	Mouse anti human Collagen IV	1250	Sigma, St. Louis, USA
Collagen IV $\alpha$ 1	Mouse anti- $\alpha$ 1 collagen	40	Wieslab, Lund, Sweden
Collagen IV $\alpha$ 5	Mouse anti- $\alpha$ 5 collagen	10	Wieslab, Lund, Sweden
Collagen I	Rabbit anti human Collagen I	40	Monosan, Caltag lab.,Burlinggame
Collagen III	Mouse anti human Collagen III	10	Monosan, Caltag lab.,Burlinggame
Macrophage	Mouse anti human CD68	2000	Dako, Glostrup, Denmark

## RESULTS

We noticed the presence of small globally sclerosed glomeruli without accompanying interstitial changes in children with recurrent nephrotic syndrome. An initial survey of 8 biopsies from children (age 3-9 years) with recurrent nephrotic syndrome and diagnosed as having minimal change nephropathy, showed that this type of sclerosed glomeruli was present in 21 out of 177 glomeruli (12%). In comparison, these small sclerosed glomeruli were never seen (0 out of 70 glomeruli) in 5 biopsies from children (age 2-10 years) with non nephrotic kidney disease. We have characterized these small sclerosed glomeruli, which will be referred to as glomerular involution, in detail and made comparison with globally sclerosed glomeruli of the glomerulopathic type and vascular type.

### *Morphology*

As compared to the classical forms of global sclerosis, in involution there is a marked reduction in diameter (approximately a quarter of the diameter of an open glomerulus). In the silverstainings with low power magnification involuted glomeruli appear as small black nodules without apparent accompanying interstitial changes (Figure 1A). For comparison see Figure 2A and 2B for globally sclerosed glomeruli of the glomerulopathic and vascular type respectively. In fact, if present in low numbers involuted glomeruli can easily be overlooked. They are mostly evenly distributed throughout the cortex, although sometimes there is a

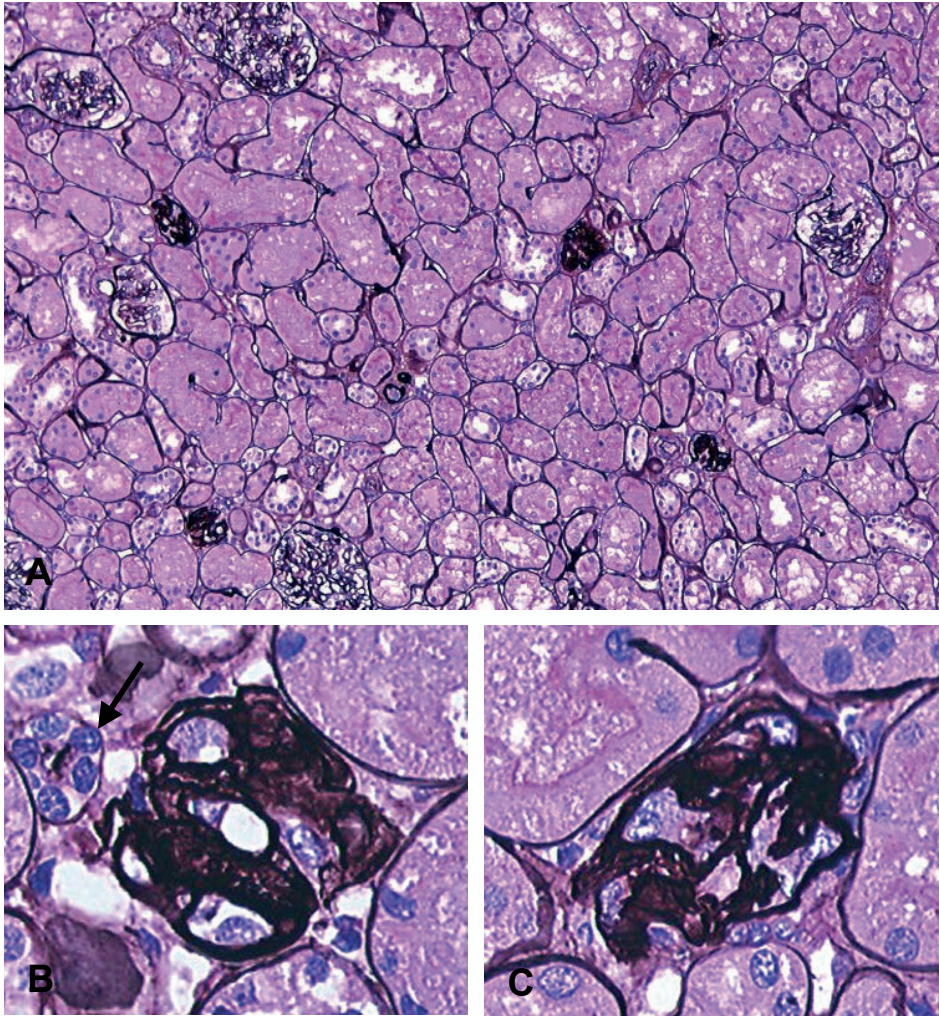


**Figure 1. Histology, silver methenamine staining:** With low magnification involuted glomeruli appear as small black nodules (panel A). They are distributed throughout the cortex, without the presence of accompanying interstitial changes. In detail, the extracellular matrix strongly stains a network composed of remnants of the GBM and Bowman's capsule (panel B,C). Embedded in the matrix there is a certain number of vital appearing cells. Sporadically atrophic tubules can be seen close to involuted glomeruli (panel B, arrow) (A x150, B,C x750).

predominant subcapsular localisation. On closer examination involuted glomeruli are made up of strong staining (non hyalinized) extracellular matrix, comparable to the matrix observed in glomerulopathic sclerosis. This matrix, likely composed of remnants of the GBM and Bowman's capsule, has the appearance of an interconnecting network in continuity (adhesions) with the former glomerular tuft and Bowman's capsule (Figure 1B,C). In addition, a small number of vital appearing cells are usually seen unlike in vascular sclerosis, where the contracted tuft does usually not contain any cells (see below). Remarkably, there is no splitting or duplication of Bowman's capsule, as is usually observed in glomerulopathic sclerosis.

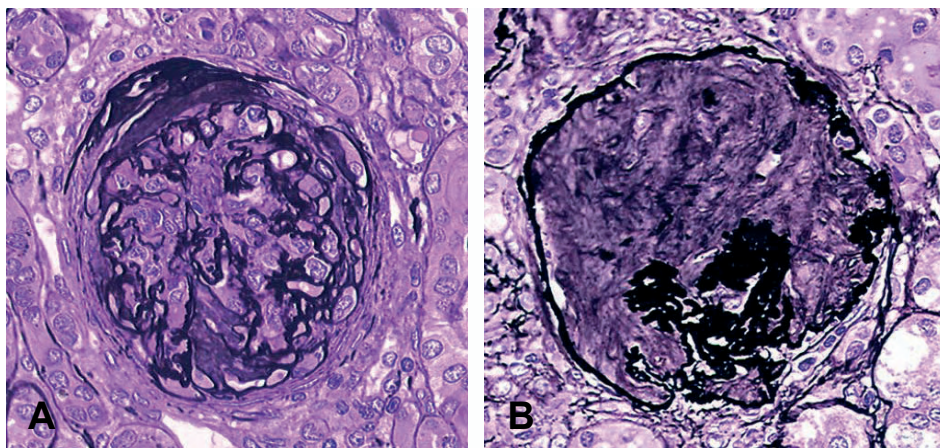


**Figure 2. Types of global glomerulosclerosis:** An example of glomerulopathic glomerulosclerosis also referred to as solidified type as shown in panel A. Glomerulopathic glomerulosclerosis is characterized by a solidified non-retracted glomerular tuft with often recognizable tuft adhesions, splitting of Bowman's capsule and prominent periglomerular fibrosis. An example of vascular glomerulosclerosis is shown in panel B. This type is characterised by the retracted glomerular tuft, surrounded by a hypocellular homogeneous collagenous matrix in the former Bowman's space, without tuft adhesions. There usually is moderate periglomerular fibrosis (A, B  $\times 500$ ).

Also, there is no stromal reaction or hypercellularity of the surrounding interstitium, which is usually markedly present in glomerulopathic sclerosis and to a lesser extent also in vascular sclerosis. A few atrophic tubular structures, probably remnants of the tubular apparatus, can often be identified in proximity of involuted glomeruli (Figure 1B, arrow). Electron microscopy confirmed the presence of vital appearing cells that cover either the GBM or Bowman's capsule in the involuted glomeruli, whereas these are absent in the other types of global glomerulosclerosis (data not shown). Identifiable interrupted stretches of glomerular basement membrane are seen and both the GBM and Bowman's capsule are in part thickened (Figure 3, arrows).

### *Immunohistochemistry*

We characterized the three types of global glomerulosclerosis, glomerular involution (Figure 4-6, A-D), glomerulopathic glomerulosclerosis (Figure 4-6, E-H), and vascular glomerulosclerosis (Figure 4-6, I-L), by immunostainings for synaptopodin and CD10 (podocytes), CK8 and PAX2 (parietal cells), CD68 (macrophages),  $\alpha$  smooth muscle actin, (myofibroblasts, mesangial cells), CD34 (endothelium), vimentin and extracellular matrix components collagen I, III and IV and the  $\alpha 1$  and  $\alpha 5$  chain of collagen IV (Table 1).

Remarkably, in involuted glomeruli some of the remaining cells stained for podocyte markers synaptopodin (Figure 4 B) and CD10 (Figure 4 C) and for PEC marker PAX-2 (Figure 4 D), whereas cells positive for these markers were neither seen in glomerulopathic sclerosis nor in vascular sclerosis (Parallel panels).

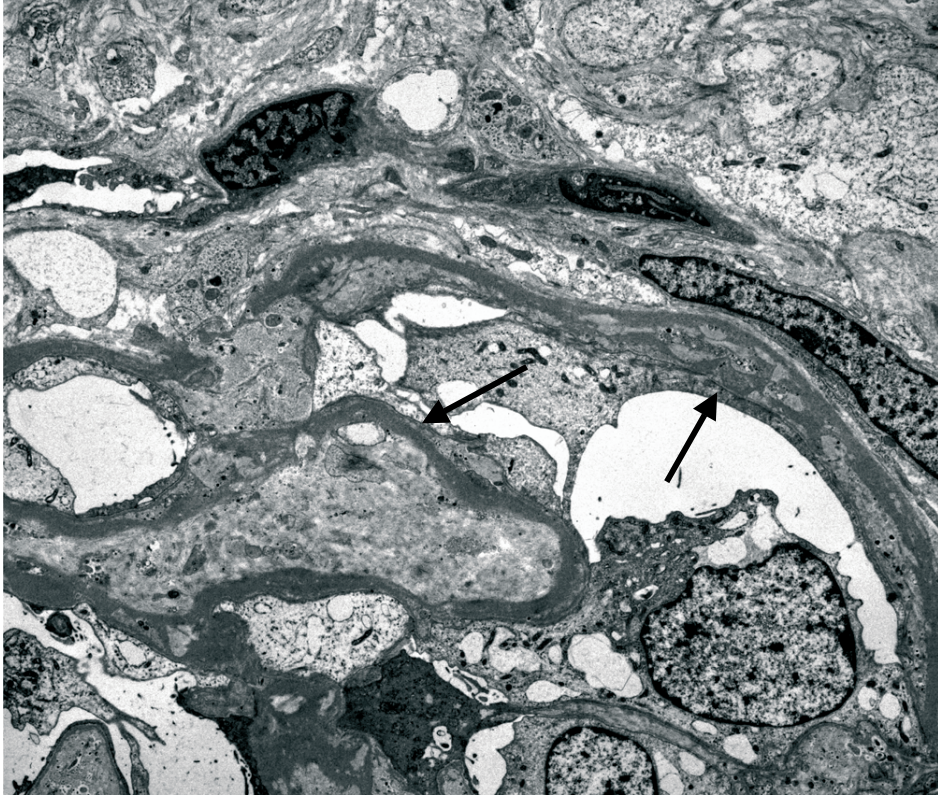


**Figure 3. Transmission electron microscopy of an involuted glomerulus:** The observations by light microscopy (Figure 1) are confirmed at high magnification by EM. Involuted glomeruli show an interconnecting network of GBM and Bowman's capsule. Vital appearing cells are present. Cells which cover the GBM show foot process effacement and sometimes a single cell forms bridges between Bowman's capsule and the GBM (arrows). The former GBM and Bowman's capsule are thickened by irregular duplication and matrix deposition (x7000).

The extracellular matrix characteristics of the different types are depicted in figure 5. Collagen III was negative in all types of sclerosis (not shown). The hyalinized extracellular matrix filling Bowman's space in vascular sclerosis was strongly positive for collagen I (Figure 5J), whereas collagen I was not detected in involuted glomeruli (Figure 5B) or glomerulopathic sclerosis (Figure 5F). Collagen IV stains all of the matrix in involution and glomerulopathic sclerosis and only the contracted glomerular tuft in vascular sclerosis (Figure 5A,E,I). There was staining for both the  $\alpha$ -1 and  $\alpha$ -5 chain of collagen IV in involuted glomeruli (Figure 5C,D), and glomerulopathic sclerosis (Figure 5G,H), whereas in vascular sclerosis the Bowman's capsule was stained for the  $\alpha$ -1 chain (Figure 5K) and the contracted tuft stained only for  $\alpha$ -5 (Figure 5L).

CK8 positivity, a marker for activated parietal epithelial cells, was not seen (Figure 6A). CK8 is not normally expressed in glomeruli, but can become expressed on parietal cells in focal and segmental glomerulosclerosis (FSGS) [7]. We observed residual staining in involuted glomeruli for smooth muscle actin (Figure 6B) and CD34 (Figure 6C), possibly representing

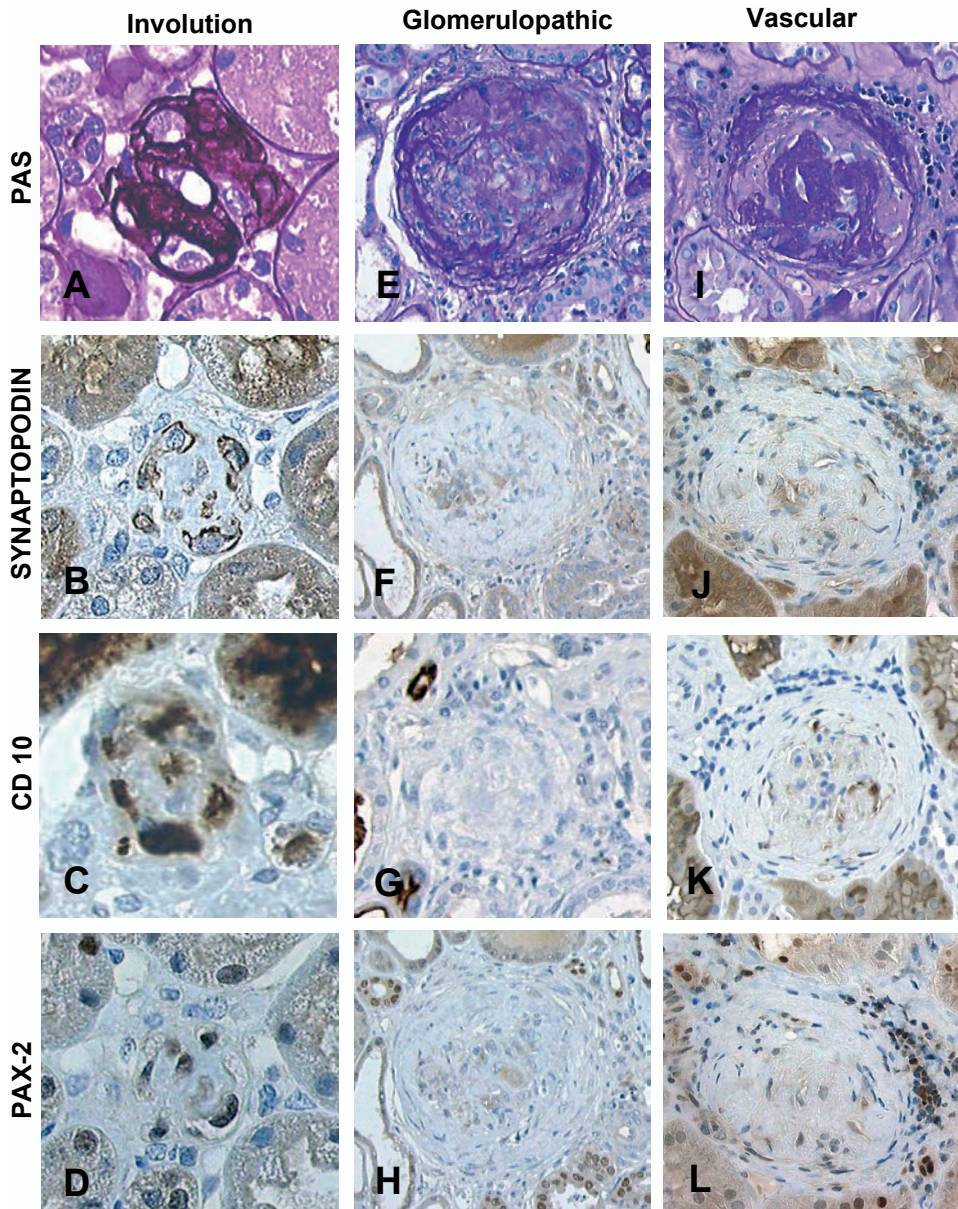


**Figure 4. Phenotype of glomerular cells:** Cells in glomerular involution (panel A-D), glomerulopathic glomerulosclerosis (panel E-H) and vascular glomerulosclerosis (panel I-L). Light microscopy (PAS staining) is shown in panel A, E and I. Podocytemarkers synaptopodin (panel B), CD 10 (panel C) and the parietal epithelial cells marker (PAX-2, panel D) are still expressed in involuted glomeruli and not in the other two types of glomerulosclerosis (A-D x400, E-L x250).



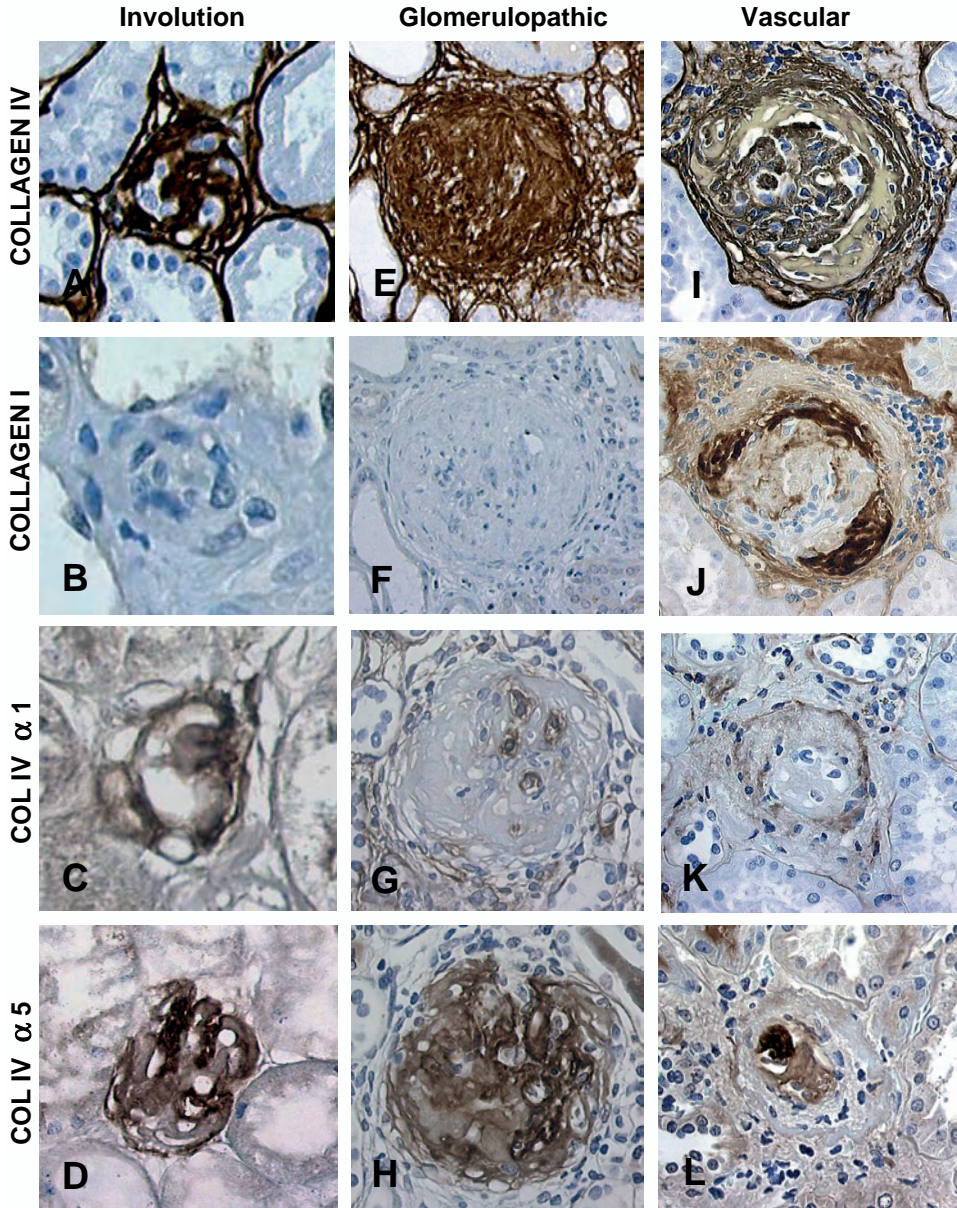


**Figure 5. Extracellular matrix characteristics:** Cells in glomerular involution (panel A-D), glomerulopathic glomerulosclerosis (panel E-H) and vascular glomerulosclerosis (panel I-L). Collagen IV stains all of the matrix in glomerular involution (panel A), glomerulopathic sclerosis (panel E) and only the contracted glomerular tuft in vascular glomerulosclerosis (panel I). Collagen I only stains the hyalinized extracellular matrix filling Bowman's space in vascular glomerulosclerosis (panel J). The interconnecting network in involuted glomeruli stains for both the  $\alpha$ -1 and  $\alpha$ -5 chain of collagen IV (panel C,D). Staining of the  $\alpha$ -1 and  $\alpha$ -5 chain of collagen IV was also seen in glomerulopathic glomerulosclerosis (panel G,H), whereas in vascular glomerulosclerosis Bowman's capsule stains for the  $\alpha$ -1 chain (panel K) and the contracted tuft stains for the  $\alpha$ -5 chain of collagen IV (panel L) (A-D x400, E-L x250).

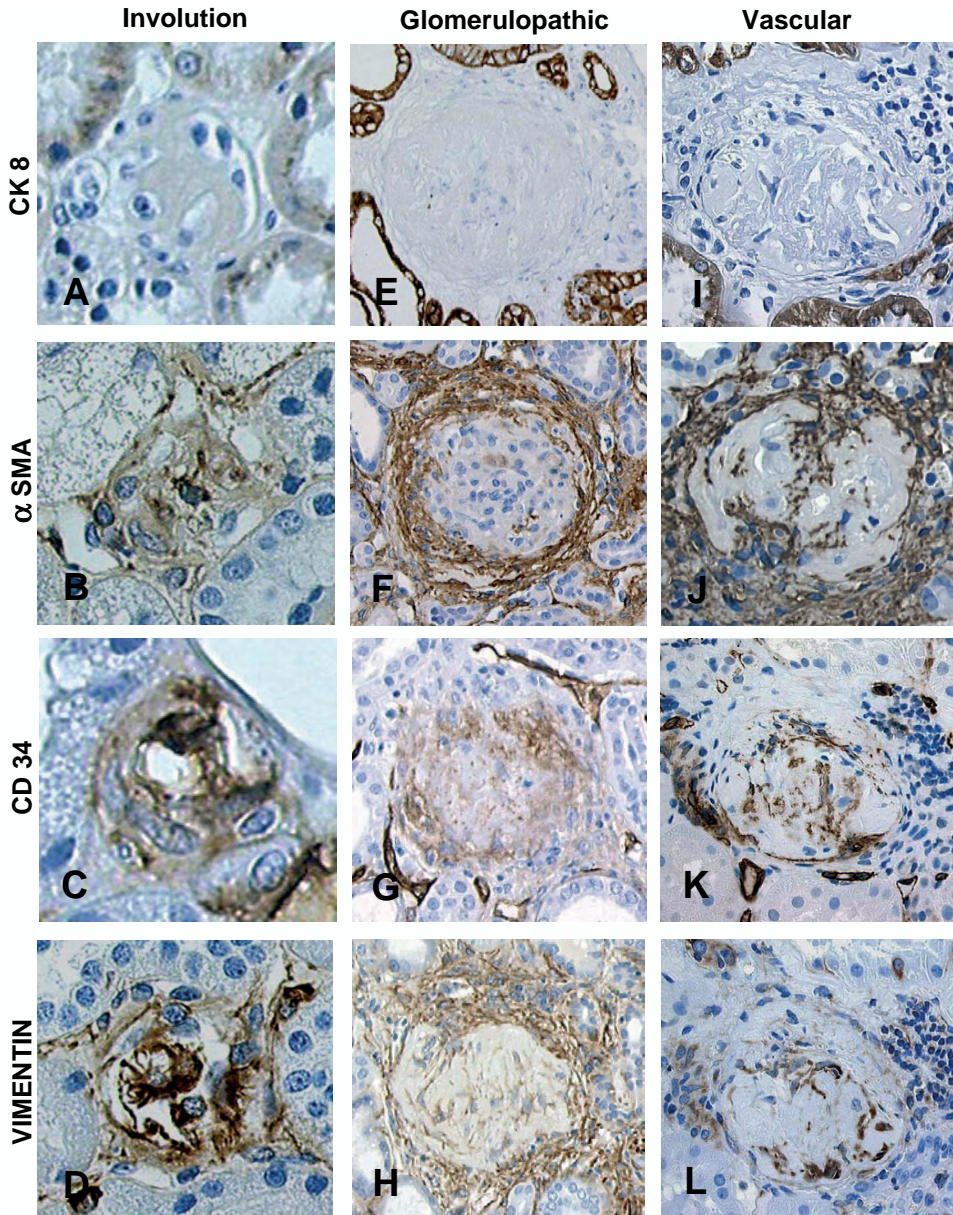


**Figure 6. Staining characteristics of the periglomerular region:** Cells in glomerular involution (panel A-D), glomerulopathic glomerulosclerosis (panel E-H) and vascular glomerulosclerosis (panel I-L). CK8 is an activation marker of PECs in FSGS, is not expressed within the different types of sclerosed glomeruli but only stains tubular epithelium (panel A,E,I). In glomerulopathic and vascular sclerosis the periglomerular fibrosis is highlighted by staining for vimentin and  $\alpha$  SMA (myofibroblasts) and CD34 (periglomerular capillaries). Note the absence of interstitial reaction in glomerular involution (panel B,D) (A-D x400, E-L x250).

residual endothelial cells and mesangial cells. Intriguingly SMA staining was almost absent in the periglomerular region of the involuted glomeruli (Figure 6B), this in contrast to the staining which was very pronounced in glomerulopathic sclerosis and in vascular sclerosis (Figure 6F,J). Staining of capillary remnants for CD34 was observed in vascular sclerosis and involuted glomeruli, but not in glomerulopathic sclerosis (Figure 6C,G,K).

The remarkable absence of interstitial changes accompanying glomerular involution was further highlighted by vimentin (Figure 6D,H,L), staining which showed prominent periglomerular expression in glomerulopathic sclerosis but not in involuted glomeruli.

All typical glomerular characteristics of the three forms of glomerulosclerosis are listed in table 2.

**Table 2:** Typical characteristics of the different types

Glomerular Components	Normal	involution	Glomerulopathic sclerosis	Vascular sclerosis
<b>Podocyte components</b>				
Synaptopodin	+++	++	=	=
CD 10	++++	++	=	=
<b>PEC components</b>				
PAX-2	+++	++	=	=
Cytokeratin 8	=	=	=	=
<b>Proliferation</b>				
KI 67	=	=	=	=
<b>Miscellaneous</b>				
Macrophage (CD68)	=	=	=	=
$\alpha$ -smooth muscle actin				
- intra glomerular	+	+	+	+
- peri glomerular	=	=	+++	+++
Endothelium (CD34)	+++	++	=	++
Collagen IV	+	++	+++	=(BS) / ++(T)
Collagen I	=	=	=/+	++++(BS)
Collagen III	=	=	=	=
<b>Glomerular volume</b>	Normal 150-250 $\mu$ m	Very small 30-70 $\mu$ m	Normal 150-250 $\mu$ m	Normal 150-250 $\mu$ m

Abbreviations: BS-Bowman's space, T-Glomerular tuft

## DISCUSSION

Our findings justify the conclusion that glomerular involution is a type of glomerulosclerosis distinct from glomerulopathic and vascular glomerulosclerosis. The most evident distinguishing features are reduced size, remaining vital cells that stain for podocyte and parietal markers and a remarkable absence of interstitial damage.

It is likely that glomerular involution has been noted by other investigators although a clear description is lacking. Emery et al described glomerular involution and scarring in children, a process unlikely to be the result of vascular injury [4]. They observed these scarred glomeruli in children, occurring predominantly in children aged < 2 years, with preferential localisation in the subcapsular region and in proximity to the arcuate vessels. In the paper glomerular involution is described as the presence of small solid masses of connective tissue like material lacking epithelial cells. Similar findings have been reported by Herxheimer, who noted hyalinised glomeruli in children < 1 year [8]. Both reports do not mention the tubulo-interstitium. However, based on the description (lacking epithelial cells) and the predominant occurrence at very young age it is unlikely that these glomeruli may match our findings. Sibley et al described the occurrence of microglomeruli in children with a congenital nephrotic syndrome. The microglomeruli averaged 20–40 µm in diameter and contained capillaries. The description of the glomeruli fits our findings, although no mention is made of tubulo-interstitial injury [6].

Many studies have addressed global glomerulosclerosis [9]. It was shown that the number of obsolescent glomeruli increased with age, and correlated with interstitial fibrosis and arteriolar intimal hyperplasia [9]. Glomerular involution appears to be very different from vascular glomerulosclerosis as there is no contraction of the glomerular tuft and no deposition of collagen I but rather production of collagen IV. Moreover, we did not detect any vascular changes in the renal tissue of patients with involuted glomeruli. The random distribution of the involuted glomeruli also argues against a vascular cause. Thus, whereas vascular sclerosis is thought to occur secondary to hypoperfusion, such a pathogenesis is unlikely in glomerular involution.

It is intriguing that glomerular involution occurs in the setting of minimal change nephropathy in patients with relapses (recurrent nephrotic syndrome) and therefore like FSGS is seen in the context of proteinuria. Therefore, one could ask if glomerular involution and glomerulopathic sclerosis in FSGS are related processes. From a histological point of view the most apparent similarity is that in both types of glomerulosclerosis solidification is the result of matrix deposition by residual glomerular cells, which results in an 'inflated' glomerulus and tuft adhesions. In the last years the pathogenesis of glomerulosclerosis in FSGS has become much clearer [10–13]. It is generally accepted that in FSGS the podocyte is the cell that is initially injured, causing proteinuria. Studies in animal models have elucidated the following sequence of events which contribute to the characteristic lesions of FSGS: podocytes lose their differentiation markers and disappear, there is activation and proliferation of parietal epithelial cells (PECs) or dedifferentiated podocytes, and deposition of matrix with the formation of the characteristic scar. The adhesions between the glomerular tuft and Bowman's capsule are responsible for misdirected filtration, moving ultrafiltrate in the periglomerular

space, stimulating myofibroblast proliferation. This periglomerular ultrafiltrate typically spreads to the peritubular space. We have confirmed these abnormalities in human FSGS, and proposed that injury to PECs is important in this process [7].

In glomerular involution there is also deposition of extracellular matrix by cells of glomerular origin, causing consolidation and tuft adhesions. However, in involuted glomeruli there is no evidence of cell proliferation, podocyte markers remain present, there is no activation of PECs and no periglomerular fibrosis or interstitial fibrosis.

Based on these findings we hypothesize that misdirected filtration does not occur in the process of glomerular involution. Apparently, glomerular involution occurs in the setting of podocyte injury with proteinuria, insufficient to cause parietal epithelial cell injury and the associated formation of a bridging adhesion allowing misdirected filtration. The injury stimulates glomerular matrix production by glomerular epithelial cells and eventually the epithelial cells disappear. We have noticed these involuted glomeruli in children with minimal change disease, who were biopsied because of a relapsing cause of the disease. Thus, most patients have suffered from many episodes of proteinuria. Future studies are needed to further clarify the relation between proteinuria, treatment and the development of glomerular involution.

## CONCLUSION

We describe a distinct type of global sclerosis that is observed in the setting of children with recurrences of minimal change nephrotic syndrome. This type of glomerulosclerosis without periglomerular and interstitial fibrosis is best described as glomerular involution.

## ACKNOWLEDGEMENTS

We thank the members of the EM-, Immuno/ISH laboratory (all of the Department of Pathology, Radboud University Medical Center Nijmegen, Nijmegen), for their expert technical assistance.

## REFERENCES

1. Kappel B, Olsen S: Cortical interstitial tissue and sclerosed glomeruli in the normal human kidney, related to age and sex. A quantitative study. *Virchows Arch A Pathol Anat Histol*; 387:271-277, 1980.
2. Kaplan C, Pasternack B, Shah H *et al*: Age-related incidence of sclerotic glomeruli in human kidneys. *Am J Pathol*; 80:227-234, 1975.
3. Jennette JC, Olson JL, Schwartz MM, *et al* (editors): *Heptinstall's Pathology of the Kidney*, 5th ed., Philadelphia, New York, LippincottWilliams & Wilkins; pp 137-167, 212-223, 949-951, 962-966, 1998.
4. Emery JL, Macdonald MS: Involuting and scarred glomeruli in the kidneys of infants. *Am J Pathol*; 36:713-23.:713-723, 1960.
5. Kriz W, Hartmann I, Hosser H *et al*.: Tracer studies in the rat demonstrate misdirected filtration and peritubular filtrate spreading in nephrons with segmental glomerulosclerosis. *J Am Soc Nephrol*; 12:496-506, 2001.
6. Sibley RK, Mahan J, Mauer SM *et al*.: A clinicopathologic study of forty-eight infants with nephrotic syndrome. *Kidney Int*; 27:544-552, 1985.
7. Dijkman H, Smeets B, van der Laak J *et al*.: The parietal epithelial cell is crucially involved in human idiopathic focal segmental glomerulosclerosis. *Kidney Int*; 68:1562-1572, 2005.
8. Herxheimer G. Über hyaline glomeruli der neugeborenen und Sauglinge. *Frankfurter Zeitschrift Pathologie*; 2:138-152, 1909.
9. Tracy RE, Ishii T: What is 'nephrosclerosis'? lessons from the US, Japan, and Mexico. *Nephrol Dial Transplant*; 15:1357-1366, 2000.
10. Kriz W, Elger M, Nagata M *et al*.: The role of podocytes in the development of glomerular sclerosis. *Kidney Int Suppl*; 45:S64-S72, 1994.
11. Kriz W, Kretzler M, Nagata M *et al*.: A frequent pathway to glomerulosclerosis: deterioration of tuft architecture-podocyte damage-segmental sclerosis. *Kidney Blood Press Res*; 19:245-253, 1996.
12. Kriz W, Gretz N, Lemley KV: Progression of glomerular diseases: is the podocyte the culprit? *Kidney Int*; 54:687-697, 1998.
13. Kriz W, LeHir M: Pathways to nephron loss starting from glomerular diseases-insights from animal models. *Kidney Int*; 67:404-419, 2005.



# 8

## CHARACTERISTICS OF GLOMERULAR INVOLUTION IN CHILDREN WITH FREQUENTLY RELAPSING MINIMAL CHANGE NEPHROTIC SYNDROME

Henry B.P.M. Dijkman, Elena N. Levtchenko<sup>1</sup>,  
J. Baede<sup>2</sup>, Eric J. Steenbergen and Jack F.M.  
Wetzels<sup>2</sup>

*Departments of Pathology, Pediatric Nephrology<sup>1</sup> and  
Nephrology<sup>2</sup>, Radboud University Nijmegen Medical  
Centre, Nijmegen, the Netherlands*

**Kidney International 2006; Accepted for  
publication in combination with chapter 7**



## ABSTRACT

We recently described the presence of small, globally sclerosed glomeruli in kidney biopsies of children with minimal change nephrotic syndrome. This abnormality, called glomerular involution, could be distinguished from the obsolescent and solidified forms of global glomerulosclerosis. These involuted glomeruli were characterised by a marked reduction in size, the persistence of vital cells within the matrix, and most notably, the absence of accompanying tubular atrophy and interstitial fibrosis.

In the present study we extend our observations on the presence of glomerular involution in biopsies of children with a frequently relapsing nephrotic syndrome due to minimal change nephropathy. Specifically, we have evaluated possible explanatory variables.

We have studied biopsies of 18 children (11 M, 7 F) with frequently relapsing minimal change nephrotic syndrome. We observed involuted glomeruli in 12 biopsies, median percentage of involuted glomeruli was 6% (range 0-33%). The percentage of involuted glomeruli correlated with age at renal biopsy and the interval between onset of disease and time of renal biopsy. The percentage of involuted glomeruli was not dependent on gender, age at onset of disease or prednisone dose. Multivariate analysis revealed that the interval between onset of disease and time of renal biopsy was the only independent predictor.

In conclusion: small, globally sclerosed involuted glomeruli are regularly observed in children with frequently relapsing minimal change nephrotic syndrome. The data suggest that glomerular involution is a slow process, related to the duration of the disease process.

Keywords: minimal change nephropathy, relapsing nephrotic syndrome, involution

## INTRODUCTION

We recently described glomerular involution as a special type of glomerular injury [1]. Glomerular involution is defined by the presence of small glomeruli, which are characterized by disorganized matrix, the presence of vital cells in between the matrix, and the striking absence of periglomerular and interstitial fibrosis. We have shown that glomerular involution can be distinguished from the other two types of global glomerulosclerosis i.e. the vascular type (also referred to as obsolescent type) and the glomerulopathic type (also referred to as solidified type).

We observed these involuted glomeruli in biopsies of children, notably of children with a nephrotic syndrome. In the present study we extend our observations. Specifically, we have evaluated possible explanatory variables.

## PATIENTS AND METHODS

### *Patients*

We have evaluated renal biopsies of children with a frequently relapsing nephrotic syndrome. These children were biopsied in the process of preparation for cyclophosphamide therapy. We only included biopsies classified as minimal change nephropathy by appropriate histological techniques (light microscopy, immunofluorescence and electronmicroscopy).

The clinical data of the patients were studied with particular emphasis on age of onset of disease, number of relapses, type and duration of immunosuppressive treatment and relapse-free interval.

### *Light microscopy*

Renal biopsies were processed according standard techniques. For light microscopy, kidney fragments were fixed in Bouin's solution or formaldehyde, dehydrated, and embedded in paraplast (Amstelslad, Amsterdam The Netherlands). 2 µm sections were stained with periodic acid-Schiff and with silver methenamine. Involved glomeruli were identified by high-power magnification. Glomeruli were scored and counted by one of us (HD), who was unaware of the clinical data of the patients.

## RESULTS

We have studied the biopsies of 18 children with a steroid-dependent or frequently relapsing minimal change nephrotic syndrome.

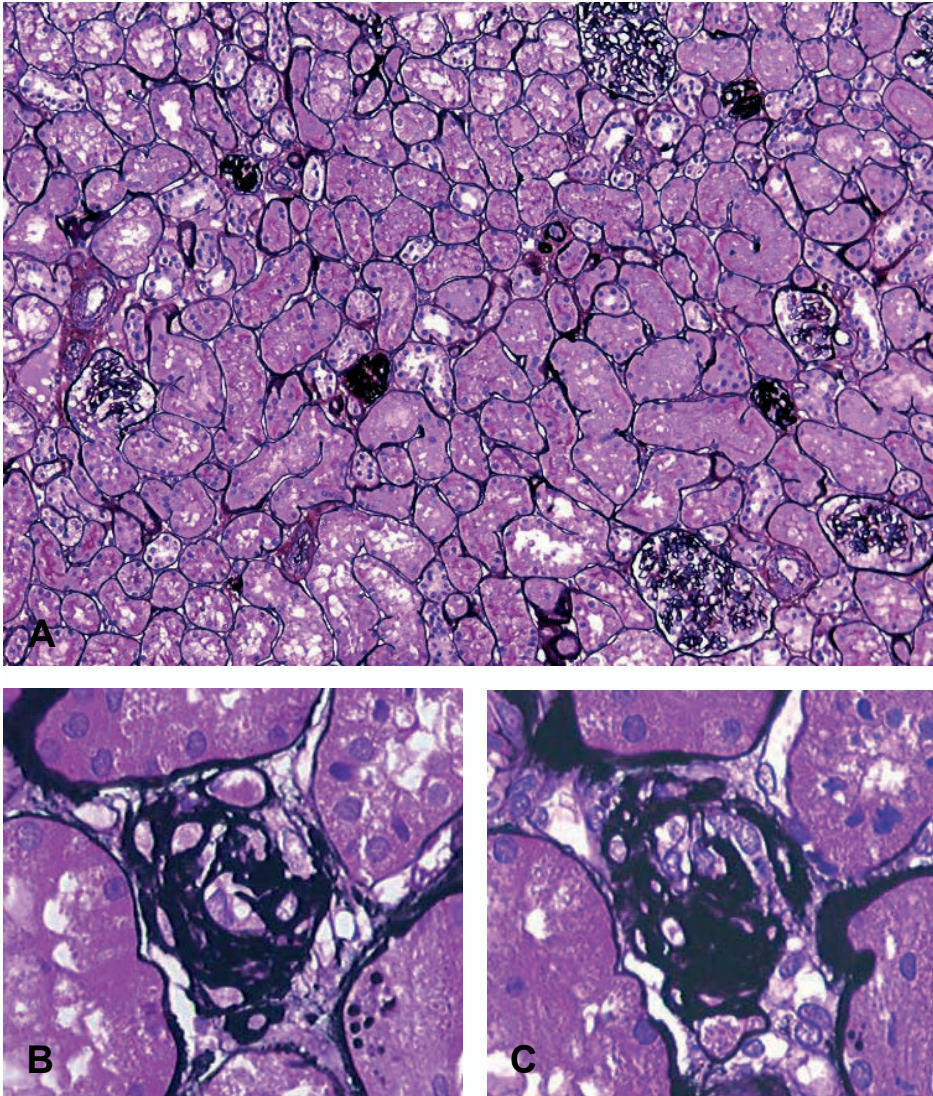


**Figure 1. Histology, silver methenamine staining:** With low magnification involuted glomeruli appear as small black nodules (panel A). They are distributed throughout the cortex and in this view the absence of tubular atrophy and periglomerular and tubulo-interstitial fibrosis is noted. At high magnification the involuted glomeruli consist of matrix, with persistence of cells within the matrix (A x 150, B-C x350).

Clinical characteristics of the patients are given in Table 1. There were 11 boys and 7 girls. Median age at disease onset was 2.8 years (1.6-10.6 years) and at biopsy 5.2 years (2.3-10.9 years). Most patients expressed a frequently relapsing course of the nephrotic syndrome. All patients had received prednisone. Other immunosuppressive agents had not been used before the renal biopsy. All patients were initially treated according guidelines of the ISKDC. Some patients with steroid-dependent nephrotic syndrome were treated with low dose pred-

nisone for prolonged time periods with titration of the prednisone dose against proteinuria assessed by urinary dipstick. The biopsies contained 19 (5-35) glomeruli. Many biopsies contained small, globally sclerosed glomeruli with the characteristics of involuted glomeruli.

Typical examples are depicted in Figure 1 B,C. Most notable is the absence of periglomerular and tubular interstitial fibrosis. The median percentage of involuted glomeruli was 6% (range 0-33%). Biopsies of six patients did not show involuted glomeruli. When comparing patients without and with involuted glomeruli we observed a significant difference in the age at renal biopsy (without involution:  $3.9 \pm 1.1$  year, with involution  $6.5 \pm 2.6$  years;  $p < 0.05$ ) and the interval between onset of disease and the renal biopsy ( $0.44 \pm 0.43$  years vs  $3.8 \pm 3.3$  years;  $p < 0.01$ ). There were no significant differences in gender distribution, maximal proteinuria at onset, serum albumin, number of recurrences or selectivity index. There was a significant correlation between the percentage of involuted glomeruli and the interval between onset of disease and renal biopsy (Figure 2, Spearman  $R = 0.64$ ;  $p < 0.01$ ), and a trend between age at biopsy and percentage involution ( $r = 0.41$ ;  $p = 0.09$ ). By logistic regression analysis the interval between disease onset and the renal biopsy was the only independent significant predictor.

**Table 1:** Clinical characteristics of the patients

Patients (N)	18
Sex (M/F)	11 / 7
Age at onset (yr)	2.8 (1.6 - 10.6)
Age at biopsy (yr)	5.2 (2.3 - 10.9)
Interval onset-biopsy (yr)	1.5 (0.2 - 6.7)
Number of relapses	2 (1 - 16)
Number of glomeruli	19 (5 - 35)
Involuted glomeruli (%)	6 (0 - 33)

Values are given as medians (range)

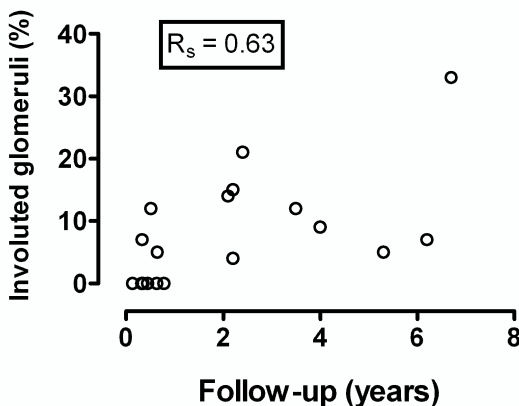


**Figure 2.** Correlation between the percentage of involuted glomeruli and the interval between disease onset and renal biopsy (Spearman  $R = 0.64$ ;  $p < 0.01$ ).

## DISCUSSION

Our study indicates that small, seemingly sclerosed glomeruli are regularly found in patients with frequently relapsing or steroid dependent minimal change nephrotic syndrome. In our series these glomeruli were observed in the majority (two thirds) of the renal biopsies. We previously have suggested to use the term glomerular involution to describe these small glomeruli [1]. Glomerular involution can be distinguished from the obsolescent and the solidified form of global glomerulosclerosis.

We observed a significant relation between the percentage of glomerular involution and the interval between onset of disease and time of renal biopsy. Thus, involuted glomeruli are predominately observed in children who are biopsied several years after onset of the disease. We did not find a relation with number of recurrences, proteinuric selectivity index, maximal proteinuria at onset or serum albumin. Obviously, our study has the limitations of a retrospective study. In particular, it was impossible to obtain accurate and meaningful data on time-averaged proteinuria. Especially patients with a more protracted course were advised to check their urine by dipstick and adjust the dose and duration of prednisone therapy accordingly. Detailed information obviously cannot be retrieved from the patient records. Therefore, we cannot draw conclusions on possible mechanisms of glomerular involution. Glomerular involution may be the consequence of initial glomerular injury, slowly developing afterward. Alternatively, it is quite possible that glomerular involution is the consequence of ongoing subtle injury, reflected by continued recurrence of proteinuria. The continued use of prednisone may offer a third explanation. In an animal model of minimal change nephropathy, the so-called puromycin aminonucleoside model, chronic administration of methylprednisolone caused glomerulosclerosis [2], an effect attributed to hyperfiltration. Chronic steroid treatment has also been implicated as cause of glomerulosclerosis. Prospective studies are needed to determine the best explanation.

The term glomerular involution has been used before to describe abnormal glomeruli in biopsies of children. Emery et al described glomerular involution and scarring in children, and considered that it was unlikely that this was the result of vascular injury [3]. They demonstrated that these scarred glomeruli occurred predominantly in children aged < 2 years, with preferential localisation in the subcapsular region or in proximity to the arcuate vessels. In Emery's paper glomerular involution is described as the presence of small solid masses of connective tissue like material lacking epithelial cells. Similar findings have been reported by Herxheimer, who noted hyalinised glomeruli in children < 1 year [4]. Both reports do not mention the tubulo-interstitium. However, based on the description of the glomeruli, the lack of epithelial cells and the clinical characteristics (predominant occurrence at very young age), it is unlikely that the glomeruli described by Emery or Herxheimer match our findings. Sibley et al described the occurrence of microglomeruli in children with a congenital nephrotic syndrome [5]. The microglomeruli averaged 20-40  $\mu\text{m}$  in diameter and contained capillaries. The

description of these glomeruli bears resemblance with our findings, although no mention is made of the presence or absence of tubulo-interstitial injury [5].

Obviously, involuted glomeruli have lost their function. The observation that up to 30% of glomeruli are involuted in biopsies of children with minimal change nephrotic syndrome thus suggest that minimal change nephropathy is not so benign as suggested. Although renal function abnormalities were not detected in these children by standard creatinine assays, loss of functional nephrons may cause problems in the future. Therefore, more information is needed in the pathogenesis of this process.

## **ACKNOWLEDGEMENTS**

We thank the members of the EM-, Immuno/ISH laboratory (all of the Department of Pathology, Radboud University Medical Center Nijmegen, Nijmegen), for their expert technical assistance.

## REFERENCES

1. Dijkman HB, Wetzels JF, Gemmink JH, Levtchenko EN, Steenbergen EJ: Glomerular involution: An unrecognized form of glomerulosclerosis? *Kidney Int* 2006, publication in combination with chapter 8.
2. Garcia DL, Rennke HG, Brenner BM, Anderson S: Chronic glucocorticoid therapy amplifies glomerular injury in rats with renal ablation. *J Clin Invest* 80:867-874, 1987.
3. Emery JL, Macdonald MS: Involuting and scarred glomeruli in the kidneys of infants. *Am J Pathol* 36:713-23.:713-723, 1960.
4. Herxheimer G. Über hyaline glomeruli der neugeborenen und Säuglinge. *Frankfurter Zeitschrift Pathologie* 2: 138-152, 1909.
5. Sibley RK, Mahan J, Mauer SM, Vernier RL: A clinicopathologic study of forty-eight infants with nephrotic syndrome. *Kidney Int* 27:544-552, 1985.

# 9

## **A MOUSE MODEL OF GLOMERULAR INVOLUTION**

Henry B.P.M. Dijkman, Karel J.M. Assmann, Eric  
J. Steenbergen and Jack F.M. Wetzels<sup>1</sup>

*Departments of Pathology and Nephrology<sup>1</sup>,  
Radboud University Nijmegen Medical Centre,  
Nijmegen, the Netherlands*

**Submitted**



## ABSTRACT

We recently described the presence of small, seemingly sclerosed glomeruli in kidney biopsies of children with recurrent minimal change nephrotic syndrome. This abnormality, called glomerular involution, can be distinguished from the vascular (obsolescent) type and glomerulopathic (solidified) type of global glomerulosclerosis. We now present a mouse model of glomerular involution. Six week old Balb/c mice received two weekly intravenous injections, on day 1 and again on day 7, of 4 mg of the combination of two monoclonal antibodies directed at aminopeptidase-A (ASD-37/41). Mice injected with the non-proteinuric combination ASD-3/41 were used as controls. We followed the groups over 12 months and tested the urine samples for albuminuria every 4 weeks by placing mice in metabolic cages. Mice were sacrificed at months 7, 10 and 12 and kidneys processed for light microscopy, immunofluorescence, immunohistochemistry and electron microscopy.

Injection of ASD-37/41 caused an acute albuminuria after each injection. Thereafter albuminuria decreased to values slightly above normal within 21 days. During follow up albuminuria averaged  $703 \pm 626 \mu\text{g}/18 \text{ hrs}$  in mice injected with ASD-37/41 as compared to  $273 \pm 225 \mu\text{g}/18 \text{ hrs}$  in controls. Involuted glomeruli were first observed in mice sacrificed 7 months after injection and the percentage of involuted glomeruli increased to 17% at 12 months. Abnormal glomeruli were not observed in control mice.

We have studied these involuted glomeruli in detail by light microscopy, electron microscopy and immunostaining and have investigated the expression of markers for podocytes (synaptopodin, WT-1, nephrin & VEGF), parietal epithelial cells (PAX-2), miscellaneous matrix components (coll I, III & IV, ASD-20), endothelium (CD 34), myofibroblasts (SMA) and made a comparison with the involuted glomeruli observed in humans.

The involuted glomeruli in mice closely resembled the abnormal glomeruli described in humans. These glomeruli were characterised by small size, increased matrix and the presence of vital cells that stained with podocyte markers (synaptopodin, WT1, nephrin and VEGF) and PEC marker (PAX-2). Most notable was the absence of periglomerular and tubulo-interstitial inflammation and fibrosis.

In conclusion; we present a mouse model of glomerular involution. This mouse model will enable studies to reveal the pathogenic pathways involved in this type of glomerular injury.

Keywords: APA, global glomerulosclerosis, parietal epithelial cell, podocyte, periglomerular fibrosis, involution.

## INTRODUCTION

We recently described the presence of small, seemingly sclerosed glomeruli in kidney biopsies of children with recurrent minimal change nephrotic syndrome [1]. This abnormality, called glomerular involution, could be distinguished from the vascular (obsolescent) form and glomerulopathic (solidified) form of global glomerulosclerosis. Glomerular involution was characterised by a marked reduction in size of the glomerulus, an apparent increase of matrix, the continued presence of vital glomerular epithelial cells and, most remarkably, the absence of periglomerular and tubulo-interstitial fibrosis. These characteristics suggested a different pathogenic pathway.

In recent years we have described a mouse model of podocytic activation and injury which resembles minimal change nephropathy. Administration of a specific combination of aminopeptidase-A (APA) mAbs in mice induces an acute albuminuria which is independent of complement, inflammatory cells or angiotensin II [2;3]. Albuminuria is massive, starts at 6 hr, reaches its maximum at 8 hr and declines to near-normal values thereafter. We have tried to induce FSGS in this model by repeating the injection of the mAbs. During follow-up we observed the development of glomerular abnormalities that resembled glomerular involution. This report details our findings. Our study indicates that the small glomeruli in our anti-APA mouse model have similar characteristics than the involuted glomeruli in humans. Our mouse model can be used to study the pathogenesis of glomerular involution.

## METHODS

### *Animals*

BALB/c mice, aged 6 weeks and weighing 20–25 g, were purchased from Charles River, Sulzfeld, Germany. All procedures involving mice were approved by the Animal Care Committee of the University of Nijmegen and conformed to the Dutch Council for Animal Care and National Institutes of Health guidelines.

### *Antibodies used for intravenous injection*

The characteristics of the three rat mAbs against different epitopes of mouse APA used in this study (ASD-3, ASD-37 and ASD-41) have been described previously [2]. The combination ASD-37/41 is nephritogenic and induces albuminuria, whereas the combination ASD-3/41 is non-nephritogenic and used as control. The anti-APA mAbs have been propagated in vitro by hollow-fiber culture (Nematology Department, Agriculture University Wageningen, The Netherlands).

### *Animal Experiments*

We have studied mice that received two intravenous injections 6 and 7 weeks after birth of 4 mg of the nephritogenic combination ASD-37/41 or the non-nephritogenic combination ASD-3/41 (both with 1:1 weight ratio). The long term effects were studied in mice which were followed for at least 6 months. Urine samples (18 hr) were collected every 4 weeks by placing mice in metabolic cages. At each specified time point thereafter (7, 10 and 12 months) mice were killed and kidneys processed for light microscopy, immunofluorescence and electron microscopy. The time-course of the acute albuminuria was studied in a separate set of experiments. Urine samples were collected by bladder puncture within 24 hours and at day 2 and 7 after the first injection and within 24 hours after the second injection. Albuminuria was measured by radial immunodiffusion as described [4].

### *Light microscopy*

For light microscopy, kidney fragments were fixed in Bouin's solution and formaldehyde, dehydrated, and embedded in paraplast (Amstelslad, Amsterdam The Netherlands). 2  $\mu\text{m}$  sections were stained with periodic acid-Schiff, and with silver methenamine.

### *Immunohistochemistry*

The expression of glomerular antigens was studied by immunohistochemistry and immunofluorescence. Immunohistochemical staining was performed on kidney sections fixed in 4% buffered formaldehyde for 24 hr and embedded in paraffin. 4  $\mu\text{m}$  sections were incubated with primary and secondary antibodies as listed in Table 1. Detection was carried out with the use of peroxidase as label and diaminobenzidine as substrate or via alkaline phosphatase (AF). For immunofluorescence (IF) kidneys were snap frozen in liquid nitrogen. Two  $\mu\text{m}$ -thick, acetone fixed sections were incubated with specific antibodies for 60 minutes at room temperature. The expression of important proteins was examined using unlabeled primary Ab and FITC-labeled secondary antibodies as listed in Table 1. The sections were analysed by a microscopical system, the Leica Discovery (Leica GmbH, Heidelberg, Germany).

### *In situ hybridisation*

Kidney sections were fixed in 4% buffered formaldehyde for 24 hr and embedded in paraffin. 4  $\mu\text{m}$  sections were incubated and subjected to VEGF in situ hybridization (ISH) using a digoxigenin-labeled VEGF-A antisense RNA probe [5]. The corresponding sense probe was used as a control.

### *Transmission Electron Microscopy*

For electron microscopy, we used immersion fixation. Small fragments of cortex were fixed in 2.5% glutaraldehyde dissolved in 0.1 M sodium cacodylate buffer, pH 7.4, overnight at 4°C and washed in the same buffer. The tissue fragments were postfixed in Palade-buffered 2%

Table 1: Antibodies used for the detection of glomerular antigens <sup>1)</sup>

Antigen	Primary antibody	Dil.	Supplier <sup>2)</sup>	Secondary antibody	Dil.	Supplier <sup>2)</sup>
<b>Podocyte components</b>						
Synaptopodin	Mouse anti-synaptopodin	1	Progen	Sheep anti-mouse Ig - FITC	100	Cappel
APA	Rat anti-mouse APA mAbs (ASD-38)	1		Sheep anti-rat IgG2b - FITC	100	Serotec
WT1	Rabbit anti-nuclear protein	50	Santa Cruz	Swine anti-rabbit Ig - FITC	40	Dako
VEGF	ISH m-RNA Probe (*ng/ml)	100*	Ref. [5]	Envision AF	1	Klimipath
Nephrin	Goat anti-nephrin (N 20)	50	Santa Cruz	Rabbit anti-goat Ig - FITC	100	Cappel
<b>PEC components</b>						
PAX-2	Rabbit anti human PAX-2	50	Zymed laboratories	Powervision, Poly+HRP-anti M/R/Ra,IgG	1	Klimipath
<b>Miscellaneous</b>						
$\alpha$ smooth muscle actin	Mouse anti human SMA	15000	Sigma	Envision AF-anti Rabbit IgG	1	Klimipath
ASD-20	Rat anti-mouse ASD-20 mAb	1		Sheep anti-rat IgG2b - FITC	100	Serotec

1) Abbreviations: APA = aminopeptidase A, mAbs = monoclonal antibodies, WT-1 = Wilms tumor suppressor gene WT-1 product, CDZAP = CD2-associated protein, Dil. = dilution

2) Serotec, Oxford, UK - Dako, Glostrup, Denmark - Progen, Heidelberg, Germany - Cappel, Organon Teknica, The Netherlands - Santa Cruz, California, USA - Zymed, San Francisco, USA - Klimipath, Duiven, The Netherlands - Sigma, St. Louis, USA

OsO<sub>4</sub> for 1 hr, dehydrated, and embedded in Epon 812, Luft's procedure (Merck, Darmstadt, Germany). Ultrathin sections were contrasted with 4% uranyl acetate for 45 min and subsequently with lead citrate for 5 min at room temperature. Sections were examined in a Jeol 1200 EX2 electron microscope (JEOL, Tokyo, Japan).

## RESULTS

### *Proteinuria*

Injection of the nephritogenic APA antibody combination ASD-37/41 in 6 weeks old mice induced an acute albuminuria which was first noted at 6 hr, peaked at 8 hr after antibody injection

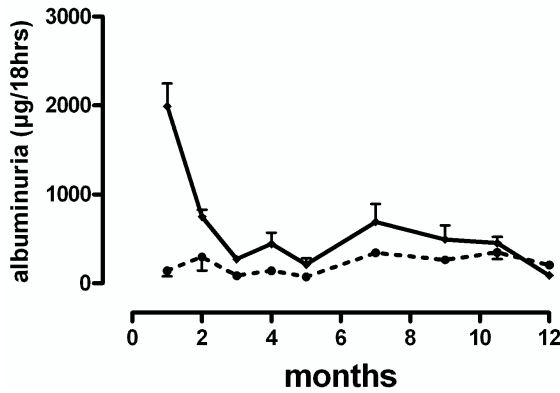


**Figure 1.** The course of albuminuria in the experimental group (injection of ASD-37/41; straight line) and the control group (injection of ASD-3/41; interrupted line). N=6 mice per group till month 6. Albuminuria is higher in the experimental group ( $p < 0.01$ ).

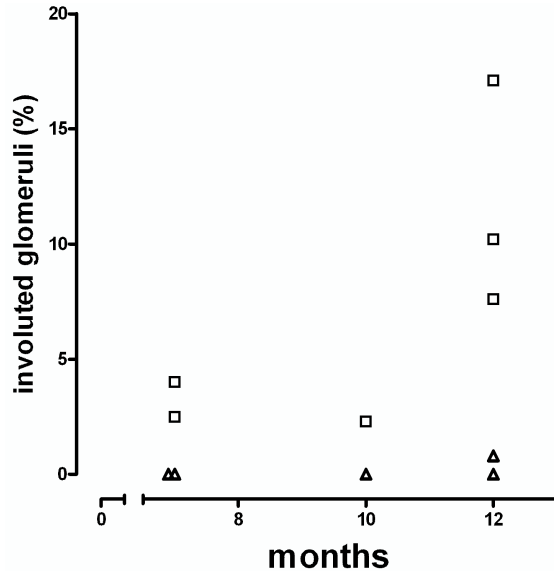


**Figure 2.** Percentage of involuted glomeruli in the experimental group (injection of ASD-37/41; □) or the control group (injection of ASD-3/41; △) in relation to time of follow-up.

tion and decreased thereafter. Albumin in urine was  $58,046 \pm 6,084 \mu\text{g/ml}$  at 8 hr,  $3,247 \pm 1,076 \mu\text{g/ml}$  at 24 hr,  $1,148 \pm 688 \mu\text{g/ml}$  at 48 hr, and  $724 \pm 334 \mu\text{g/ml}$  at day 7. Mice injected with the non-nephritogenic combination ASD-3/41 did not develop albuminuria ( $102 \pm 24 \mu\text{g/ml}$ ). The second injection of ASD-37/41 at day 7 also resulted in an acute albuminuria ( $13,412 \pm 16,905 \mu\text{g/18 hrs}$ ) and decreased thereafter ( $1,989 \pm 811 \mu\text{g/18 hrs}$  at 4 weeks). Albuminuria measured during long-term follow-up is presented in Figure 1. Albuminuria was consistently higher in mice that received ASD-37/41, although levels were only mildly increased.

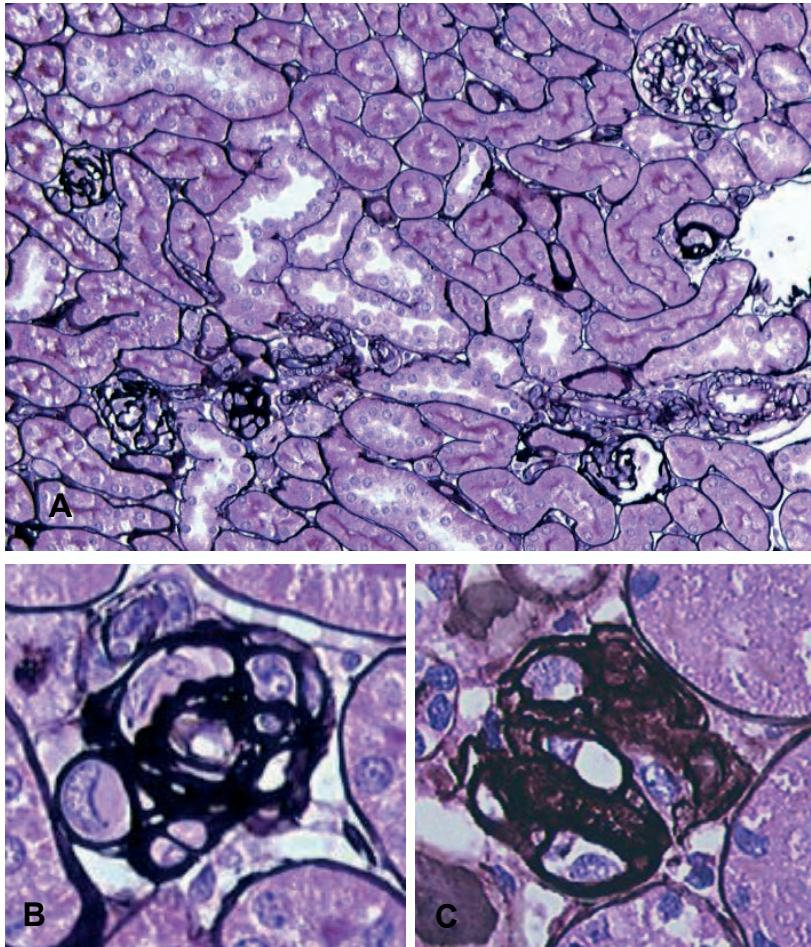


**Figure 3. Histology, silvermethenamine staining:** Involuted glomeruli appear as small black nodules (panel A). In an overview the involuted glomeruli are distributed throughout the cortex, without the presence of accompanying interstitial changes. The aspect of the extracellular matrix becomes evident in detail (panel B). Remnants of the glomerular basement membrane and Bowman's capsule can be seen and form an interconnecting network. There is continuity between the former glomerular tuft and Bowman's capsule and a small number of vital appearing cells can be seen (panel B). These glomeruli are characterised by the small size, seemingly increased matrix and the persistent presence of vital cells and resembled the involuted glomeruli in humans. For comparison an involuted glomerulus in a child with relapsing minimal change nephrotic syndrome is shown (panel C) (A x150, B,C x750).

### Glomerular morphology

In mice sacrificed after 7 months we noted the presence of small, seemingly sclerosed glomeruli. The percentage of these involuted glomeruli increased with time of follow-up (Figure 2). Abnormal glomeruli were not observed in control mice.

With low power magnification the involuted glomeruli appear as small black nodules without apparent accompanying interstitial changes (Figure 3A). With higher magnification the relative increase of extracellular matrix becomes evident. Remnants of the glomerular basement membrane and Bowman's capsule can be seen and form an interconnecting network. There is continuity between the former glomerular tuft and Bowman's capsule and a small number of vital appearing cells can be seen. Morphologically the small glomeruli found in our mouse model are very similar to the involuted glomeruli that can be observed in humans (Figure 3B and 3C). Notable is the absence of periglomerular fibrosis or inflammation of the surrounding interstitium (Figure 4A). This finding is in clear contrast with the marked periglomerular fibrosis that is always present in our mouse model of FSGS (Figure 4B).

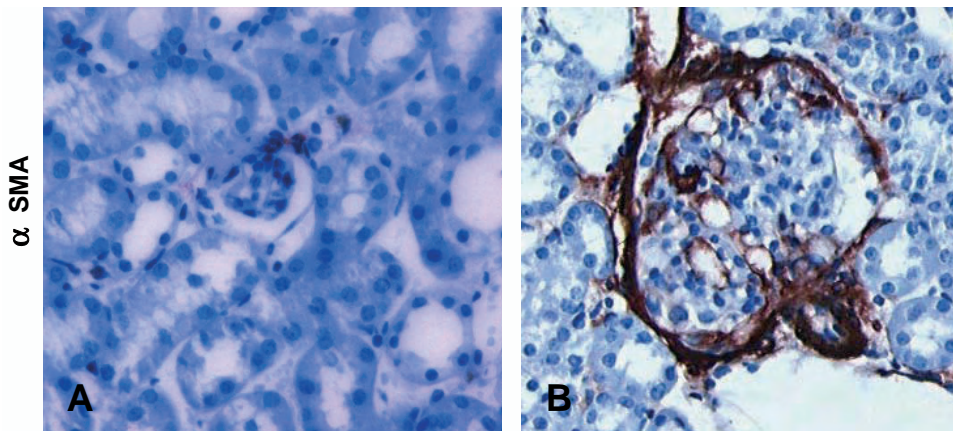


**Figure 4. Immunostaining with  $\alpha$  SMA to characterize the periglomerular and interstitial inflammation / fibrosis (panel A,B).** Notable is the absence of periglomerular fibrosis or inflammation of the surrounding interstitium in glomerular involution (panel A). For comparison, marked periglomerular fibrosis is always present in a mouse model of FSGS (Thy-1.1 transgenic mouse: panel B) (A,B x400).

We have analysed the cells that remain present in the involuted glomeruli by immunohistochemistry and immunofluorescence. Cells were positive for either the podocyte markers nephrin, synaptopodin, WT1, ASD-38 and VEGF or the parietal epithelial cell marker PAX-2 (Figure 5 A-J). We have performed additional stainings using ASD-20, an antibody that predominately stains the matrix of Bowman's capsule in normal mouse glomeruli (Figure 5 D). Staining is more prominent and more diffuse in the involuted glomeruli (Figure 5 D and 5 I). Electron microscopy is depicted in Figure 6. There is thickening of the GBM and Bowman's capsule. Podocytes show foot process effacement. There is an increase of matrix, which connects the tuft and Bowman's capsule. Notably, cells are uniformly present between this newly

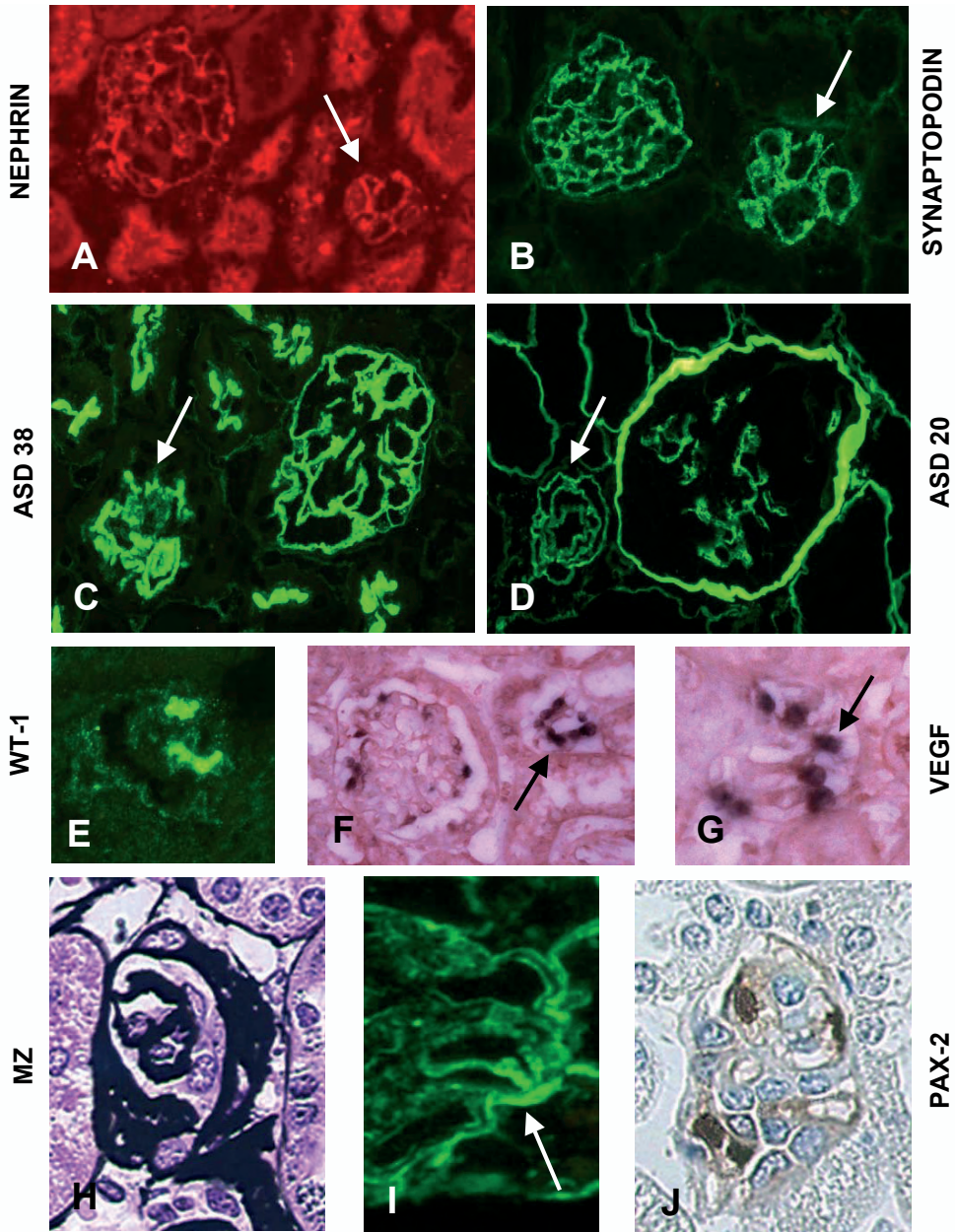


**Figure 5. Phenotype of glomerular cells and extracellular matrix characteristics in glomerular involution.** The vital cells in the involuted glomeruli (marked via white or black arrow) still express podocytemarkers such as nephrin (panel A), synaptopodin (panel B), ASD-38 (panel C), WT-1 (panel E), mRNA VEGF (panel F,G). The parietal epithelial cell marker (PAX-2, panel J) is also still present in involuted glomeruli. We have used staining with ASD-20, an antibody that predominately stains the matrix of Bowman's capsule in normal mouse glomeruli (panel D). Involuted glomeruli show more diffuse staining (panel D-arrow), in more detail adhesions can be recognized (panel I-arrow). For comparison light microscopy (silvermethenamine) is shown in panel H (A-G x350, H-J x500).



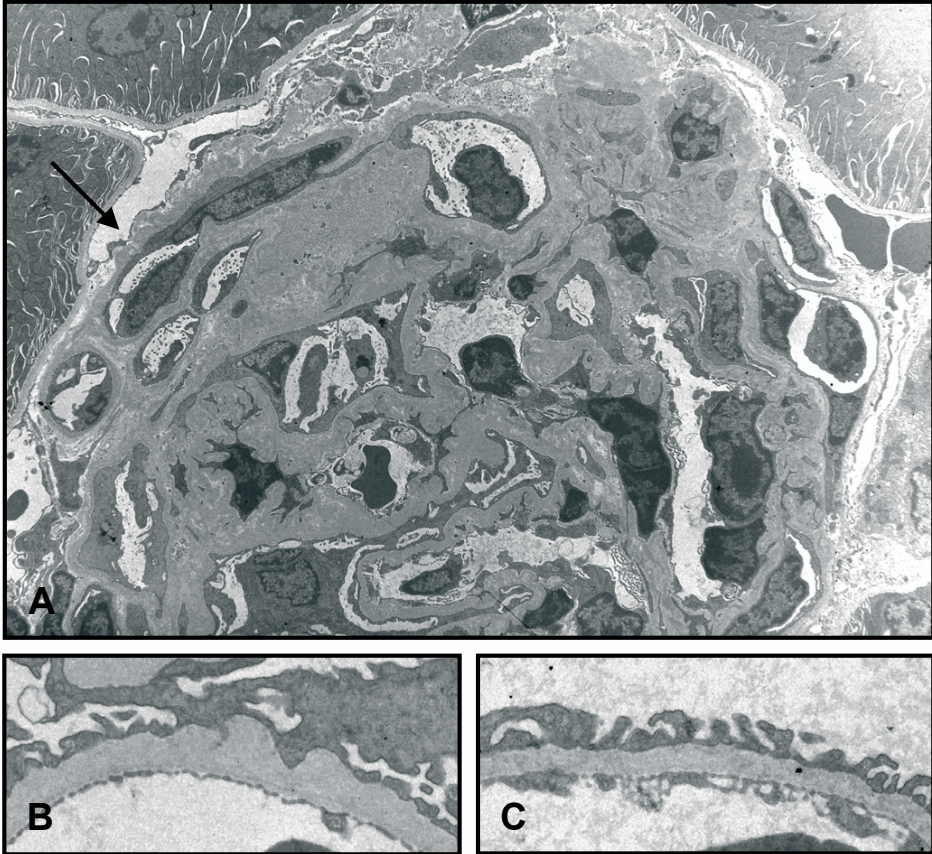


**Figure 6. Transmission electron microscopy of an involuted glomerulus:** Electron microscopy confirmed the observations by light microscopy (Figure 3). Involuted glomeruli show a matrix network that interconnect the GBM and Bowman's capsule (panel A). Vital appearing cells are present and cells which cover the GBM show foot process effacement. The former GBM and Bowman's capsule are thickened. In normal appearing glomeruli of ASD-37/41 injected mice GBM thickness was increased (panel B) whereas GBM thickness was normal in age-matched control mice and ASD-3/41 injected mice (panel C) (A x7000, B,C x10,000).

formed matrix. We have also analysed normal appearing glomeruli of ASD-37/41 injected mice and age-related control mice by electron microscopy. GBM thickness was increased in ASD-37/41 injected mice (Figure 6 B) whereas GBM thickness was normal in ASD-3/41 injected mice (Figure 6 C). Also, foot processes were partially effaced in ASD-37/41 injected mice.

We were intrigued by the notable absence of periglomerular and tubulo-interstitial fibrosis and the absence of atrophic tubuli. To further evaluate the relationship between the involuted glomeruli and the tubular system we have cut serial sections and analyzed several small globally sclerosed glomeruli in different stages. Figure 7 presents serial sections of such an involuted glomerulus. We did not observe atrophic tubuli and did not find a connection between the glomerulus and a proximal tubule. Figure 8 shows serial sections of a segmental

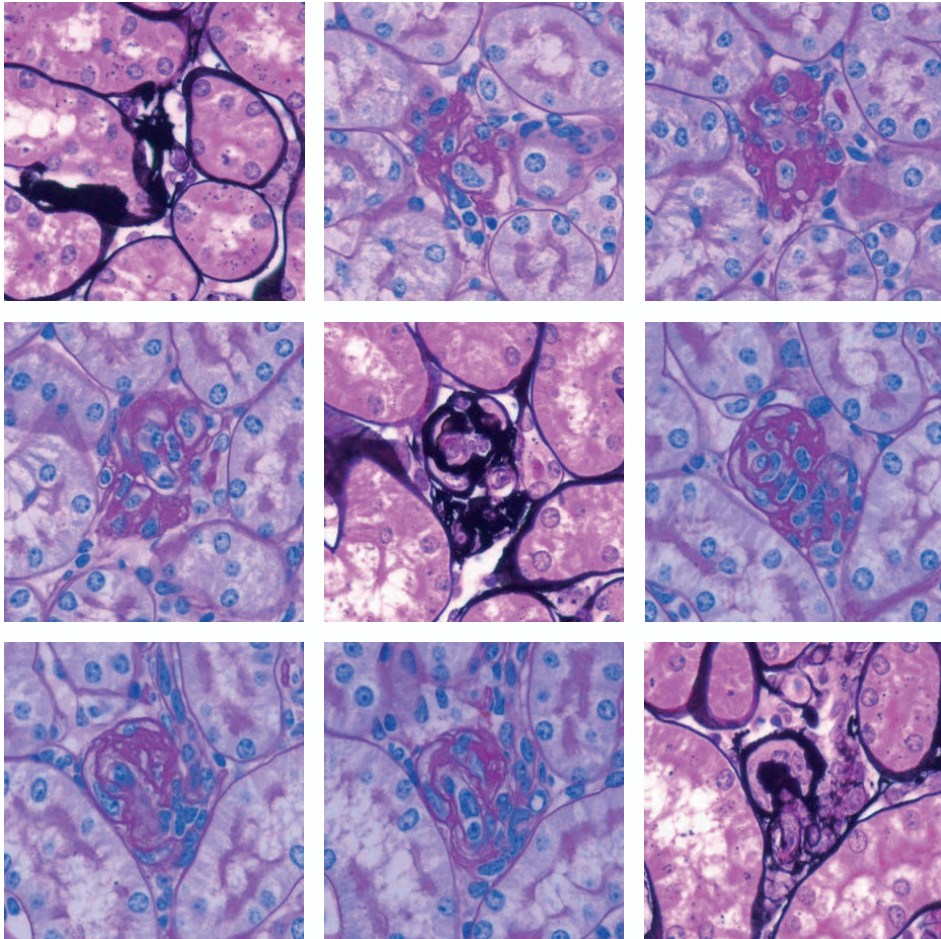


**Figure 7. Relation between involuted glomeruli and the tubuli.** We have used serial sections and analyzed several small globally sclerosed glomeruli in different stages. Atrophic tubuli were not observed and also a connection between the glomerulus and a proximal tubule was not found (serial sections are depicted in the gallery starting at the upper left) (silvermethenamine and PAS staining, A-I x350).

lesion. Apparently in the early stage there is formation of matrix along Bowman's capsule, where cells remain present. Adhesions are formed but proliferation of glomerular cells does not occur. There is no inflammatory response outside Bowman's capsule.

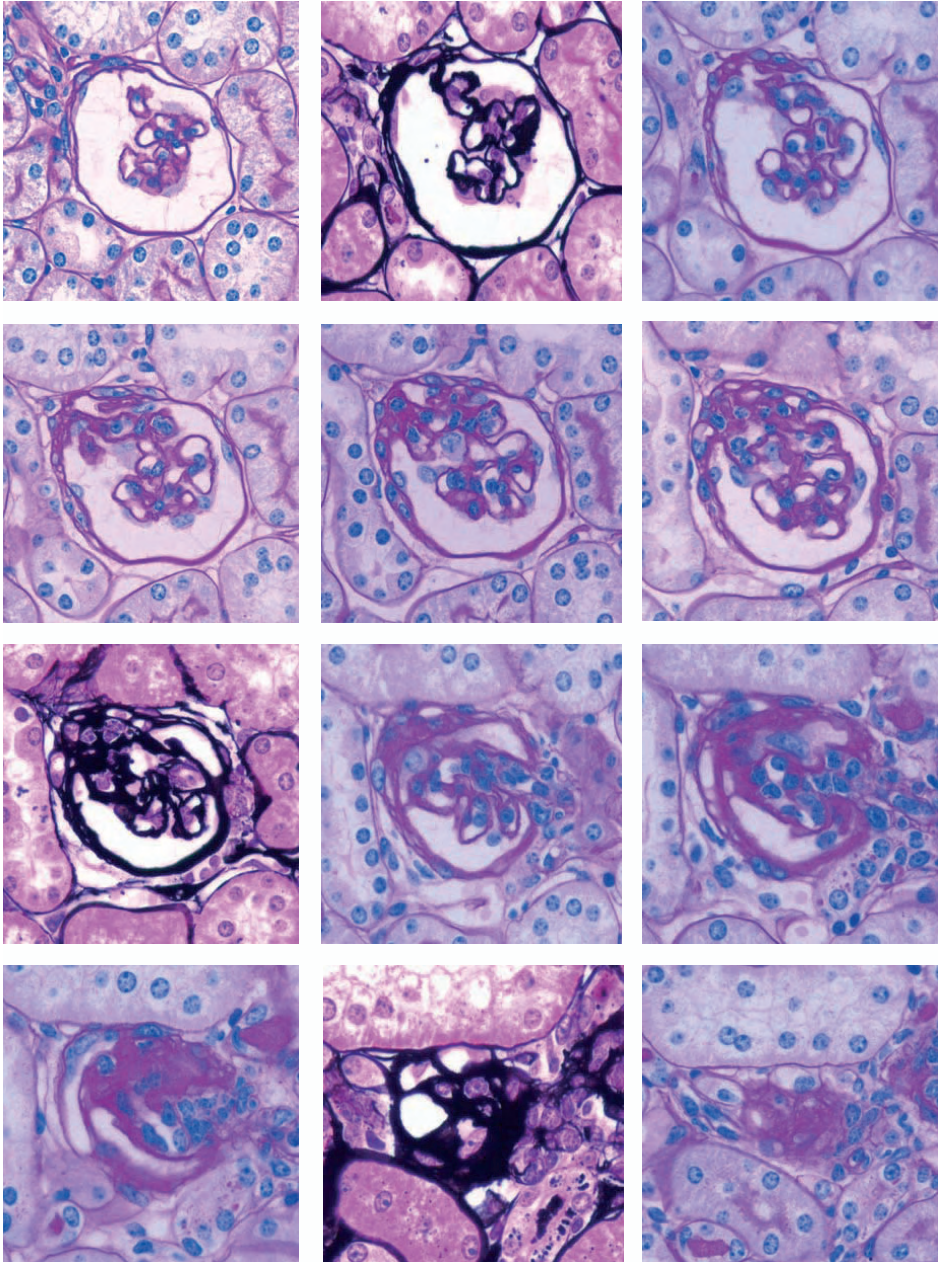


**Figure 8. Early involuted glomeruli, a segmental lesion.** In this figure serial sections are shown of a segmental lesion. In the early stage there is formation of matrix along Bowman's capsule. Adhesions are formed but proliferation of glomerular cells does not occur. There is no inflammatory response outside Bowman's capsule (serial sections are depicted in the gallery starting at the upper left) (silvermethenamine and PAS staining, A-L x350).

## DISCUSSION

Most authors distinguish two types of global glomerulosclerosis i.e. the vascular type (also referred to as obsolescent type) and the glomerulopathic type (also referred to as solidified type) [6]. Vascular glomerulosclerosis is characterised by retraction of the glomerular tuft, the absence of tuft adhesions and the prominent filling of Bowman's space with collagen I matrix. Glomerulopathic sclerosis is characterised by a solidified non-retracted glomerular tuft, with increased matrix, recognizable tuft adhesions and disappearance of vital cells.

We recently have described a new type of global glomerular injury, so called glomerular involution, which we observed in biopsies of children with a nephrotic syndrome [1]. These glomeruli were characterised by small size, seemingly increased matrix, the persistent presence of vital cells in the matrix and the notable absence of periglomerular fibrosis and tubulo-interstitial inflammation.

We now describe a mouse model of glomerular involution. Injection of mice with anti-APA monoclonal antibodies that induced an acute proteinuria resulted in the late development of abnormal and small glomeruli. These small glomeruli resembled the involuted glomeruli in humans in every detail. Specifically, the glomeruli were small, contained seemingly increased matrix, vital cells remained present with staining characteristics of podocytes and PECs, and periglomerular and tubulo-interstitial fibrosis was absent. Thus, this mouse model can be used to study the pathogenesis of glomerular involution in more detail.

We have hypothesized that glomerular involution and glomerulopathic glomerulosclerosis differ with respect to the extent of damage to the PECs and Bowman's capsule [1]. Tuft adhesions are typically present in FSGS. The tuft adhesions are areas of matrix that connect the glomerular tuft and the periglomerular region. These synechia contain matrix. The parietal epithelial cells that normally line Bowman's capsule are absent. It has been suggested that misdirected filtration is present thru these adhesions, moving ultrafiltrate into the periglomerular space, stimulating myofibroblast proliferation [7]. This periglomerular ultrafiltrate typically spreads to the peritubular space and is the cause of the local inflammatory response and fibrosis [7]. Thus, misdirected filtration provides an explanation linking focal glomerular sclerosis to periglomerular and tubulo-interstitial fibrosis. Based on our findings we have suggested that glomerular involution lacks misdirected filtration, possibly as the consequence of the persistence of vital PECs that remain present along Bowman's capsule.

In the older literature there has been a discussion if glomeruli can disappear without leaving a scar [8]. We suspect that the process of glomerular involution may eventually lead to the disappearance of glomeruli, which will be unnoticed in the absence of fibrosis. By serial sectioning we have analyzed the relationship between the involuted glomerulus and the proximal tubular system. Apparently involuted glomeruli are no longer connected to a proximal tubules. Most remarkable is the fact that we did not observe many atrophic tubuli.

Again, our observations provide some support for studies by Oliver [9] more than 60 years ago who already suggested that tubuli may not degenerate after loss of the glomerulus. We have made another interesting observation. We observed thickening of the GBM in normal appearing glomeruli of ASD-37/41 injected mice. Thus, thickening of the GBM preceded glomerular involution. Thickening of the GBM is characteristically observed in patients with diabetes and patients with vascular ischaemia and may point to the role of growth factors in the process of involution. Further studies in this mouse model are warranted.

## **CONCLUSION**

We describe a mouse model which resembles glomerular involution in humans. This mouse model will enable further studies into the pathogenesis of glomerular involution.

## **ACKNOWLEDGEMENTS**

We thank the members of the EM-, Immuno/ISH laboratory (all of the Department of Pathology, University Medical Center Nijmegen, Nijmegen), for their expert technical assistance.

## REFERENCES

1. Dijkman HB, Wetzels JF, Gemmink JH, Levtschenko EN, Steenbergen EJ: Glomerular involution: An unrecognized form of glomerulosclerosis? *Kidney Int* 2006, publication in combination with chapter 8.
2. Mentzel S, van Son JP, Dijkman HB *et al.*: Induction of albuminuria in mice: synergistic effect of two monoclonal antibodies directed to different domains of aminopeptidase-A. *Kidney Int* 55:1335-1347, 1999.
3. Gerlofs-Nijland ME, Assmann KJ, Dijkman HB *et al.*: Albuminuria in mice after injection of antibodies against aminopeptidase-A: role of angiotensin II. *J Am Soc Nephrol* 12:2711-2720, 2001.
4. Assmann KJ, Tangelder MM, Lange WP *et al.*: Membranous glomerulonephritis in the mouse. *Kidney Int* 24:303-312, 1983.
5. Leenders WP, Kusters B, Verrijp K *et al.*: Antiangiogenic therapy of cerebral melanoma metastases results in sustained tumor progression via vessel co-option. *Clin Cancer Res* 10:6222-6230, 2004.
6. Jennette JC, Olson JL, Schwartz MM, *et al* (editors): *Heptinstall's Pathology of the Kidney*, 5th ed., Philadelphia, New York, Lippincott Williams & Wilkins, 1998, pp 137-167, 212-223, 949-951, 962-966.
7. Kriz W, Elger M, Hosser H *et al.*: How does podocyte damage result in tubular damage? *Kidney Blood Press Res* 22:26-36, 1999.
8. Samuel T, Hoy WE, Douglas-Denton R *et al.*: Determinants of glomerular volume in different cortical zones of the human kidney. *J Am Soc Nephrol* 16:3102-3109, 2005.
9. Oliver J: problems of aging, biological and medical aspects, Baltimore, Williams & Wilkins, 1939, pp 257-277.



# 10

## GENERAL DISCUSSION





## **PARIETAL EPITHELIAL CELL INJURY: TIPPING THE BALANCE BETWEEN GLOMERULOSCLEROSIS AND GLOMERULAR INVOLUTION?**

### *Focal segmental glomerulosclerosis*

FSGS is defined by the focal and segmental presence of lesions that are characterized by mesangial sclerosis, obliteration of glomerular capillaries with hyalinosis and intracapillary foam cells, adhesions between the glomerular tuft and Bowman's capsule, and podocyte hypertrophy. It is important to note that FSGS is not a disease entity, but rather a pattern of glomerular injury. Various morphological variants have recently been described [1]. It is as yet undecided if these variants have a different pathogenesis. In recent years the podocyte has become the culprit in the pathogenesis of FSGS [2;3]. One line of evidence comes from studies in patients with hereditary FSGS. In many patients mutations of podocytic proteins have been discovered [4]. Involved proteins are important in maintaining the slit-pore complex (e.g. nephrin, podocin, CD2AP,  $\alpha$ -actinin-4) or function as transcription factors (WT-1, LmX1b). Thus, dysfunction of podocytic proteins causes FSGS in humans. Other evidence is put forward by animal experiments. Especially studies by Kriz and coworkers have pointed to the role of podocytic injury in the pathogenesis of FSGS [5-7]. Notably, the models used by Kriz et al were characterized by glomerular hypertension and / or glomerular hyperfiltration. Podocytic injury was always recognized in the early phase, with later development of hypocellular FSGS lesions. In the pathogenesis proposed by these authors the podocyte is positioned as a terminally differentiated cell which is unable to replicate. Thus, podocytes are unable to compensate for injured podocytes that no longer adhere to the GBM and are lost in the urine. As a result there is denudation of the GBM, which is covered by parietal epithelial cells. Subsequently, a firm adhesion forms, which is composed of matrix and allows passage of proteins and filtrate from the capillaries to the periglomerular space. This latter process, also called misdirected filtration, is the cause of the periglomerular fibrosis and peritubular inflammation that is typically observed in FSGS.

Obviously, the above-mentioned pathogenesis is not applicable to collapsing FSGS. In collapsing FSGS there is always abundant cellular proliferation in Bowman's space. Collapsing FSGS is typically seen in HIV associated nephropathy, and has been associated with parvovirus B19 infection and pamidronate toxicity. Sometimes collapsing FSGS is observed in patients with idiopathic FSGS. Initially, most authors suggested that the proliferating cells were podocytes. Their conclusions were based on observations in light microscopy, which showed that the proliferating cells covered the capillary loops. In further studies it was noted that the proliferating cells did not express well known podocyte markers such as nephrin, synaptopodin or WT-1. These observations have introduced the concept of the dysregulated, proliferating podocyte. In this concept podocytes have dedifferentiated, have lost their podocytic markers and have regained the ability to proliferate. In the later phase of collapsing FSGS adhesions are formed.

Recent observations of our group in a mouse model of FSGS provided strong arguments against the above mentioned pathways of podocyte injury and suggested involvement of parietal epithelial cells. Our mouse model of FSGS is the Thy-1.1 transgenic mouse [8-10]. Thy-1.1 transgenic mice ectopically express the mouse Thy-1.1 antigen on podocytes. Injection of anti Thy-1.1 mAbs induces FSGS. The initial lesions show prominent epithelial cell hyperplasia. In this mouse model we observed dedifferentiation of the podocytes as reflected by the loss of some but not all podocyte markers. Most remarkably, we did not observe proliferating podocytes and we identified the proliferating cells as parietal epithelial cells. We also found that the matrix produced by these cells resembled Bowman's capsule. These findings suggested that parietal epithelial cells are involved in FSGS.

### *The parietal epithelial cell in human FSGS*

We conducted phenotypic analysis in a nephrectomy specimen of a patient with recurrence of idiopathic FSGS after transplantation [11]. In some glomeruli, glomerular epithelial cell hyperplasia was observed. The proliferating cells stained positively for cytokeratin and other PEC markers, and did not express podocyte markers. Many cells were located adjacent to the glomerular tuft, which suggested that these cells could be podocytes that newly expressed cytokeratin. However, we have been able to invalidate this conclusion using 3-dimensional analysis of the glomeruli. We could show that cytokeratin positive cells on the tuft were always in continuity with cytokeratin positive cell lining Bowman's capsule [11]. From these studies we concluded that PECs contributed to the cellular lesions in idiopathic FSGS. Similar conclusions were reached by Nagata et al and Kihara et al [12;13].

We have extended these observations in patients with collapsing FSGS related to HIV and pamidronate [14]. Based on double staining for CD10/CK8 and synaptopodin/CK8 we were able to demonstrate that the proliferating cells in HIV associated collapsing FSGS were PECs. Another important observation in our studies is related to the composition of the newly formed matrix. We showed that the staining characteristics of the matrix were similar to Bowman's capsule. Based on our studies we propose that the current views of the development of FSGS must be changed. Obviously, injury to the podocyte with resulting proteinuria is the first step. However, we never observed non-adherent podocytes or denudation of the GBM. Rather, there is injury of the PECs with denudation of Bowman's capsule. Hereafter adhesions develop as a result of contacts between the podocyte (tuft) and PECs and possibly denuded Bowman's capsule. Activated PECs produce matrix that covers the podocytes. These podocytes disappear and eventually a hypocellular scar lesion is formed. Adjacent PECs may proliferate, explaining the hypercellular lesions that can be observed in FSGS. Finally, the adhesions provoke periglomerular fibrosis and tubulo-interstitial fibrosis, likely thru misdirected filtration of plasma proteins, a process elegantly demonstrated by Kriz et al [15].

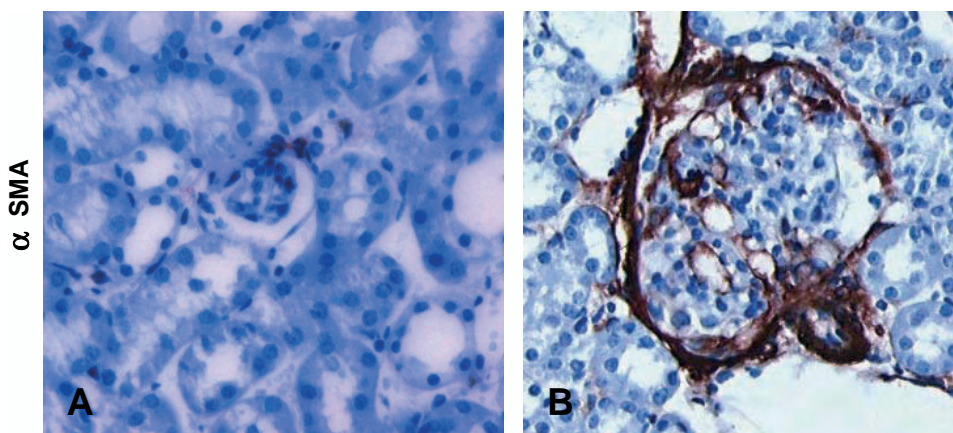


**Figure 1. Staining characteristics of the periglomerular region in glomerular involution (panel A) and in FSGS (panel B):** Notable is the absence of interstitial reaction or inflammation of the surrounding interstitium in glomerular involution (panel A). This is in clear contrast with the marked periglomerular fibrosis in our mouse model of FSGS (panel B).

### *Glomerular involution, a new type of glomerular injury*

We have identified abnormal glomeruli in renal biopsies of children with frequently relapsing nephrotic syndrome due to minimal change nephropathy. These glomeruli were characterized by their small size, the presence of vital cells in the matrix, and the notable absence of periglomerular and tubulo-interstitial fibrosis. We have proposed the term glomerular involution to describe this abnormality. Involuted glomeruli can be distinguished from vascular sclerosis (also referred to as obsolescent glomerulosclerosis) and glomerulopathic sclerosis (also referred to as solidified glomerulosclerosis). We have developed a mouse model of glomerular involution by repeatedly injecting nephritogenic anti-APA mAbs in mice. These mice did not develop FSGS. However, after 12 months we observed small glomeruli that resembled the involuted glomeruli that we observed in children. Again, most notable was the complete absence of periglomerular and tubulo-interstitial fibrosis. This finding is in clear contrast with the marked periglomerular fibrosis that always accompanies glomerulosclerosis in the Thy-1.1 mouse model (Figure 1). The absence of periglomerular fibrosis is clear evidence that glomerulosclerosis and glomerular involution differ in pathogenesis.

Based on our studies we have developed a new scheme that illustrates the development of FSGS and glomerular involution (Figure 2).

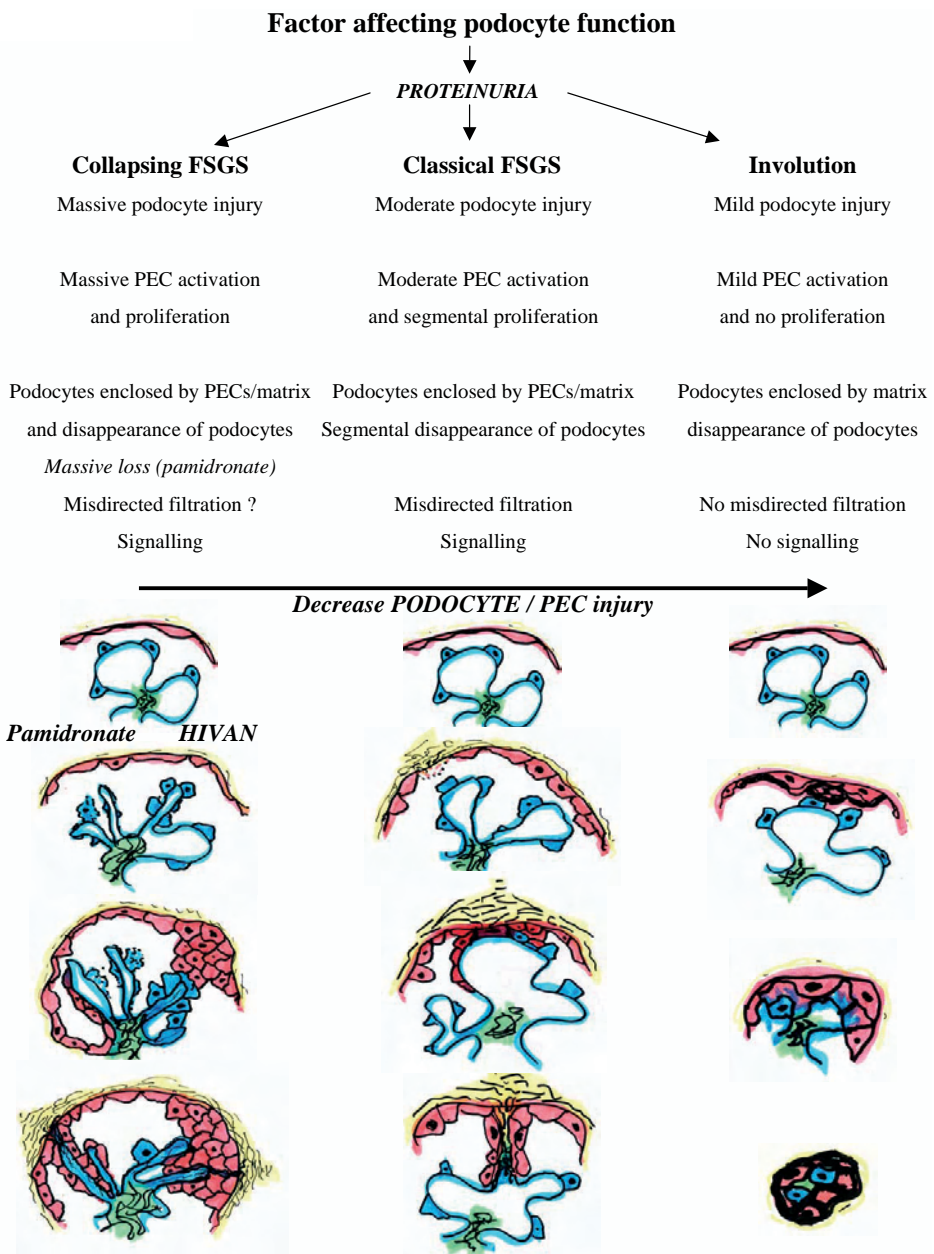


**Figure 2. A new scheme that illustrates the development of FSGS and glomerular involution:** The proposed scheme describes the relation between proteinuria, podocyte injury, PEC activation/proliferation, matrix production, misdirected filtration/signalling and the development of glomerulosclerosis and glomerular involution.

## DEVELOPMENT OF FGSG AND GLOMERULAR INVOLUTION

### *PECs are important in FSGS and involution*

Podocyte injury is the initial event in the development of glomerulosclerosis and glomerular involution. Podocyte injury is clinically characterized by proteinuria. Although there is a relation between proteinuria and FSGS, the mere presence of proteinuria is not sufficient to cause FSGS. This is well known from clinical examples such as minimal change disease and membranous nephropathy. Patients with minimal change disease do not develop FSGS. In membranous nephropathy the situation is somewhat more complex, with approximately 40-50% of patients developing FSGS. The latter patients are more likely to develop progressive renal insufficiency. Podocyte injury has to reach a certain level to cause FSGS. Mild injury, as in minimal change, may not lead to glomerular loss or may lead to glomerular involution in case podocytes are repeatedly injured.

How activated / injured podocytes exactly induce FSGS remains unclear. Factors such as proteinuria, direct interaction between podocytes or PECs may be involved. Also denudated segments of GBM or Bowman's capsule may provide a growth stimulus. Activated glomerular cells may produce cytokines and growth factors stimulating cell proliferation and matrix production. Naked GBM may especially play a role in 'toxic FSGS' or for instance pamidronate associated FSGS, when podocytes are rapidly lost due to toxicity.

We propose that if podocyte injury is severe enough, PEC activation and proliferation is the next step in the development of FSGS. The extent of PEC proliferation depends on the level of podocytic injury. We propose that podocyte / parietal cell injury may differ in extent or severity, thus explaining the divergent histological pictures. Parietal cell injury may lead to disappearance of the PECs or loss of cell-cell contacts. As a consequence there is denudation of Bowman's capsule. Alternatively, sub lethally damaged PECs may become activated, produce matrix and proliferate.

In classical FSGS parietal injury is moderately severe. The podocytes attach to Bowman's capsule or form cell bridges with activated PECs, there is mild PEC proliferation and production of matrix that covers the podocytes. As a result, the podocytes get enclosed by PECs and disappear, thus resulting in the hypocellular adhesion. At the site of this adhesion periglomerular inflammation starts, followed by fibrosis, a process possibly related to misdirected filtration of proteinaceous fluid or the production of exocrine factors by glomerular cells. The adhesion is infiltrated by myofibroblasts, matrix accumulates and neighboring capillaries disappear, ultimately leading to a sclerosed portion of the glomerulus.

Injury to the podocytes and PECs is more severe in collapsing FSGS, such as seen in HIV infection. The podocytes are hypertrophic and activated. There is more prominent prolifera-

tion of the PECs, thus filling Bowman's space. This process gives the glomerulus the typical appearance with collapsed glomerular capillaries. In seldom cases podocyte injury may be so severe as to cause their disappearance, with PECs filling in their place. Such events may occur in pamidronate induced FSGS, characterized by severe injury of the podocytes.

If PEC injury is limited, another pathway toward glomerular involution is followed. In this case, there is initially no loss of PECs and cell-cell contacts between PECs remain intact. There is no denudated Bowman's capsule, cell bridges between podocytes and PECs occur, matrix is produced but there is no periglomerular inflammation or fibrosis. Still, podocytes disappear, and the loss of podocytes is accompanied by loss of endothelial cells and thus capillaries. Also, the injured PECs produce matrix, but do not proliferate and eventually disappear. The result is the decrease in size and ultimate disappearance of the glomerulus.

We hypothesize that podocyte and PEC injury are linked. Possibly PEC injury is triggered by podocytic proteins (cytokines, growth factors) that are produced during podocyte activation. Alternatively, PEC injury may be the mere consequence of proteinuria, whereby the severity and the extent of injury is determined by the amount and type of proteinuria. Clinically, it is well known that both the amount of proteinuria and the type of proteinuria (as reflected by protein selectivity index) are related to prognosis in proteinuric renal diseases. Whenever adhesions (matrix continuity) between the glomerular tuft and Bowman's capsule are formed, misdirected filtration may occur and cause interstitial fibrosis. Alternatively, it cannot be excluded that factors produced by activated PECs / podocytes directly induce periglomerular fibrosis and that during glomerular involution such stimulating factors are not produced.

## CONCLUSION

Our proposed scheme describes the relation between podocyte injury, proteinuria and the development of glomerulosclerosis and glomerular involution. Our model attributes a central role to the PEC. Specifically, the reponse of the PEC determines if the initial podocytic insult is followed by the development of FSGS or glomerular involution.

Further studies are needed to clarify the relation between podocyte injury, proteinuria, PEC injury and the balance between development of FSGS or glomerular involution.

From a therapeutic perspective it seems worthwhile to pursue strategies that are capable of interfering with PEC activation or injury.

## REFERENCES

1. D'Agati V: Pathologic classification of focal segmental glomerulosclerosis. *Semin Nephrol* 23:117-134, 2003.
2. Kriz W, Elger M, Nagata M *et al.*: The role of podocytes in the development of glomerular sclerosis. *Kidney Int Suppl* 45:S64-S72, 1994.
3. Kretzler M, Koepfen-Hagemann I, Kriz W: Podocyte damage is a critical step in the development of glomerulosclerosis in the uninephrectomised-desoxycorticosterone hypertensive rat. *Virchows Arch* 425:181-193, 1994.
4. Tryggvason K, Patrakka J, Wartiovaara J: Hereditary proteinuria syndromes and mechanisms of proteinuria. *N Engl J Med* 354:1387-1401, 2006.
5. Kriz W: Progressive renal failure--inability of podocytes to replicate and the consequences for development of glomerulosclerosis. *Nephrol Dial Transplant* 11:1738-1742, 1996.
6. Kriz W, Gretz N, Lemley KV: Progression of glomerular diseases: is the podocyte the culprit? *Kidney Int* 54:687-697, 1998.
7. Kriz W, Lemley KV: The role of the podocyte in glomerulosclerosis. *Curr Opin Nephrol Hypertens* 8:489-497, 1999.
8. Assmann KJ, van Son JP, Dijkman HB *et al.*: Antibody-induced albuminuria and accelerated focal glomerulosclerosis in the Thy-1.1 transgenic mouse. *Kidney Int* 62:116-126, 2002.
9. Smeets B, Dijkman HB, Te Loeke NA *et al.*: Podocyte changes upon induction of albuminuria in Thy-1.1 transgenic mice. *Nephrol Dial Transplant* 18:2524-2533, 2003.
10. Smeets B, Te Loeke NA, Dijkman HB *et al.*: The parietal epithelial cell: a key player in the pathogenesis of focal segmental glomerulosclerosis in Thy-1.1 transgenic mice. *J Am Soc Nephrol* 15:928-939, 2004.
11. Dijkman H, Smeets B, van der LJ *et al.*: The parietal epithelial cell is crucially involved in human idiopathic focal segmental glomerulosclerosis. *Kidney Int* 68:1562-1572, 2005.
12. Nagata M, Hattori M, Hamano Y *et al.*: Origin and phenotypic features of hyperplastic epithelial cells in collapsing glomerulopathy. *Am J Kidney Dis* 32:962-969, 1998.
13. Kihara I, Yaoita E, Kawasaki K *et al.*: Origin of hyperplastic epithelial cells in idiopathic collapsing glomerulopathy. *Histopathology* 34:537-547, 1999.
14. Dijkman HB, Weening JJ, Smeets B *et al.*: Proliferating cells in HIV and pamidronate-associated collapsing focal segmental glomerulosclerosis are parietal epithelial cells. *Kidney Int* 70: 338-344, 2006.
15. Kriz W, Hartmann I, Hosser H *et al.*: Tracer studies in the rat demonstrate misdirected filtration and peritubular filtrate spreading in nephrons with segmental glomerulosclerosis. *J Am Soc Nephrol* 12:496-506, 2001.





# 11

## SUMMARY



## THE ROLE OF THE GLOMERULAR EPITHELIAL CELLS IN FOCAL SEGMENTAL GLOMERULOSCLEROSIS

Proteinuria is an important hallmark of glomerular diseases. In recent years we have described a mouse model of acute proteinuria. Injection of a combination of two mAbs directed against specific epitopes of mouse aminopeptidase-A (APA) induces a massive but transient acute albuminuria. This model was used to evaluate possible mechanisms of proteinuria.

Aminopeptidase-A (APA) (EC 3.4.11.7) is a membranebound zinc metalloprotease. In mouse kidney, it is predominately expressed on podocytes and the brush borders of the proximal tubules. APA is involved in the degradation and uptake of filtered peptides. The best-known substrate of APA is angiotensin II (Ang II), the most active component of the renin-angiotensin system (RAS).

Injection of a combination of anti-APA antibodies that inhibit the enzyme activity increased intrarenal levels of angiotensin II. Angiotensin II is important for the normal development of the kidney. The role of APA has not been studied. Therefore, we have used the anti-APA mAbs as tools to study the expression of APA in the kidney during nephrogenesis (Chapter 2). In addition, we evaluated the effect of APA-enzyme inhibition on nephrogenesis by injecting anti-APA mAbs in 1-day old mice.

In developing glomeruli APA expression was observed from the comma stage onwards, predominantly in the developing podocytes and brush borders of proximal tubular cells. Although APA is highly expressed, complete inhibition of APA during nephrogenesis for 9 days after birth did not affect normal development of nephrons. We only observed podocyte effacement at days 9 and 21 which disappeared after 3 months. Our study suggests that APA has only a minor role during embryonal development.

An injection of the anti-APA mAbs combination ASD-37/41 induces a massive but transient albuminuria which peaked at 8 hr, and declined thereafter. Induction of the albuminuria is not related to any of the known systemic mediators of glomerular injury, such as complement, coagulation factors, monocytes, neutrophils, or platelets. Recently, we demonstrated that the induction of albuminuria is not dependent on the presence of angiotensin II. Thus it is unlikely that systemic factors or hemodynamic changes are relevant for the development of proteinuria in our anti-APA model.

We have performed additional studies to evaluate possible mechanisms involved in the development of proteinuria. In the experiments described in chapter 3, we have examined the expression of several important podocytic proteins in relation to the time course of the albuminuria. We have included cytoskeleton (-associated) proteins, adhesion molecules, slit-diaphragm proteins and heparan sulfate proteoglycans, all known to affect podocyte integrity.

In addition, we measured ultrastructurally foot process retraction (the number of foot processes per  $\mu\text{m}$  GBM) and the width of the slit pore between the podocytes by morphometric methods. An injection of the mAbs combination ASD-37/41 induced a massive albuminuria that started at 6 hr, peaked at 8 hr, and decreased thereafter. However, at day 7 after injection of the mAbs still some albuminuria was present. Changes in the expression of two slit-pore-associated proteins, CD2AP and podocin coincided with the start of the albuminuria. The normal homogeneous staining along the capillary loops of podocin became more granular at 6 hr with evidence of a recovery at day 7. At the same time, CD2AP expression changed from a normal fine granular into a granular pattern at 6 hr that persisted unchanged until day 7. At the early time point, no changes in the expression of nephrin were noted. The staining for nephrin at 24 hr was slightly less than in previous hours and podocytic actin staining became more granular only at a time point that albuminuria was declining (24 hr). The number of foot processes per  $\mu\text{m}$  GBM was already decreased at 4 hr, with further reduction thereafter. The width of the slit pore was unchanged at the time of peak albuminuria and gradually decreased thereafter. At day 7, podocytic foot process effacement was even more prominent although albuminuria was only slightly abnormal. Expression of CD2AP was still granular. We observed however a change toward normal in the expression of podocin. Our data show that the onset of albuminuria in the anti-APA model is related to alterations in CD2AP and podocin, proteins that are important for maintaining slit diaphragm structure and podocytic function.

To quantitate the degree of foot process retraction and the width of the slit pore we had to calibrate our system and used replicas. Especially calibration of the magnification in digital images from transmission electron microscopy is not always accurate. We have developed a better procedure that allows automated measurement of the calibration on electron microscopical images with high precision. The procedure is described in chapter 4.

We have next focussed on focal segmental glomerulosclerosis. FSGS has become one of the most common glomerular diseases and is characterized by focal and segmental occurrence of lesions with mesangial sclerosis, obliteration of glomerular capillaries with hyalinosis, intra-capillary foam cells and formation of adhesions. Based on findings in a mouse model of FSGS we questioned if PECs play a role in human FSGS. In chapter 5 we describe the relative role of PECs and podocytes in human idiopathic FSGS. We investigated the nephrectomy specimen of a patient who suffered from recurrent FSGS after transplantation. We performed a detailed study of lesions by serial sectioning, marker analysis and three-dimensional reconstruction of glomeruli. We have studied the expression of markers for podocytes, PECs, mesangial cells, endothelium, and myofibroblasts. Also proliferation and composition of the deposited extracellular matrix (ECM) were investigated. Our study demonstrated that the proliferating epithelial cells in FSGS lesions were negative for podocyte and macrophage markers, but

stained for PEC markers such as PAX-2, CK8 and pancadherin. The staining characteristics of the matrix deposited by these cells was identical to Bowman's capsule. Sometimes these proliferating cells were observed on the glomerular tuft, but they were always connected to cells lining Bowman's capsule. We have used sophisticated three-dimensional analysis (3-D) to prove this.

Taken together, these data argue that proliferating epithelial cells in active FSGS lesions are PECs and question the contribution of the so-called 'dedifferentiated' podocyte. The concept of the dedifferentiated podocyte was based on findings in human immunodeficiency virus (HIV)-induced collapsing FSGS (cFSGS). It is therefore conceivable that podocyte proliferation might occur in this condition, probably related to incorporation of viral genome in podocytic DNA. Therefore, we also investigated the origin of the proliferating cells in cFSGS associated with HIV and pamidronate (chapter 6). Both entities are characterized by global collapse and the absence of adhesions. We performed a detailed study of glomerular lesions in biopsies of two patients with HIV associated cFSGS and a nephrectomy specimen of a patient with pamidronate associated cFSGS. Glomeruli were studied by serial sectioning using light and electron microscopy and immunohistochemistry. The proliferating cells were negative for the podocyte markers, but stained positive for the PEC markers and the cell proliferation marker Ki-67. The proliferating PAX-2 and CK8 positive cells that covered the capillary tuft were always in continuity with PAX-2/CK8 positive cells lining Bowman's capsule. Double staining experiments provide additional evidence for the role of PECs. We were able to show CK8 positive PECs covering CD10 positive podocytes. The staining of the matrix deposited by these proliferating cells was identical to Bowman's capsule. So, also in HIV and pamidronate associated cFSGS most of the proliferating cells are PECs.

Thus our studies show that the parietal epithelial cells constitute the hypercellular lesions in cFSGS. The concept of the dedifferentiated-proliferating podocyte needs revision.

Progressive FSGS will eventually lead to global glomerulosclerosis. Global glomerulosclerosis is often observed in patients with renal disease or patients with nephrosclerosis. Two types of global glomerulosclerosis are described: the obsolescent type and the solidified type. The obsolescent type (vascular sclerosis) is characterised by retraction of the tuft and Bowman's space is filled with collagenous material. The solidified type (glomerulopathic sclerosis) is characterised by global solidification of the tuft, without deposition of collagenous material in Bowman's space.

We noticed the presence of abnormal glomeruli in biopsies of children with a recurrent nephrotic syndrome. The glomeruli were small and globally sclerosed, and we have suggested the term involution to describe this process (chapter 7). We have investigated these involuted glomeruli in more detail and compared them with the other types of global glomerulosclerosis. Involved glomeruli were characterised by their reduced size, and a global increase of

matrix. However, these glomeruli appeared distinct from obsolescent or solidified globally sclerosed glomeruli in view of the continuing presence of glomerular cells. Most remarkable was the absence of periglomerular and tubulo-interstitial fibrosis. Our data suggested that these glomeruli present an unique form of glomerular injury.

We have extended our studies and evaluated the renal biopsies of 18 children with frequently relapsing or steroid dependent minimal change nephrotic syndrome due to minimal change nephropathy (chapter 8). We counted the abnormal glomeruli, and evaluated the relation with clinical parameters. We have studied 11 boys and 7 girls. Median age at disease onset was 2.8 years (1.6-10.6 years) and at biopsy 5.2 years (2.3-10.9 years). The biopsies contained 19 (5-35) glomeruli. Many biopsies contained small, globally sclerosed glomeruli with the characteristics of involuted glomeruli. The median percentage of involuted glomeruli was 6% (range 0-33%). Biopsies of six patients did not show involuted glomeruli. When comparing patients without and with involuted glomeruli we observed a significant difference in the age at renal biopsy (without involution:  $3.9 \pm 1.1$  year, with involution  $6.5 \pm 2.6$  years;  $p < 0.05$ ) and the interval between onset of disease and the renal biopsy ( $0.44 \pm 0.43$  years vs  $3.8 \pm 3.3$  years;  $p < 0.01$ ). There were no significant differences in gender distribution, maximal proteinuria at onset, serum albumin, number of recurrences or selectivity index. There was a significant correlation between the percentage of involuted glomeruli and the interval between onset of disease and renal biopsy (Spearman  $R = 0.64$ ;  $p < 0.01$ ). By logistic regression analysis the interval between disease onset and the renal biopsy was the only independent significant predictor.

As described in chapter 9 we have more or less by chance developed a mouse model of glomerular involution. We have tried to induce FSGS by multiple injections of anti-APA mAbs in mice. We followed the mice for a long time period and evaluated albuminuria and podocyte injury. Specifically, we used 6 weeks old mice, injected them on day 1 and again on day 7. We followed the groups over 12 months and tested the urine samples for albuminuria every 4 weeks. The treated mice developed acute albuminuria after each injection. Thereafter albuminuria decreased to values slightly above normal. Mice were sacrificed at months 7, 10 and 12. Light microscopy of the kidneys revealed up to 17% of small, dense glomeruli. These small glomeruli had the same characteristics as the involuted glomeruli described in children with minimal change disease. Electron microscopy revealed partial foot process effacement and thickening of the GBM in the early phase of glomerular involution. Our mouse model will enable us to investigate in more detail the pathogenesis of glomerular involution.

In chapter 10 we discuss our findings and propose a new scheme for the development of FSGS and glomerular involution. We attribute a central role to parietal epithelial cell injury in determining if podocyte injury and proteinuria progress to FSGS or glomerular involution. If confirmed by further studies the PEC might become a new target for therapy.

# 12

**SAMENVATTING**





## **DE ROL VAN DE GLOMERULAIRE EPITHEELCEL (PODOCYT) EN DE PARIETALE EPITHEELCEL (PEC) BIJ HET ONTSTAAN VAN PROTEÏNURIE EN FOCALE SEGMENTALE GLOMERULOSCLEROSE.**

Eiwitverlies is een belangrijk kenmerk van nierziekten. Wij maken gebruik van een muismodel voor de bestudering van mogelijke mechanismen die betrokken zijn bij het ontstaan van eiwitverlies. Wij kunnen in een muis proteïnurie opwekken door injectie van een combinatie van twee monoklonale antilichamen (ASD-37/41) die gericht zijn tegen verschillende epitopen van het aminopeptidase-A (APA) eiwit. APA (EC 3.4.11.7) is een membraangebonden zink-metalloprotease, dat in de muizenier voornamelijk voorkomt op de glomerulaire epitheelcel, ook wel de podocyt genoemd en op de borstelzoom van de proximale tubulus. APA is betrokken bij de afbraak en de opname van gefiltreerde peptiden. Het bekendste substraat van APA is angiotensine II (Ang II). Ang II is de meest actieve component van het renine-angiotensine systeem. Ang II speelt ook een belangrijke rol bij de normale ontwikkeling van de nier. De rol van APA hierbij is tot op heden niet bestudeerd. Wij hebben de anti-APA antilichamen gebruikt om de expressie van APA in de nier te bestuderen tijdens de nephrogenese of wel ontwikkeling van de nier (hoofdstuk 2). Tevens hebben wij gekeken naar het effect van de enzymremming van APA tijdens de nephrogenese. Bij deze studie hebben wij muizen van 1 dag oud, ingespoten met anti-APA monoclonalen. De nefrogenese van de nier voltooit zich pas 10 dagen na de geboorte, vandaar dat wij in deze experimenten de ontwikkeling van het nefron in verschillende stadia nog uitgebreid kunnen bestuderen. Tijdens de nefrogenese bleek APA al vroeg tot expressie te komen en wel vanaf de kommafase. APA expressie was met name zichtbaar op de tot ontwikkeling komende podocyt en op de borstelzoom van de proximale tubulus cellen. Complete remming van de enzymactiviteit gedurende de eerste 9 dagen na de geboorte bleek geen effect te hebben op de normale ontwikkeling van de nephronen. Het enige wat we konden waarnemen was geringe versmelting van de voeten van de podocyt, die nog zichtbaar was op dag 9 en 21 na de geboorte. Na 3 maanden waren ook deze afwijkingen verdwenen. Onze studie suggereert dat APA geen belangrijke rol speelt tijdens de nephrogenese.

Zoals vermeld leidt toediening van de combinatie van anti-APA monoklonale antistoffen tot een massief eiwitlek. Dit eiwitlek is maximaal 8 uur na inspuiting en neemt daarna geleidelijk af. De albuminurie wordt niet veroorzaakt door ontstekingsmediatoren zoals complement, stollingsfactoren, monocyten, granulocyten of bloedplaatjes. Recent hebben wij aangetoond dat het ontstaan van albuminurie onafhankelijk is van de aanwezigheid van Ang II. Daarom lijkt het onwaarschijnlijk dat systemische factoren of hemodynamische veranderingen betrokken zijn bij het ontstaan van het eiwitverlies in ons anti-APA muismodel.

Wij hebben aanvullende studies uitgevoerd om andere mechanismen die betrokken kunnen zijn bij de ontwikkeling van het eiwitverlies te onderzoeken. In de experimenten beschreven in hoofdstuk 3, hebben wij de expressie bestudeerd van een aantal belangrijke podocytaire eiwitten in relatie tot de ontwikkeling van albuminurie. Wij hebben hierbij gekeken naar cytoskelet geassocieerde eiwitten, adhesiemoleculen, slit-diafragma eiwitten en heparan-sulfaat proteoglycanen. Van al deze eiwitten is bekend dat zij de integriteit van de podocyt kunnen beïnvloeden. Tevens hebben wij op ultrastructureel niveau het aantal podocytvoetjes gemeten per micrometer glomerulaire basaalmembraan (GBM) en wij hebben de afstand gemeten tussen de voetjes, de zogenaamde slit-pore. Hiervoor hebben wij gebruik gemaakt van beeldanalyse van elektronenmicroscopische opnamen.

Een injectie van de combinatie ASD-37/41 induceerde een massief eiwitlek dat optrad op 6 uur na inspuiting, piekte op 8 uur en daarna geleidelijk afnam tot een licht verhoogd niveau op dag 7. Veranderingen in de expressie van twee belangrijke slit-pore geassocieerde eiwitten te weten CD2AP en podocine, vielen samen met het ontstaan van het eiwitlek. Podocine laat normaal een homogene aankleuring langs de capillaire lisswand zien maar werd echter granulaair op 6 uur na inspuiting. Na 7 dagen leek er herstel te zijn. Tevens veranderde de CD2AP-expressie van fijn granulaair naar een meer grof granulaair patroon op 6 uur; dit bleef echter onveranderd op dag 7. Nefrine liet op 6 uur na inspuiting van de antilichamen geen verandering zien in expressie maar na 24 uur nam de eiwitexpressie licht af. Het actineskelet van de podocyt werd eveneens meer granulaair, echter pas na 24 uur. Dit was enigszins opmerkelijk aangezien het eiwitverlies toen al fors was afgenomen. Het aantal podocytvoetjes per GBM-lengte was al afgenomen na 4 uur en de voetjesversmelting nam verder toe in de tijd. De slit-pore was onveranderd tijdens de piek van het eiwitlek maar werd smaller in de daaropvolgende dagen. De podocytversmelting was het duidelijkst op dag 7, hoewel de albuminurie op dat moment bijna verdwenen was. Het expressiepatroon van CD2AP was nog steeds granulaair in tegenstelling tot het expressiepatroon van podocine wat weer homogeen werd. Onze data suggereren dat veranderingen in CD2AP en Podocine een rol kunnen spelen bij het ontstaan van de albuminurie in ons APA-model. Deze eiwitten zijn belangrijk bij de instandhouding van het slit-diafragma.

Bij het meten van het aantal podocytvoetjes per lengte-eenheid en de slit-pore breedte speelt de calibratie van het meetstelsel een belangrijke rol. Hierbij maken we gebruik van meetreplica's. Hiermee kunnen we de vergroting die gegenereerd wordt in het transmissie electronenmicroscopie precies berekenen. Het omzetten van het replicabeeld in een vergrotingsfactor hebben wij in een vernieuwde meetprocedure verder ontwikkeld en gedeeltelijk geautomatiseerd. Hierdoor kunnen we de replicavergroting nauwkeuriger en sneller berekenen. Deze procedure is beschreven in hoofdstuk 4.

Vervolgens hebben wij ons gericht op de ontwikkeling van focale segmentale glomerulosclerose (FSGS). FSGS is een van de meest voorkomende glomerulaire ziekten. FSGS wordt gekenmerkt door het voorkomen van afwijkingen in een deel (segment) van de glomerulus, waarbij slechts een beperkt aantal glomeruli (focaal) zijn aangedaan. Karakteristiek voor FSGS zijn de mesangiale sclerose en het samenvallen van glomerulaire capillairen, met hyalinose van de vaatwand en vorming van schuimcellen. Meest kenmerkend zijn de verbindingen tussen de capillaire kluwen en het kapsel van Bowman, de zogenaamde adhesies of senechiën. Bij sommige vormen van FSGS wordt een toename van het aantal cellen in de ruimte van Bowman gezien. In het algemeen werd aangenomen dat het podocyten betrof, die gedifferentieerd waren en weer proliferatieve eigenschappen hadden verworven. Wij hadden in een muizenmodel voor FSGS aanwijzingen gevonden dat de PEC een belangrijke rol zou kunnen spelen bij FSGS. Daarom onderzochten wij de rol van de pariëtale epitheelcel (PEC) bij de ontwikkeling van FSGS in de mens. Allereerst bestudeerden wij een nefrectomie preparaat van een patiënt, waarbij de FSGS was teruggekeerd in de transplantaatnier (Hoofdstuk 5).

Wij hebben seriële coupes kunnen bestuderen en een driedimensionale reconstructie van glomerulaire laesies uitgevoerd. De prolifererende cellen hadden alle kenmerken van PECs. Podocytmarkers werden niet aangetroffen. Toch gaven de lichtmicroscopische beelden de indruk dat we te maken hadden met podocyten omdat soms de prolifererende cellen op de capillaire kluwen lagen en geen contact leken te maken met de pariëtale cellen van het kapsel van Bowman. Door middel van driedimensionale analyse van de glomerulus konden wij echter aantonen dat deze cellen altijd in contact bleken te staan met pariëtale cellen langs het kapsel van Bowman. De nieuw gevormde matrix had de kenmerken van het kapsel van Bowman. Deze studie toonde dus aan dat pariëtale epitheelcellen prolifereren en verantwoordelijk zijn voor de epitheelcelhyperplasie bij idiopathische FSGS. Pariëtale epitheelcellen produceren de matrix die een rol speelt bij de ontwikkeling van de sclerotische laesies. Het concept van de prolifererende, gedifferentieerde podocyt is ontwikkeld in studies van collapsing FSGS (cFSGS) in combinatie met een HIV infectie. Daarom hebben wij de herkomst van de prolifererende cellen in collapsing FSGS, geassocieerd met HIV of pamidronaat, onderzocht (Hoofdstuk 6). Wij bestudeerden nierbiopten van 2 patiënten met HIV en een nefrectomie preparaat van een patient met pamidronaat-geïnduceerde FSGS. Het bleek dat alle prolifererende cellen negatief waren voor podocytmarkers (synaptopodine en CD10), maar wel aankleurden voor PECmarkers (PAX-2 en CK8) in combinatie met de proliferatiemarker KI-67. Deze PAX-2 en CK8 positieve prolifererende cellen bekleden de capillaire kluwen en bleken wederom altijd in contact te staan met PAX-2/CK8 positieve cellen op het kapsel van Bowman. Met dubbelkleuringen zijn wij erin geslaagd onze conclusies te versterken. We konden aantonen dat CK8 positieve PECs lagen op CD10 positieve podocyten. De prolifererende cellen produceerden matrix die wederom identiek bleek te zijn aan de matrix van het kapsel van Bowman. Dus ook in de cFSGS die geassocieerd is met HIV en pamidronaat blijken de meeste prolifererende cellen PECs te zijn. Onze studies tonen aan dat de pariëtale epitheelcel

een belangrijke rol speelt in de pathogenese van FSGS en zowel bijdraagt aan de cellulaire hyperplasie als aan de matrixproductie. Onze studies suggereren dat het concept van de gedifferentieerde prolifererende podocyt moet worden aangepast.

Uiteindelijk zal progressieve FSGS leiden tot complete (globale) glomerulosclerose. Globale glomerulosclerose wordt vaak gezien bij patiënten met nierziekten of patiënten met nephrosclerose. Wij kunnen twee typen van globale glomerulosclerose onderscheiden, te weten de vasculaire vorm en de glomerulopathische vorm. Vasculaire sclerose wordt gekarakteriseerd door het inkrimpen van de capillaire kluwen. Hierdoor ontstaat er een leegte in de ruimte van Bowman, die wordt opgevuld met collageen materiaal (met name collageen type I). Glomerulopathische sclerose wordt gekarakteriseerd door een algehele sclerose van de capillaire kluwen. Beide vormen van glomerulosclerose worden gekenmerkt door het voorkomen van periglomerulaire en tubulo-interstitiële fibrose.

In biopten van kinderen met een recidiverend nefrotisch syndroom ontdekten wij abnormale glomeruli. Deze glomeruli waren globaal afwijkend, maar duidelijk te onderscheiden van de twee bekende vormen van globale glomerulosclerose. Deze glomeruli, door ons in Hoofdstuk 7 beschreven als involuerende glomeruli, werden gekenmerkt door de geringe grootte, de vorming van matrix waarbij vitale cellen tussen de matrix aanwezig bleven. Het meest opvallend was de totale afwezigheid van periglomerulaire en tubulo-interstitiële fibrose. Wij veronderstellen dat deze glomeruli een uiting zijn van een nieuwe vorm van glomerulaire beschadiging. In hoofdstuk 8 hebben wij onze studies uitgebreid door bestudering van nierbiopten afkomstig van een groep van 18 kinderen, die leden aan een frequent recidiverend of steroid afhankelijk nefrotisch syndroom ten gevolge van minimale laesies nefropathie. Wij hebben van deze totale groep (11 jongens en 7 meisjes) het aantal abnormale glomeruli in kaart gebracht en dit gerelateerd aan klinische parameters. De gemiddelde leeftijd bij het optreden van de ziekte was 2,8 jaar (1,6 -10,6 jaar). De gemiddelde leeftijd waarop het nierbiopt werd genomen was 5,2 jaar (2,3 – 10,9 jaar). De biopten bevatten gemiddeld 19 (5 – 35) glomeruli. Veel biopten bevatten kleine glomeruli met de karakteristieken van involuerende glomeruli. Het gemiddelde percentage van involuerende glomeruli was 6% (0 – 33%). 6 biopten bleken geen involuerende glomeruli te bevatten. Bij vergelijking van de patiënten met en zonder involuerende glomeruli viel op dat kinderen met involuerende glomeruli ouder waren op het moment van de biopsie. Ook was het tijdsinterval tussen het ontstaan van de ziekte en de nierbiopsie langer. Er waren geen andere significante verschillen. Met behulp van logistische regressieanalyse bleek het tijdsinterval tussen het ontstaan van de ziekte en het nemen van het nierbiopt de enige onafhankelijke voorspellende factor te zijn.

In hoofdstuk 9 beschrijven wij dat wij min of meer bij toeval een muismodel van glomerulaire involutie hebben ontwikkeld. Het oorspronkelijke doel was om door twee opeenvolgende

injecties van anti-APA monoclonale antilichamen een muismodel voor FSGS te ontwikkelen. Wij vervolgden deze muizen gedurende 12 maanden en onderzochten de urine elke maand op albuminurie. De behandelde muizen ontwikkelden een acute albuminurie na elke injectie. De proteïnurie nam vervolgens geleidelijk af, maar bleef significant hoger dan in de controle groep. Abnormale glomeruli werden gezien in muizen van de experimentele groep vanaf maand 7. Het percentage geïnvolueerde glomeruli nam toe tot maximaal 17% op maand 12. Deze abnormale glomeruli bleken identiek te zijn aan de involuerende glomeruli zoals beschreven bij de kinderen met minimale laesie nefropathie. Onderzoek met behulp van elektronenmicroscopie liet podocytoetversmelting en verdikking van de GBM in de vroege fase van glomerulaire involutie zien. Dit muizenmodel kan ons helpen om de pathogenese van glomerulaire involutie nader in kaart te brengen.

In hoofdstuk 10 bediscussiëren wij onze bevindingen. Wij hebben een nieuw schema opgesteld met betrekking tot de ontwikkeling van FSGS en glomerulaire involutie. In dit vernieuwde concept kennen wij een belangrijke rol toe aan de pariëtale epitheelcel. Schade aan deze cel en het kapsel van Bowman, bepaalt de balans tussen progressie tot FSGS of ontwikkeling naar glomerulaire involutie.

Indien verder onderzoek de rol van de PEC bevestigt, dan wordt deze cel mogelijk een belangrijk doelwit van therapeutische strategieën.





**DANKWOORD**





## WOORDEN VAN DANK

Ik wil allen die mij hebben bijgestaan bij de totstandkoming van dit proefschrift van harte danken. Velen hebben een bijdrage geleverd maar ik kan niet een ieder bij naam bedanken.

Echter enkele personen wil ik in het bijzonder noemen. Op de eerste plaats twee personen die zeer veel voor mij betekend hebben en nog steeds veel voor me betekenen, mijn promotor prof. dr. Jack Wetzels en mijn co-promoter dr. Karel Assmann.

Beste Jack, bedankt voor het vertrouwen dat je me hebt gegeven en de onaflatende steun waar ik altijd op kon rekenen. Jouw visie en enthousiasme hebben me altijd gestimuleerd om nieuwe wegen te bewandelen. Ik heb je leren kennen als een zeer bewogen hartelijk mens, die altijd voor iemand klaar staat en zich met de juiste argumenten graag laat overtuigen.

Beste Karel, jij was voor mij altijd een oprecht persoon, een leider en een prima collega. Over veel zaken dachten we hetzelfde en vanaf het begin dat ik je leerde kennen klikte het. Voor jezelf legde je de lat hoog. Je was zeer belezen en ik kon daardoor op ieder moment een beroep doen op je uitgebreide parate kennis, je was een wandelende bibliotheek. Veel heb ik van je mogen leren en ik wil je dan ook bedanken voor alle prettige discussies.

Ook mijn tweede co-promotor dr. Eric Steenbergen wil ik bedanken voor de samenwerking en steun in het onderzoek.

Mijn directe collega's van het laboratorium voor elektronenmicroscopie wil ik bedanken voor de prettige sfeer en de bereidheid om altijd voor elkaar klaar te staan. Ria, ook al ben je al even weg van de afdeling, vergeten zal ik je niet. Irene, Lilian en Maria, bedankt voor de steun in de afgelopen jaren. Fijn dat jullie mijn paranimfen wilden zijn, drie was net teveel maar ook dat hebben we prima opgelost.

De collega's van de niergroep, Mark, Nathalie, Bart, Kiek en Fieke, wil ik bedanken voor hun inzet en de prettige samenwerking. Bart, we hebben elkaar vaak gesteund en samen iets op de kaart gezet. Een persoon uit het verleden wil ik hier nog graag noemen. Ondanks het feit dat hij al bijna 7 jaar elders werkzaam is, heb ik met name prettige herinneringen aan Jacco die ik leerde kennen toen ik in 1988 begon bij de niergroep. Het aminopeptidase-A werk kreeg gestalte en de ASD-antilichamen (Assmann-Son-Dijkman) werden de basis voor verder onderzoek.

De collega's van de afdelingen Pathologie, Nierziekten, Antropogenetica, Kindergeeneeskunde en Biochemie ben ik zeer erkentelijk voor hun hulp, informatie, kennisoverdracht, antilichamen, materiaal en of samenwerking. Met name bedankt, dr. Jeroen van der Laak, Anita Gemmink, Monique Link, prof. dr. Jo Berden, dr. Johan van der Vlag, dr. Bert van den Heuvel, prof. dr. Nine Knoers-van Slobbe en dr. Toin van Kuppevelt.

Ook de collega's van de afdeling Pathologie van het AMC Amsterdam wil ik hartelijk bedanken voor hun samenwerking, met name bedankt prof. dr. Jan Weening.

Mijn collega's van het dierenlaboratorium (CDL) wil ik bedanken voor de verzorging van de proefdieren en de prettige samenwerking. Ook het secretariaat (staf & patiëntenzorg), de ICT medewerkers en het beheer van de afdeling Pathologie wil ik hierbij danken voor hun medewerking. Prof. dr. Dirk Ruiter en prof. dr. Han van Krieken wil ik dank zeggen voor de vrijheid die zij mij hebben gegeven om naast mijn vaste taak op de afdeling te werken aan mijn promotiestudie.

Mijn ouders wil ik bedanken voor hun steun en de gelegenheid die ze mij hebben geboden om dit te kunnen bereiken. Jolanda, jij was vaak mijn beschermer, een zus om trots op te zijn.

Lieve Marian, ik wil jouw bedanken voor je opbouwende kritiek en alle steun. Jij bent mijn stimulan. We hebben samen al vele mooie dingen bereikt.

Henry



## **CURRICULUM VITAE**



## CURRICULUM VITAE

Henry Dijkman werd geboren op 11 oktober 1962 te 's-Heerenberg. In 1978 behaalde hij het MAVO diploma aan de Andreas scholengemeenschap te Zevenaar. Hierna begon hij in 1978 aan de opleiding tot analist aan de Hoge school van Arnhem en Nijmegen (OLAN/HAN). Na het behalen van zijn MBO diploma in 1982 startte hij met de HBO opleiding met als differentiatie histopathologie/morfologische technieken. Na de afronding hiervan in 1984 was hij werkzaam als research analist op de afdeling Dermatologie van de Erasmus Universiteit te Rotterdam onder begeleiding van dr. J. Boddington en deed veel ervaring op binnen het gebied van de Immunoelektronenmicroscopie met als specialisatie de ultracryotomie.

In augustus 1988 startte hij als research analist op de afdeling Pathologie van het Universitair Medisch Centrum Nijmegen onder de begeleiding van dr. K.J.M. Assmann. Hij participeerde in het nefropathologisch onderzoek en hieruit ontstond de stimulans voor het promotieonderzoek. Momenteel is hij werkzaam als wetenschappelijk laboratorium medewerker aan het instituut voor Pathologie van het Universitair Medisch Centrum Nijmegen (Hoofd: Prof. dr. H. van Krieken).





## LIST OF PUBLICATIONS





## REFERENCES

1. Dijkman HB, Weening JJ, Smeets B, Verrijp KC, van Kuppevelt TH, Assmann KJ, Steenbergen EJ, Wetzels JF. Proliferating cells in HIV and pamidronate-associated collapsing focal segmental glomerulosclerosis are parietal epithelial cells. *Kidney Int* 70: 338-344, 2006.
2. Huls M, van den Heuvel JJ, Dijkman HB, Russel FG, Masereeuw R. ABC transporter expression profiling after ischemic reperfusion injury in mouse kidney. *Kidney Int* 69: 2186-2193, 2006.
3. Straathof-Galema L, Wetzels JF, Dijkman HB, Steenbergen EJ, Hilbrands LB. Sirolimus-associated heavy proteinuria in a renal transplant recipient: evidence for a tubular mechanism. *Am J Transplant* 6: 429-33, 2006.
4. van der Laak JA, Dijkman HB, Pahlplatz MM. Automated magnification calibration in transmission electron microscopy using Fourier analysis of replica images. *Ultramicroscopy* 106: 255-60, 2006.
5. Dijkman HB, Assmann KJ, Steenbergen EJ, Wetzels JF. Expression and effect of inhibition of aminopeptidase-A during nephrogenesis. *J Histochem Cytochem* 54: 253-62, 2006.
6. Wilmer MJ, de Graaf-Hess A, Blom HJ, Dijkman HB, Monnens LA, van den Heuvel LP, Levtschenko EN. Elevated oxidized glutathione in cystinotic proximal tubular epithelial cells. *Biochem Biophys Res Commun* 337: 610-4, 2005.
7. Dijkman H, Smeets B, van der Laak J, Steenbergen E, Wetzels J. The parietal epithelial cell is crucially involved in human idiopathic focal segmental glomerulosclerosis. *Kidney Int* 68: 1562-72, 2005.
8. Vogtlander NP, Dijkman H, Bakker MA, Campbell KP, van der Vlag J, Berden JH. Localization of alpha-Dystroglycan on the Podocyte: from Top to Toe. *J Histochem Cytochem* 53: 1345-53, 2005.
9. Heil SG, De Vriese AS, Kluijtmans LA, Dijkman H, van Strien D, Akkers R, Blom HJ. Cytochrome P450-2C11 mRNA is not expressed in endothelial cells dissected from rat renal arterioles. *Nephron Physiol* 99: 43-9, 2005.
10. Rops AL, van der Vlag J, Jacobs CW, Dijkman HB, Lensen JF, Wijnhoven TJ, van den Heuvel LP, van Kuppevelt TH, Berden JH. Isolation and characterization of conditionally immortalized mouse glomerular endothelial cell lines. *Kidney Int* 66: 2193-201, 2004.
11. de Graaf AO, van den Heuvel LP, Dijkman HB, de Abreu RA, Birkenkamp KU, de Witte T, van der Reijden BA, Smeitink JA, Jansen JH. Bcl-2 prevents loss of mitochondria in CCCP-induced apoptosis. *Exp Cell Res* 299: 533-40, 2004.
12. Smeets B, Te Loeke NA, Dijkman HB, Steenbergen ML, Lensen JF, Begieneman MP, van Kuppevelt TH, Wetzels JF, Steenbergen EJ. The parietal epithelial cell: a key player in the pathogenesis of focal segmental glomerulosclerosis in Thy-1.1 transgenic mice. *J Am Soc Nephrol* 15: 928-39, 2004.
13. Marchio S, Lahdenranta J, Schlingemann RO, Valdembri D, Wesseling P, Arap MA, Hajitou A, Ozawa MG, Trepel M, Giordano RJ, Nanus DM, Dijkman HB, Oosterwijk E, Sidman RL, Cooper MD, Bussolino F, Pasqualini R, Arap W. Aminopeptidase-A is a functional target in angiogenic blood vessels. *Cancer Cell* 5: 151-62, 2004.
14. Smeets B, Dijkman HB, Te Loeke NA, van Son JP, Steenbergen EJ, Assmann KJ, Wetzels JF, Groenen PJ. Podocyte changes upon induction of albuminuria in Thy-1.1 transgenic mice. *Nephrol Dial Transplant* 18: 2524-33, 2003.
15. Matschurat S, Blum S, Mitnacht-Kraus R, Dijkman HB, Kanal L, De Waal RM, Claus M. Negative regulatory role of PI3-kinase in TNF-induced tumor necrosis. *Int J Cancer* 92: 30-7, 2003.
16. Dijkman HB, Gerlofs-Nijland ME, van der Laak JA, Wetzels JF, Groenen PJ, Assmann KJ. Podocyte changes after induction of acute albuminuria in mice by anti-aminopeptidase-A mAb. *Nephron Exp Nephrol* 94: e85-e93, 2003.
17. van Dijk MC, Rombout PD, Dijkman HB, Ruiter DJ, Bernsen MR. Improved resolution by mounting of tissue sections for laser microdissection. *Mol Pathol* 56: 240-3, 2003.
18. Gerlofs-Nijland ME, Assmann KJ, van Son JP, Dijkman HB, Te Loeke NA, van der ZR, Wetzels JF, Groenen PJ. Epitope mapping of monoclonal antibodies directed to aminopeptidase-A and their relevance for albuminuria in mice. *Nephron Exp Nephrol* 94: e25-e34, 2003.
19. de Jong AS, Wessels E, Dijkman HB, Galama JM, Melchers WJ, Willems PH, van Kuppeveld FJ. Determinants for membrane association and permeabilization of the coxsackievirus 2B protein and the identification of the Golgi complex as the target organelle. *J Biol Chem* 278: 1012-21, 2003.
20. van Kuppeveld FJ, de JA, Dijkman HB, Andiono R, Melchers WJ. Studies towards the potential of poliovirus as a vector for the expression of

- HPV 16 virus-like-particles. *FEMS Immunol Med Microbiol* 34: 201-8, 2002.
21. Assmann KJ, van Son JP, Dijkman HB, Mentzel S, Wetzels JF. Antibody-induced albuminuria and accelerated focal glomerulosclerosis in the Thy-1.1 transgenic mouse. *Kidney Int* 62: 116-26, 2002.
  22. Gerlofs-Nijland ME, Assmann KJ, Dijkman HB, Dieker JW, van Son JP, Mentzel S, van Kats JP, Danser AH, Smithies O, Groenen PJ, Wetzels JF. Albuminuria in mice after injection of antibodies against aminopeptidase-A: role of angiotensin II. *J Am Soc Nephrol* 12: 2711-20, 2001.
  23. van Lent PL, Licht R, Dijkman H, Holthuysen AE, Berden JH, van den Berg WB. Uptake of apoptotic leukocytes by synovial lining macrophages inhibits immune complex-mediated arthritis. *J Leukoc Biol* 70: 708-14, 2001.
  24. van Spruiel AB, Leusen JH, van EM, Dijkman HB, Assmann KJ, Mayadas TN, van de Winkel JG. Mac-1 (CD11b/CD18) is essential for Fc receptor-mediated neutrophil cytotoxicity and immunologic synapse formation. *Blood* 97: 2478-86, 2001.
  25. Pijpers AH, van Setten PA, van den Heuvel LP, Assmann KJ, Dijkman HB, Pennings AH, Monnens LA, van Hinsbergh VW. Verocytotoxin-induced apoptosis of human microvascular endothelial cells. *J Am Soc Nephrol* 12: 767-78, 2001.
  26. van Leenders G, Dijkman H, Hulsbergen-van de Kaa C, Ruiter D, Schalken J. Demonstration of intermediate cells during human prostate epithelial differentiation in situ and in vitro using triple-staining confocal scanning microscopy. *Lab Invest* 80: 1251-8, 2000.
  27. Engbersen R, Moons MM, Wouterse AC, Dijkman HB, Kramers C, Smits P, Russel FG. Sulphonylurea drugs reduce hypoxic damage in the isolated perfused rat kidney. *Br J Pharmacol* 130: 1678-84, 2000.
  28. Raats CJ, van den BJ, Bakker MA, Oppers-Walgreen B, Pisa BJ, Dijkman HB, Assmann KJ, Berden JH. Expression of agrin, dystroglycan, and utrophin in normal renal tissue and in experimental glomerulopathies. *Am J Pathol* 156: 1749-65, 2000.
  29. Mentzel S, Dijkman HB, van Son JP, Wetzels JF, Assmann KJ. In vivo antibody-mediated modulation of aminopeptidase-A in mouse proximal tubular epithelial cells. *J Histochem Cytochem* 47: 871-80, 1999.
  30. Mentzel S, van Son JP, Dijkman HB, Wetzels JF, Assmann KJ. Induction of albuminuria in mice: synergistic effect of two monoclonal antibodies directed to different domains of aminopeptidase-A. *Kidney Int* 55: 1335-47, 1999.
  31. Bernsen MR, Dijkman HB, de Vries E, Figdor CG, Ruiter DJ, Adema GJ, van Muijen GN. Identification of multiple mRNA and DNA sequences from small tissue samples isolated by laser-assisted microdissection. *Lab Invest* 78: 1267-73, 1998.
  32. Latijnhouwers MA, Bergers M, Kuijpers AL, van der Vleuten CJ, Dijkman H, van de Kerkhof PC, Schalkwijk J. Tenascin-C is not a useful marker for disease activity in psoriasis. *Acta Derm Venereol* 78: 331-4, 1998.
  33. van Setten PA, van Hinsbergh VW, van den Heuvel LP, Preyers F, Dijkman HB, Assmann KJ, van der Velden TJ, Monnens LA. Monocyte chemoattractant protein-1 and interleukin-8 levels in urine and serum of patients with hemolytic uremic syndrome. *Pediatr Res* 43: 759-67, 1998.
  34. Groffen AJ, Ruegg MA, Dijkman H, van de Velden TJ, Buskens CA, van den Born J, Assmann KJ, Monnens LA, Veerkamp JH, van den Heuvel LP. Agrin is a major heparan sulfate proteoglycan in the human glomerular basement membrane. *J Histochem Cytochem* 46: 19-27, 1998.
  35. Groffen AJ, Hop FW, Tryggvason K, Dijkman H, Assmann KJ, Veerkamp JH, Monnens LA, van den Heuvel LP. Evidence for the existence of multiple heparan sulfate proteoglycans in the human glomerular basement membrane and mesangial matrix. *Eur J Biochem* 247: 175-82, 1997.
  36. van Kuppeveld FJ, Hoenderop JG, Smeets RL, Willems PH, Dijkman HB, Galama JM, Melchers WJ. Coxsackievirus protein 2B modifies endoplasmic reticulum membrane and plasma membrane permeability and facilitates virus release. *EMBO J* 16: 3519-32, 1997.
  37. Mentzel S, van Son JP, de Jong AS, Dijkman HB, Koene RA, Wetzels JF, Assmann KJ. Mouse glomerular epithelial cells in culture with features of podocytes in vivo express aminopeptidase-A and angiotensinogen but not other components of the renin-angiotensin system. *J Am Soc Nephrol* 8: 706-19, 1997.
  38. Latijnhouwers M, Bergers M, Ponc M, Dijkman H, Andriessen M, Schalkwijk J. Human epidermal keratinocytes are a source of tenascin-C

- during wound healing. *J Invest Dermatol* 108: 776-83, 1997.
39. Mentzel S, Assmann KJ, Dijkman HB, de Jong AS, van Son JP, Wetzels JF, Koene RA. Inhibition of aminopeptidase-A activity causes an acute albuminuria in mice: an angiotensin II-mediated effect? *Nephrol Dial Transplant* 11: 2163-9, 1996.
  40. de Jong DJ, Assmann KJ, de Abreu RA, Monnens LA, van Liebergen FJ, Dijkman HB, Huysmans FT. 2,8-Dihydroxyadenine stone formation in a renal transplant recipient due to adenine phosphoribosyltransferase deficiency. *J Urol* 156: 1754-5, 1996.
  41. Pfundt R, van RF, van Vlijmen-Willems IM, Alkemade HA, Zeeuwen PL, Jap PH, Dijkman H, Fransen J, Croes H, van Erp PE, Schalkwijk J. Constitutive and inducible expression of SKALP/elafin provides anti-elastase defense in human epithelia. *J Clin Invest* 98: 1389-99, 1996.
  42. Kramers K, van Bruggen MC, Rijke-Schilder TP, Dijkman HB, Hylkema MN, Croes HJ, Fransen JA, Assmann KJ, Tax WJ, Smeenk RJ, Berden JH. In vivo ANA is a fixation artifact: nucleosome-complexed antinucleosome autoantibodies bind to the cell surface and are internalized. *J Am Soc Nephrol* 7: 946-54, 1996.
  43. Mentzel S, Dijkman HB, van Son JP, Koene RA, Assmann KJ. Organ distribution of aminopeptidase-A and dipeptidyl peptidase IV in normal mice. *J Histochem Cytochem* 44: 445-61, 1996.
  44. van den Born J, van Kraats AA, Bakker MA, Assmann KJ, Dijkman HB, van der Laak JA, Berden JH. Reduction of heparan sulphate-associated anionic sites in the glomerular basement membrane of rats with streptozotocin-induced diabetic nephropathy. *Diabetologia* 38: 1169-75, 1995.
  45. Mentzel S, de Leeuw EP, van Son JP, Dijkman HB, de Jong AS, Koene RA, Assmann KJ. Characterization of a 43 kD protein associated to aminopeptidase-A from murine kidney. *Biol Chem Hoppe Seyler* 375: 623-7, 1994.
  46. Kramers C, Hylkema MN, van Bruggen MC, van de Lagemaat R, Dijkman HB, Assmann KJ, Smeenk RJ, Berden JH. Anti-nucleosome antibodies complexed to nucleosomal antigens show anti-DNA reactivity and bind to rat glomerular basement membrane in vivo. *J Clin Invest* 94: 568-77, 1994.
  47. Termaat RM, Assmann KJ, van Son JP, Dijkman HB, Koene RA, Berden JH. Antigen-specificity of antibodies bound to glomeruli of mice with systemic lupus erythematosus-like syndromes. *Lab Invest* 68: 164-73, 1993.
  48. Termaat RM, Assmann KJ, Dijkman HB, van Gompel F, Smeenk RJ, Berden JH. Anti-DNA antibodies can bind to the glomerulus via two distinct mechanisms. *Kidney Int* 42: 1363-71, 1992.
  49. Assmann KJ, van Son JP, Dijkman HB, Koene RA. A nephritogenic rat monoclonal antibody to mouse aminopeptidase-A. Induction of massive albuminuria after a single intravenous injection. *J Exp Med* 175: 623-35, 1992.
  50. Boddington J, Dijkman H. Subcellular localization of Mycobacterium leprae-specific phenolic glycolipid (PGL-I) antigen in human leprosy lesions and in M. leprae isolated from armadillo liver. *J Gen Microbiol* 136: 2001-12, 1990.
  51. Boddington J, Dijkman H. Immunogold labeling method for Mycobacterium leprae-specific phenolic glycolipid in glutaraldehyde-osmium-fixed and Araldite-embedded leprosy lesions. *J Histochem Cytochem* 37: 455-62, 1989.
  52. Boddington J, Dijkman H. In situ locations of Mycobacterium leprae-specific antigens. Immunoelectronoptical studies. *Acta Leprol* 7 Suppl 1:107-12.: 107-12, 1989.
  53. Boddington J, Dijkman H, van der Meijden W, Schmitz P, van Joost T, Stolz E. Replication characteristics and core size of intranuclear herpes simplex virus (HSV-1) in genital skin lesions: electronmicroscopy studies of a biopsy from a female patient. *J Med Microbiol* 24: 93-103, 1987.
  54. Boddington J, Dijkman H, Hendriksen E, Schift R, Stolz E. HSV-2 replication sites, monocyte and lymphocytic cell infection and virion phagocytosis by neutrophils, in vesicular lesions on penile skin. Electronoptical studies of a biopsy. *J Cutan Pathol* 14: 165-75, 1987.

